The inflammatory infiltrate of high-grade serous carcinoma omental metastasis

Everitt, Gemma Louise Ann

The inflammatory infiltrate of high-grade serous carcinoma omental metastasis

Gemma Louise Ann Everitt

Submitted in partial fulfilment of the requirements of the Degree of Doctor of Philosophy

March 2014

The Centre for Cancer and Inflammation
Barts Cancer Institute
Queen Mary University of London
Charterhouse Square
London
EC1M 6BQ

"Learn from yesterday, live for today, hope for tomorrow. The important thing is to not stop questioning." ~ Albert Einstein

Statement of originality

I, Gemma Everitt, confirm that the research included within this thesis is my own work or that where it has been carried out in collaboration with, or supported by others, that this is duly acknowledged below and my contribution indicated. Previously published material is also acknowledged below.

I attest that I have exercised reasonable care to ensure that the work is original, and does not to the best of my knowledge break any UK law, infringe any third party's copyright or other Intellectual Property Right, or contain any confidential material.

I accept that the College has the right to use plagiarism detection software to check the electronic version of the thesis.

I confirm that this thesis has not been previously submitted for the award of a degree by this or any other university.

Signature:

Date: 26th March 2014

Details of collaboration and publications:
In collaboration with AstraZeneca and MedImmune.

Acknowledgements

This work was supported by the BBSRC (Biotechnology and Biological Sciences Research Council) and AstraZeneca in an Industrial Case Studentship, grant number BB/G017867/1.

I would like to thank….

My primary supervisor Prof Fran Balkwill for all of her reassurance, help and guidance with the project. I particularly want to thank her for her endless patience and belief in me throughout the duration of my PhD. For this I am very grateful to her.

My secondary supervisor Dr John Marshall for all of his advice and direction with the project. I would also like to especially thank him for his overwhelming support and the time that he was always only too willing to spend helping and encouraging me when I have found things particularly challenging.

Dr Hagen Kulbe as my postdoctoral supervisor for all of his support and guidance with the project.

Dr Ernst Lengyel for his huge amount of guidance with helping me establish the 3D cell culture model in our laboratory when he visited us for a month in August 2010. I would also like to thank him and Dr Hilary Kenny at The University of Chicago for all of their support since then.

Dr Robert Wilkinson, Dr Richard Sainson, Dr Nadia Luheshi, Dr Judith Anderton and Dr Gareth Davies at MedImmune, Cambridge for being so welcoming and supportive during my time spent there, and throughout the collaboration.

Dr Simon Barry at AstraZeneca for all his support and advice with the project.

Dr John McCafferty in Cambridge for the collaboration and providing the CXCL12 targeting antibody as a part of a Cancer Research UK Discovery committee grant.

Prof David Bowtell at The Peter MacCallum Cancer Centre, Melbourne for providing support with the Australian Ovarian Cancer Study data set and the AOCS1 high-grade serous cell line.

Dr Probir Chakravarty at the London Research Institute for all of his help with the bioinformatics work in chapter 6, and for very kindly guiding me through the analysis of the gene expression microarray data sets and explaining everything so clearly.

Prof Iain McNeish, Dr Michelle Lockley, Dr Darren Ennis, Dr Steffen Boehm, and Tom Dowe for all of their incredibly hard work helping me establish the human omental metastases tissue bank. I really appreciate all of their support with this.

I would particularly like to thank Dr Steffen Boehm for his unlimited support in the laboratory and as a friend! I really enjoyed working with him and I hope that we will work together again in the future!

I would especially like to thank Dr Juliana Candido. We went through the rollercoaster of PhD life together in the laboratory and she was overwhelmingly supportive throughout the duration of the four years, and particularly at difficult times. I can’t thank her enough, and really appreciate everything that she has done for me! She is a true friend!

My lab sisters, Dr Kyra Archibald, Ganga Gopinathan and Laura King for their advice with the project, and continuous encouragement and support. Thank you for keeping me smiling!

All of the staff, but especially George Elia in the Barts Cancer Institute Histopathology Department for their huge amount of help with processing samples and their advice with immunohistochemistry.

Linda Hammond for her huge amount of support, guidance and tuition with using the confocal microscope and other facilities in the Barts Cancer Institute Imaging Suite.

Guglielmo Rosignoli in the Barts Cancer Institute FACS suite. Dr Anne Montfort and Dr Eleni Maniati in the lab for all their help and guidance particularly with the FACS.

Dr Christina Ghirelli for her guidance on PBMC isolations and Dr Raphael Zollinger for his advice with qRT-PCR.

Zohra Gueroui, Emily Mclean-Inglis and Monica Canosa for their endless support and help around the lab.

Richard Thompson, Dr Modhassar Kahn, Dr Simon Hallam, and Daniel Andritschke for the laughter shared that kept me going!

All of my colleagues, past and present in The Centre for Cancer and Inflammation for their continuous support, advice and guidance.

Dr Michael Allen in the Tumour Biology department for his support and help with the project, particularly with analysing the 3D cell culture model work.

Andrew Clear in the Haemato-Oncology department and Dr Andrew Leinster for their continuous help and support with the immunohistochemistry and the Leica Ariol System.

Dr Shah-Jalal Sarker for his advice with the statistics in the project.

Dr Naveena Singh for taking the time to explain the pathology of human omental metastases to me.

All of the hospital and theatre staff at Barts for accommodating me and being so welcoming whilst I was collecting the tissue samples.

Niall Morrissey for his incredible confidence boosting support, inspiration and reassurance at particularly difficult times. Thank you for teaching me to be mindful!

All of my friends and family for their unlimited patience and continuous support….I could not have done this without you!

My dad and Jennifer for their endless encouragement, reassurance, support and interest in my work. Thank you for all the hours you have spent listening and for being there!

My mum and Dave for standing by me through the rollercoaster of successes and uplifting me during the difficult times. Thank you for listening, dealing with my stresses, and for your overwhelming support!

My sisters Sara, Laura, Sarah and my little niece Lilah for keeping me motivated and always making me smile!!

My friends Dr Annie Baker, Dr Alex Avgustinova, Dr Morgane Gourlaouen, Laura Tooth and Dr Amanda Ayling for being absolute pillars of strength and support for me during the last four years.

I would like to warmly remember my friend David Randall who was diagnosed and lost his battle with cancer during the course of my PhD. He was Inspirational!

Abstract

The aim of this thesis is to investigate the role of inflammatory infiltrates and chemokines in metastasis of high-grade serous ovarian cancer, HGSC, to the omentum using human tissue biopsies and a 3-dimensional (3D) cell culture model.

In ten patients with metastatic HGSC, omental tumour deposits contained a prominent leukocyte infiltrate of CD3+ T cells (9% of total cells) and CD68+ macrophages (11% of total cells). The presence of CD68+ macrophages showed a significant positive correlation with tumour cell proliferation analysed by Ki67 expression.

Four ovarian cancer cell lines were co-cultured on a 3D model mimicking the microenvironment of the omentum for two weeks. The model was composed of collagen embedded human fibroblasts covered in a confluent layer of human primary mesothelial cells. The mesothelial cells in the 3D model significantly increased the growth ($p = 0.002$) and invasion ($p = 0.0004$) of the ovarian cancer cells.

CXCL12 is the macrophage chemoattractant and ligand for the major chemokine receptor expressed on ovarian cancer cells. An association between CXCL12 and extracellular matrix remodelling was identified in two independent gene expression microarrays of ovarian cancer biopsies. The expression of CXCL12 in the HGSC omental metastases measured by quantitative Real Time-PCR positively correlated with decorin expression. Antibody mediated neutralisation of CXCL12 reduced growth ($p = 0.012$) and invasion ($p = 0.029$) in the 3D model. Mimicking an infiltrate of CD68+ macrophages in this multicellular 3D *in vitro* system also produced measurable changes in inflammatory cytokine and chemokine expression.

There is currently a demand for more accurate models of HGSC and a necessity to study its metastasis that presents itself as the major clinical problem in patients. Therefore the development of this 3D model to mimic tumour-promoting inflammation in HGSC metastasis will provide researchers with an essential tool for testing novel therapeutic strategies.

Table of Contents

List of Figures

List of tables

Abbreviations

2D	2-dimensional
3D	3-dimensional
ACTB	β-actin
ADP	adenosine diphosphate
ANOVA	One-Way Analysis of Variance
AOCS	Australian Ovarian Cancer Study
ARID1A	AT – rich interactive domain-containing protein 1A
ASC	adipose stem cell
BBSRC	Biotechnology and Biological Sciences Research Council
BCG	Bacillus Calmette-Guerin
BCI	Barts Cancer Institute
BRCA	breast cancer gene
BSA	bovine serum albumin
CA-125	cancer antigen 125
CCC	clear cell ovarian carcinoma
CCL	chemokine (C-C motif) ligand
CD	cluster of differentiation molecule
CLL	chronic lymphocytic leukaemia
CLOVAR	classification of ovarian cancer survival signatures
CO_2	carbon dioxide
COSP	calculator of subtype prediction
CSF	colony-stimulating factor
CTLA4	cytotoxic T-lymphocyte antigen 4
CXCL	chemokine (C-X-C motif) ligand
CXCR	C-X-C chemokine receptor
DAB	3,3'diaminobenzidine
DMBA	7, 12 – dimethylbenzanthracene
DMEM	Dulbecco's Modified Eagle Medium

DNA	deoxyribonucleic acid
dNTP	deoxyribonucleotide triphosphate
DTT	dithiothreitol
ECM	extracellular matrix
EDTA	ethylenediaminetetraacetic acid
EGF	epidermal growth factor
EGFR	epidermal growth factor receptor
ELISA	enzyme – linked immunosorbent assay
EMT	epithelial-mesenchymal transition
EPAS1	endothelial PAS (Period circadian protein, Aryl hydrocarbon receptor nuclear translocator protein, Single-minded protein) domain – containing protein 1
ER	estrogen receptor
ERK	extracellular signal – related kinases
FACS	fluorescence activated cell sorting
FAP	fibroblast activation protein
FBS	fetal bovine serum
FDA	Food and Drug Administration
FH	follicle stimulating hormone
FN	fibronectin
FOXP3	forkhead box P3
GAPDH	glyceraldehyde 3-phosphate dehydrogenase
GEO	Gene Expression Omnibus
GFP	green fluorescent protein
H & E	hematoxylin and eosin
HBV	Hepatitis B virus
HCl	hydrochloride
HEF	human embryo fibroblast
HGSC	high-grade serous ovarian carcinoma
HIF1α	hypoxia – inducible factor 1α
HIV	Human Immunodeficiency Virus
HMBS	hydroxymethylbilane synthase

HNF1B	hepatocyte nuclear factor 1 homeobox B
HPF	human primary fibroblasts
HPMC	human primary mesothelial cells
HPRT	hypoxanthine phosphoribosyltransferase
HPV	human Papilloma virus
HR	homologous recombination
HRP	horseradish peroxidase
HUVEC	human umbilical vein endothelial cell
IFN-γ	interferon - γ
IKK-β	IκB kinase - β
IL	interleukin
JAK	Janus kinase
JNK	Jun N-terminal kinase
Lam	Laminin
LH	luteinizing hormone
M-CSF	macrophage colony-stimulating factor
MAP	mitogen activated protein
MDM	mouse double minute
MHC	major histocompatibilty complex
MISR	müllerian inhibiting substance receptor
MLC	myosin light chain
MMP	matrix metalloproteinase
MOSEC	mouse ovarian surface epithelial cell
MPS	mononuclear phagocyte system
mRNA	messenger ribonucleic acid
MSC	mesenchymal stem cell
MYD88	myeloid differentiation primary response gene (88)
NCBI	National Center for Biotechnology Information
NF-κB	nuclear factor kappa B
NK	natural killer
NO	nitric oxide
NSAID	non-steroidal anti-inflammatory drug

OCT	optimal cutting temperature compound
PARP	poly ADP ribose polymerase
PAX	paired box gene
PBMC	peripheral blood derived monocyte
PBS	phosphate buffer solution
PCR	polymerase chain reaction
PD-L1	programmed cell death ligand 1
PDGFR	platelet – derived growth factor receptor
PET	positron emission tomography
PI3K	phosphoinositide 3 - kinase
PIK3CA	phosphatidylinositol 3 – kinase, catalytic, alpha polypeptide
PKC	protein kinase C
PMA	phorbol 12-myristate 13-acetate
PROVAR	protein-driven index of ovarian cancer
PS	penicillin/streptomycin
PTEN	phosphatase and tensin homolog
qRT-PCR	quantitative real-time polymerase chain reaction
Rb	retinoblastoma
RET	rearranged during transfection
RNA	ribonucleic acid
RPL34	ribosomal protein L34
RPMI	Roswell Park Memorial Institute
RT-PCR	reverse transcription polymerase chain reaction
SDF-1α	stromal derived factor - 1α
shRNA	short hairpin ribonucleic acid
siRNA	small interfering ribonucleic acid
STAT	signal transducer and activator of transcription
STIC	serous tubal intraepithelial carcinoma
STR	short tandem repeat
SV40 TAg	Simian virus 40 T antigen
TAM	tumour associated macrophage
TBP	TATA-binding protein

TCGA	The Cancer Genome Atlas
TEN	tumour-entrained neutrophils
TERT	telomerase reverse transcriptase
TGF-β	transforming growth factor - β
TGFB1	TGFβ-induced protein
TH	T helper
TMA	tissue microarray
TNF-α	tumour necrosis factor - α
TP53	tumour protein p53
TUNEL	terminal transferase dUTP nick end labelling
UBC	ubiquitin C
UK	United Kingdom
US	United States
VEGFA	vascular endothelial growth factor A
VEGFR	vascular endothelial growth factor receptor
WT1	Wilms tumour 1
YWHAZ	tyrosine 3-monooxygenase/ tryptophan 5-monooxygenase activation protein, zeta
α-SMA	α - smooth muscle actin
β2M	beta-2 microglobulin

1. Introduction

Ovarian cancer is the fifth most common cancer affecting women in the United Kingdom (UK). Generally women who are older, overweight or infertile are at a greater risk of developing ovarian cancer (Vaughan et al., 2011). Platinum therapies were introduced approximately thirty years ago, and together with Paclitaxel, Carboplatin treatment followed by interval-debulking surgery remains to be the standard regime of care for ovarian cancer patients

The latest recorded five-year survival rates in the UK equates to 42.9% (Cancer Research UK). Given the stagnated survival rates since current therapeutic strategies were introduced, there is a demand for novel drug targets.

1.1. The origin and pathogenesis of 'ovarian' carcinoma

The theory that acquired general consensus until recent times was that ovarian cancer originated from aberrations in the ovarian surface epithelium, (Radisavljevic, 1977). Two modes of malignant transformation of the epithelial cells were thought to exist (Erickson et al., 2013). Firstly overstimulation of the surface epithelial cells with follicle stimulating hormone (FSH) and luteinizing hormone (LH) were thought to promote the occurrence of genetic mutations (Cramer and Welch, 1983). Perimenopausal women produced high levels of these gonadotropin hormones, and there was an increased incidence of ovarian cancer in women ten years after their menopause. Secondly the process of ovulation itself was thought to cause malignant transformation through the development of cortical inclusion cysts (Nik et al., 2014). This was first identified where an excessive production of

eggs in hens increased the development of epithelial ovarian cancer (Fathalla, 1971). It was thought that the surface epithelial cells became damaged during the ovulation process, and within the inclusion cyst were exposed to growth factors that would normally be dispersed in the peritoneal fluids. These abnormal cellular interactions were thought to promote malignant transformation. This theory was supported by the lower incidence of ovarian cancer in women who had experienced breaks in ovulation through pregnancy, and also those who had reduced ovulation cycles regulated by the oral contraceptive pill (Cramer et al., 1982). Malignant ovarian surface epithelial cells were then thought to disseminate from the ovarian surface, where they were then free-floating in the peritoneal fluids and metastasised to surrounding tissues (Shield et al., 2009).

Attempts to try and identify the precursor lesions of ovarian cancer on the ovaries themselves however, were met with very little success (Nik et al., 2014). In fact, the molecular pathology of ovarian carcinoma carried very little resemblance to that of the ovaries. The disease was considered to be so heterogeneous that it was doubted a disease of single origin (Kurman and Shih Ie, 2010). It is now clear that there are five defined histological subtypes of ovarian carcinoma, each showing similarities to the epithelium of tissues within close proximity to the ovaries (Table 1-1) (Kurman and Shih Ie, 2011; Li et al., 2011). Early lesions of high-grade serous carcinoma (HGSC) originated as serous tubal intraepithelial carcinoma (STIC) involving the secretory cells of the endosalpinx of the fallopian tubes (Crum et al., 2012). It appeared that the original concept of a ‘cortical inclusion cyst’ initiating malignant transformation still applied, but the cells of the cyst may have originated in the fimbria, and were included in the ovaries as a secondary site during cyst development (Kurman, 2013).

Histological ovarian carcinoma subtype	Tissue resemblance
High grade serous	Fallopian tube
Low grade serous	Fallopian tube
Endometrioid	Endometrium
Clear cell	Endometrium
Mucinous	Gastrointestinal tract

Table 1-1 Summary of the histological subtypes of ovarian carcinoma.

The five histological subtypes of ovarian carcinoma bear more molecular and pathological resemblance to different tissues that are anatomically close to the ovaries, than they do to the ovaries themselves. A new and alternative theory with growing supportive evidence suggests that the tissue types resembled by the carcinomas are in fact the true origin of the precursor lesions, and the ovaries are sites of secondary metastases (Kurman and Shih Ie, 2011; Li et al., 2011).

Figure 1-1 illustrates the differences in the histopathology of four of the ovarian cancer subtypes, HGSC, endometrioid, clear cell and mucinous carcinoma. Figure 1-1 also diagrammatically indicates the tissue source of each subtype.

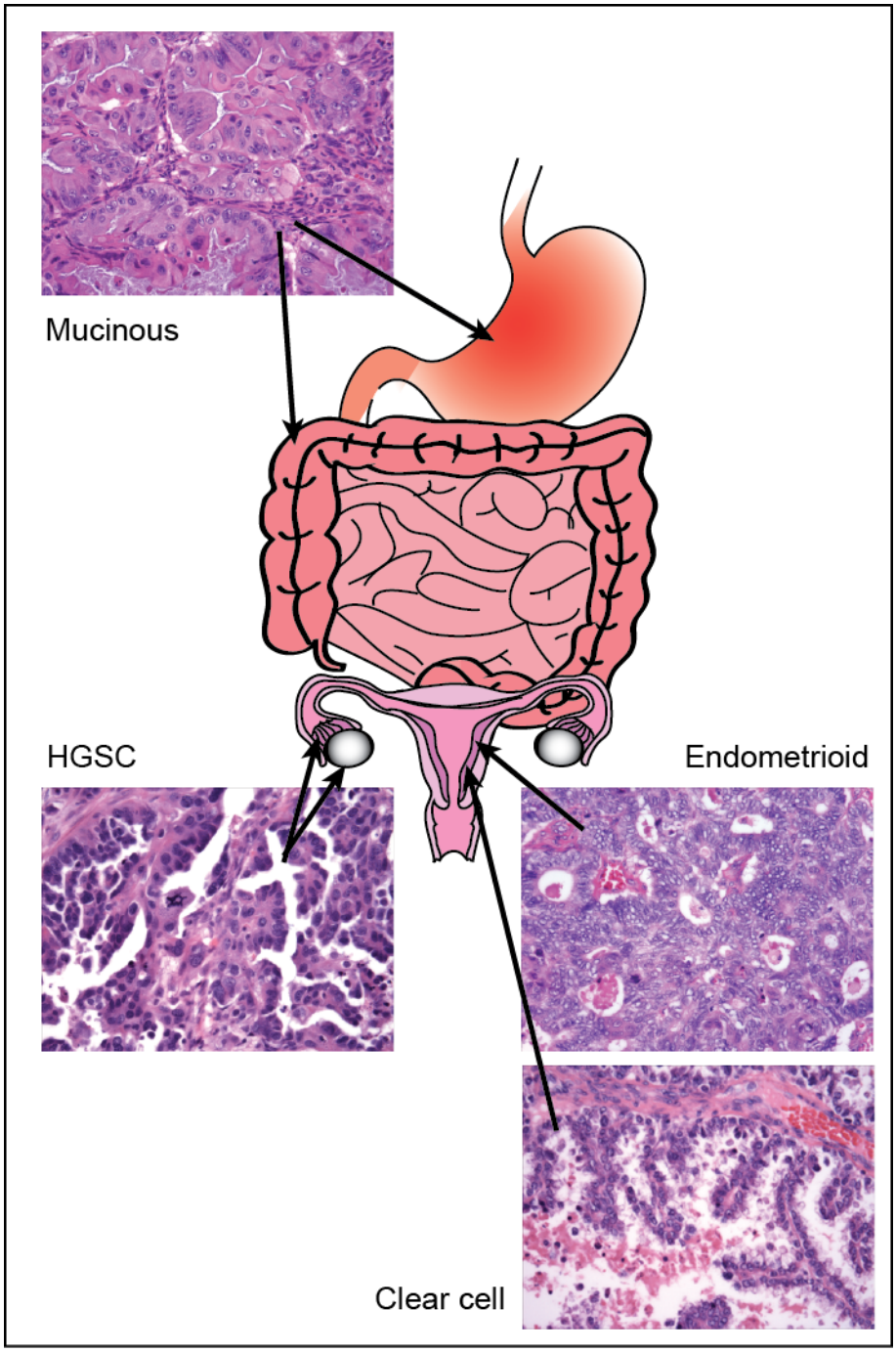

Figure 1-1 The origins and histopathology of four subtypes of ovarian carcinoma.

Diagram illustrating H & E stained sections of four of the subtypes of ovarian cancer, and arrows indicating the tissue of origin. Mucinous ovarian cancers arise from the gastrointestinal tract, including the colon, appendix and stomach. High-grade serous carcinoma (HGSC) may originate from the ovaries but are more likely to involve the epithelial cells of the fimbria. Endometrioid and clear cell carcinoma is initiated in the endometrium (Kurman and Shih Ie, 2011; Li et al., 2011).

1.1.1. High grade serous ovarian carcinoma (HGSC)

HGSC is the most common and the most aggressive of the histological subtypes accounting for approximately 60% of ovarian cancer deaths (Bowtell, 2010; Kurman, 2013). HGSC is generally sensitive to platinum-based therapies at least initially, but due to the clonal diversity of the disease, it quickly adapts and acquires resistance (Vaughan et al., 2011). Resistance to therapy in HGSC may develop from the selected survival of a sub-clonal population that pre-exists within the tumour (Cooke et al., 2010). Genomic aberrations were studied in a group of sensitive and resistant HGSC cell lines derived from the same patient. The degree of aneuploidy between the sensitive and resistant lines was highly dissimilar suggesting the resistant cell population was not a descendant of the sensitive cell lines. This was further supported when paired pre- and post chemotherapy samples collected from six HGSC patients were also divergent in their genetic instability and copy number aberrations.

1.1.1.1. HGSC is a cancer of the fallopian tube

Recently pre-neoplastic lesions were identified in the fimbria of the fallopian tubes in patients with HGSC. (Ahmed et al., 2010; Kindelberger et al., 2007; Nik et al., 2014). This suggested that the epithelial cells of the fimbria themselves were the true initiating cells of HGSC. 75% of patients with sporadic HGSCs were found to have STICs (Kindelberger et al., 2007). Involvement of the fallopian tube equally applied to HGSC patients with BRCA mutations who had an inherited genetic predisposition to the disease (Crum et al., 2007). In the HGSC cases positive for fimbria involvement the same TP53 mutation signature found in the carcinoma was also identified in the STICs (Lee et al., 2007b). TP53 mutations were identified in 96% of HGSCs (Cancer Genome Atlas Research, 2011). A comprehensive study of the type and frequency of TP53 mutations in HGSC patients did not significantly

associate with patient prognosis (Ahmed et al., 2010). 56.3% of the mutations studied were missense mutations and located within exons 4-8. The most frequently mutated codon was 273 involving R273C, R273H and R273L mutations occurring in 13.4% of all cases. The high frequency of TP53 mutations in high stage disease suggested that it was an early driver of HGSC development and progression. Ahmed and colleagues noted that in HGSC cases that were negative for TP53 mutations, there were copy number gains in MDM (mouse double minute) 2 and 4, which regulate and target p53 for degradation, indicating that there was still a loss of p53 function where mutations were absent.

An array of secreted proteins from an *ex vivo* culture model of the human fallopian tube were collectively very representative of secreted markers seen in HGSC (Levanon et al., 2010) and very few of these proteins were detected in the ovarian surface epithelium. This further supported the theory that HGSCs did not originate in the ovary at all, but were actually carcinomas of the fallopian tube incorporated within the ovary by the process of endosalpingiosis (Nik et al., 2014).

1.1.1.2. The quest for prognostic biomarkers of HGSC

In recent years there has been a significant expansion in data sets of gene expression analyses of HGSC. The Australian Ovarian Cancer Study (AOCS) lead by the laboratory of Prof David Bowtell in Melbourne is a collaborative project uniting scientific and clinical data to search for predictive biomarkers for earlier diagnosis, chemotherapy response and survival of HGSC patients. Tothill and colleagues (Tothill et al., 2008) used an unbiased clustering statistical analysis of microarray gene expression data to collate data from 285 HGSC and endometrioid biopsies into six molecular subtypes on the basis of patient clinical outcome and their response to chemotherapy. Four of those subtypes (C1, C2, C4 and C5) related to HGSC and collectively showed an up-

regulation in pathways associated with a reactive stromal signature, such as cell signalling pathways, angiogenesis, mesenchymal expression markers, and extracellular matrix and cell adhesion proteins. The C1 and C2 subtypes expressed high levels of pro-inflammatory cytokines and chemokines of the described TNF (tumour necrosis factor) network; interleukin (IL)-6, TNF-α and CXCL12 (Kulbe et al., 2012). Biopsies of the C1 subtype related to a poor prognosis and response to chemotherapy, and expressed markers such as FAP (fibroblast activation protein) and α-SMA (smooth muscle actin). These C1 subytype biopsies were also highly desmoplastic defined by excessive collagen deposition (Tothill et al., 2008). More recently the BRCA1 and BRCA2 mutated C2 molecular subtype was further annotated with increased T cell infiltrates and an immunoreactive signature (George et al., 2013).

Interrogation of a further gene expression data set of more than 500 HGSC ovarian cancer biopsies derived from The Cancer Genome Atlas (TCGA) (Cancer Genome Atlas Research, 2011), recently aided the formulation of the CLOVAR model (classification of ovarian cancer survival signatures)(Verhaak et al., 2013). Four described gene signature groups were identified on the basis of patient prognosis. Patients of HGSC with a mesenchymal and immunoreactive signature had the worst prognosis, with disease recurrence in less than six months from treatment and the development of resistance to platinum therapy. This highlights the relevance of the tumour microenvironment in disease severity.

In a later study Yang J and colleagues generated a second model using the biopsies of the TCGA based on high throughput protein expression arrays, named the PRotein-driven index of OVARian cancer (PROVAR) model (Yang et al., 2013b). This model was composed of 9 protein markers that were predictive of progression free survival, and was more robust than the CLOVAR model. Similarly to the CLOVAR model, four

distinct protein clusters were identified that related to patient prognosis. These PROVAR model protein clusters correlated with the molecular subtypes of the CLOVAR model. High-risk patients with a poor prognosis as predicted by the PROVAR model, clustered and associated with the mesenchymal and immunoreactive gene signature subytpes as predicted by the CLOVAR model. Three of the protein markers found to be associated with poor prognosis STAT (signal transducer and activator of transcription) 5α, pPKC (protein kinase C) α and pMAP (mitogen activated protein) 2 kinase 1 were all in downstream signalling pathways of EGFR (epidermal growth factor receptor) involved in tumour cell proliferation, survival and invasion.

1.1.1.3. Potential new therapeutic strategy for HGSC

Women with a family history of breast or ovarian cancers carrying genetic mutations in the DNA repair molecules RAD51C and BRCA1/2 fall within the high-risk group for developing HGSC (Vaughan et al., 2011). Hence poly adenosine diphosphate ribose polymerase (PARP) inhibitors are one of the most promising new leads for advancing the treatment of HGSC patients. These molecular inhibitors take advantage of the inefficiency of BRCA1 and BRCA2 mutated HGSC cells to repair double-strand breaks in DNA (Banerjee et al., 2010). In primary cell cultures established from the ascites of 50 women, RAD51 positive nuclear foci were used as a marker of DNA double-strand break repair by homologous recombination (HR) (Mukhopadhyay et al., 2012). 96% of the cultures that were deficient in HR mechanisms were also sensitive to the PARP inhibitor rucaparib, compared with none of the HR competent cultures. In the patients that the cultures were derived from, HR deficiency also correlated with increased platinum sensitivity and improved overall survival.

It was thought that acquired resistance to such PARP inhibitors might jeopardise the efficacy of subsequent treatments with platinum-based

chemotherapy. This was disproved in a recent retrospective study of patient responses (Ang et al., 2013). Therefore PARP inhibitors are still strong candidates for HGSC care.

1.1.2. Clear cell ovarian carcinoma (CCC)

Clear cell carcinoma, CCC, is the second most common subtype of ovarian cancers and responds poorly to current chemotherapeutic strategies. In advanced cases, it actually has a worse prognosis than HGSC (Goff et al., 1996). CCC often presents in younger women and is strongly associated with endometriosis (Kennedy et al., 1989). Approximately 50% of CCCs carry a mutation in the chromatin-remodelling gene and tumour supressor *ARID1A* (AT-rich interactive domain containing protein 1A) (Jones et al., 2010; Wiegand et al., 2010). Pathologically CCC is rich in basement membrane components and glycogen. The latter is reflective of the enrichment in gene expression profile signatures associated with metabolic pathways that are distinctive to this subtype (Anglesio et al., 2011a). CCCs are also molecularly characterised by enrichment in cytokine signalling, oxidative stress and hypoxia driven pathways.

CCCs present with activating mutations in *PIK3CA*, a regulator of the phosphoinositide (PI) 3 kinase pathway (Campbell et al., 2004). On a molecular level, CCCs are very similar to renal carcinomas, both showing an up regulation in *HIF1A* (hypoxia-inducible factor 1A) *(Lee et al., 2007a)* and *EPAS1* (endothelial (Period circadian protein, Aryl hydrocarbon receptor nuclear translocator protein, Single-minded protein) domain-containing protein 1). Sunitinib is a tyrosine kinase inhibitor that targets angiogenesis through inhibition of VEGFR (vascular endothelial growth factor receptor), PDGFR (platelet-derived growth factor receptor) and KIT signalling pathways amongst others. The success of the anti-angiogenic drug sunitinib in renal cancers (Kumar et al., 2009) prompted an investigation involving sunitinib treatment in CCC

(Anglesio et al., 2011b). High IL-6 levels are also found in CCC and endometriosis, which activate STAT3, HIF and VEGFA (vascular endothelial growth factor A). Two sunitinib-treated CCC patients showed a significant decrease in tumour size with an associated reduction in monitored CA-125 (cancer antigen 125) levels suggesting that high IL-6 levels drive early events in the development of CCC.

In contrast to HGSCs, CCCs specifically express *HNF1B* (hepatocyte nuclear factor 1 homeobox B), which may be involved in the deregulation of apoptosis (Tsuchiya et al., 2003). CCCs also have no *TP53* mutations and have a low frequency of *BRCA1/BRCA2* mutations (Nik et al., 2014).

These further supports the notions that the two subtypes of ovarian cancer are more distinct from one another than the term 'subtype' suggests, and are in fact completely different diseases. It is becoming increasingly important that we recognise this when considering treatments for these diseases. Given that the predominant proportions of ovarian cancer deaths are attributed to HGSC, this subtype is the focus of this thesis. The contribution of the microenvironment to tumour development and chemotherapy resistance is particularly important in HGSC (Vaughan et al., 2011; Verhaak et al., 2013). Given the malignant cells of HGSC are characterised by their clonal diversity and ability to quickly acquire resistance to therapies, the supporting cells of the microenvironment may be a favourable target for HGSC treatment.

1.2. Inflammatory cells of the tumour microenvironment

The involvement of the immune system in malignant transformation and development is a well recognised hallmark of cancer progression (Cavallo et al., 2011). It is widely accepted that the presence of an inflammatory infiltrate within a tumour can often support its growth and metastasis (Erez and Coussens, 2011). The first observation of the presence of an immune infiltrate in cancers was noted by Rudolf Virchow in 1863 (Balkwill and Mantovani, 2001). The inflammatory infiltrate within malignant disease can switch from a tumour promoting response which is detrimental to patient survival to a tumour-targeted response that is beneficiary (Hanahan and Weinberg, 2011). Therefore the signature of inflammatory infiltrate may provide useful information as a prognostic marker, and also aid the design of more personalised therapies (Fridman et al., 2012). The roles of immune cell infiltrates studied in ovarian cancer are discussed in this chapter and summarised in table 1-2.

Immune cell infiltrate	Patient prognosis	Reference
Neutrophils	Poor	(Carus et al., 2013)
B cells	Poor	(Yang et al., 2013a)
CD4+ FOXP3+ T cells	Poor	(Curiel et al., 2004)
T Helper (TH) 1 & TH17 CD4+ T cells	Good	(Fridman et al., 2012)
TH2 CD4+ T cells	Poor	(Fridman et al., 2012)
CD8+ T cells	Good	(Fridman et al., 2012; Stumpf et al., 2009)
Macrophages	Poor	(Kryczek et al., 2007; Vaughan et al., 2011)

Table 1-2 The effect of immune cell infiltrates on ovarian cancer patient prognosis.

Table summarising the role of immune cell infiltrates in ovarian cancer progression on the basis of their impact on patient prognosis when present in the tumour microenvironment at high densities. The associated references are also indicated.

1.2.1. Neutrophils

Neutrophils release reactive oxygen species that can contribute to malignant transformation by damaging DNA and deregulating the action of DNA repair, cell cycle control and apoptosis proteins (Schafer and Werner, 2008). Neutrophils can adopt an angiogenesis inducing pro-tumorigenic role within the tumour microenvironment (Fridlender et al., 2009; Polyak et al., 2009). Additionally and conversely 'tumour entrained neutrophils' (TENs) can be anti-metastatic. Granot et al demonstrated that hydrogen peroxide production by TENs at the metastatic site prevented metastasis to the lung in the 4T1 breast carcinoma *in vivo* model (Granot et al., 2011).

In ovarian cancer patients increased numbers of neutrophils in the blood correlates with a poor response to chemotherapy (Carus et al.,

2013)(Table 1-2). Recently in a randomised trial involving 964 ovarian, fallopian and peritoneal cancer cases, patients were treated with a constant or increasing dose of carboplatin. (Banerjee et al., 2013; Donskov, 2013). There was no significant improvement on survival. However within both arms of the study increased baseline neutrophil blood counts correlated with a reduced progression free survival, suggesting that these may be a useful prognostic marker. Tumour-infiltrating neutrophils within the microenvironment of HGSC omental metastases were quantified by immunohistochemical analysis (Leinster et al., 2012). Conversely to the baseline blood counts the overall number of neutrophils in the microenvironment was relatively low in comparison with T cell and macrophage infiltrates. However there were no data linking HGSC infiltrating neutrophils with patient survival.

1.2.2. B and T cell lymphocytes

B and T cell lymphocytes of the adaptive immune system are also found within the tumour microenvironment (Balkwill et al., 2012). Classically B cells produce antibodies and the deposition of immune complexes can polarise macrophages to become tumour promoting (Balkwill et al., 2013). B cells promoted tumour progression in a mouse model of skin carcinoma mediated by the recruitment of inflammatory cells and Fcγ receptor interactions on the surface of macrophages (Andreu et al., 2010). B cells also had an immunosuppressive function on T cell activity through interactions with CD40 and secretion of IL-10 (Qin et al., 1998; Shah et al., 2005). Depleting B cell populations with the CD20 targeted antibody rituximab, is used for the treatment of Non-Hodgkin's lymphoma and chronic lymphocytic leukaemia (CLL) (Balkwill et al., 2013). However research into B cell activity in tumour progression is largely hindered through a lack of definitive B cell markers. A recent report correlated CD19 positive B cells with poor overall survival in a cohort of 49 omental metastases of HGSC (Yang et al., 2013a)(Table 1-

2), but in general very little is known about the role of B cells in ovarian cancer.

B cell-cell interactions with CD4 positive T cells together with TGF (transforming growth factor) β production stimulates the differentiation of the T cell into a regulatory T cell (Balkwill et al., 2013). Different T cell subsets can have either tumour-targeted cytotoxic effector functions, or regulatory functions that counteract and dampen the immune response to the developing tumour (Balkwill and Mantovani, 2012; Mantovani et al., 2008). CD3 positive T cells are broadly sub-categorised into CD4 positive regulatory or memory T cells and CD8 positive cytotoxic T cells. T regulatory cells are generally associated with a poor prognosis in cancers (Bates et al., 2006; Hiraoka et al., 2006), and characterised by the expression of FOXP3 (forkhead box P3) and CD25 (Balkwill et al., 2012). They promote tumour progression through preventing tumour cell interactions with cytotoxic T cells via blockade of the cytotoxic T-lymphocyte antigen 4 (CTLA4). In some cases T regulatory cells can also hinder tumour growth. High levels of CXCL12 in cervical cancers, which correlated with a poor prognosis, repelled the infiltration of regulatory T cells (Jaafar et al., 2009). However in ovarian cancer an infiltrate of these cells rather impairs patient survival (Curiel et al., 2004)(Table 1-2).

Other CD4 positive T helper (TH2 and TH17) cells found in the tumour microenvironment are believed to promote tumour progression, but in some cases they correlate with a good prognosis (Balkwill et al., 2012)(Table 1-2). Differences in the clinical response to CD4 positive T cell infiltrates across a panel of cancer types illustrates the complexity of the subpopulations within this group of inflammatory cells (Fridman et al., 2012). Using alternative CD4 positive T cell markers correlated with patient response will aid studying the role of these cells in different tumour microenvironments.

CD4 positive TH1 cells producing IL-2 and IFNγ support the activity of CD8 positive cytotoxic T cells. These CD8 positive inflammatory cells in the tumour microenvironment are overall associated with a good prognosis (Balkwill et al., 2012; Fridman et al., 2012). CD8 positive T cells can be found at both the invasive margin and core of the developing tumour. For example, a high infiltrate of CD8 positive T cells within the invasive margin of human colorectal cancer liver metastases correlated with an improved response to chemotherapy and increased patient survival (Halama et al., 2011).

CD8 positive T cell infiltrates are also associated with an increased survival in ovarian cancer patients, which has been supported by many studies (Fridman et al., 2012; Hamanishi et al., 2007; Sato et al., 2005; Zhang et al., 2003). Investigation into the tumour infiltrating lymphocytes of one hundred stage III HGSC biopsies linked the presence of intraepithelial CD8 positive T cells with an improved overall survival in all cases, inclusive of patients whom had received chemotherapy (Stumpf et al., 2009)(Table 1-2).

More recently Webb and colleagues associated CD8 positive T cells that were also positive for CD103 with an increased progression free survival compared with those that were CD103 negative (Webb et al., 2014). The epithelial regions of HGSCs in particular were rich in CD103 positive T cells, and it was thought that the proximity of the T cells with the epithelial cells was mediated by interactions between CD103 and E-Cadherin.

Furthermore, activation of the programmed cell death (PD)-1 receptor expressed on tumour infiltrating lymphocytes with its ligand PD-L1 has a tumour targeted immunosuppressive function (Duraiswamy et al., 2013). Antibody mediated inhibition of this pathway in the syngeneic ID8 ovarian cancer mouse model caused tumour regression, which was related to an increased infiltrate, proliferation and function of CD8 positive T cells.

1.2.3. Macrophages

Given there is a focus on macrophage infiltrates in this thesis following the work described in chapter 3, more background information will be provided in this chapter about these inflammatory cells and their role in the tumour microenvironment.

Monocytes can differentiate, according to the cues of chemokine and cytokine signalling within the microenvironment, to macrophages or dendritic cells. CD68 positive macrophages can also be divided into two broad groups. M1 or classically polarised macrophages are pro-inflammatory, displaying markers such as CD40, CD80, and MHC (major histocompatibility complex) class II and releasing cytokines such as, interferon (IFN)-γ, TNF-α, IL-6 and IL-12. The pro-inflammatory properties of these macrophages are tumour-promoting, however the phagocytic functions of these macrophages can engulf tumour cells (Wynn et al., 2013).

M2 polarised or tumour-associated macrophages (TAMs) release anti-inflammatory cytokines such as IL-10, and express IL-4 and its receptor. TAMs support tumour growth and metastasis. One of the first studies to show that TAMs promote the development of cancer was in a mouse breast carcinoma model (Lin et al., 2001). Tumours grown in mouse models that had been genetically engineered to be completely depleted of macrophages failed to develop lung metastases. TAMs can increase the invasion and proliferation of malignant cells by the release of chemotactic and growth factors such as TGF-β and EGF (epidermal growth factor) (Bonecchi et al., 2011). They secrete VEGF promoting angiogenesis (Yang et al., 2004) and suppress the adaptive tumour-targeted immune response including CD8 positive T cell activation (Mantovani et al., 2008; Sica and Bronte, 2007). Macrophages are also very important in the remodelling of the extracellular matrix (ECM) in tumours. Matrix metalloproteinase (MMP) production facilitates tumour

cell invasion and in addition TAMs regulate ECM stabilisation through promoting collagen fibrillogenesis (Pollard, 2008).

1.2.3.1. Multiple macrophage subtypes and their origins

The binary sub-classification of macrophages is really too basic. There is in fact a very complex transitional spectrum of intermediate phenotypes (Wynn et al., 2013). Gene expression profiles for tissue resident macrophages of different mouse organs have been established to identify unique molecular subytpes (Gautier et al., 2012). Efforts are currently underway to translate these studies in humans to better understand the mechanisms underpinning the transition between the subtypes. Frankenberger and colleagues identified distinct gene expression profiles for CD16 positive and negative monocyte populations in the blood, which are further unique to tissue resident macrophages (Frankenberger et al., 2012). The mononuclear phagocyte system (MPS) model hypothesised that monocytes circulating in the blood extravasate into tissues and differentiate according to localised molecular cues (Gomez Perdiguero and Geissmann, 2013). The model proposed that within the tissue the macrophages then contribute to inflammation, tissue remodelling and tumour progression. However the identification of macrophages in embryos, such as those in the peritonea, the microglia in the central nervous system, and the Kupffer cells in the liver negated this theory. A mouse model deficient for the transcription factor Myb revealed that the hematopoietic stem cell derived CD11b positive macrophage population found in the fetal liver was ablated (Schulz et al., 2012). F4/80 positive tissue resident macrophages were however still present suggesting a completely separate origin for these cells that were able to self-renew and were Myb independent. A normal number of macrophages were found in the yolk sac of these developing mice, proposing that this may be the origin of tissue resident macrophages, which unlike their bone marrow derived counterparts differ in function (Gomez Perdiguero and Geissmann,

2013). Tissue resident macrophages are thought to be less involved in inflammation, as they do not activate nuclear factor (NF)-κB, and do not secrete inflammatory cytokines, but they are more involved in tissue homeostasis.

1.2.3.2. Macrophage targeted therapies

Current therapeutic strategies, such as those targeting CCL2 aim to ablate macrophage recruitment to tumours (Qian et al., 2011; Wynn et al., 2013). Tumour cells secrete colony-stimulating factor (CSF) 1 which macrophages are responsive to through expression of the receptor on their cell surface. In a recent study involving a viral mammary tumour *in vivo* model, targeting the CSF1 receptor with a blocking antibody in combination with inhibition of CXCR4 signalling significantly reduced invasion and metastasis (Boimel et al., 2012). This work demonstrated that EGF stimulated breast cancer invasion and metastasis is co-dependent upon macrophage infiltration and CXCR4 signalling. Agents targeting CSF1 and its receptor are in clinical trials (Hamilton and Achuthan, 2013). However such strategies affecting all macrophage subtypes deprive the tumour of their favourable phagocytic and antigen presentation functions that would stimulate a tumour-targeted immune response.

Further genomics, transcriptomics and proteomics studies could herald the development of therapeutic strategies that could re-educate TAMs to a tumour-targeting phenotype that prolongs patient survival (Wynn et al., 2013). For example, murine models of melanoma and neuroblastoma treated with an established regime of immunotherapy and chemotherapy that controlled tumour growth, gave promising indications of the re-polarisation of infiltrating TAMs to a more classical phenotype (Buhtoiarov et al., 2011).

1.2.3.3. Macrophages in ovarian cancer

Overall an infiltrate of macrophages in the ovarian cancer microenvironment correlates with a poor patient outcome (Kryczek et al., 2007; Vaughan et al., 2011)(Table 1-2). This is also true of BRCA mutation positive ovarian cancers (Mhawech-Fauceglia et al., 2013). The release of pro-inflammatory cytokines by ovarian cancer cells induced the differentiation of M1 macrophages into the tumour associated M2 phenotype in *in vitro* co-culture assays (Hagemann et al., 2006). The co-cultured ovarian cancer cells also showed an increase in their ability to invade. This was dependent on MMP activity and TNF-α induced activation of the transcription factor NF-κB and the MAP kinase pathway through JNK (Jun N-terminal kinase) (Hagemann et al., 2005). The role of macrophages in an *in vivo* model of ovarian cancer also further validated their ability to promote ovarian cancer invasion and metastasis (Robinson-Smith et al., 2007).

IKKβ (IκB kinase β) is the activator of NF-κB, and targeting this in bone marrow derived macrophages or TAMs derived from ID8 tumour bearing mice reduced tumour cell invasion in *in vitro* co-culture assays (Hagemann et al., 2008). The co-cultured ID8 tumour cells showed increased caspase 3/7 activation and consequent increased apoptosis, mediated by macrophage tumoricidal activity. The IKKβ targeted macrophages reduced tumour burden in mice following adoptive transfer of the cells. Both *in vitro* and *in vivo* the macrophages showed reduced expression of IL-10, TNF-α and arginase 1, with associated increases in IL-12, nitric oxide (NO) and NO synthase 2. This work suggested that inactivation of IKKβ in macrophages within the ovarian cancer microenvironment could ‘re-educate’ the tumour-promoting inflammatory cells to switch their activities to those that are tumoricidal. This was linked to MyD88 (myeloid differentiation primary response gene) and IL-1 receptor signalling, and IL-12 mediated recruitment of natural killer (NK) cells to the microenvironment.

A recent report describes how chemoresistance induced IL-6 signalling in ovarian cancer cell lines can promote the differentiation of monocytes to the M2 tumour-associated polarised macrophage *in vitro* (Dijkgraaf et al., 2013). This is suggestive of a link between macrophages in the ovarian cancer microenvironment and the development of resistance to therapies. Targeting the polarisation mechanisms of the macrophages such as IKKβ activation may therefore increase sensitivity of tumours to current chemotherapy treatments and reduce resistance.

The concept of further intermediate macrophage phenotypes is supported in a recent study of TAMs isolated from the ascites of thirty HGSC patients (Reinartz et al., 2013). These TAMs expressed the 'M2' cell surface marker CD163. This correlated with a reduced relapse free survival, and increased levels of both the pro-inflammatory cytokine IL-6 and the anti-inflammatory cytokine IL-10 in the ascitic fluids. In addition the gene expression profile of the CD163 positive TAMs carried no relationship to the "Beyer Signature" which has previously been used to distinguish 'M1 and M2" macrophage phenotypes (Beyer et al., 2012). This work highlights a void in our understanding for the true transcriptional and molecular profile of ovarian cancer associated macrophages.

1.2.3.4. Macrophage and adipocyte interactions

More specific to the metastatic microenvironment of ovarian cancer is the abundance of adipocytes in the omentum. In a gene expression array of adipose tissues, in control and obese mice, 30% of the genes that correlated with an increased body mass were those associated with macrophages (Weisberg et al., 2003). The recruitment of macrophages to adipose tissues was confirmed in histopathology sections, including that of the mesentery. This recruitment initiated a positive feedback loop leading to an increase in adipose tissue mass and therefore further

macrophage recruitment (Sun et al., 2011). Adipose tissue macrophages isolated from obese mice expressed higher levels of the pro-inflammatory cytokines TNF-α and IL-6, whereas from the control mice, the macrophages expressed increased anti-inflammatory IL-10 (Lumeng et al., 2007). These studies suggested that there is interplay between adipocytes and macrophages that regulates adipocyte function and macrophage polarisation. Tumour cell and adipocyte interactions have already been reported in ovarian cancer metastasis (Nieman et al., 2011). They may be potential targets for future therapeutic intervention.

1.3. Cytokines and chemokines in cancer

For almost 25 years cancers have been described as “wounds that do not heal” (Dvorak, 1986). During wound healing and pathogen stimulation, chemokines and cytokines released by the resident fibroblasts and damaged epithelial cells recruit inflammatory cells (Dranoff, 2004; Mantovani et al., 2008). Inflammatory cells release proteases and reactive oxygen species for anti-bacterial defence mechanisms (Schafer and Werner, 2008). Inflammatory cytokine and chemokine-mediated processes in their chronic form are mirrored in the development and progression of cancer. In the majority of solid tumours, associated chronic inflammation reduces the efficacy of chemotherapy (Grivennikov et al., 2010).

The long-term usage of non-steroidal anti-inflammatory drugs reduces the risk of developing some cancers. For instance the daily use of aspirin minimised the risk of developing estrogen receptor (ER)-positive breast cancer (Gierach et al., 2008). Large-scale clinical trials where patients were treated with aspirin daily for 5 years or longer reduced the incidence (Rothwell et al., 2011) and the development of distant metastases (Rothwell et al., 2012) for many solid cancers. Death by colorectal cancers in particular was reduced by 30-40% (Rothwell, 2013).

1.3.1. Inflammatory cytokines

Acute inflammation is a rapid response to pathogen stimulation. The work of the New York surgeon William Coley in the 19th century gave the first indication that microbial preparations and an induction of an acute inflammatory response can be used to treat cancer (Balkwill, 2009). The treatment of bladder cancer with Bacillus Calmette-Guerin (BCG); a vaccine for tuberculosis, is based on these ideas (Grivennikov et al., 2010).

Chronic inflammation is also known to promote malignant transformation and metastasis (Balkwill and Mantovani, 2001). Many types of cancer are initiated by bacterial or viral infections that also induce long and sustained chronic inflammation. *Helicobacter Pylori* infections are involved in the development of gastric cancer, and the Hepatitis B virus (HBV) causes liver cancers (Cavallo et al., 2011). Vaccinations against the Human Papilloma Virus (HPV) are now routinely administered for the prevention of cervical cancer (Mesher et al., 2013).

Many oncogenic mutations are also drivers of inflammatory signalling pathways. RET (rearranged during transfection) activation in thyroid carcinomas induced the expression of the pro-inflammatory cytokine IL-1β and the angiogenesis inducing cytokine IL-8 (Grivennikov et al., 2010; Mantovani et al., 2008). Similarly Myc expression induced under the insulin promoter in β-islet cells in a pancreatic cancer mouse model increased angiogenesis via IL-1β (Shchors et al., 2006). When supernatant from explanted islet cells were cultured with human umbilical vein endothelial cells (HUVECs), there was an increase in endothelial cell proliferation and tubule formation. This was accompanied by the release of VEGF-A that was redistributed in the tumours upon Myc activation. IL-1β was immediately up regulated in response to Myc activation and the release of ECM sequestered VEGF-A and endothelial cell proliferation was significantly reduced when mice were treated with IL-1β neutralising antibodies. In addition Ras activation in human ovarian surface epithelial cells induced transformation and tumour growth in animal models that was coupled with an increase in cytokine production, including IL-1β, IL-6 and IL-8 (Liu et al., 2004). Furthermore tumour growth in xenograft models with induced Ras activation in cervical and lung cancer cells was reduced by approximately 60% when treated with IL-8 neutralising antibodies (Sparmann and Bar-Sagi, 2004). This was accompanied by a decrease

in endothelial cell recruitment, vascularisation and infiltration of macrophages and granulocytes.

The malignant epithelial cells in tumours as well as the stromal cells produce cytokines and chemokines (Balkwill, 2002). Perturbed expression of these inflammatory mediators blocks the progression of cancer in experimental models. The deletion of the cytokine TNF-α or its receptor in mice prevented the development of DMBA (7, 12-dimethylbenzanthracene) initiated skin carcinogenesis (Moore et al., 1999). NF-κB regulates the transcription of inflammatory cytokines. The deletion of its activator IKKβ and inhibition of the NF-κB pathway in the epithelial cells of a colitis induced colon cancer model reduced the risk of tumour development (Greten et al., 2004). Targeting the same pathway in the myeloid subpopulation of leukocytes in this model also significantly reduced tumour growth. The importance of TNF-α and the downstream signalling pathways in cancer associated inflammation has lead to several phase I and II clinical trials with single agent antagonists and antibodies targeting TNF-α (Balkwill, 2009).

1.3.1.1. The TNF network

Kulbe et al (Kulbe et al., 2005) correlated high CXCR4 expressing ovarian cancer cell lines with the expression of TNF-α. TNF-α stimulated CXCR4 and CXCL12 expression in the malignant cells, which then fed back into an autocrine signalling loop.

Malignant cell driven inflammatory cytokine networks maintain a tumour-promoting microenvironment through both autocrine and paracrine signalling. The TNF network in ovarian cancer cells involves the autocrine-stimulated expression of other inflammatory cytokines and chemokines including IL-6 and the angiogenesis-inducing VEGF (Kulbe et al., 2007). This TNF network was described following gene set enrichment analyses of gene expression microarray data from the AOCS

(Kulbe et al., 2012). This and supporting immunohistochemistry on a tissue microarray (TMA) of 53 HGSC patients showed significant associations between the expression of TNF-α, IL-6 and CXCL12. Stable knock down of CXCR4 in the IGROV1 ovarian cancer cells reduced the secretion of these inflammatory cytokines and increased survival in a xenograft *in vivo* model. Targeting TNF-α with the antibody Infliximab produced the same results *in vitro* and *in vivo*. Supporting this further, treating the same xenograft model with the IL-6 targeted antibody Siltuximab inhibited IL-6 signalling and reduced tumour burden (Coward et al., 2011). This antibody in a Phase II clinical trial of eighteen ovarian cancer patients also reduced plasma levels of VEGF and CXCL12, whilst inducing disease stabilisation for seven patients and generating a partial response for one patient.

Interestingly in all three cases, inhibition of the TNF network reduced the vasculature area and the macrophage infiltrate *in vivo* (Coward et al., 2011; Kulbe et al., 2012). Comparing biopsies of the AOCS data set displaying high expression levels of the TNF network with those displaying low expression levels identified an enrichment in cell adhesion, cell cycle, NOTCH signalling, angiogenesis and immune cell signatures (Kulbe et al., 2012). Analysis of 21 human ovarian cancer biopsies derived from the AOCS revealed an increased CD68 positive macrophage population in the stromal areas of biopsies associated with high expression of the TNF network. VEGF itself increases the expression of CXCR4 in vascular endothelial cells and therefore CXCL12 may support VEGF-induced angiogenesis in ovarian cancers. CXCL12 alone increases angiogenesis *in vivo*, but only at concentrations that are much higher than what would naturally be seen in a tumour microenvironment (Kryczek et al., 2005).

1.3.2. Chemokines and receptors

Inflammatory chemokines promote immune cell recruitment, activation and differentiation. Constitutively expressed homeostatic chemokines regulate and maintain the levels of inflammatory responses (Kucia et al., 2004; Moser and Loetscher, 2001). In wound repair the signalling pathways that chemokines activate support the proliferation and survival of resident cells.

The nomenclature for chemokines is derived from the location of conserved cysteine residues in their molecular structure. Chemokines induce their downstream effects by binding to G-protein coupled chemokine receptors on the cell surface. The numbers given to chemokine receptors denote the chronological order that they were discovered (Raz and Mahabaleshwar, 2009). Chemokine receptors have seven transmembrane domains, and chemokines will often bind to numerous chemokine receptors and vice versa. There are approximately 50 different chemokines and 20 different receptors in humans offering to the complexity of their pathological roles (Kucia et al., 2004).

Deregulated expression of chemokines can lead to the development of various inflammatory diseases and can also initiate and promote tumour development in over-reactive tissue (Kulbe et al., 2004; Schafer and Werner, 2008). The chemokines within the tumour microenvironment influences the described immune infiltrate (Coussens and Werb, 2002; Fridman et al., 2012). Chemokine receptors on the surface of malignant cells, allows them to utilise the downstream proliferative and cell survival signalling pathways. Exploitation of chemokine: receptor signalling allows CXCR4-expressing malignant cells to metastasise to CXCL12-expressing sites (Muller et al., 2001).

One of the aims of this thesis was to study chemokine signalling in ovarian cancer metastasis to the omentum. CXCR4 is the major chemokine receptor expressed on malignant epithelial cells in ovarian

cancer biopsies (Scotton et al., 2001). Therefore the literature review here focuses on the role of CXCR4 and its ligand CXCL12 in the ovarian cancer microenvironment.

1.3.3. CXCR4 and CXCL12 signalling in the tumour microenvironment

In the last twenty years research has significantly advanced around the biology of the chemokine receptor CXCR4. This is since the discovery of its role as an entry co-receptor with CCR5 for Human Immunodeficiency Virus (HIV) into CD4 positive T lymphocytes and macrophages (Feng et al., 1996). Epithelial and stromal cells, including leukocytes, secrete its ligand CXCL12. Under normal conditions, the generated concentration gradient regulates the homing of CXCR4-expressing leukocytes and haematopoietic progenitor cells to sites of inflammation (Aiuti et al., 1997; Tchernychev et al., 2010), and controls cell migration in embryogenesis (Doitsidou et al., 2002; Raz and Mahabaleshwar, 2009). It has later been elucidated as a key player in angiogenesis, tumour development and metastasis (Murdoch, 2000). Hypoxic conditions up regulate the expression of CXCL12 within the core of a tumour and its receptor CXCR4 on infiltrating immune cells, endothelial cells and metastasising malignant cells (Schioppa et al., 2003). It is potentially an attractive therapeutic target for cancer treatment as its sole ligand CXCL12 interacts only with CXCR4 (Balkwill, 2004). Following its discovered involvement in HIV infection, there was a boom in production of receptor targeted molecular inhibitors and antibodies, that have since been readily available for experimentation in cancer models and clinical trials (Domanska et al., 2013).

CXCR4 is expressed by a number of different malignant cells, for example in haematopoietic, glioma, colorectal, prostate, renal (Burger and Kipps, 2006), lung and breast cancers, and generally not expressed by their normal counterparts. Integrin-mediated cell adhesion is

increased by CXCR4 signalling. It has been suggested that CXCR4 induced integrin signalling may confer the development of resistance to chemotherapeutic agents in lung cancers (Hartmann et al., 2005).

1.3.3.1. CXCR4 expression in the early transformation events of ovarian cancer

Immortalised ovarian surface epithelial cells that spontaneously transformed when grown in soft agar acquired TP53 mutations typical of those seen in HGSC, and also genomic amplification of the CXCR4 receptor (Archibald et al., 2012). The transformed cells demonstrated increased CXCR4 dependent growth and migration, and showed epigenetic silencing of the chemokine receptor's ligand CXCL12. This work suggests that increased CXCR4 expression on ovarian surface epithelial cells may be important in the early stages of their transformation to a malignant phenotype. Their silencing of CXCL12 expression may sensitise their evasion potential from the ovarian epithelium into the chemokine rich peritoneal fluids. Given the recent advances in our understanding of the origins of HGSC, it would be interesting to investigate the amplification of CXCR4 in the early transformation events of the surface epithelial cells of the fimbria (section 1.1.1.1).

1.3.3.2. CXCR4 expression in ovarian cancer cell lines

Supporting this work, Son and colleagues recently studied a panel of ovarian cancer cell lines covering wild type, null and mutant TP53 statuses. Cell lines with low level expression or mutated TP53 showed increased mRNA (messenger ribonucleic acid) expression of CXCR4 and pro-inflammatory cytokines including TNF-α (Son et al., 2012). Either restoring TP53 status in the null or mutant cell lines, or stabilisation of the protein with Nutlin-3 in the low expressors, reduced NF-κB promoter activity and expression of the pro-inflammatory

cytokines. This together with the work of Archibald and colleagues (Archibald et al., 2012) suggests that the TP53 mutations typical of HGSC may drive cancer-associated inflammation.

The ovarian cancer cell lines IGROV1 and CAOV-3 migrated towards a CXCL12 chemokine gradient (Scotton et al., 2001). Activation of the receptor sent signals through the MAP kinase and PI3 kinase pathways, promoting cell adhesion, survival, proliferation and invasion, (Kulbe et al., 2005; Kulbe et al., 2007; Scotton et al., 2002), which were inhibited by the CXCR4 antagonist AMD3100 (Scotton et al., 2002).

1.3.3.3. CXCR4 expression in ovarian cancer metastasis and its clinical significance

When the SKOV3 ovarian cancer cells were transfected with CXCR4, they showed increased metastasis to the peritoneum in *in vivo* models compared to controls (Balkwill, 2004). In a xenograft *in vivo* model of HGSC, short hairpin RNA (shRNA) interference of the receptor reduced tumour burden and delayed the angiogenic switch. However it did not alter tumour cell attachment to the bowel mesentery (Leinster et al., 2012). The nature of ovarian cancer metastasis may exclude the processes of intra- and extravasation, unlike other cancers such as breast cancer (Muller et al., 2001). This might therefore suggest that CXCR4 expression does not play such a pivotal role in targeting ovarian cancer cells to the peritoneum per se, but becomes of greater importance for the development of metastases once *in situ*. This is perhaps supported by a recent report that investigated copy number variations in matched ovarian primary tumours and peritoneal metastases of nine patients (Malek et al., 2011). Gene set enrichment analysis highlighted a role for the JAK/STAT and cytokine signalling pathways when comparing the two groups. For example many CC cytokines and their receptors were deleted in the primary tumours, but expressed in the metastases. Conversely, many CXC chemokines,

including CXCL12 were amplified in the primary tumour but not in the metastases. These data were validated with that of the TCGA (Cancer Genome Atlas Research, 2011) and this highlighted the concerning issue that the majority of chemotherapy targets are amplified in the primary tumours but not in the metastases. Given that the major clinical problem of ovarian cancer is the spread to the peritoneum, it is important to identify druggable targets amplified in the metastases.

Both paracrine and autocrine signalling are responsible for the downstream effects of CXCL12. CXCL12 is largely sourced from the surrounding stroma but is, in fact, also produced by the malignant cells (Kajiyama et al., 2008b; Kulbe et al., 2007). Immunohistochemical analysis of ovarian cancer biopsies showed CXCL12 expression in the malignant cells and a weak expression in the surrounding stromal fibroblasts (Scotton et al., 2002). In a more recent study, 20% of a cohort of 289 ovarian cancer biopsies expressed CXCL12 in the cytoplasm of the tumour cells (Popple et al., 2012). 69% of the biopsies were serous carcinomas. Increased levels of CXCL12 in this cohort correlated with a poor overall patient survival, and patient biopsies negative for CXCL12 benefited a 51-month survival advantage.

1.3.3.4. Inhibition of CXCR4 signalling

AMD3100 is a small molecular inhibitor of CXCR4 and was identified as a useful agent for HIV-1 entry blockade (Donzella et al., 1998). It is also used to mobilise hematopoietic progenitor cells for transplants (Liles et al., 2003). As a potential cancer treatment, AMD3100 has been predominantly assessed for its efficacy in acute promyelocytic leukemia. It was shown to sensitise these malignant cells to chemotherapeutic agents through mobilising them away from the protective microenvironment of the bone marrow and into the peripheral blood stream (Nervi et al., 2009). In solid cancers not only has the inhibitor been shown to minimise invasion and tumour burden (Domanska et al.,

2013), it has also been utilised as an imaging tool. Coupled with the radioactive Copper-64, it offered its potential for visualising solid tumours expressing CXCR4 in positron emission tomography (PET) scans (Jacobson et al., 2009). In December 2008, the Food and Drug Administration (FDA) agency approved the use of the inhibitor for medical purposes (Pusic and DiPersio, 2010). In a recent publication Salomonnson and colleagues showed that in a combination therapy with cisplatin, AMD3100 decreased tumour burden in an *in vivo* model of ovarian cancer greater than either treatment alone (Salomonnson et al., 2013).

Infiltration of immune cells and the expression of inflammatory mediators within the microenvironment promote tumour growth and metastasis. Evidence suggests that intervention of the molecular pathways that regulate tumour-associated inflammation can increase patient survival and improve their response to chemotherapy. The aims of this thesis were to study these processes in HGSC. The following sections of this review discuss available experimental models of HGSC with a particular focus on 3-dimensional (3D) cell culture assays.

1.4. Models of HGSC

1.4.1. *In vitro* models of human HGSC ovarian cancer

1.4.1.1. Cell line models of HGSC ovarian cancer

The subtype of ovarian cancer under question (section 1.1) must be reflected in the models we use to study the disease. Experiments on cell lines often formulate baseline ideas and hypotheses that are later tested in animal models and clinical trials. In recent years there has been huge emphasis on short tandem repeat (STR) profiling of cell lines due to identified discrepancies within and between laboratory cell line banks. Therefore researchers need to employ extra caution when working with these models. Also commonly used cell lines were established and characterised before the detailed study of cancer genomes revealed specific genetic types and subtypes.

In respect of this Domcke and colleagues recently evaluated the genomic profiles of 47 ovarian cancer cell lines from the Broad-Novartis Cell Line Encyclopedia with those of approximately 500 HGSC ovarian cancer biopsies studied in the TCGA (Domcke et al., 2013). The cell lines were ranked by their resemblance to the HGSC ovarian cancer biopsies, notably revealing that the SKOV3, A2780 and IGROV1 ovarian cancer cells that were originally thought to be HGSC cell lines, are not representative of HGSC tumours at all. The strength of the resemblance was based upon the presence of a TP53 mutation, the absence of other subtype related mutations, a low frequency of non-synonymous mutations and a correlation between chromosomal copy numbers. It is concerning that these cell lines in particular are amongst those that have been most frequently cited in publications.

Later work by Anglesio and colleagues (Anglesio et al., 2013) reported the use of an established calculator of subtype prediction (COSP) algorithm (Kalloger et al., 2011) to create a reliable panel of CCC cell lines from 32 tested lines. The group assessed the expression of nine markers by immunohistochemistry, the presence of common mutations, the chromosomal copy number variations and the transcriptomic profiles of the 32 cell lines. *ARID1A* mutations typical of CCC produce a truncated protein, which cannot be detected by immunohistochemistry. Most of the cell lines previously annotated as CCC were negative for this marker by immunohistochemistry and closely resembled primary tumours of CCC. For the interests of this thesis the TOV21G cells were representative of CCC, but the RMG1 cells line were unclassified by this group's methods. Many cell lines with *TP53* mutations previously used to model HGSC also had *ARID1A* mutations, with an immunohistochemistry profile of endometrioid carcinomas. This was true for the IGROV1 cell line. Consistent with the work of Domcke et al (Domcke et al., 2013), Anglesio and colleagues also classified the SKOV3 cells as non-HGSC, owing to their mutations in *ARID1A* and *PIK3CA*, despite their positive expression for HGSC related immunohistochemistry markers (Anglesio et al., 2013). The message of this work is that the subtype of ovarian cancer that cell lines represent must be clearly defined at the onset of any experiments. Without this inaccurate conclusions regarding targeted therapy efficacies will be relayed through translational studies and clinical trials. What is also important to consider is that cell lines cultured particularly in 2D (2-dimensional) are subject to adverse changes through a lack of normal cell-cell and cell-matrix interactions.

Recently optimised methods were established to isolate and culture epithelial ovarian cancer cells from the ascites and solid tumours with a 91% success rate (O Donnell et al., 2014). These primary cultures were positive for ovarian cancer cell markers such as pan-cytokeratin, EpCam, CA-125 and vimentin. Using primary cell cultures such as this will better represent the heterogenecity of ovarian cancer and also

allows the performance of experimental assays that could not otherwise be reproduced on paraffin or frozen tissue sections.

1.4.1.2. Ovarian cancer cell spheroid formation *in vitro*

One frequently used *in vitro* 3D model for ovarian cancer is spheroid formation (Lengyel et al., 2013). The drop assay allows gravity to bring ovarian cancer cells together for adhesion and compaction into spheroid aggregates (Kelm et al., 2003). This is appropriate for modelling the aggregates that are free-floating in the peritoneal cavity of HGSC patients. However it is unknown whether these have detached from the primary tumour as multicellular aggregates or whether they have formed from single cells in the peritoneal fluids (Lengyel, 2010; Pease et al., 2012). A clustering antibody for αVβ1 integrin and its ligand fibronectin encouraged spheroid development. (Casey et al., 2001). Some cell lines are unable to form spheroids, and this is due to defects in actinomysin contractility. Cell lines that do grow into spheroids have myofibroblast characteristics with increased expression of TGFβ1 regulated genes (Sodek et al., 2009). Cell lines that form more compact spheroids also have a greater ability to invade collagen matrices. Recently fluidic forces that would naturally be experienced by metastasising ovarian cancer aggregates increased expression of EGF and drove an epithelial–mesenchymal transition (EMT) (Rizvi et al., 2013), perhaps making the cells more viable for survival in spheroid formation. EMT is a process that normally occurs during embryonic development, where a loss of epithelial intercellular adhesion and polarisation transitions the cell to a migratory mesenchymal state (Wan et al., 2013). Cancer cells utilise this transition for invasion and metastasis, supporting the development of chemoresistance. Regulated by the transcription factors Slug, Snail and Twist, EMT was also driven in a pancreatic cancer mouse model by inflammation (Rhim et al., 2012). Dexamethasone treatment reduced EMT and dissemination of the tumour. However EMT is a phenomenon under huge debate, since it is especially difficult to capture cells in transit

particularly in clinical samples. Rizvi and colleagues observed a reduction in E-Cadherin expression in ovarian cancer spheroids, which is characteristic of EMT (Rizvi et al., 2013), but not so typical in the development of chemoresistance in the aggregates (Green et al., 2004).

Multicellular aggregates of ovarian cancer express matrix interacting receptors that prepare them for metastasis to the peritoneum and omentum. For example, they express α_2, α_5 and $\alpha_6\beta_1$ integrins (Figure 1-2) that bind to collagen type IV, fibronectin and laminin respectively (Lengyel, 2010). These are the most abundant matrix proteins of the sub-mesothelial layer (Witz et al., 2001). Before interacting with these underlying matrix proteins, the ovarian cancer cells must negotiate the protective mesothelial cell layer. MMP2 expression in the malignant cells potentiates adhesion to the mesothelial layer through proteolysis of the ECM proteins fibronectin and vitronectin. These cleavage reactions expose the binding sites for $\alpha V\beta 1$ and $\alpha V\beta 3$ integrins on the surface of the malignant cells (Kenny et al., 2008).

1.4.2. Multicellular culture models of HGSC ovarian cancer

1.4.2.1. 2D multicellular culture models

Early *in vitro* models incorporating cell-cell interactions involved culturing ovarian cancer cells on 2D mesothelial cell monolayers (Lengyel et al., 2013) (Figure 1-3a). For example such a model was used to describe the contractile nature of mesothelial cells to give clearance of the sub-mesothelial matrix to invading ovarian cancer spheroids (Figure 1-2) (Iwanicki et al., 2011). Iwanicki and colleagues used time-lapse video microscopy of fluorescently labelled ovarian cancer spheroids and immortalised mesothelial cells from the lung mesothelium to demonstrate that the ovarian cancer cells spread on the surface of the mesothelial cells before penetrating beneath them. This observed

localised de-adhesion of the mesothelial cells occurred when they were cultured on glass or fibronectin-coated polyacrylamide gels. Short-interfering RNAs targeting myosin II expression in the ovarian cancer cells reduced mesothelial cell clearance. Talin I dependent interactions connected the myosin network to the fibronectin receptor αVβ1 integrin. Antibodies blocking the function of this receptor also reduced mesothelial cell clearance. Fluorescently labelled fibronectin fibrils on the surface of the mesothelial layer revealed the detachment and reorganisation of these fibrils around invading spheroids. Interactions between the myosin network, talin I and αVβ1 integrin were all required to exert the maximal strain energy on the extracellular matrix as determined by displacement of fluorescent beads within the matrix. Collectively this work identified molecular mechanisms relevant to ovarian cancer metastasis to the peritoneum. However further work is required to investigate the cues that drive migration of the mesothelial cells away from the invading ovarian cancer cells.

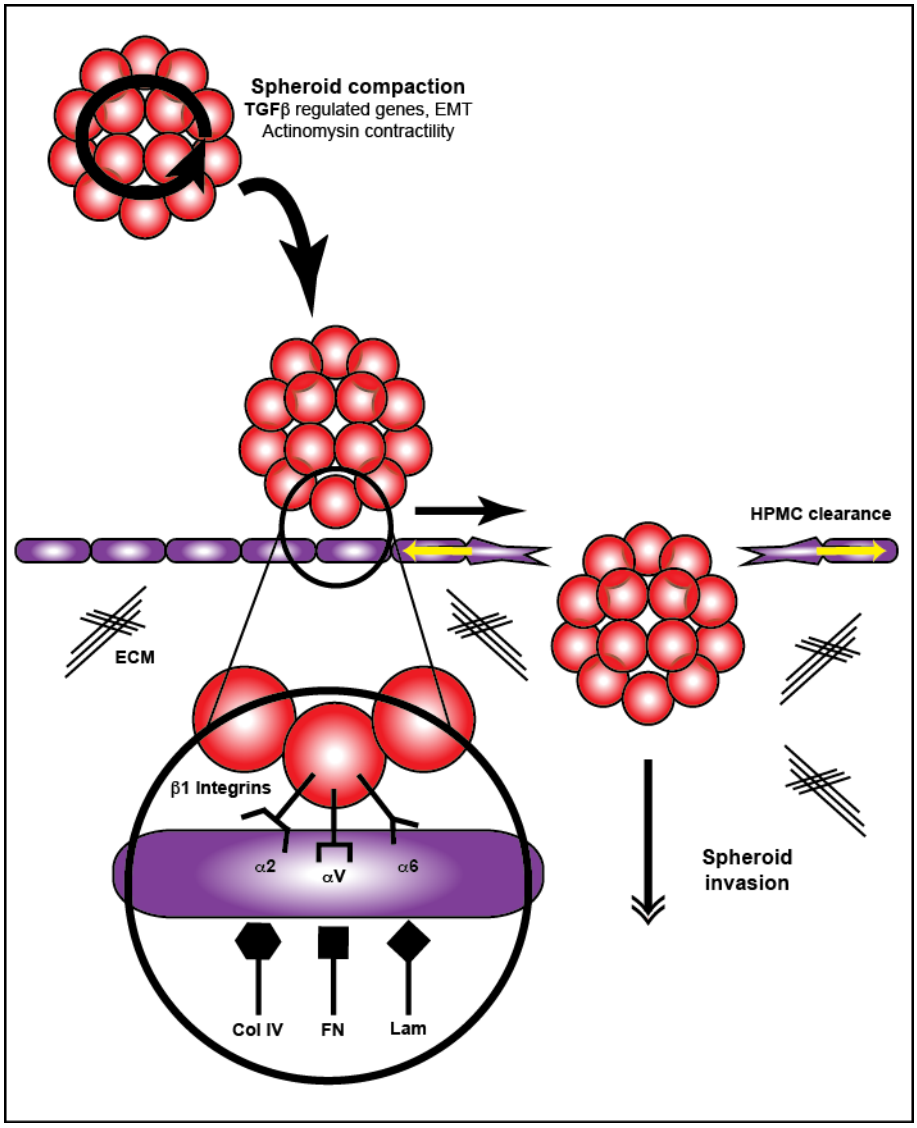

Figure 1-2 Ovarian cancer cell aggregate development and interactions with HPMC layers.

Spheroid development and compaction is promoted by TGFβ stimulated epithelial-mesenchymal transition (EMT) and actinomysin contractility (Sodek et al., 2009). Ovarian cancer cell aggregates express the β1 integrin receptors (α2, αV and α6) for interactions with the extracellular matrix (ECM) proteins collagen (Col) IV, fibronectin (FN) and laminin (Lam) in the sub-HPMC (human primary mesothelial cell) compartment (Lengyel, 2010). Spheroids induce localised clearance (yellow arrows) of the HPMCs for invasion into the ECM (Iwanicki et al., 2011).

1.4.2.2. 3D multicellular culture models

Despite our increasing awareness of the impact of a 3D matrix microenvironment on tumour cell survival and differentiation (Levental et al., 2009), the repertoire of 3D organotypic models that have been utilised for studies into ovarian cancer tumourigenesis has been rather limited. Some earlier 3D organotypic models have co-cultured murine embryonic fibroblasts with human ovarian cancer cells in a collagen matrix (Guruswamy et al., 2001). These models have often been raised on a metal mesh platform within a culture dish or well to generate an air-medium interface (Gregoire et al., 1998) (Figure 1-3b). This not only mixed cells of different species origin, but also more closely resembled a skin carcinogenesis model with an air-medium interface than an ovarian cancer model that should have exposure to medium recapitulating the peritoneal fluids.

More recently the work of Kenny and colleagues (Kenny et al., 2007) advanced the complexity of 3D *in vitro* models available for research into ovarian cancer metastasis. Human primary fibroblasts (HPFs) and mesothelial cells (HPMCs) isolated from human omentum removed at surgery, were co-cultured in and on the surface of a collagen I matrix respectively (Figure 1-3c). This omentum-mimicking microenvironment formed the substrate on which to culture ovarian cancer cells to monitor their stromal interactions.

Cai et al (Cai et al., 2012) used the 3D omental model established by Kenny and colleagues to show the importance of cell-cell interactions in the stimulation of MMP2 expression in the omental fibroblasts. They illustrated the role of TGFβ1 signalling in omental fibroblast activation and measured the invasion of HGSC cells through the ECM.

Subsequent to its establishment, the Kenny et al 3D omental model has further offered insights into the role of α_5 integrins (Kenny et al., 2008; Sawada et al., 2008) in the early adhesion events of ovarian cancer

metastasis. Undoubtedly there is a void in our understanding of these early events due to the absence of accurate genetic mouse models and the late stage presentation of patients in the clinic. However in none of the studies carried out thus far has anyone ventured to maintain these cultures for longer time periods than five days.

The Kenny et al 3D omental model also offered the opportunity to experiment with novel therapies. Zillhardt et al (Zillhardt et al., 2011) utilised the 3D omental model to test the effect of a clinically available oral multikinase inhibitor of c-Met and VEGFR2, which reduced the adhesion and invasion of the ovarian cancer cell line SKOV3ip1. However this work in particular highlighted one of the limitations of the model as it currently stands. VEGFR2 is a regulator of angiogenesis, the synthesis of new blood vessels. The study described by Zilhardt et al could not effectively test the inhibition of VEGFR2 in the 3D omental model, due to the absence of endothelial cells in the co-culture system. The potential to introduce further cell types to the model provides huge opportunity to develop its complexity and increase its likeness to the microenvironment of the human omentum as it is *in situ*.

1.4.3. Prospects for further developing 3D cell culture models of ovarian cancer

The tumour microenvironment of ovarian cancer includes many cell types including adipocytes (Nieman et al., 2011). The abundance of lipids serves as a fuel source for ovarian cancer cell proliferation and adipokines are direct drivers of cancer cell invasion. Recently a 3D cell culture model of breast cancer has been described incorporating adipose stem cells (ASCs) (Delort et al., 2013). Culturing the ASCs with fibroblasts for three weeks led to the development of an adipose substrate. Breast cancer cells were then cultured on the surface for a week before being raised to an air-medium interface for a further two weeks. In comparison with keratinocyte and non-malignant mammary

epithelial control cell lines, the breast cancer cells induced differentiation of the ASCs to adipocytes as measured by oil red staining. Following culture on the model, the surface epithelial cells were subjected to a thermolysin treatment to selectively remove them from the surface of the substrate. Quantitative reverse transcription polymerase chain reaction (qRT-PCR) analysis on the epithelial cells revealed a role for the adipose microenvironment in promoting cell cycle, anti-apoptotic, angiogenesis and cytokine signalling pathways (Delort et al., 2013). Despite the microenvironment having no significant effect on aromatase expression, it was postulated that the increase in inflammatory cytokines TNF-α and IL-6 may stimulate aromatase activity leading to promoted androgen conversion to estrogen. This was hypothesised because the basal breast cancer cell line MDA-MB-231 that is ER negative, was less responsive to the adipose microenvironment than the luminal ER positive cell line MCF7. The MCF7 cells demonstrated increased invasive capacity in the 3D model. Kenny and colleagues are currently working to introduce adipocytes to their previously established 3D omental model of ovarian cancer (Figure 1-3d) (communications with Prof Ernst Lengyel).

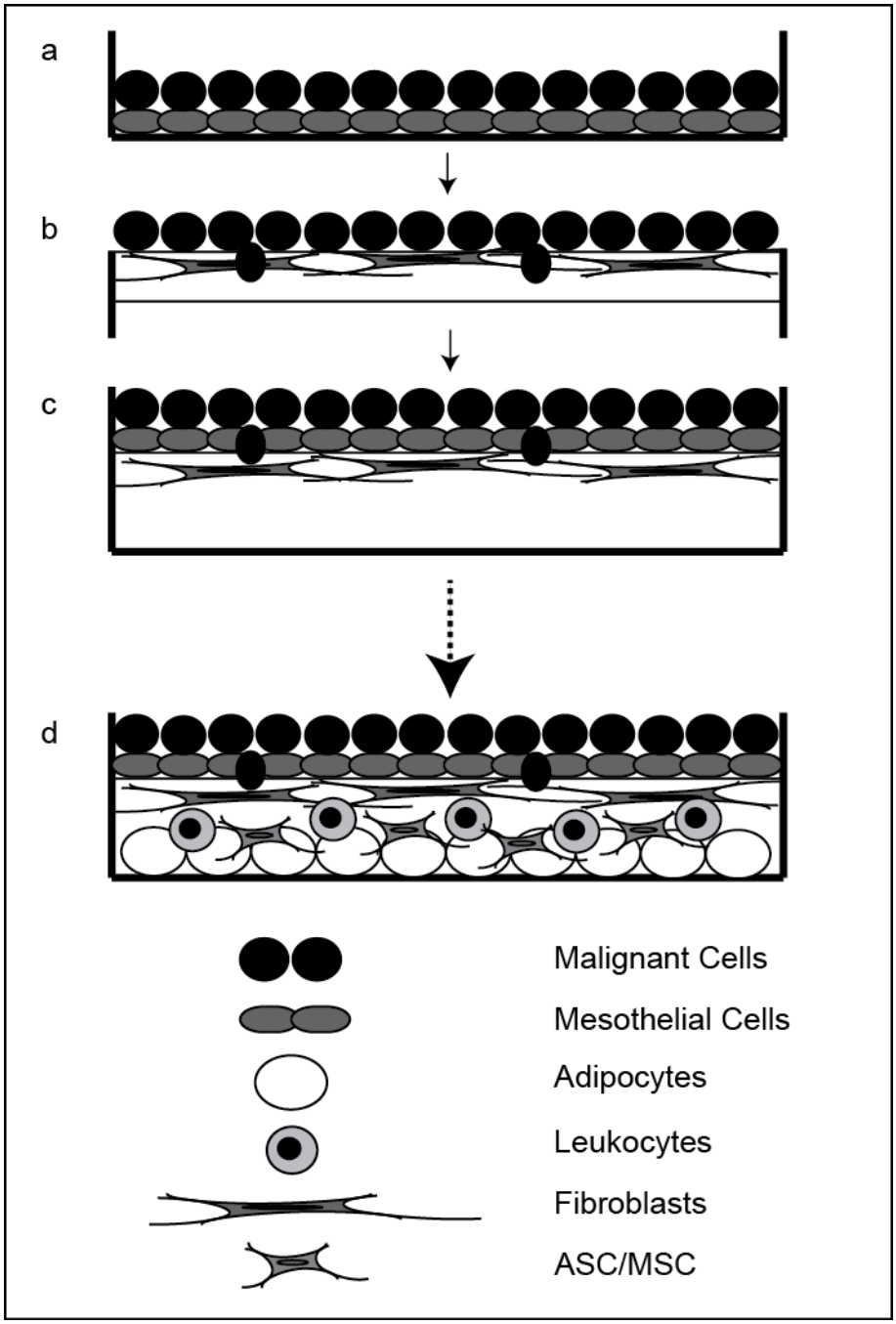

Figure 1-3 The development of 3D cell culture models of ovarian cancer.

a) Early 2D cell culture models involved culturing ovarian cancer cells on mesothelial cell layers (Lengyel et al., 2013). **b)** Early organotypic models cultured ovarian cancer cells on raised fibroblast embedded collagen gels (Gregoire et al., 1998). **c)** The most advanced current 3D cell culture model mimics ovarian cancer metastasis to the omentum and includes the growth of primary mesothelial cells and fibroblasts on the surface and within a collagen matrix respectively (Kenny et al., 2007). **d)** Developing 3D models of ovarian cancer will involve introducing further cell types normally present within the ovarian cancer microenvironment including adipocytes, leukocytes, adipocyte (ASC) and mesenchymal (MSC) stem cells (Lengyel et al., 2013; Nieman et al., 2011; Touboul et al., 2013).

Instead of reassembling an artificial tumour microenvironment methods have been employed involving *ex vivo* tissue explant cultures. Kahn and colleagues maintained murine *ex vivo* omentum cultures for ten days, and demonstrated the potential for human ovarian cancer cells to colonise areas of the tissue rich in inflammatory cells and proliferate (Khan et al., 2010b). More recently human ovarian cancer cell line spheroids adhered to and infiltrated a human amniotic membrane scaffold over a course of 72 hours (Touboul et al., 2013). This demonstrated enhanced interactions with mesenchymal stem cells, mediated by IL-6 signalling. The limitations of such *ex vivo* culture models do however lie in the duration that they can be maintained in the absence of a blood supply and the variability of microenvironmental elements between tissue explants (Lengyel et al., 2013).

The inflammatory infiltrate in ovarian cancer is yet to be modelled in a 3D cell culture system (Lengyel et al., 2013) (Figure 1-3d). A newly improvised breast cancer model co-cultured tumour spheroids of the MDA-MB-231 basal cell line with *in vitro* polarised peripheral blood derived monocytes (PBMCs). This work demonstrated that tumour cell conditioned medium educated the PBMCs to stimulate the invasive capacity of the breast cancer cell spheroids, but these PMBCs also retained the ability to respond to tumour antigen targeted phagocytosis cues (Grugan et al., 2012). Therefore the influx of infiltrating macrophages in the tumour microenvironment could potentially be monopolised for their maintained tumouricidal activity with tumour antigen targeted monoclonal antibody therapies. The impact of the immune cells on ovarian cancer progression is well documented (section 1.2), and a 3D cell culture model mimicking this could further delineate their multivariate interactions within the metastatic microenvironment. Ultimately the aim for the development of *in vitro* models of human ovarian cancer is to incorporate all components of the tumour microenvironment (Figure 1-3d), and this is the long-term endeavour of the newly established CANBUILD project team in the Balkwill laboratory of Barts Cancer Institute, London (YouTube video web reference).

1.4.4. Animal models of HGSC ovarian cancer

1.4.4.1. Xenograft models

Modelling metastasis for most tumour types necessitates tumour cell entry into a vascular or lymphatic system, and the development of metastases in distant organs. This can only be reproduced in animal models. The nature of ovarian cancer metastasis however removes the requirement to recreate tumour cell intra- and extravasation. Most ovarian cancer cells are thought to metastasise via the ascitic fluids to exposed surfaces of the peritoneal cavity, where they invade to the surrounding organs and eventually to the lymphatic vasculature. Therefore mouse models of late stage ovarian cancer can be created by intraperitoneal injection of malignant cells to generate xenografts. The first xenograft model was developed approximately thirty years ago with the drug resistant human ovarian cancer cell line NIH-OVCAR-3 (Hamilton et al., 1984). In more recent times patient-derived aggregates of fibroblasts, tumour and immune cells were engrafted in the ovary, omentum, pancreas and liver of intraperitoneal injected mice. These later developed ascites and corresponding increments in CA-125 levels both in the peritoneal fluids and serum (Bankert et al., 2011), however the patient-derived cells did not survive for long. Unfortunately, xenograft models require the use of mouse strains with an impaired adaptive immune system to prevent xenograft rejection. This limits investigating the role of immunity and other microenvironment interactions in tumour progression.

1.4.4.2. Syngeneic mouse models

Mouse ovarian surface epithelial cells (MOSECs) were isolated by gentle trypsinisation of the ovaries from five adult C57BL/6 mice (Roby et al., 2000). These isolated cells were transformed by more than twenty passages *in vitro* in the presence of EGF. The ID8 cells were one of ten

clones established from these MOSECs. Intraperitoneal injection of the ID8 cells in immunocompetent mice caused tumour growth throughout the peritoneal cavity including the omentum, and the production of ascites. However this syngeneic model of ovarian cancer was not representative of HGSC since the ID8 cells were wild type for TP53 (unpublished data).

1.4.4.3. Genetically engineered mouse models

At the beginning of the work for this thesis there was no genetically engineered mouse model available that displayed true HGSC characteristics, including high rates of TP53 mutations and genomic instability (Cancer Genome Atlas Research, 2011). The existence of such a model will greatly benefit research into the early development stages of HGSC ovarian cancer. Generating models has previously been problematic due to difficulties finding the precursor lesions of HGSC and a lack of tissue specific promoters.

The first transgenic mouse model of ovarian cancer was generated using expression of the viral SV40 Tag (Simian virus 40 T antigen) protein under the promoter region of the Müllerian inhibiting substance receptor (MISR) type II gene (Connolly et al., 2003). The *MISRII* gene is expressed and involved in the development of the female reproductive tract and is also expressed in ovarian cancer (Masiakos et al., 1999). The SV40 TAg protein transforms cells through perturbing the function of tumour-suppressors such as TP53 and Retinoblastoma (Rb) protein (DeCaprio et al., 1988; Garson et al., 2012; Hahn et al., 1999; Kierstead and Tevethia, 1993). The transgenic mice in this model developed ovarian epithelial tumours that gave rise to ascites and metastases in the peritoneum. However the mice developed tumours too quickly and did not survive long.

To remove the need for tissue specific promoters, cells can be genetically manipulated with viral vector transported Cre recombinase inserted transgenes (Wang et al., 1996). These can be injected directly into the tissue of preference. However different cell types can have variable infection efficiencies and the virus can stimulate an immune response (Garson et al., 2012). Recently transgenic mice expressing Cre recombinase under the MISRII promoter were crossed with transgenic mice bearing LoxP sites flanking the genes *Dicer* and *PTEN* (phosphatase and tensin homolog). The resultant mouse was a double knock–out for the miRNA synthesis gene and the negative regulator of PI3K gene respectively. All the mice developed tumours in the fallopian tube that closely resembled HGSC seen in patients (Kim et al., 2012). The tumours generated ascites, peritoneal metastases, and elevated levels of CA-125; currently the most reliable serum marker of HGSC (Bast, 2003). Deregulated PI3K pathway activation is frequent (45% of cases) in HGSC, however *PTEN* deletion is not so, occurring in 2% of cases (Cancer Genome Atlas Research, 2011). In addition, despite low expression levels of the TP53 protein, the tumour in this model did not have a TP53 mutation. Kim and colleagues argue that the role of TP53 mutations as drivers of HGSC tumourigenesis is unknown (Kim et al., 2012). Nevertheless we cannot deny the 96% frequency rate of these mutations in this disease (Cancer Genome Atlas Research, 2011), and therefore the current gap in the field for a more appropriate genetic mouse model of HGSC.

The TCGA provides publically available exomic sequencing data for more than 500 HGSC ovarian tumours (Cancer Genome Atlas Research, 2011). Interrogation of these data and an shRNA screen of 25 ovarian cancer cell lines identified *PAX8* (paired box gene 8) as an essential gene for cell survival (Cheung et al., 2011). Under normal circumstances PAX8 is a transcription factor involved in the organogenesis of the thyroid, kidney and müllerian system, whereby expression in the latter is specifically in the epithelial cells of the fimbria (Bowen et al., 2007). The Drapkin laboratory of the Harvard Cancer

Centre, United States (US) have recently developed a genetic mouse model of HGSC (Perets et al., 2013). The group first generated a model that used a reverse tetracycline-controlled transactivator under the promoter of *PAX8* to express Cre-recombinase. The expression of a LacZ transgene in this model confirmed specificity of the driver to the fallopian tube. This model was then crossed with models mutant for *BRCA2* and *TP53*, and negative for *PTEN*. Following induced expression with doxycycline, the resultant models developed STICs in the fallopian tubes that were characterised by increased secretory cell proliferation, loss of polarity and structural abnormalities. The developing tumours metastasised to the ovaries and the peritoneum and expressed markers typical of HGSC, such as PAX2 and WT-1 (Wilms tumour 1). The tumours were also positive for nuclear TP53. Omental metastases were not any more frequent than those in other areas of the peritoneum. Interestingly however, the performance of oophorectomies following the induction of tumour development reduced peritoneal metastases, suggesting that hormones secreted by the ovaries are important for metastasis. A comparative genomic hybridisation array confirmed that the tumours had high genomic copy number alterations that correlated with those seen in the human TCGA data set. Colleagues in the Balkwill laboratory have been endeavouring to produce the same genetic mouse model (unpublished data). This mouse model represents and mimics HGSC as seen in human patients with far greater accuracy than any other that is currently available, and will be an essential tool for research particularly benefiting earlier detection of the disease.

The value of mouse models here for research into HGSC cannot be negated, but like all models, they have their limitations. Despite the remarkable similarities between the mouse and human genome (Mural et al., 2002) there are unquestionably anatomical and biochemical differences between the two. The phenotype of murine models can be greatly affected by the method employed to generate the model, the productivity of potential heterozygotes, and the strain of the mouse used (Garson et al., 2012). Therefore this can affect the translation of animal

experiments to clinical trials. Results from mouse models ideally need to be complimented with human *in vitro* 3D model systems.

The Drapkin animal model of HGSC was published very recently (Perets et al., 2013). Prior to this there were no animal models available that accurately represented HGSC. Therefore for the work of this thesis, the 3D cell culture model mimicking HGSC metastasis to the omentum, established by Kenny and colleagues (Kenny et al., 2007) was constructed and developed. The model was used to investigate the role of the chemokine CXCL12 and macrophages in HGSC progression. Advancements to this model system will later support the drug discovery process for identifying novel therapies for HGSC treatment.

Thesis aims

I. Characterise the immune infiltrate of HGSC metastasis to the omentum.

II. Establish and optimise a 3D primary cell culture model mimicking ovarian cancer metastasis to the omentum.

III. Test the efficacy of a neutralising antibody targeting CXCL12 on the growth of ovarian cancer cell lines on the 3D omental model.

IV. Validate the association between CXCL12 and ECM gene expression in HGSC omental metastasis.

V. Investigate the effect of introducing an immune cell subtype to the pre-established 3D omental metastasis model.

Chapter 2

2. Materials and Methods

2.1. Cell culture

The SKOV3ip1-cGFP (green fluorescent protein) human ovarian cancer cell line (a kind donation from Prof Ernst Lengyel, The University of Chicago), the PA1 human cancer cell line, and the human breast carcinoma cell line MCF7 were cultured in DMEM, High Glucose (4.5g/L) with L-Glutamine, (PAA, E15-810), 10% Fetal Bovine Serum (FBS; PAA, A15-104) and 1X Penicillin/Streptomycin (PS; PAA, P11-010, 100X). The AOCS1 (a kind donation from Prof. David Bowtell, Peter MacCallum Cancer Centre, Australia), TOV21G-GFP (kindly donated by Dr Michael Salako) and RMG1 human ovarian cancer cell lines, the ICRF27 human embryo fibroblasts (HEFs), and all the primary cells isolated were cultured in RPMI-1640 with L-Glutamine, (PAA, E15-840), 10% FBS, and 1X PS.

The THP1 monocytic cell line were cultured in suspension in RPMI-1640 with L-Glutamine, 10% FBS, 1X PS and 0.05mM β–mercaptoethanol (Sigma, M-6250). The THP1 cells were differentiated in 5ng/mL phorbol 12-myristate 13-acetate (PMA) (Sigma, P-8139).

PBMC-derived macrophages were differentiated in RPMI 1640, Glutamax I (Invitrogen, 61870), 10% FBS (HI/GI) (SAFC Biosciences, 12006C), 1% PS (Invitrogen, 15140) and 100ng/mL macrophage colony-stimulating factor M-CSF (R&D Systems, 216-MC).

All cultures were kept under standard conditions at 37^{o}C and 5% CO_2. Adherent cells were passaged after washing in Dulbecco's phosphate

buffer solution (PBS) without Ca & Mg, (PAA, H15-002) and detachment with 0.1%/0.04% Trypsin-EDTA in PBS, (PAA, L11-003, 0.5%/0.2%).

2.2. Human omental metastasis sample processing

All human omentum samples were collected from surgery on ovarian cancer patients at St. Bartholomew's hospital. All samples were taken under the guidelines of the Human Tissue Authority Act 2004 and only from patients whom had given prior consent under the Research Ethical Committee Project reference 10/H0304/14. Samples were transported in sterile PBS back to the laboratory. On arrival this PBS was centrifuged at 1500rpm for five minutes, and the pelleted cells were re-suspended in full medium and plated in a T75 flask, (Corning, 430641). Photographs of the samples in a 150mm dish petri dish (Corning, 430599) were taken before they were processed. In an additional 20mL of PBS, the tissue was cut with a scalpel to give an approximately 20mm x 20mm piece to fix in Formal Saline Solution (equivalent to 4% formaldehyde; Adams Healthcare, 416479) and be embedded in paraffin. Four 10mm x 10mm sections were cut each to be embedded in O.C.T. Compound, (Tissue-Tek, 4583) and to prepare snap frozen samples. The tissue was stored in a bijoux and placed directly on to dry ice for snap freezing. OCT blocks and snap frozen samples were stored at -80^{o}C. All human omentum samples were stored under the Barts Gynae Tissue Bank. The 20mL PBS was centrifuged at 1500rpm for five minutes, and the pelleted cells were resuspended in full medium and plated in a T75 flask.

2.3. Human primary fibroblast and mesothelial cell isolation

The human omental tissue remaining from processing was cut into approximately 5mm x 5mm pieces and a maximum of 5mL volume of tissue was placed into a single 50mL centrifuge tube (Falcon, Becton

Dickinson). The number of centrifuge tubes required was dependent on the size of the tissue received. To each tube, 15mL of PBS was added to the tissue together with 15mL of 0.25%/0.1% Trypsin-EDTA. The tissue was then agitated at 200rpm at 37^{o}C for 15 minutes. The solution was passed through a cell strainer and centrifuged at 1500rpm for five minutes. The pelleted cells were re-suspended in full medium and plated in a T75 flask. Cells were cultured for approximately four days, when 10mL of fresh medium was added to each flask. After a total of one week in culture the entire medium was discarded and complete fresh medium was added to the cultures. The cells were further cultured until confluent. Note that on average I obtained primary tissue at a rate of approximately one every two weeks.

2.4. Peripheral blood monocytic cell (PBMC) preparation

PBMCs were prepared by density gradient centrifugation (Figure 2-1). Approximately 6-8mL of whole blood was diluted in PBS to a total volume of 25mL. The diluted blood was slowly layered on top of 15mL of Ficoll-Paque Plus (GE Healthcare, 17-1440-03) in a 50mL centrifuge tube (Falcon, Becton Dickinson). This was immediately centrifuged at 2600rpm, 18^{o}C for 20 minutes without braking. The supernatant was discarded to the level of 20mL in the centrifuge tube, and the ring of cells containing the PBMCs was gently aspirated and transferred to a new 50mL centrifuge tube. The total volume of PBMCs was made to 50mL with PBS and centrifuged at 1600rpm, 18^{o}C for ten minutes with maximal brake. The pelleted PBMCs were re-suspended in PBS and viable cells were counted with Trypan blue (Sigma, 93595) exclusion staining. The PBMCs were then seeded in 40mL of RPMI 1640 without supplements at a density of 2 x 10^{6} cells/mL in T175 flasks. The monocyte population within the preparation were allowed to adhere for one hour at 37°C, 5% CO_2 in a humidified incubator. The non-adherent cells were then removed and the monocytes were washed in RPMI 1640

before allowed to differentiate in complete medium supplemented with 100ng/mL M-CSF (R&D Systems, 216-MC) for one week.

PBMC-derived macrophages were dissociated from the flask before inclusion into the 3D omental model with accutase (PAA Laboratories, L11-007). The PBMC preparations were performed at MedImmune, Cambridge.

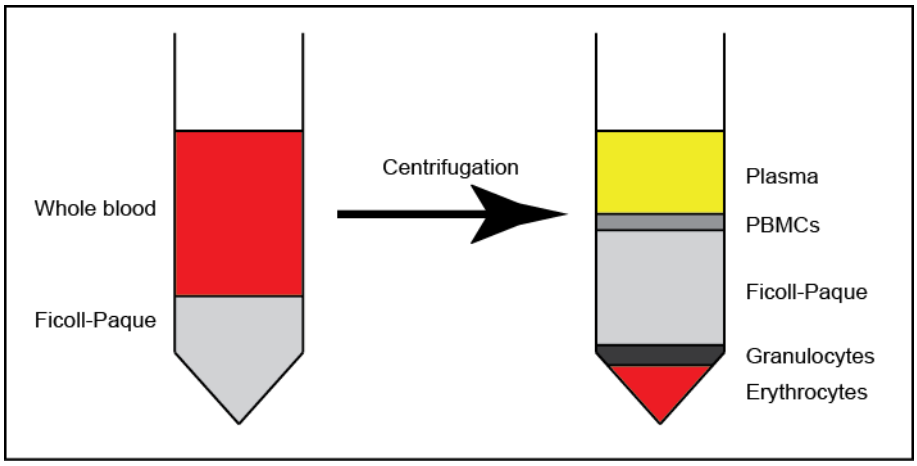

Figure 2-1 Peripheral blood monocytic cell preparation by density gradient centrifugation.

2.5. 3D Omental model construction

A collagen mix was made up on ice constituting one part 10X RPMI-1640 (powder dissolved in distilled water and Sodium Bicarbonate; Sigma, R6504), one part 0.33M Sodium Hydroxide, (Sigma, S-8045), one part FBS, and seven parts Rat-tail Collagen, Type 1, (BD Biosciences, 354236). 50μL of the mix was added to each well of a 24 well Corning Transwell-Clear, plate 12 inserts, 3μm pore size, 6.5mm diameter, (Fisher, TKT-525-090R), and allowed to set for 30 minutes. 50,000 HEFs or HPFs were mixed into 50μL of the collagen mix per well, and allowed to set on top of the pre-set layer. 500μL and 100μL of full medium were placed in the bottom and top part of the transwell

respectively and left in culture for 24 hours. 20,000 HPMCs were then seeded in 100μL of full medium to the top part of each transwell and left to culture for 24 hours. 50,000 ovarian cancer cells were then seeded in 100μL of full medium to the top part of each transwell and left to culture for a further 24 hours. The top and bottom compartment of each transwell was washed in PBS, and full medium was placed in the bottom compartment and serum-free medium was placed in the top compartment to generate a serum concentration gradient. The models were left in culture for 14 days.

2.6. Histopathology

All human tissue and 3D model gels were fixed in formal saline solution (Adams Healthcare, 416479) at room temperature over night, and dehydrated in 30%, 50% and 70% Ethanol, (VWR, 10107EP) series. Samples were then stored in 70% Ethanol at 4^{o}C. The samples were embedded in paraffin, sectioned and stained with hematoxylin and eosin by the staff in the Barts Cancer Institute (BCI) Histopathology department.

2.7. Antibodies

All human antibodies were monoclonal and of mouse origin unless indicated.

Monoclonal Rabbit Anti-CD3, (Labvision, RM-9107-S)
Anti-CD4, Clone 1F6, (Novocastra, NCL-CD4-368)
Anti-CD68, Clone KP1 (Dako, M0814)
Anti-CD8, Clone C8/144B, (Dako, M7103)
Anti-CXCR4 (Fusin), Clone 44716, (R&D Systems, MAB172)
Polyclonal Rabbit Anti-Pan-Cytokeratin (Dako, Z0622)
Monoclonal Rabbit Anti-Cytokeratin 8, (Epitomics, 2032-1)

Polyclonal Rabbit Anti-GFP, (Invitrogen, A11122)
Anti-Ki67 Antigen clone MIB-1 (Dako, M7240)
Anti-Vimentin, (Dako, M0725)

John McCafferty in Cambridge (under a Cancer Research UK Discovery committee grant) kindly provided a lead compound, single chain variable fragment antibody to neutralise CXCL12. The antibody was denoted as 114_3H1.

2.8. Flow cytometry

For flow cytometry cells were detached with enzyme-free PBS-based cell dissociation buffer (Gibco, Invitrogen, 13151-014). 500,000 cells were pelleted and washed twice in buffer (PBS, 2% BSA (Albumin from bovine serum, Cohn V fraction, Sigma, A4503), 2mM EDTA (Ambion, AM9262)). All antibodies and dyes were diluted in buffer. The cells were incubated in the primary antibody for 45 minutes on ice. The cells were pelleted and washed twice again in buffer. The cells were then incubated in a secondary 546nm Alexa Fluor antibody (Invitrogen) diluted 1:1000 for a further 45 minutes on ice. The cells were then pelleted and washed twice in buffer before incubation in Fixable Viability Dye eFluor 450 (eBioscience, 65-0863). The cells were washed twice and finally fixed in 20% Formal Saline Solution (Adams Healthcare, 416479). The cells were analysed on the FACS (fluorescence activated cell sorting) Calibur in the Barts Cancer Institute FACS suite, having compensated with FITC and PE labelled anti-mouse Ig Comp beads (BD Biosciences, 552843). These data were processed with the FlowJo 9.4.11 software.

2.9. Immunofluorescence

Cells on 13mm glass cover slips were washed once in PBS and fixed in formal saline solution for one hour at room temperature. They were then washed twice with PBS and made permeable with a ten minute incubation in 0.5% Triton X-100 in PBS. The cells were washed twice again with PBS and once with PBS, 1% BSA, 2% FBS. This solution was further used to dilute all the antibodies. The cells were incubated with the primary antibody for one hour at room temperature.

3D model paraffin embedded sections were prepared for immunofluorescence staining by initially deparaffinising and rehydrating the sections. This was carried out by two five-minute incubations in Xylene, (Fisher Scientific, X620017) followed by two two-minute incubations in each of 100%, 95%, 70% and 50% ethanol series. The sections were then washed twice for two minutes in distilled water. Boiling the sections for nine minutes in the microwave in a solution containing 2.5mL of Antigen Unmasking Solution, (Vector, H-3300) in 250mL of distilled water was carried out for antigen retrieval. The sections were allowed to cool for 15 minutes and then washed three times for three minutes in PBS. A PAP hydrophobic pen was used to mark around the sections, and they were blocked for one hour at room temperature in a humidified chamber with 5% Goat Serum, (Invitrogen, Gibco, 16210072), 2.5% BSA, in PBS. After removal of the block solution, the sections were left to incubate in the primary antibodies diluted in the same blocking solution over night at 4^{o}C.

The cells or sections were washed three times with PBS and incubated with the appropriate secondary Alexa Fluor antibody (Invitrogen) diluted 1:1000 for one hour at room temperature. The cells/sections were then washed twice with PBS and incubated in Hoechst diluted 1:200 for 30 minutes at room temperature. The cells/sections were washed three times in PBS. The cover slips were dipped three times in distilled water

before mounting on to a frosted glass slide with 5μL Mowiol (1% Mowiol 4.88, Calbiochem, 475904, one part Citifluor, Electron Microscopy Services, AF1-17970-25, one part distilled water, two parts 200mM Tris-HCl (pH 8.5)). The cover slips were sealed with clear nail varnish and stored at 4°C before analysis. Sections were mounted with 10μL of Mowiol under a square glass cover slip and also stored at 4°C. The cells or sections were visualised and photographed on the Zeiss LSM 510 META laser scanning confocal microscope in the Barts Cancer Institute imaging suite.

2.10. Immunohistochemistry

For immunohistochemistry, sections were deparaffinised and rehydrated as above. Sections were also incubated with the primary antibody over night at 4°C after antigen retrieval and blocked for one hour at room temperature. The sections were then washed three times in PBS, and incubated in the appropriate biotinylated secondary antibody diluted 1:200 for 45 minutes; Goat Biotinylated Anti-Rabbit, (Vector, BA-1000), Goat Biotinylated Anti-Mouse, (Vector, BA-9200). The sections were then washed twice in PBS and endogenous peroxidase activity was blocked in a solution containing Methanol, (Fisher, M4000PC17) and Hydrogen peroxide 30% w/v, (Fisher, BPE2633-500) in a ratio 50:1 for 20 minutes at room temperature. Vectastain ABC Kit, Standard, (Vector, PK-6100) was diluted by manufacturer's instructions in 0.5M Sodium Chloride, (Sigma, S3014), and allowed to sit on ice for 30 minutes before use. Following blocking endogenous peroxidase activity, the sections were washed three times in PBS and were incubated in the ABC solution for 30 minutes at room temperature. One DAB tablet and one Tris/Peroxide tablet FAST 3,-3'-Diaminobenzidine Tablet, (Sigma, D4418) was dissolved in 15mL of distilled water, and after washing the sections three times in PBS, the sections were developed in the DAB solution for 3 – 5 minutes. The sections were then washed twice in distilled water and counterstained with Hematoxylin Solution, Gill No. 3,

(Sigma, GHS316) for 30 seconds. The sections were washed again in distilled water and dunked ten times in an acid differentiating solution of 750μL Ammonium Hydroxide, (Sigma, A6899) in 250mL of distilled water. The sections were then dunked twenty times in 100% isobutanol, (Fisher, B/5100/PB17) and then incubated in isobutanol for four minutes, and twice in Xylene for two minutes at room temperature. The sections were mounted in General Purpose Grade DPX mounting medium, (Fisher, D/5319/05) under a square glass cover slip and left flat until dry.

2.11. Automated Immunohistochemistry

Sections of human omental tissue were stained for the immunohistochemical markers CD68, CD3, CD4 and CD8 using a Dako Autostainer Plus with a Super Sensitive Polymer-HRP DAB (Launch Diagnostics Ltd, QD430-XAKE).

2.12. Immunohistochemistry Analysis

Quantification of the tumour-infiltrating inflammatory cells and Ki67 positive tumour cells was determined using the Ariol computer-controlled microscope and image analysis software (Leica Microsystems).

2.13. Measurement of growth on the 3D omental model

Confocal or bright field images were taken across the paraffin embedded centre cross-section of each gel at 20x magnification. On average two images were taken per immunofluorescence section and up to ten images were taken of each H & E stained section respectively. This was performed for triplicate gels in each treatment group. The images were made binary using the Image J software, and the area covered by any visible fibroblasts was omitted from the image. The software was then

used to calculate the area covered by the growing tumour cells in μm^2. The average tumour cell area per image was calculated for each gel. This average tumour cell area was then used as a measure of tumour growth.

2.14. Calculation of Invasion Index in the 3D omental model

The average tumour cell area was calculated as described in section 2.13. As previously published (Nystrom et al., 2005), the cells sitting on the surface of the gels were then omitted from the binary images within the Image J software. The software was used to analyse the number of invading particles greater than $1\mu m^2$. Measurements of the distance invaded by the particles were taken at three different points across the image and the average distance invaded was calculated. The product of the distance invaded, the number of invading particles and the total tumour cell area was calculated to give an Invasion Index.

2.15. Enzyme-linked immunosorbent assay (ELISA)

The assay procedure was carried out as advised by manufacturer's instructions. All reagents were provided in the Quantikine Human CXCL12/SDF-1α ELISA kit, (R & D Systems, DSA00).

2.16. Bioinformatics

Protocols provided by Dr Probir Chakravarty at the London Research Institute who conducted all of the bioinformatics analyses for this thesis:

The cohort of 285 ovarian cancer biopsies from the Australian Ovarian Cancer Study (AOCS) was selected as a second data set to confirm the

CXCL12 and extracellular matrix-remodelling link initially identified in the GSE 6008 and 3149 data set. The NCBI GEO (Gene Expression Omnibus web reference) accession number for the AOCS arrays was GSE 9891. Raw CEL files were downloaded and analysed using Bioconductor 1.9 (Gentleman et al., 2004) running on R 2.6.0 (Statistical computing text book reference). Probe set expression measures were calculated using the Affymetrix package's Robust Multichip Average (Gautier et al., 2004) default method. All samples were ranked on the normalised expression of CXCL12 [probe set ID: 209687_at] from highest expression to the lowest expression. The 50 highest CXCL12-expressing biopsies were compared with the 50 lowest CXCL12-expressing biopsies with an eBayes t-test from the limma package (Limma package text book reference). Amongst these two groups of 50 biopsies, more than 95% of the biopsies were from HGSC, and the remaining biopsies were from endometrioid ovarian cancers. A total of 5167 genes were differentially expressed between the two groups. Each gene was identified with multiple probes. Only probe sets with p values equal to or less than a multiple testing corrected (Multiple testing text book reference) p value of 0.05 were considered differentially expressed. There was no filtering based on fold change.

The biological processes enriched in the 5167 differentially expressed genes were elucidated using the Metacore Pathway Analysis software (Metacore Analysis web reference). This process used a hyper-geometric test to look for enrichment of genes within a gene list relative to a background list, which in this case were all genes present on the Affymetrix Human Genome U133 plus2 Array.

Gene set signatures defining macrophage and other immune cell infiltrates (Abbas et al., 2005) were used to interrogate the differentially expressed genes associated with high levels of CXCL12.

The function GeneSetTest from the limma package was used to assess whether the t-statistic from the high CXCL12 versus low CXCL12

comparison had a tendency to be associated with an up or down-regulation of members of each immune cell signature. The function employed Wilcoxon's t test to generate p values.

2.17. RNA Extraction

Omental metastases samples were lysed in 1mL of lysis buffer and 10µL of β–mercaptoethanol (Sigma, M-6250). The tissue was homogenised in a gentle MACS tube (MACS Miltenyi Biotec, 130-093-236). The homogenised tissue was centrifuged at 1200rpm for five minutes, and the supernatant was centrifuged through a QIAShredder column (Qiagen, 79654) as advised by the manufacturer's instructions.

Two 3D omental model gels were lysed in 0.5mL of lysis buffer and 5µL of β–mercaptoethanol by vortexing.

350µL of the lysed tissue samples or gels were mixed with an equal volume of 70% ethanol. The two solutions were mixed by pipetting, not vortexing. The total 700µL final volume was then transferred to a RNA binding column. The columns and lysis buffer are both provided in the RNeasy Mini kit (Qiagen, 74104). The remainder of the RNA extraction was performed as advised by the kit manufacturer's instructions. An on-column DNA digest was carried out using Qiagen's RNase-Free DNase I set (Qiagen, 79254). The resultant concentration of the eluted RNA was measured on the Nanodrop. The RNA was then stored at -80^{o}C.

2.18. cDNA Synthesis

Up to 2µg of RNA can be reverse transcribed in a single reaction, and the final reaction volume was made up to 20µL. A master mix of the appropriate volumes of the required reagents was generated containing 1X concentration of first strand buffer (Invitrogen, 18064-014), 10mM

dithiothreitol (DTT) (Invitrogen, 18064-014), 0.5mM dNTP (deoxyribonucleotide triphosphate) (Promega, U1240), 12.5ng/μL random hexamers (Promega, C1181), 6.25 ng/μL oligo dT 15 mers (Promega, C1101), 1U/μL RNasin (Promega, N2111) and 5U/μL SuperScript II reverse transcriptase (Invitrogen, 18064-014). 8.75μL of master mix was added to 11.25μL of the diluted RNA in PCR tubes or a 96 well PCR plate. The tubes or plate were placed in to a PCR machine and subjected to the program of one hold at 25^{o}C for ten minutes, 42^{o}C for 60 minutes, 90^{o}C for five minutes, and then continuously held at 4^{o}C. The cDNA was then stored at -20^{o}C.

2.19. TaqMan gene expression assays

All TaqMan gene expression assays were purchased from Applied Biosystems, 4331182.

IFNγ (Hs00989291_m1), TNFα (Hs01113624_g1), IL-12 (Hs01073447_m1), IL-10 (Hs00961622_m1), IL1-β (Hs01555410_m1), IL-6 (Hs00985639_m1), IL-8 (Hs00174103_m1), VEGF (Hs00900055_m1), CXCL12 (Hs00171022_m1), ACTB (Hs01060665_g1), YWHAZ (Hs03044281_g1), TBP (Hs00427620_m1), HPRT1 (Hs02800695_m1), POSTN (Hs00170815_m1), VCN (Hs00171642_m1), LUM (Hs00929860_m1), DCN (Hs00754870_s1), COL6a3 (Hs00365098_m1), THBS1 (Hs00962908_m1).

2.20. Quantitative Real-time PCR (qRT-PCR)

The cDNA was diluted to a concentration that corresponded to 0.625ng/μL of RNA. A master mix of the appropriate volumes of the required reagents was generated containing 1X TaqMan Universal PCR master mix (Applied Biosystems, 4318157), 1X target gene Fam labelled gene expression array (Applied Biosystems, 4331182) and 1X 18S Vic

labelled gene expression assay (Applied Biosystems) or water if the second Vic labelled primer was not required. 8µL of the diluted cDNA was added to 11.25µL of the master mix per reaction in a MicroAmp Fast Optical 96-well reaction plate (Applied Biosystems, 4346906). The plate was covered with MicroAmp optical adhesive film (Applied Biosystems, 4311971), and centrifuged at 1500rpm for one minute. The quantitative real-time PCR was then run on a StepOnePlus Real-Time PCR system (Applied Biosystems).

Chapter 3

3. Characterising the tumour microenvironment of HGSC metastases

3.1. The omentum

The omentum is a fold in the peritoneal lining that overlies and physically protects the stomach and bowels. A monolayer of mesothelial cells creates a non-abrasive, non-adhesive surface between the adipose-rich, well-vascularised tissue of the omentum and the peritoneal cavity. These mesothelial cells regulate the transfer of solutes between the two compartments, and elicit a defensive barrier against invading pathogens (Khan et al., 2010a). Just below the mesothelial cells there is a layer of fibroblasts, which are likely to contribute significantly to collagen and fibronectin synthesis in the sub-mesothelial compartment (Kenny et al., 2007). The omentum is the area of the peritoneal cavity that is most dominantly colonised by disseminated HGSC cells during metastasis (Sehouli et al., 2009). At the beginning of the project a tissue bank of human omental metastases of HGSC was started and established, and the microenvironment of these metastatic deposits was characterised.

3.2. Collection of human omental metastases specimens

After 3-4 cycles of neoadjuvant chemotherapy, ovarian cancer patients undergo interval-debulking surgery to remove as much of the tumour as possible before the next cycle of chemotherapy. For the purpose of this thesis, I collected a total of 112 samples of human omentum removed during this surgery on ovarian cancer patients at St. Bartholomew's hospital. For patient confidentiality purposes, each sample was given an anonymous code. The letter 'G' denoted this code followed by a number

representing the order that the samples were collected in. Therefore the first sample collected was given the anonymous G-code ‘G1,’ and this continued to the final sample collected which was G-coded ‘G112.’ During 2011, 18 out of the total 44 (41%) samples collected that year were from HGSC patients. The majority of the patients had received on average 3 cycles of carboplatin and paclitaxel before surgery. The majority of the patients were between 50 and 70 years of age. The samples ranged from relatively non-involved samples (Figure 3-1a) to predominantly metastatic disease (Figure 3-1b). Omenta with metastatic lesions are often termed ‘omental cake,’ describing the increase in mass and density of the tissue as the malignant cells promote a huge stromal reaction and monopolise the normal adipose tissue. Approximately 20% of the samples I have collected were colonised by tumour deposits, as determined by the hematoxylin and eosin (H & E) stained sections (Figure 3-2 & Figure 3-3). Ten HGSC diseased samples were selected to investigate the degree of inflammatory infiltrate in these omental metastases. All of these ten patients had received chemotherapy. The relevant clinical information for these samples is recorded in Table 3-1.

Anon. Code	Collection Date	Age	Histotype	Grade	Stage	Treatment prior to biopsy
G9	09/08/2010	59	SP	HG	3	23/07/2010 – C & P
G11	23/09/2010	70	SP	HG	3	April 2010 - C
G15	11/01/2011	73	SP	HG	3	6 cycles: incomplete debulking
G17	10/03/2011	62	SP	HG	3	
G20	17/03/2011	46	SP	HG	4	22/12/10 - C & P
G33	28/06/2011	70	SP	HG	3	03/2011 - C & P
G34	30/06/2011	63	SP	HG	3	22/2/11 – C & P. Post surgery C & T 07/2011.
G73	21/08/2012	67	SP	HG	3	4 cycles, first 3 including AVASTIN
G75	30/08/2012	47	SP	HG	3	
G77	13/09/2012	66	SP	HG	3	

Table 3-1 Clinical information for disease colonised biopsies

Each patient was identified with an individual anonymous code as denoted in the first column. The table shows for each patient the date the biopsy was collected, the patient's age at collection, and the histopathology (SP – Serous Papillary), grade (HG – High Grade) and stage of the disease. Information is also given about the treatment the patient received before the biopsy was taken. All the biopsies received were interval-debulking specimens. If known, the date the patient started chemotherapy and the combination of chemotherapy (C – Carboplatin, P – Paclitaxel) they received is recorded.

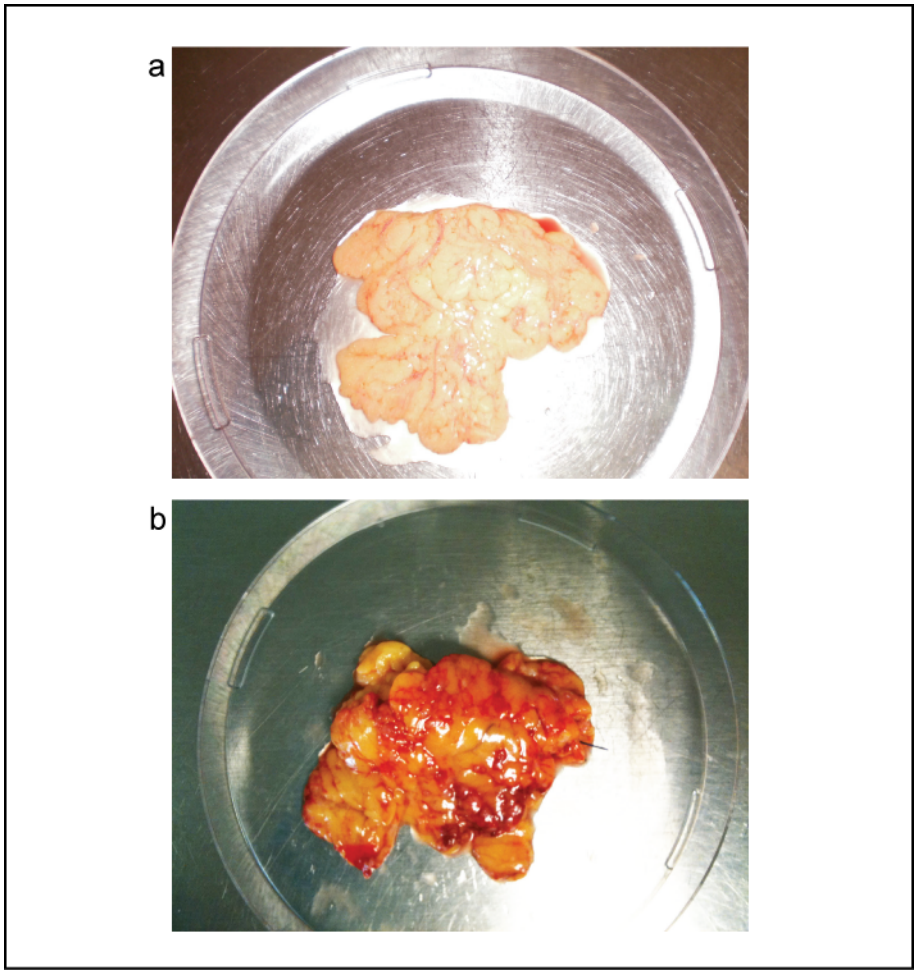

Figure 3-1 Human omentum is removed during routine de-bulking surgery on ovarian cancer patients.

Human omentum tissue samples were collected from ovarian cancer patients. Samples were taken for paraffin-embedded and frozen sections, snap freezing, and isolation of human primary mesothelial cells and fibroblasts. **a)** Normal omentum and **b)** diseased omentum. Tissue is photographed in a 150mm dish.

Representative H & E images of non-involved (Figure 3-2) and diseased (Figure 3-3) omentum samples from four different patients are shown. The non-involved omental samples are largely adipose tissue and highly vascularised. They are covered in a monolayer of mesothelial cells as illustrated in Figure 3-2a. Figure 3-2b shows fibrous septa in the omentum that can be exploited by invading malignant cells following adhesion to the mesothelial cell surface to invade deeper into the tissue. Surrounding the tumour deposits within the omentum one can identify infiltrating leukocytes, as well as a dense fibroblastic and vascularised stroma that engulfs the normal adipose tissue (Figure 3-3a). Figure 3-3b

indicates the presence of calcium deposits known as psammoma bodies that are found within the stroma of the omental metastases. It has been suggested that the presence of these psammoma bodies, which is particularly characteristic of HGSC, is associated with an increased overall survival. It is argued that the formation of these psammoma bodies is a result of the deposition of crystallised calcium during apoptosis, and the production of osteopontin by infiltrating CD68 positive macrophages (Motohara et al., 2010).

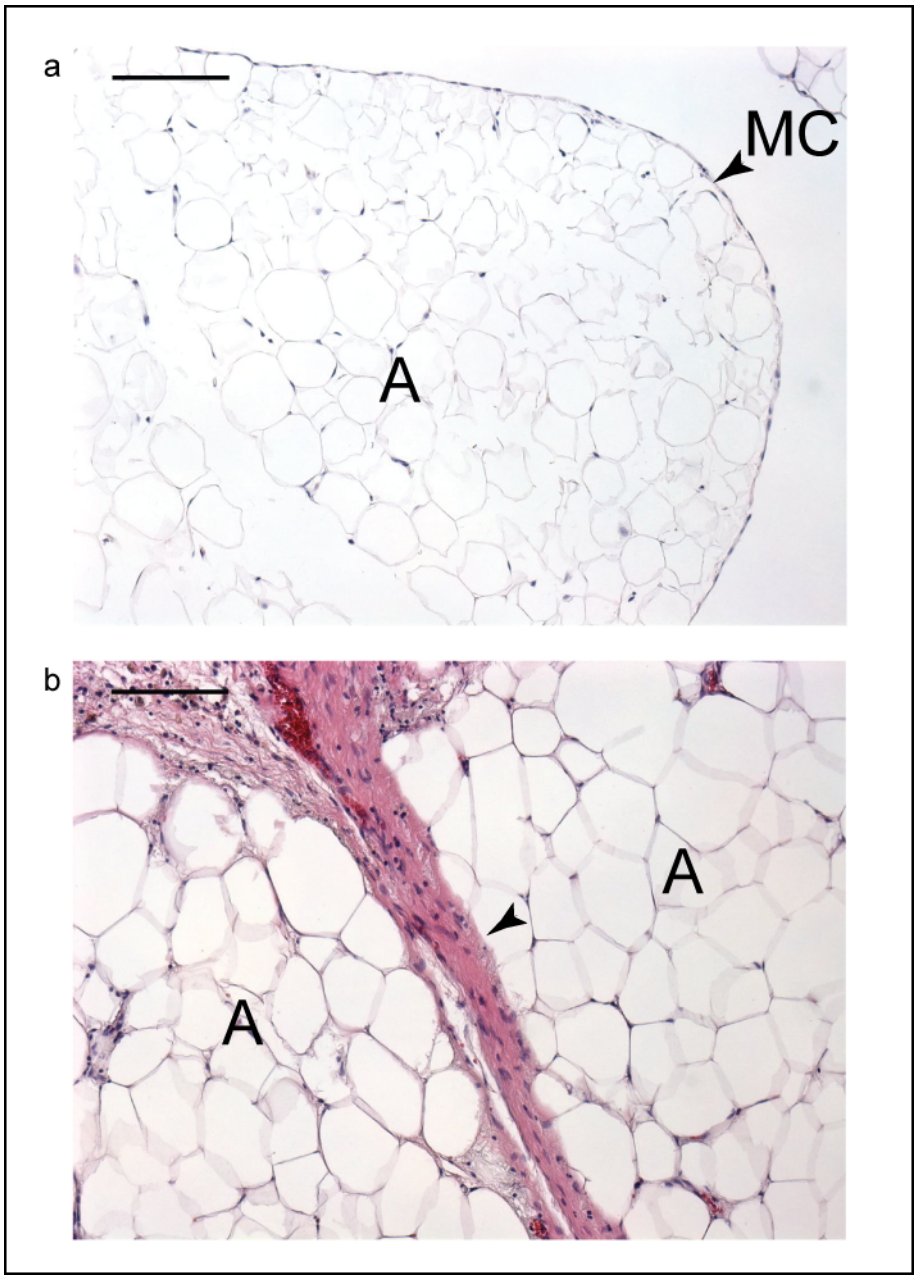

Figure 3-2 Histopathology of normal human omentum.

Hematoxylin and eosin histochemical staining of 5μm thick paraffin-embedded omentum sections. **a)** Normal omentum characterised by an abundance of adipose tissue (A) covered by a monolayer of mesothelial cells (MC) (indicated by arrow). **b)** Arrow indicates a fibrous septum passing through adipose tissue (A). 10x magnification, black bar = 200μm.

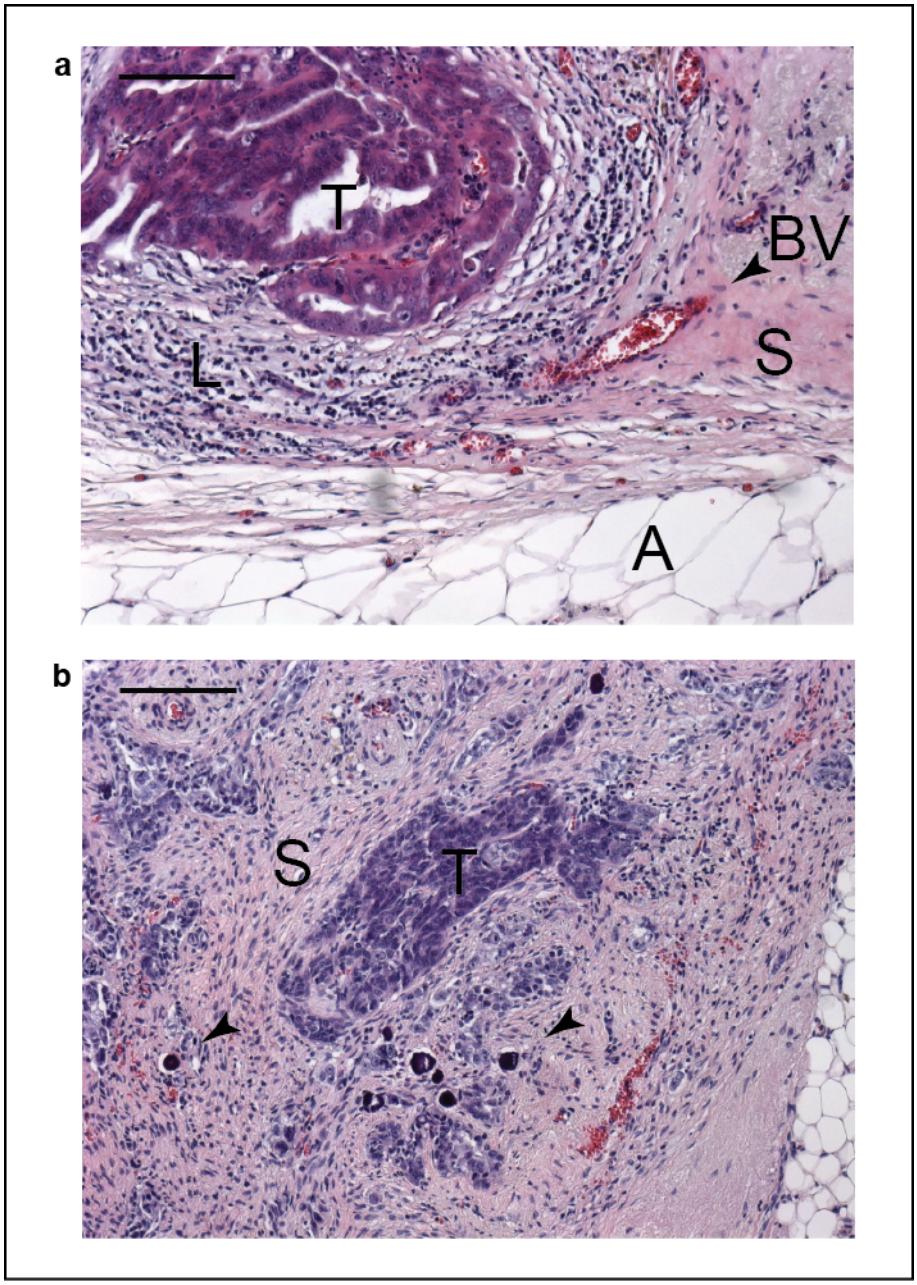

Figure 3-3 Histopathology of human omental metastases of HGSC.

Hematoxylin and eosin histochemical staining of 5μm thick paraffin-embedded omentum sections. **a)** Diseased omentum characterised by the presence of tumour deposits (T) surrounded by a leukocyte infiltrate (L), blood vessels (BV) (indicated by arrow) and stroma (S). **b)** Arrows indicate the location of psammoma bodies, which are calcium deposits found in ovarian cancer metastases. 10x magnification, black bar = 200μm.

3.3. Characterisation of the microenvironment of the omental metastases

To develop an overview of immune cell infiltrate involvement in HGSC metastasis to the omentum, the localisation and the percentage of macrophages and T cells within the human omental metastatic lesions was investigated by immunohistochemistry analysis. The tumour deposits in the entire tissue section of the ten individual biopsies were scanned using a computer-operated microscope, and analysed with the Leica Ariol software. The number of positively stained cells was quantified and illustrated as a percentage of the total number of cells in the deposits determined by the hematoxylin nuclear counterstain. The quantification of the immune cell infiltrates was represented as a percentage so the number of immune cells to be introduced to the 3D omental model later in chapter 7 could be calculated.

3.3.1. Predominant macrophage and T cell infitrate in human omental metastases

CD3 positive T cells surrounded the tumour deposits within the omentum and CD68 positive macrophages infiltrated within the tumour deposits (Figure 3-4 & 3-5). T cells and macrophages were the most prominent inflammatory infiltrate in these omental metastases of those analysed here, comprising 9.4% and 11.3% of the tumour volume respectively (Figure 3-6). These data were included in a paper I co-authored (Leinster et al., 2012)(Appendix II).

It has been shown that neutrophils can both promote tumour-associated angiogenesis (Fridlender et al., 2009; Polyak et al., 2009), but can also prevent tumour metastasis (Granot et al., 2011). Neutrophils were rarely observed in the human omental metastases of HGSC accounting for less than 1% of the total tumour volume (Leinster et al., 2012).

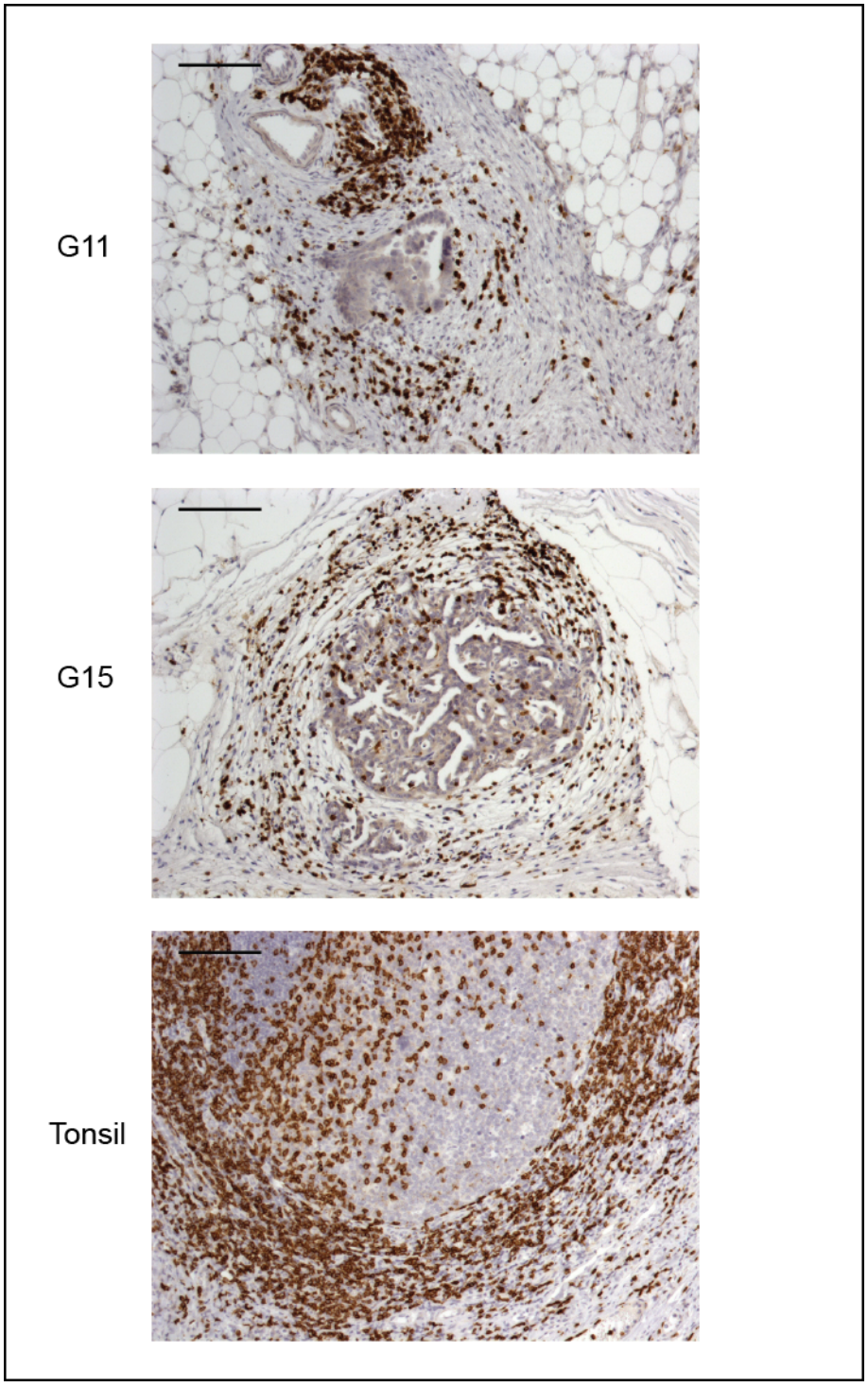

Figure 3-4 CD3 positive T cell infiltrate in human omental metastases of HGSC.

Representative immunohistochemical staining of CD3 positive T cells in paraffin-embedded sections of human omental metastases from two patients, G11 and G15. Human tonsil is used as a positive control. 10x magnification, black bar = 200μm.

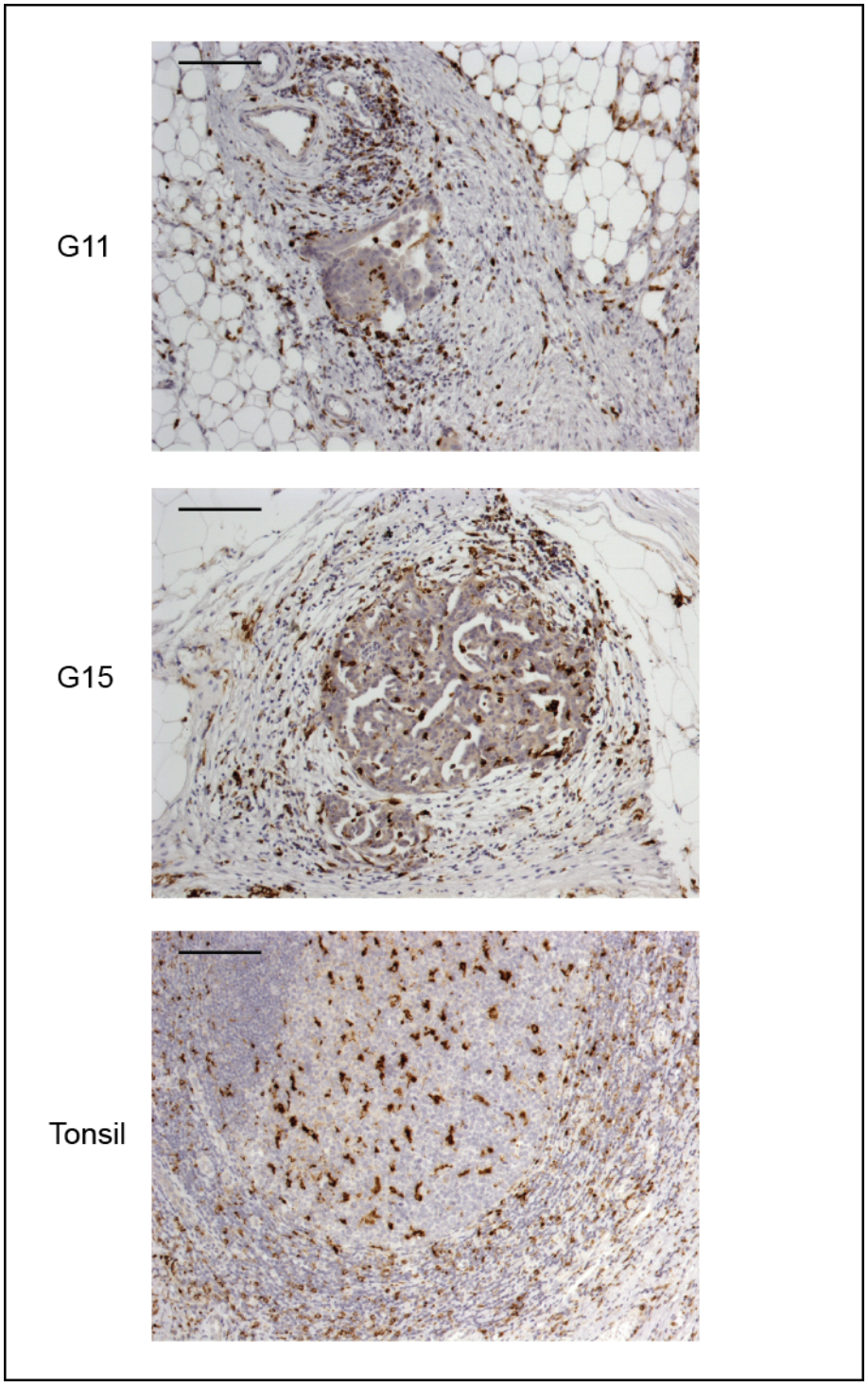

Figure 3-5 CD68 positive macrophage infiltrate in human omental metastases of HGSC.

Representative immunohistochemical staining of CD68 positive macrophages in paraffin-embedded sections of human omental metastases from two patients, G11 and G15. Human tonsil is used as a positive control. 10x magnification, black bar = 200μm.

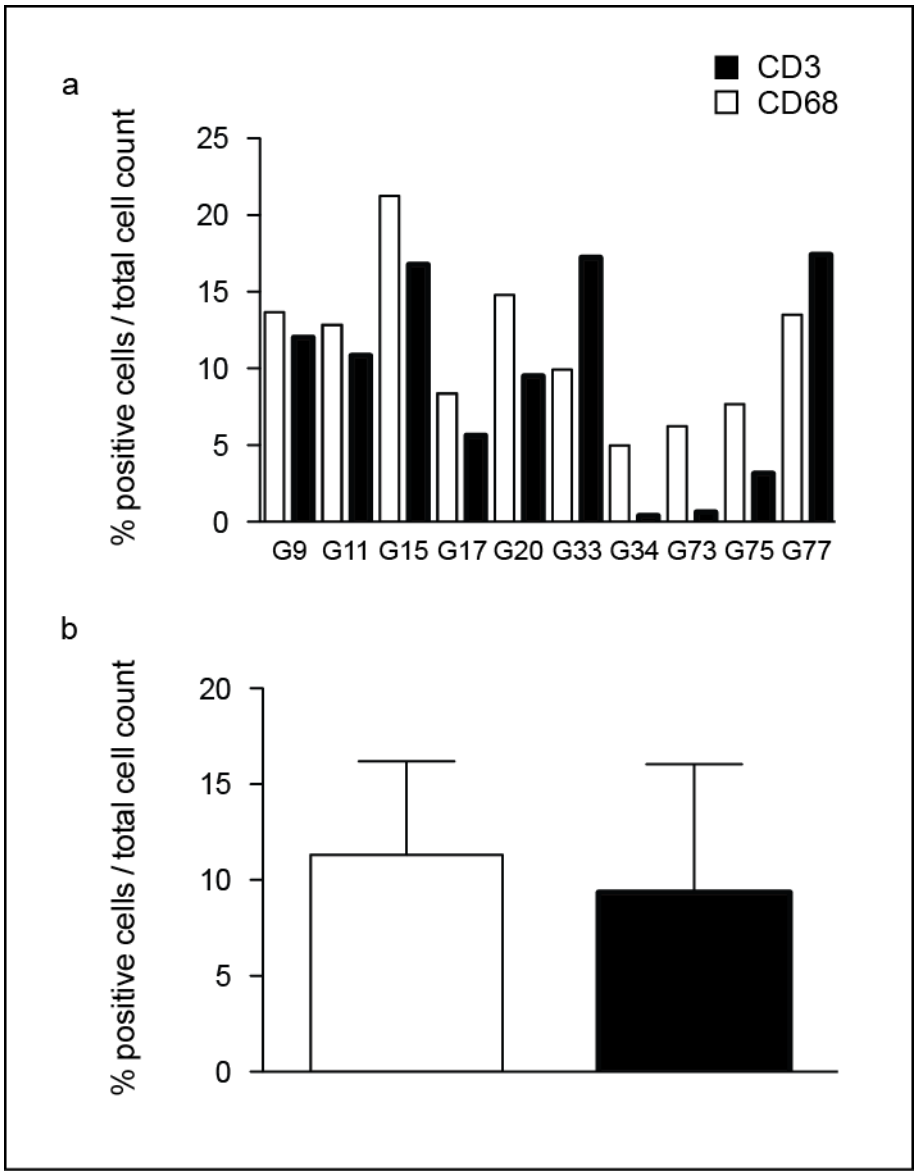

Figure 3-6 Immune cell infiltrate in human omental metastases of HGSC.

Quantification of the immune cell infiltrate in **a)** ten of the disease involved omentum. Tumour deposits within entire consecutive tissue sections of biopsies analysed by computer-aided microscopy and Leica Ariol software. Values are the percentage of positively stained cells in relation to the hematoxylin nuclear counterstain. **b)** Summary of data. All values represent mean and standard deviation.

3.3.2. The effect of the immune cell infiltrate on malignant epithelial cell proliferation

Figure 3-7 shows the proliferating population of malignant epithelial and stromal cells in the human omental metastases detected by Ki67 positivity. Using the Leica image analysis software the tumour deposit areas were carefully drawn around and selected (Figure 3-7). Undoubtedly stromal cells were found infiltrating the selected tumour deposit areas, however the majority of the cells within these areas were epithelial cells. Within these selected areas the software quantified the number of Ki67 positive and hematoxylin counterstained cells. The sum of these values was used determine the total number of cells within the designated areas. The percentage of Ki67 positive cells relative to the total cell count in these selected areas was then calculated for each omental specimen. To investigate the hypothesis that the balance of inflammatory cell infiltrate can influence tumour growth, the number of CD68 positive macrophages and CD3 positive T cells was correlated with the percentage of Ki67 positive cells in each of the omental metastases (Figure 3-8).

Figure 3-8a shows there was a significant positive correlation between tumour-infiltrating macrophages and tumour cell proliferation, where as there was no significant correlation between T cell infiltrate and tumour cell proliferation (Figure 3-8b). The Shapiro-Wilk normality test defined both data sets to form parametric distributions and therefore the Pearson rank correlation coefficient was employed to test the strength of the correlations. This is therefore supportive of the argument that an infiltrate of macrophages in ovarian cancer can promote tumour growth and correlate with a poor patient outcome (Kryczek et al., 2007; Vaughan et al., 2011).

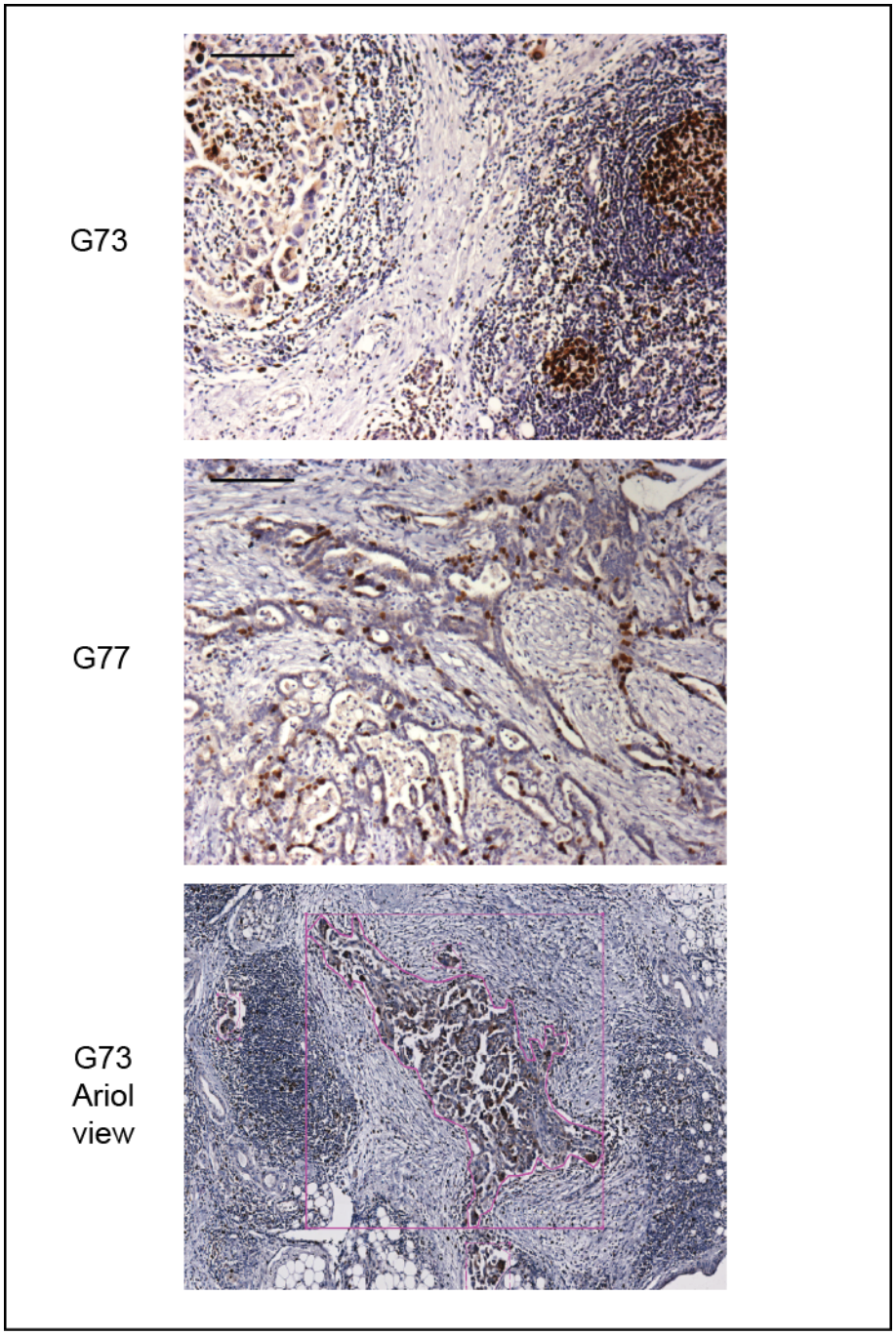

Figure 3-7 Ki67 positive cells in human omental metastases of HGSC.

Representative immunohistochemical staining of Ki67 positive epithelial cells in paraffin-embedded sections of human omental metastases from two patients, G73 and G77. 10x magnification, black bar = 200μm. G73 Ariol view shows a screen shot from the Leica image analysis software when a zoom factor of 0.23 was used to view the section. Purple lines indicate the enclosed tumour deposit areas analysed.

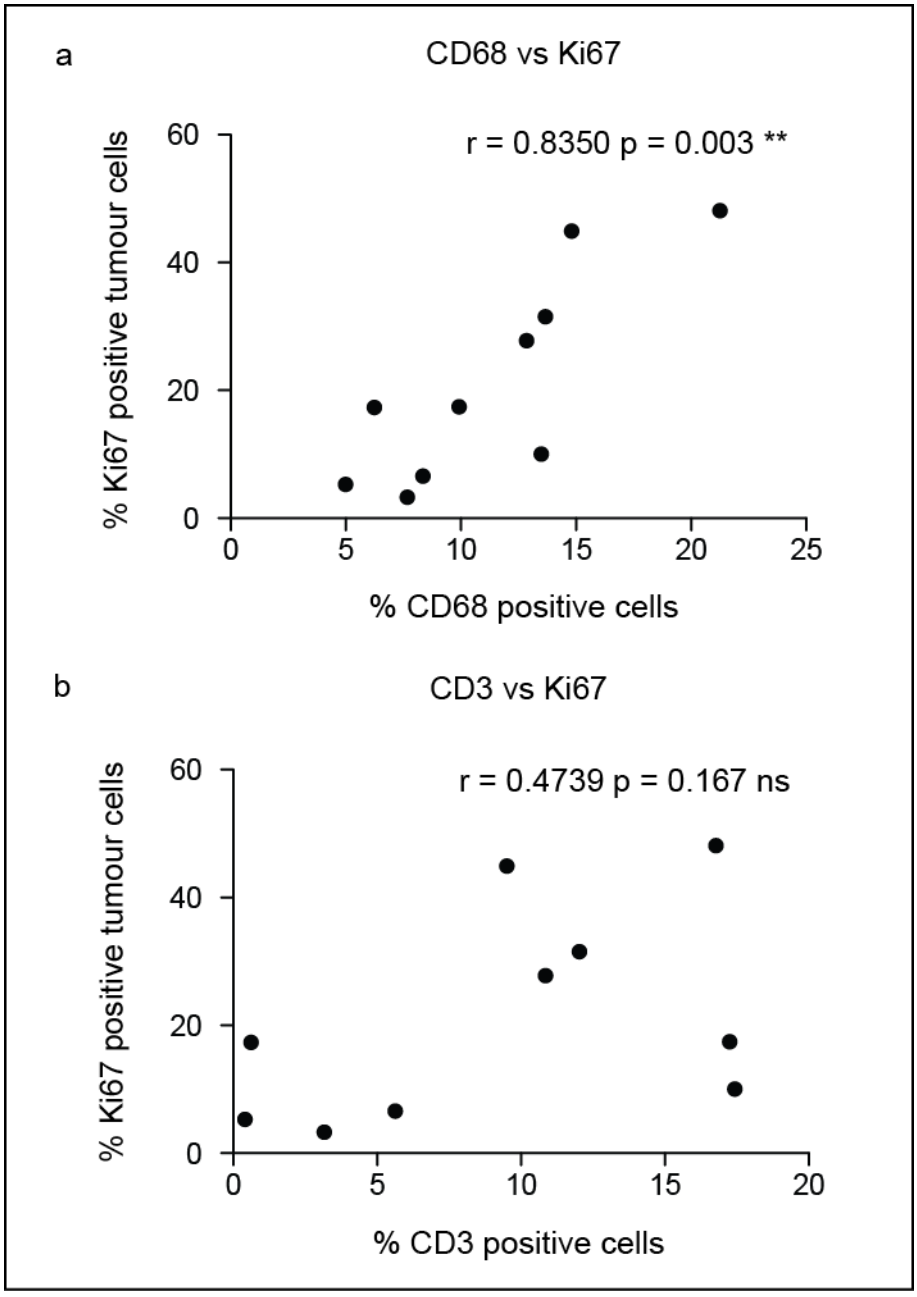

Figure 3-8 The correlation between CD68 positive macrophage and CD3 positive T cell infiltrates with tumour cell proliferation in human omental metastases of HGSC.

Correlation between Ki67 positive tumour cells with **a)** CD68 positive macrophages and **b)** CD3 positive T cells in disease involved omenta. Tumour deposits within entire tissue sections of biopsies analysed by computer-aided microscopy and Leica Ariol software. Values are the percentage of positively stained cells in relation to the hematoxylin nuclear counterstain. r = Pearson rank correlation coefficient. ns = not significant.

A further analysis was performed by Dr Steffen Boehm in the laboratory investigating the relationships between CD4 and CD8 positive T cell infiltrates with tumour cell proliferation in omental metastases of HGSC. This study utilised a tissue microarray (TMA) of the omental metastases that he established after my study was completed. Figures 3-9 and 3-10 (images kindly provided by Dr Anne Montfort and Dr Steffen Boehm) illustrate the infiltrate of CD4 and CD8 positive T cells respectively surrounding the tumour deposits within the TMA cores of the biopsies.

The same patient derived samples were analysed in the TMA for CD4 and CD8 positive T cell infiltrates as with the whole sections studied for CD68 positive macrophages and CD3 positive T cells (Table 3-1). The Shapiro-Wilk normality test defined the data sets to form non-parametric distributions. Therefore the Spearman rank correlation coefficient was employed to test the strength of the correlations between CD4 (Figure 3-11a) and CD8 (Figure 3-11b) positive T cell infiltrates with the percentage of Ki67 positive tumour cells. Of the specimens studied here in this chapter there were no significant correlations between either T cell subsets and tumour cell proliferation.

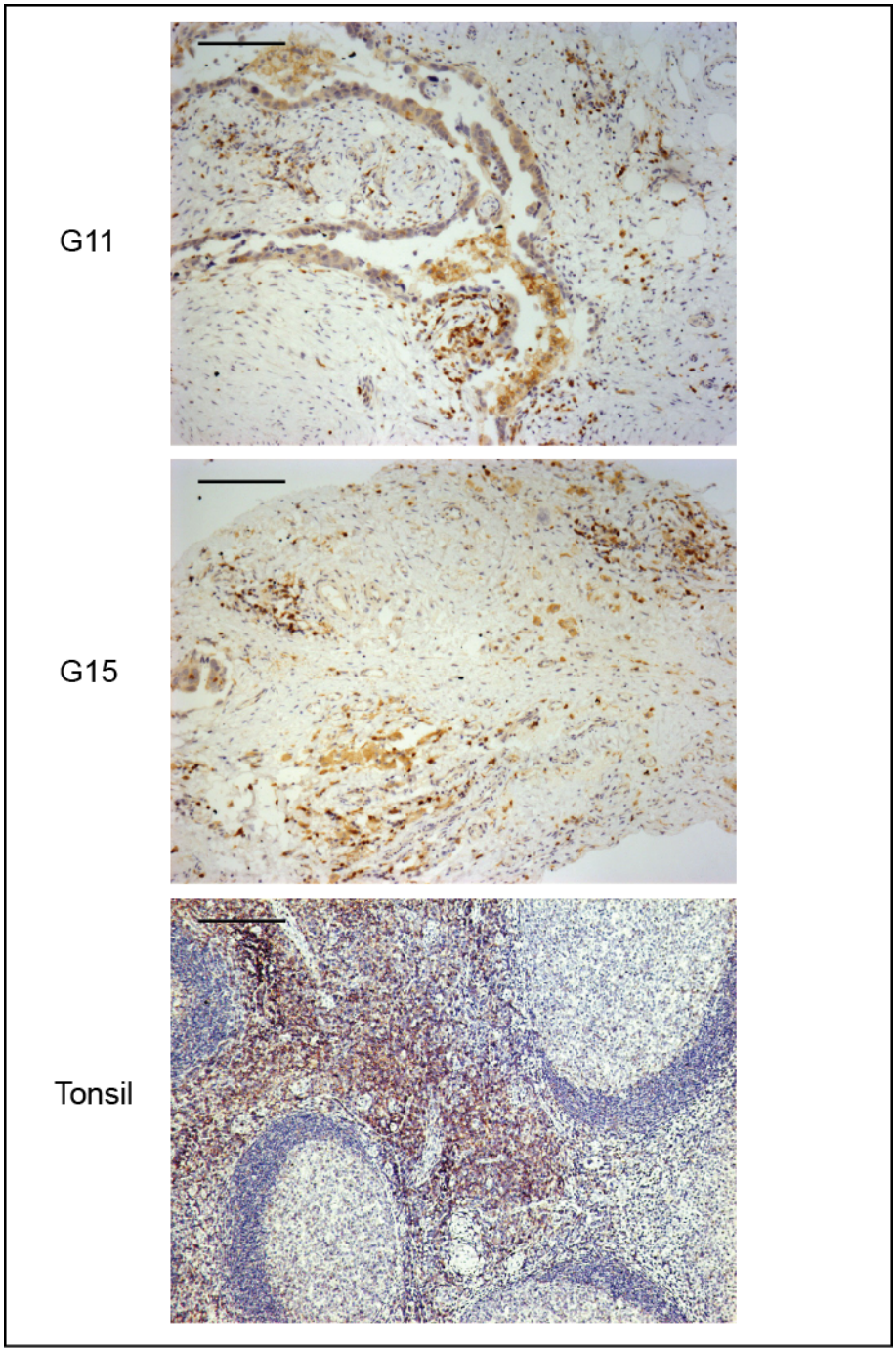

Figure 3-9 CD4 positive T cell infiltrate in human omental metastases of HGSC.

Representative immunohistochemical staining of CD4 positive T cells in paraffin-embedded tissue microarray cores of human omental metastases from two patients, G11 and G15. Human tonsil is used as a positive control. 10x magnification, black bar = 200μm. Images provided by Dr Anne Montfort and Dr Steffen Boehm.

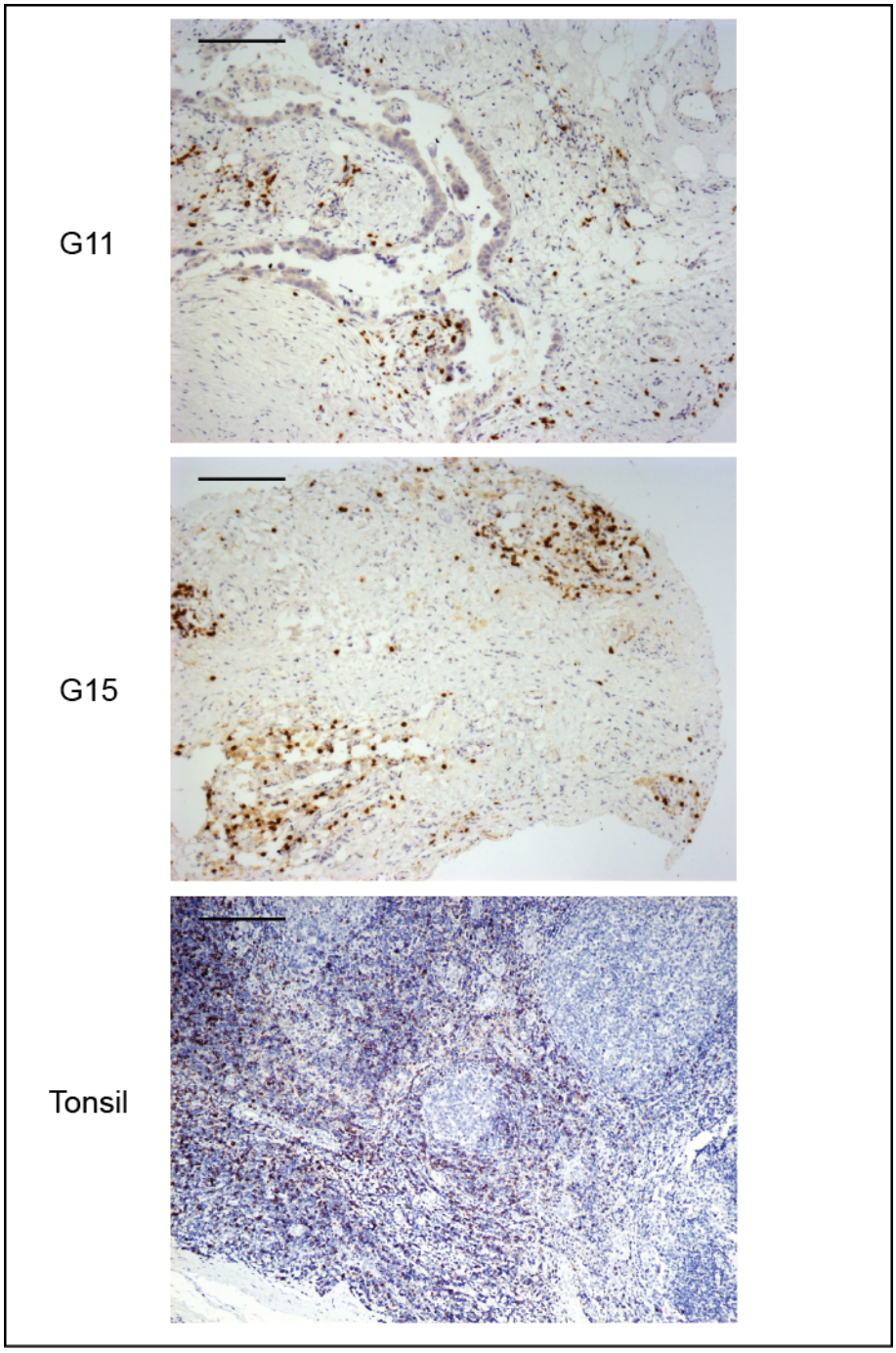

Figure 3-10 CD8 positive T cell infiltrate in human omental metastases of HGSC.

Representative immunohistochemical staining of CD8 positive T cells in paraffin-embedded tissue microarray cores of human omental metastases from two patients, G11 and G15. Human tonsil is used as a positive control. 10x magnification, black bar = 200μm. Images provided by Dr Anne Montfort and Dr Steffen Boehm.

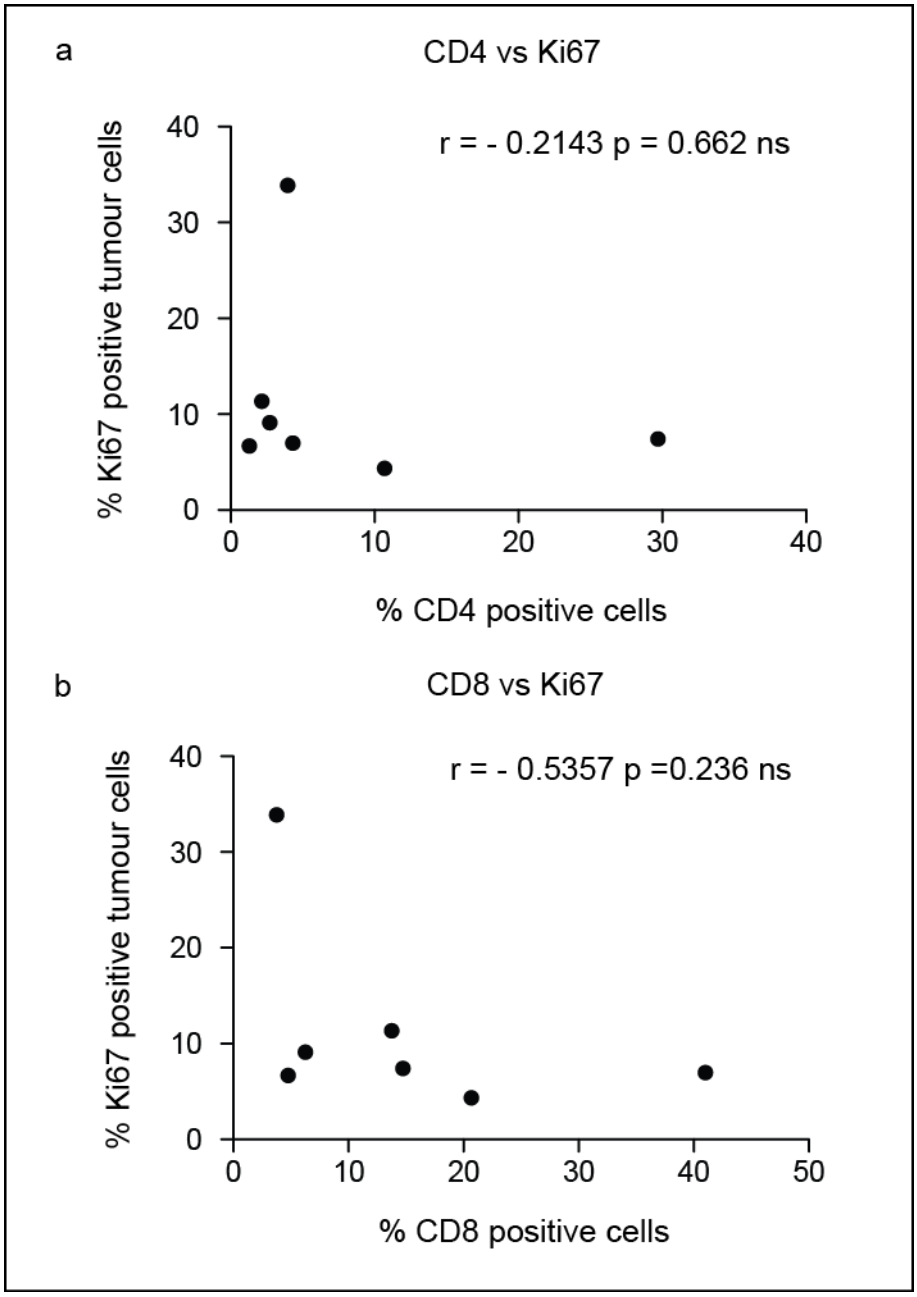

Figure 3-11 The correlation between CD4 and CD8 positive T cell infiltrates with tumour cell proliferation in human omental metastases of HGSC.

Correlation between Ki67 positive tumour cells with **a)** CD4 and **b)** CD8 positive T cells in disease involved omenta. Tumour deposits within tissue microarray cores of biopsies analysed by computer-aided microscopy and Leica Ariol software. Values are the percentage of positively stained cells in relation to the hematoxylin nuclear counterstain. r = Spearman rank correlation coefficient. ns = not significant. Data collected and provided by Dr Steffen Boehm.

Ki67 is expressed in cells in all phases of the cell cycle, but not in quiescent cells. It seems controversial as to whether Ki67 scoring can be predictive of patient prognosis (Dowsett et al., 2011). All of the human omental metastases described in this chapter were removed from patients whom had received chemotherapy prior to surgery (Table 3-1). At the time of writing this thesis, the omental metastases tissue bank was four years old. Survival rates are usually based upon five-year intervals following diagnosis (Cancer Research UK). Therefore information regarding patient survival and response to treatment was not available. Consequently a correlation between the CD68 positive macrophage infiltrate and chemoresistance or overall survival could not be determined directly here, but a relationship with the proliferation index in the omental metastases can be considered indicative of macrophages supporting a tumour-promoting microenvironment.

3.4. Summary

• The omentum is a common site for HGSC metastasis**.**

• Interactions with the mesothelial cells and fibroblasts of the omentum potentiates malignant cell invasion.

• Of the ten patient samples studied, all of the patients had received chemotherapy prior to the removal of the omentum during interval debulking surgery.

• In the samples studied there was a prominent infiltrate of CD3 positive T cells (9.4% of total cells) and CD68 positive macrophages (11.3% of total cells).

• An increase in CD68 positive macrophages in the omental deposits significantly correlated with an increase in tumour cell proliferation ($r = 0.835$, $p = 0.003$), whereas the extent of the CD3, CD4 and CD8 positive T cell infiltrate did not correlate with tumour cell proliferation.

3.5. Discussion

At the time of writing this thesis many points raised by the preliminary data presented in this chapter have been followed up. Dr Steffen Boehm, a Clinical Research Fellow in The Centre for Cancer and Inflammation generated a TMA with the omental metastases of 47 patients (11 pre-treatment, and 36 post-treatment unmatched samples). This was complimented also with a TMA of the primary ovarian tumour masses of 15 patients (seven pre-treatment, and eight post-treatment unmatched samples). The same analyses into the immune infiltrate carried out here was applied to the TMAs, but the CD3 positive T cell population was sub-divided and the CD4 and CD8 positive populations were analysed separately. This showed significant positive correlations between CD68 positive macrophages and Ki67 (Pearson rank correlation coefficient $r = 0.81$, $p = 0.002$), and also CD4 positive T cells and Ki67 (Pearson rank correlation coefficient $r = 0.72$, $p = 0.012$) in the primary tumour TMA but not in the omental metastases TMA. In the omental metastases, only a significant negative correlation was identified between the CD8 positive cytotoxic T cells and Ki67 (Pearson rank correlation coefficient $r = -0.52$, $p = 0.027$) (Boehm S manuscript in preparation).

Dr Steffen Boehm was also able to access pre and post chemotherapy matched patient paraffin embedded omental biospies, and again applied the same analyses into the immune infiltrate to those samples. These preliminary data suggest a decrease in the percentage of CD68 positive macrophages following chemotherapy and a significant increase in CD3 positive T cells post treatment. Correlation of these data with Ki67 positive epithelial cells indicated an increase in tumour cell proliferation in the presence of CD68 positive macrophages also in the pre-treatment samples (Boehm S manuscript in preparation).

These data from this chapter informed the next stage of this project which was to establish a 3D *in vitro* model of ovarian cancer metastasis to the omentum. The primary aim was to use malignant cells, fibroblasts and mesothelial cells in the model, with a further aim to introduce macrophages since the association between these cells and malignant cell proliferation.

Chapter 4

4. A 3D cell culture model that mimics ovarian cancer metastasis to the omentum

4.1. The 3D omental cell culture model

Approximately 80% of all women that present with HGSC have metastases in the omentum (Nieman et al., 2011). Consequently it is clear that ovarian cancer omental metastasis is not a random process. There are molecular and cellular cues specific to the microenvironment of the omentum that attracts the tumour cells there. Kenny et al (Kenny et al., 2007) established a 3D cell culture model that incorporated both cell-cell and cell-matrix interactions, and recapitulated the human omental microenvironment better than any other experimental *in vitro* model previously described.

I first set out to establish and optimise the model described by Kenny and colleagues. A panel of two HGSC ovarian cancer cell lines (AOCS1 and SKOV3ip1) and two CCC cell lines (TOV21G and RMG1) were originally chosen for establishment of the model in the laboratory. However, since this work was completed a study comparing the genomic profiles of cell lines with HGSC biopsies revealed that the SKOV3ip1 ovarian cancer cells are not comparable to HGSC (Domcke et al., 2013). The TOV21G cell line was confirmed to be CCC in this study. In an additional study, a panel of nine markers was used to test the resemblance of 32 cell lines to CCC, and this again confirmed the TOV21G cells as CCC cell line, but the RMG1 cells were unclassified (Anglesio et al., 2013). The AOCS1 ovarian cancer cells were kindly donated to the laboratory from Prof David Bowtell in Australia. These cells were not evaluated in the recent publication by Domcke and colleagues (Domcke et al., 2013), however Dr Carla Milagre in the

laboratory recently confirmed that they carry a W146* mutation in *TP53*, and *TP53* mutations are characteristic of HGSC (section 1.1.1.1).

Therefore the cell lines cultured on the 3D omental model throughout this thesis were the HGSC cell line AOCS1, the CCC cell line TOV21G, and the unclassified cell lines SKOV3ip1 and RMG1. For brevity the term ‘ovarian cancer cell lines’ was used to collectively describe them.

4.2. 3D Omental cell culture model construction

Figure 4-1a shows how the 3D omental cell culture model was constructed. The HPMCs classically had a cobblestone appearance in culture (Figure 4-1b) and the HPFs had a mesenchymal spindle-like morphology (Figure 4-1c). The HPFs were cultured in a collagen I matrix, with a monolayer of HPMCs on the surface. Ovarian cancer cell lines were then cultured on top of the 3D omental model for two weeks, and their growth and invasion into the matrix was analysed. A serum gradient was applied to the model to mimic the nutrient rich microenvironment of the well-vascularised omentum relative to the peritoneal fluids that are in contact with its surface.

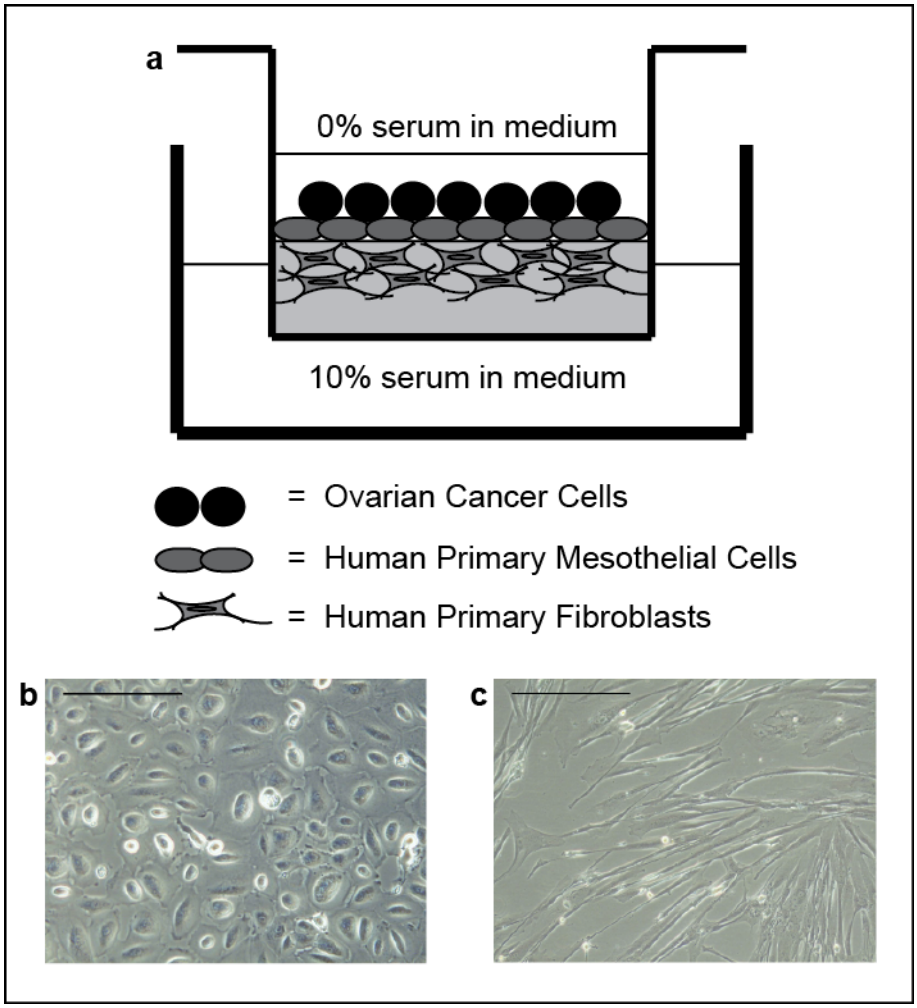

Figure 4-1 Omental 3D cell culture model construction.

a) Within a well of a 24 transwell plate ovarian cancer cells were seeded on to a 3D rat tail collagen I gel containing HPFs covered in a monolayer of HPMCs. **b)** Cobblestone morphology of HPMCs. **c)** Spindle morphology of HPFs. 20x magnification. Bar = 200 μm. Primary cells were isolated from human omentum removed during the debulking surgical treatment of ovarian cancer patients.

4.3. Human primary fibroblast and mesothelial cell characterisation

HEFs were utilised as a non cancer-associated fibroblast in the 3D omental model. These cells were positive for the expression of the intermediate filament protein vimentin that is expressed by mesenchymal cells (Figure 4-2a), and negative for the expression of cytokeratin 8/18 that is expressed by cells of epithelial origin. The human breast carcinoma cell line MCF7 served as a control for the negative expression of vimentin and the positive expression of cytokeratin 8/18 (Figure 4-2b). The HPFs mirrored the expression profile of the HEFs (Figure 4-2c), but the cell populations were not always pure and often contaminated with HPMCs. The HPMCs were characterised by their positive expression of both vimentin and cytokeratin 8/18 (Figure 4-2d) (Kenny et al., 2007).

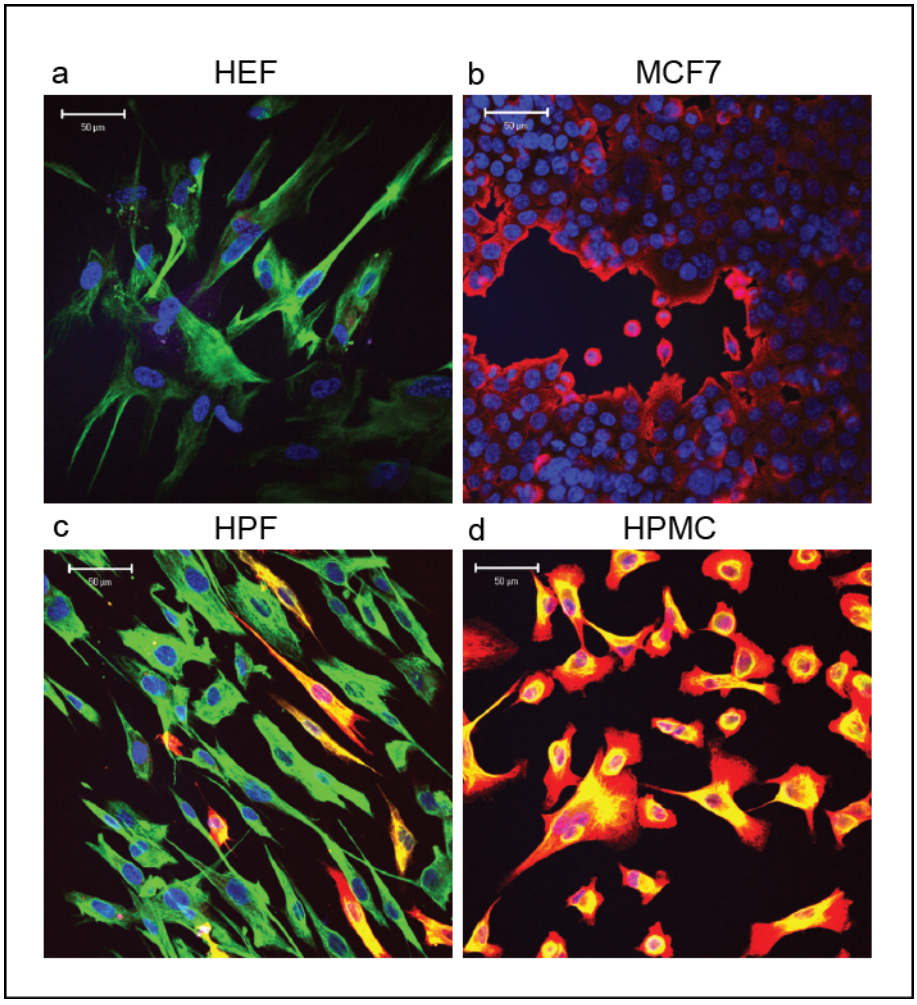

Figure 4-2 Molecular characterisation of human primary mesothelial cells and fibroblasts by Vimentin and Cytokeratin expression.

Immunofluorescence staining of cells cultured on glass cover slips. **a)** HEF **b)** MCF7 **c)** HPFs with contaminating HPMCs **d)** HPMC. Blue = Hoechst nuclear stain, Green = Vimentin, Red = Cytokeratin 8/18. 40x magnification, bar = 50 μm.

The percentage of vimentin and cytokeratin 8/18 positive cells was measured to determine the purity of a number of different cell populations taken from different patients (Figure 4-3). The cell populations were initially classified as HPF (Figure 4-3a) or HPMC (Figure 4-3b) by assessment of the cell morphology at confluency. On average the percentage of vimentin positive cells in the HPF populations was higher than the percentage of cytokeratin 8/18 positive cells (96.44% vimentin positive, st dev 4.834, 70.33% cytokeratin 8/18 positive, st dev 34.13, Mann-Whitney test p = 0.010), and the reverse

was true for the HPMC populations (75.67% vimentin positive, st dev 31.25, 98.54% cytokeratin 8/18 positive, st dev 2.975, Mann-Whitney test p = 0.009). However there were still a high number of cytokeratin 8/18 positive cells in the HPF populations (Figure 4-3a), suggestive that despite their mesenchymal morphology, a good proportion of these cells were epithelial cells. These may have been activated HPMCs. There are reports that HPMCs can differentiate into mesenchymal derived lineages (Lansley et al., 2010), and it is quite possible that their culture on plastic may initiate this. Likewise in the HPMC populations where the cells were supposed to be equally positive for both cytokeratin 8/18 and vimentin, there were a number of populations that expressed lower levels of vimentin (Figure 4-3b). In these particular cases the observed difference may have been indicative of contamination with other cells in the omentum with epithelial origins, such as endothelial cells or invading tumour cells.

In HPF and HPMC cell populations extracted from three different patients; G18, G20 and G34, the purity of the populations was determined with increasing passage number (Figure 4-3). In most cases the relative percentage of cytokeratin 8/18 positive cells declined and the percentage of vimentin positive cells increased. This may represent the differentiation of cells in culture as previously mentioned or the monopolisation of the culture with contaminating fibroblasts.

Absence of appropriate and specific cell surface markers for both the HPF and HPMCs meant that cell sorting by FACS or magnetic beads was not feasible for improving the purity of the cell populations. Given the reassurance that there was no significant difference between the vimentin expression in HPF versus HPMC populations (Mann-Whitney test p = 0.053) and the cytokeratin 8/18 expression was significantly higher in the HPMCs versus the HPFs (Mann-Whitney test p = 0.002) it was concluded that the best approach to using the primary cells in the 3D omental model would be to base the cell type on the cell

morphology at confluency. Experiments would be conducted primarily with the HEFs, and repeated with HPFs where possible.

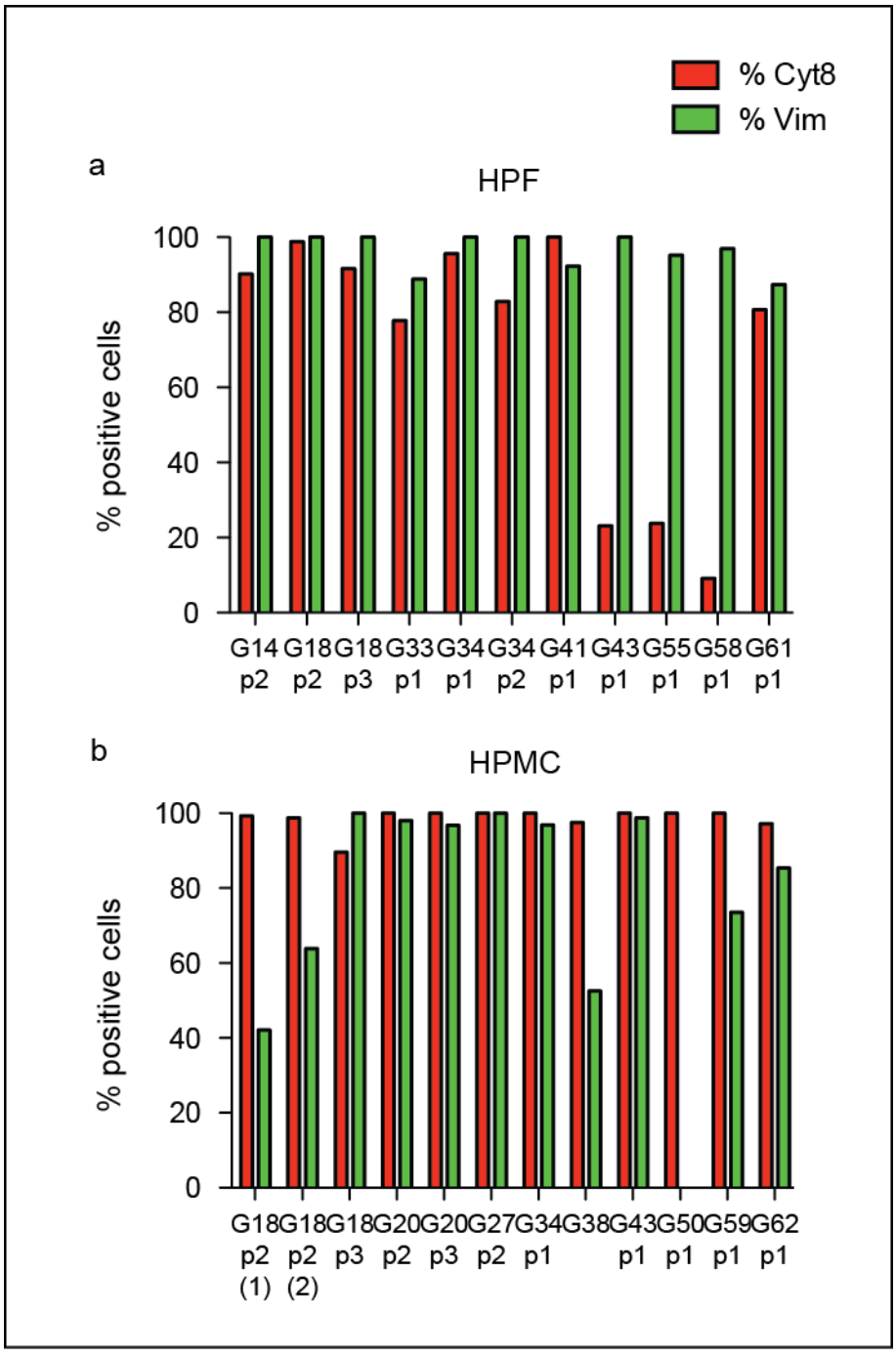

Figure 4-3 Assessment of human primary mesothelial cell and fibroblast culture purification determined by Vimentin and Cytokeratin expression.

Quantification of the percentage of cytokeratin 8/18 (red bars) and vimentin (green bars) positive cells in **a)** HPF and **b)** HPMC cultures from the omentum of different patients (G-coded) at varying culture passage numbers (p1-3). The number of positive stained cells was quantified from four fields of view at 40x magnification.

4.4. Optimisation of the growth of ovarian cancer cell lines on the 3D omental model

Kenny and colleagues maintained the 3D omental models in culture for up to five days. For this thesis long-term cultures of two weeks were developed to allow sufficient time for true tumour-stroma interactions and to better represent the established omental metastases of ovarian cancer. 24 well transwell inserts were utilised to maximise the number of experimental conditions that could be tested with limited numbers of primary cells.

The aim of this chapter was firstly to optimise the culture conditions for four ovarian cancer cell lines on the 3D omental model. Secondly the purpose of the experiments was to investigate the effects of the fibroblasts, the mesothelial cells and ascitic fluids on the growth and invasion of the ovarian cancer cell lines on the 3D omental model. For simplicity throughout this thesis, ‘K’ has been used to denote 1,000 cells where cell titrations have been performed.

These data collected in this chapter are summarised in the two tables below.

		Increase in growth		
Cell line	No. tumour cells	HEF/HPF	HPMCs	Ascitic fluids
AOCS1	200K	ns	10.5 p=0.002**	1.9 p=0.026*
SKOV3ip1	50K	ns	1.7 p=0.029*	ns
TOV21G	50K	No data	No data	No data
RMG1	50K	ns	ns	ns

Table 4-1 Table summarising the growth of ovarian cancer cell lines on the 3D omental model

The ovarian cancer cell lines AOCS1, SKOV3ip1, TOV21G and RMG1 were cultured on the 3D omental model for two weeks. The number of ovarian cancer cells (K=1000) seeded on the model was optimised for each cell line. The effect of increasing numbers of HEFs, HPFs and HPMCs as well as the presence of ascitic fluids was assessed on ovarian cancer cell growth. No data were available for cell lines that did not grow collectively on the surface of the model. Statistically significant fold changes in growth are denoted with the associated p-values. ns = not significant.

	Increase in invasion		
Cell line	HEF/HPF	HPMCs	Ascitic fluids
AOCS1	No data	No data	No data
SKOV3ip1	ns	From zero to 61.8 p=0.027*	5.3 p=0.032*
TOV21G	534.9 p=0.035*	1466.5 p=0.0004***	ns
RMG1	No data	No data	No data

Table 4-2 Tables summarising the invasion of ovarian cancer cell lines in the 3D omental model

The ovarian cancer cell lines AOCS1, SKOV3ip1, TOV21G and RMG1 were cultured on the 3D omental model for two weeks. The effect of increasing numbers of HEFs, HPFs and HPMCs as well as the presence of ascitic fluids was assessed on ovarian cancer cell invasion. No data were available for cell lines that were non-invasive. Statistically significant fold changes in invasion are denoted with the associated p-values. ns = not significant

.

The number of each of the ovarian cancer cell lines to be seeded on to the 3D omental models was first optimised (Table 4-1).

To measure growth, confocal or brightfield images were taken across the expanse of the cross-section of each 3D omental model. The average area covered by the tumour cells in the images was calculated using the image-processing program ImageJ.

4.4.1. Statistical analyses of data

To analyse these data where there were two test conditions, a non-parametric Mann-Whitney test (two-tailed) was applied. Due to the intra-experimental variation given by the impurity of primary cell cultures, a parametric distribution of these data could not be assumed.

To compare more than two given test conditions a non-parametric Kruskal-Wallis One-Way Analysis of Variance (ANOVA) was utilised (as advised by Dr Shah-Jalal Sarker, Lecturer in Biostatistics, Barts Cancer Institute). The One-Way ANOVA test reduces the potential for generating false positive results (Type I error) that would occur through applying multiple t tests across a single data set. A 95% confidence interval was applied for the calculation of all p values and a Dunns post-test was used to compare all experimental conditions following the Kruskal-Wallis test.

Each experiment was conducted with primary mesothelial cells extracted from patient samples. Intratumoral heterogeneity and patient differences for example, age (Table 3-1), proliferative capacity of tumour bulk (Figure 3-8 & 3-11), and response to chemotherapy etc, created significant variation between samples. This generated huge inter-experimental variation, and so actual values from one experiment could not be collated with the repeated experiment for statistical

analysis. Therefore each measurement was normalised to the average of the control measurements for each experiment. These values across repeated experiments were pooled for statistical analyses.

4.4.2. The effect of fibroblasts on the growth of ovarian cancer cell lines on the 3D omental model

Within a tumour microenvironment fibroblasts are recruited and activated to secrete an abundance of chemotactic and growth factors (Bhowmick et al., 2004). Therefore the effect of these fibroblasts on ovarian cancer cell growth and invasion in the 3D omental model was investigated.

There was no significant increase in ovarian cancer cell growth with increasing numbers of fibroblasts (Table 4-1).

4.4.3. The effect of mesothelial cells on the growth of ovarian cancer cell lines on the 3D omental model

Mesothelial cells are the first line of contact for metastasising HGSC cells. It was therefore asked whether HPMCs would influence the growth of the ovarian cancer cell lines on the 3D omental model. Figure 4-4 shows H & E photographs of the 3D omental model cross sections, when the HGSC cell line AOCS1 was grown with increasing numbers of HPMCs. There was a significant increase ($p = 0.002$) in ovarian cancer cell growth as the number of HPMCs increased from 0 to 40,000 (Figure 4-4a, b & c) followed by a slight drop in growth where 80,000 HPMCs were seeded (Figure 4-4d & e). This drop is perhaps indicative of the HPMCs eliciting too much of a defensive barrier for the tumour cells to break for attachment to the underlying ECM.

It has been reported that the tumour cells can induce contractile forces within the HPMCs via integrin and talin signalling which drives clearance of the HPMCs away from the invading tumour cells, so that they can

access the underlying matrix (Iwanicki et al., 2011). It is clear that these cell-cell interactions are critical in activating the signalling cascades necessary for tumour cell metastasis to the omentum, and this proved to be modelled in the 3D omental co-culture system. It was concluded that 40,000 HPMCs (Figure 4-4c) would be used in future experiments to maximise these cell-cell interactions, without exhibiting the potential to block tumour cell attachment with as many as 80,000 HPMCs (Figure 4-4d & e). Additionally, the numbers of HPFs and HPMCs used in experiments were kept as low as possible because of their limited supply.

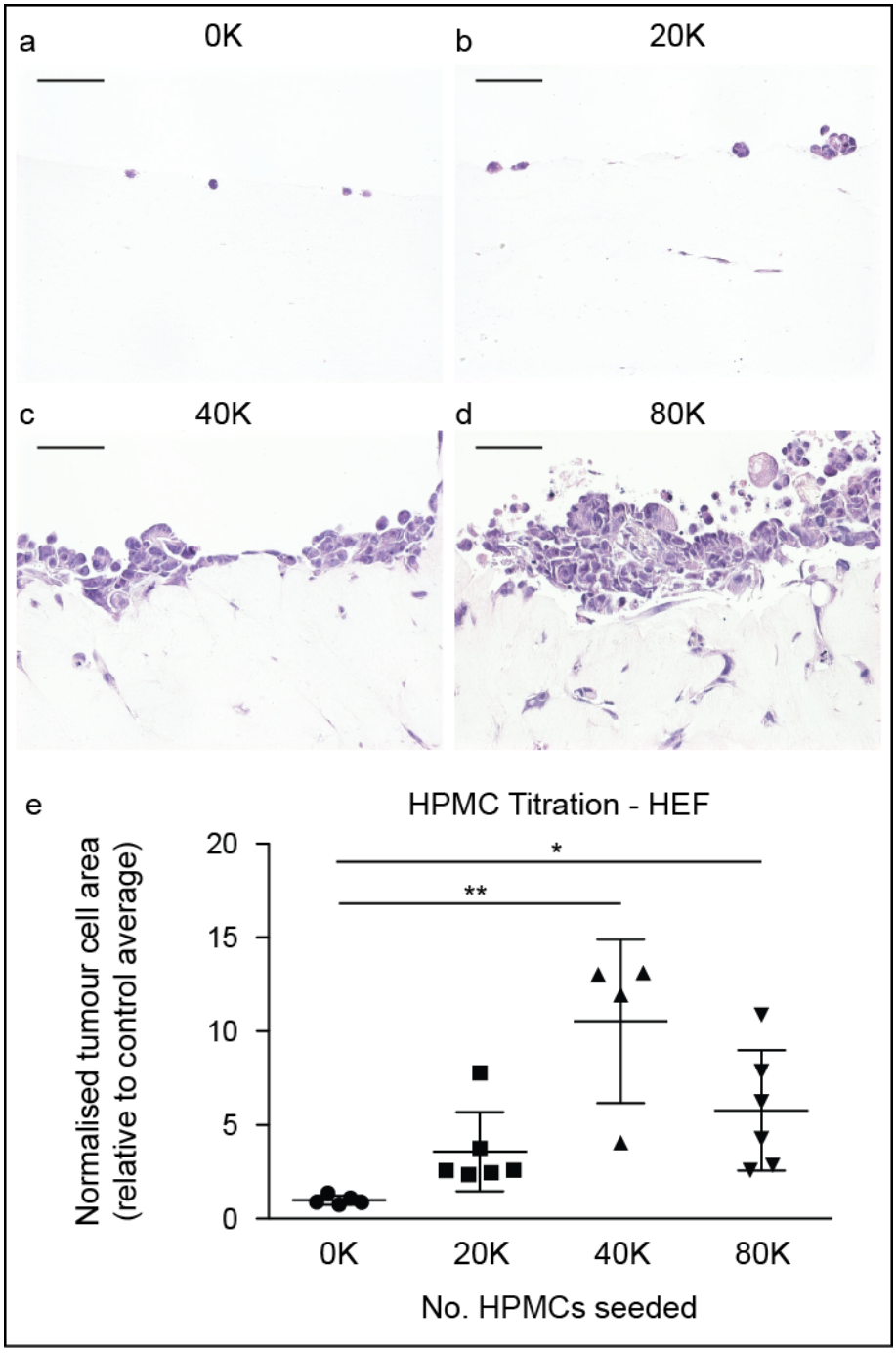

Figure 4-4 The effect of increasing numbers of HPMCs on the growth of the ovarian cancer cell line AOCS1 on the 3D omental model.

The ovarian cancer cell line AOCS1 was cultured on the 3D omental model for two weeks. Representative H & E stained images of 5 μm thick cross sections of the 3D models when **a)** 0K, **b)** 20K, **c)** 40K and **d)** 80K HPMCs were grown on each model. 20x magnification, bar = 100 μm. **e)** Graph illustrating the growth of the AOCS1 cells in the presence of increasing numbers of HPMCs and co-cultured with HEFs. Photographs of H & E stained sections were taken across the whole section of each model. Each treatment group was tested with triplicate models. The tumour area (μm^2) on each photograph was quantified as a measure of tumour growth. Bars indicate the means and standard deviations across all measurements. Collective data from two experiments. p = 0.002**

Similarly, increasing numbers of HPMCs within the 3D omental culture model had a significant effect (p = 0.029) on the growth of the ovarian cancer cell line SKOV3ip1 when co-cultured with HEFs (Figure 4-5). There was no significant increase in the growth of the RMG1 ovarian cancer cell line with increasing HPMCs. No data were collected on the growth of the TOV21G cells since they were invasive in the model and did not grow on the surface of the model as the other three cell lines did (Table 4-1).

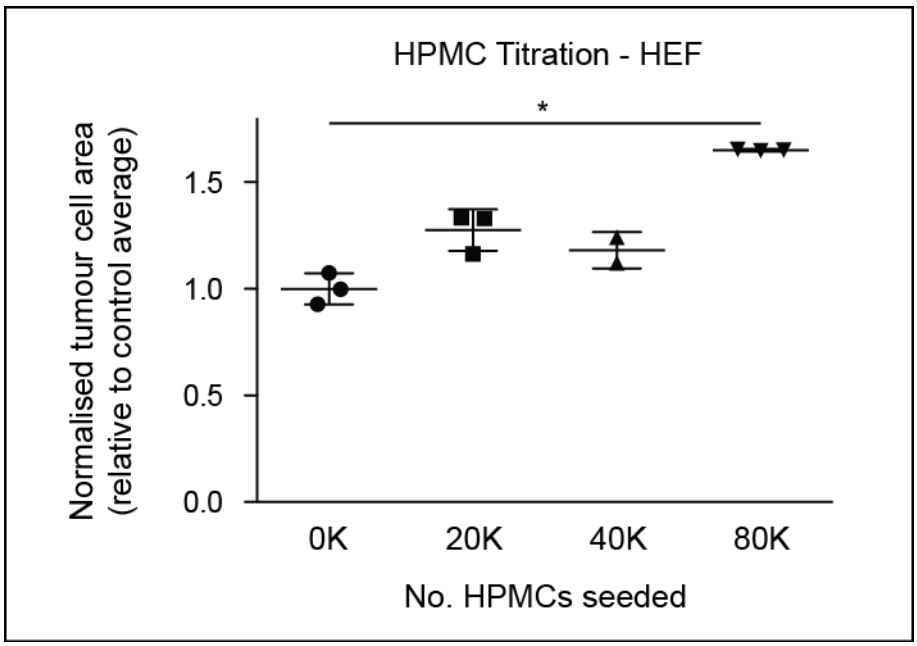

Figure 4-5 The effect of increasing numbers of HPMCs on the growth of the ovarian cancer cell line SKOV3ip1 on the 3D omental model.

Graph illustrating the growth of the ovarian cancer cell line SKOV3ip1 in the presence of increasing numbers of HPMCs and co-cultured with HEF. Tumour cells were cultured on the 3D omental model containing zero to 80K HPMCs for two weeks. Photographs of H & E stained sections were taken across the whole section of each model. Each treatment group was tested with triplicate models. The tumour area (μm^2) on each photograph was quantified as a measure of tumour growth. Bars indicate the means and standard deviations across all measurements. Data from one experiment. p = 0.029*

4.4.4. The effect of ascitic fluids on the growth of ovarian cancer cell lines on the 3D omental model

Ascites is an excessive production of peritoneal fluids produced in response to the developing tumour. Ascitic fluid is drained from patients prior to surgery and the fluid carries metastatic free-floating tumour cells and immune cells. The fluid also contains a host of growth factors (Mills et al., 1990) and pro-inflammatory cytokines (Moradi et al., 1993). To further mimic the microenvironment of omental metastases within the 3D cell culture model, I set out to test the effect of ascitic fluid on the growth of the tumour cells in the model. Experiments were conducted with pooled ascitic fluid from six patients and with low numbers (20,000 per model) of HPMCs so that conditions were sub-optimal.

Figure 4-6 shows these data collected when the ovarian cancer cell line AOCS1 was co-cultured on the 3D omental model, and the serum-free medium in the top compartment of the transwell was substituted with 50% ascitic fluid. The ascitic fluids caused a significant increase in tumour growth ($p = 0.026$).

Figure 4-7 illustrates the effect of the ascitic fluid on the growth of the AOCS1 3D omental models together with a titration in HPMC numbers. There was a trend increase (data not statistically significant) in tumour growth with lower numbers of HPMCs, but when this was increased beyond 40,000 HPMCs per well, the growth of the AOCS1 ovarian cancer cells was reduced (data not statistically significant) in the presence of ascitic fluid. It is possible that the ascitic fluid may have been a source of cellular waste products from carrying the free-floating malignant cells and immune cells within the peritoneal cavity. This in the presence of increasing numbers of cells in the cultures may result in the concentration of the cellular waste products becoming toxic for cell growth.

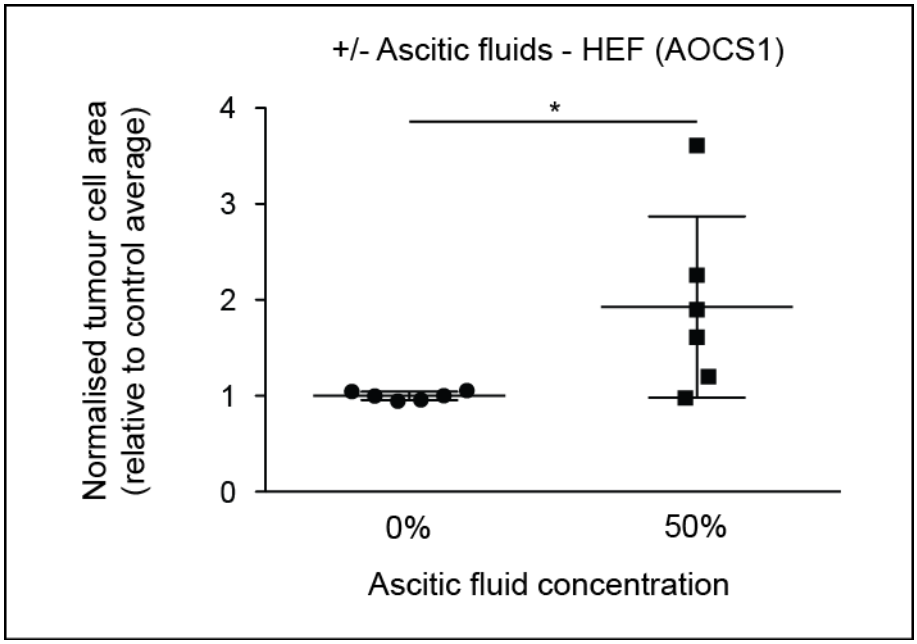

Figure 4-6 The influence of ascitic fluid on the growth of the ovarian cancer cell line AOCS1 on the 3D omental model.

Graph illustrating the growth of the ovarian cancer cell line AOCS1 in the absence and presence of human ascitic fluid. Co-cultured with HEFs, tumour cells were cultured on the 3D omental model for two weeks. Photographs of H & E stained sections were taken across the whole section of each model. Each treatment group was tested with triplicate models. The tumour area (μm^2) on each photograph was quantified as a measure of tumour growth. Bars indicate the means and standard deviations across all measurements. Collective data from three experiments. p = 0.026*

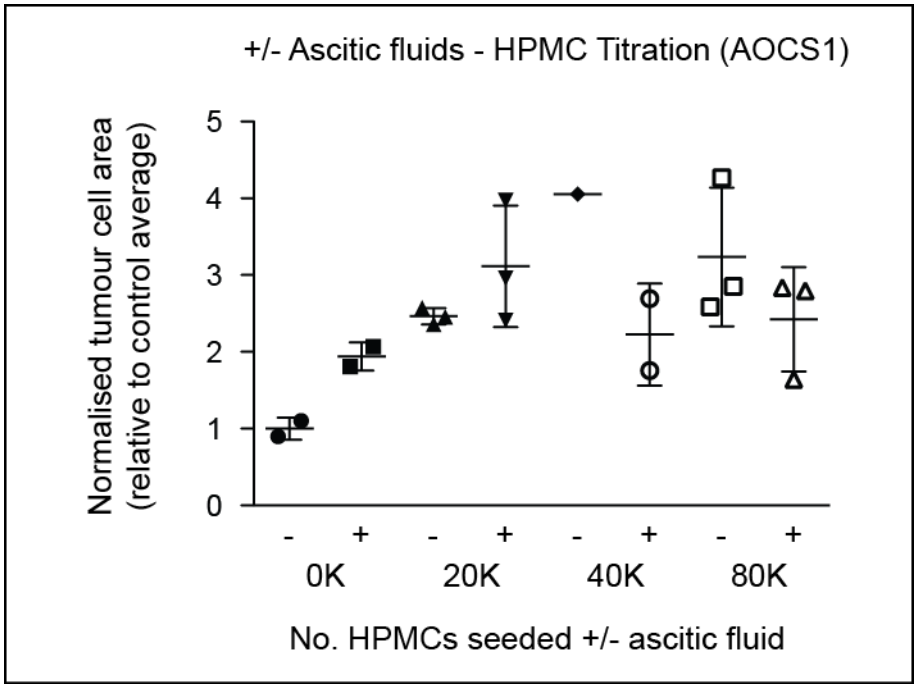

Figure 4-7 The influence of ascitic fluid together with the HPMCs on the growth of the ovarian cancer cell line AOCS1 on the 3D omental model.

Graph illustrating the growth of the ovarian cancer cell line AOCS1 in the absence and presence of human ascitic fluid when co-cultured with HEFs and increasing numbers of HPMCs from zero to 80K. Tumour cells were cultured on the 3D omental model for two weeks. Photographs of H & E stained sections were taken across the whole section of each model. Each treatment group was tested with triplicate models. The tumour area (μm^2) on each photograph was quantified as a measure of tumour growth. Bars indicate the means and standard deviations across all measurements. Data from one experiment. Data not statistically significant.

The growth of the ovarian cancer cell line SKOV3ip1 on the 3D omental model was not significantly altered when treated with ascitic fluid (Figure 4-8).

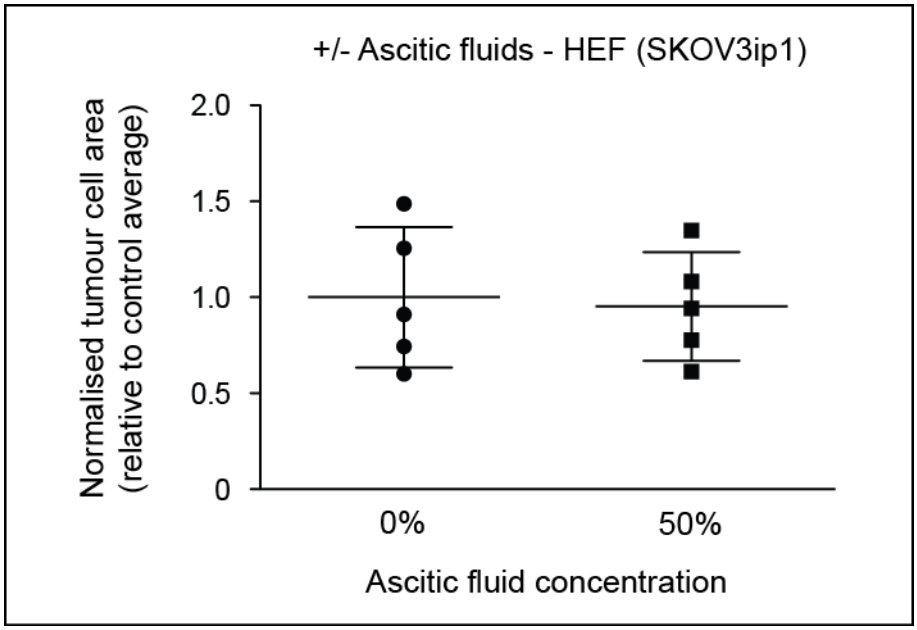

Figure 4-8 The influence of ascitic fluid on the growth of the ovarian cancer cell line SKOV3ip1 on the 3D omental model.

Graph illustrating the growth of the ovarian cancer cell line SKOV3ip1 in the absence and presence of human ascitic fluid and co-cultured with HEFs. Tumour cells were cultured on the 3D omental model for two weeks. Photographs of H & E stained sections were taken across the whole section of each model. Each treatment group was tested with triplicate models. The tumour area (μm^2) on each photograph was quantified as a measure of tumour growth. Bars indicate the means and standard deviations across all measurements. Collective data from two experiments. Data not statistically significant.

Similarly, there was no significant increase in the growth of the RMG1 ovarian cancer cell line in the presence of ascitic fluid. Again, no data were collected on the growth of the TOV21G cells since they were invasive in the model and did not grow on the surface of the model as the other three cell lines did (Table 4-1).

Overall it was concluded that higher numbers of HPMCs in the 3D omental model were advantageous with regard to the cell-cell and cell-matrix interactions. The presence of ascitic fluids under these conditions

did not consistently promote ovarian cancer cell growth on the model (Table 4-1). For future work it would perhaps be beneficiary to titrate the ascitic fluid concentration in the 3D omental model to better investigate its impact on tumour cell growth. It is possible that lower concentrations would reduce the toxicity of the cellular waste products present in the cultures, but would have enough cytokines and growth factors to stimulate proliferative signalling pathways and promote tumour cell growth.

4.5. Optimisation of the invasion of ovarian cancer cell lines in the 3D omental model

Invasion is a complex process. Conditions within the tumour microenvironment regulate a plethora of cell-matrix and cell-cell interaction proteins to allow the migration of the tumour cells through the surrounding ECM (Friedl and Alexander, 2011). Fibroblasts and TAMs release chemokines and growth factors that form gradients to which the corresponding receptors on the surface of the tumour cells are responsive to (Schioppa et al., 2003) (Bonecchi et al., 2011). MMP production by the tumour cells, fibroblasts and TAMs facilitates the remodelling of the surrounding ECM structures to develop tracks for tumour cell migration (Hagemann et al., 2005; Pollard, 2008). Dependent upon the pattern of ECM remodelling and cell-matrix interactions, tumour cells can either invade collectively or as single cells (Friedl and Gilmour, 2009; Friedl and Wolf, 2010). This is mediated by Rho and Rac signalling pathways that regulate the dynamics of the cell cytoskeleton, and which can induce either an amoeboid or mesenchymal form of migration (Sanz-Moreno and Marshall, 2010).

Nystrom and colleagues developed a method of image analysis for quantifying invasion in 3D organotypic models which incorporates the growth, depth and dissemination of the invasion within the model (Nystrom et al., 2005). The output is an invasion index which taken from

the images analysed is an arbitrary factor of the tumour cell area, the average invasion depth, and the number of invading particles. Therefore the common component between the measurements of tumour growth and invasion used in this thesis is the tumour cell area, and those distinguishing them are the measurements of the number of invading particles and the invasion distance. I applied this method of analysis to the 3D omental model. Of the four cell lines tested, only the ovarian cancer cell lines SKOV3ip1 and TOV21G showed invasion into the matrix of the model (Figure 4-9, Figure 4-11, Table 4-2).

Given the known role of cancer-associated fibroblasts in promoting tumour cell invasion (Wan et al., 2013), the effect of increasing the number of fibroblasts in the 3D omental model was tested on the invasive capacity of the ovarian cancer cell line SKOV3ip1. Increasing the number of fibroblasts in the 3D omental model had no significant effect on the invasion of the tumour cells (Table 4-2).

Interestingly however tumour cell invasion increased ($p = 0.027$) when the ovarian cancer cell line SKOV3ip1 were co-cultured in the 3D omental model with increasing numbers of HPMCs. Figure 4-9 illustrates the collective cell invasion exhibited by the green fluorescent protein (GFP)-labelled SKOV3ip1 cells in the model. It is clear that there was no tumour cell invasion in the absence of HPMCs (Figure 4-9), but there was a significant ($p = 0.027$) increase in invasion in the presence of 80,000 HPMCs (Figure 4-9b – e). This result reinforced the importance of tumour cell interactions with the HPMC layer to allow invasion into the underlying matrix as described in section 4.4.3.

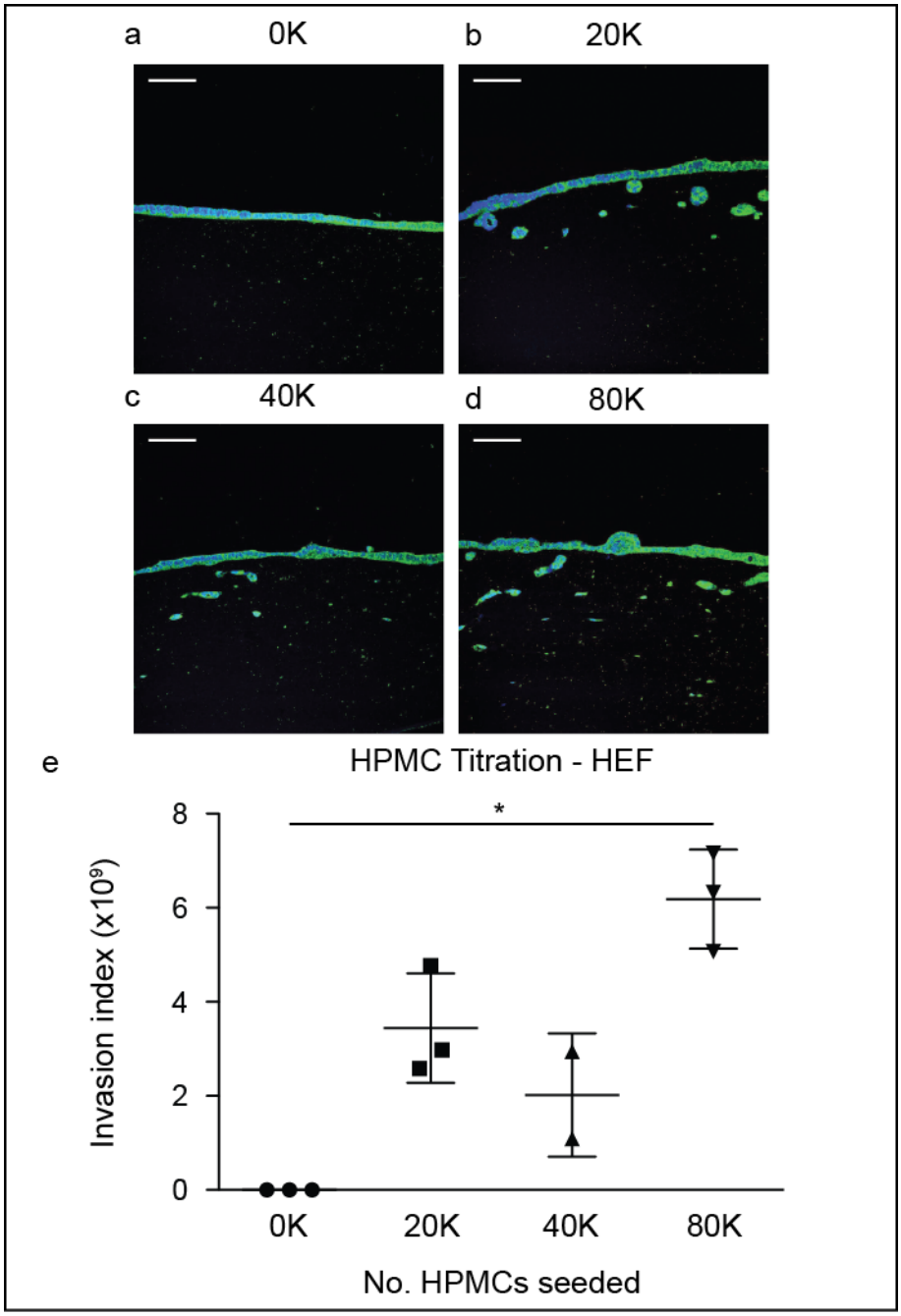

Figure 4-9 The effect of increasing numbers of HPMCs on the invasion of the ovarian cancer cell line SKOV3ip1 in the 3D omental model.

The GFP labelled human ovarian cancer cell line SKOV3ip1 was cultured on the 3D omental model for two weeks. Representative immunofluorescence images of 5 μm thick cross sections of the 3D models when **a)** 0K, **b)** 20K, **c)** 40K and **d)** 80K HPMCs were grown on each model. Blue = Hoechst nuclei stain, Green = GFP. 20x magnification, bar = 200 μm. **e)** Graph illustrating the invasion index of the SKOV3ip1 cells in the presence of increasing numbers of HPMCs and co-cultured with HEFs. Photographs of immunofluorescence stained sections were taken across the whole section of each model. Each treatment group was tested with triplicate models. The invasion index is a factor of the number of invading particles, tumour area (μm^2) and invasion distance (μm). Bars indicate the means and standard deviations across all measurements. Data from one experiment. p = 0.027*

Despite the ascitic fluid treatment having no effect on tumour growth in the SKOV3ip1 3D omental models (Figure 4-8), it did cause a significant increase ($p = 0.032$) in tumour cell invasion (Figure 4-10). This highlighted how tumour growth and tumour cell invasion are independent of one another, but also proved the strength of the model where both processes can be monitored simultaneously.

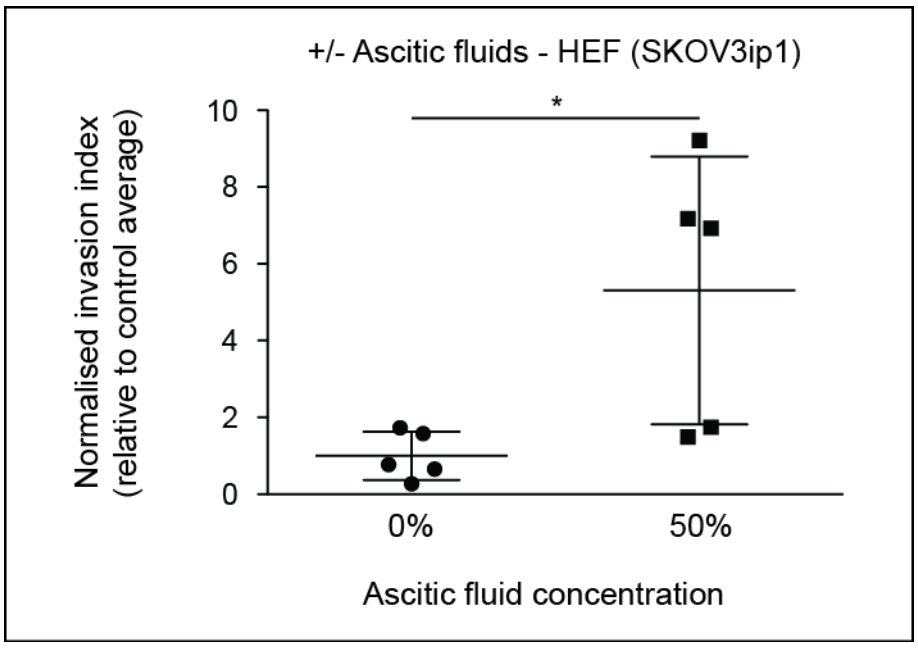

Figure 4-10 The influence of ascitic fluid on the invasion of the ovarian cancer cell line SKOV3ip1 in the 3D omental model.

Graph illustrating the invasion index of the ovarian cancer cell line SKOV3ip1 in the absence and presence of human ascitic fluid and co-cultured with HEFs. Tumour cells were cultured on the 3D omental model for two weeks. Photographs of immunofluorescence stained sections were taken across the whole section of each model. Each treatment group was tested with triplicate models. The invasion index from each photograph was determined. The invasion index is a factor of the number of invading particles, tumour area (μm^2) and invasion distance (μm). Bars indicate the means and standard deviations across all measurements. Collective data from two experiments. $p = 0.032$*

Conversely to the SKOV3ip1 cells, the ovarian cancer cell line TOV21G displayed the single-cell invasion in the 3D omental model, which is illustrated in Figure 4-12. Increasing the number of HPFs co-cultured in the model (Figure 4-11) caused a significant increase ($p = 0.035$) in TOV21G cell invasion.

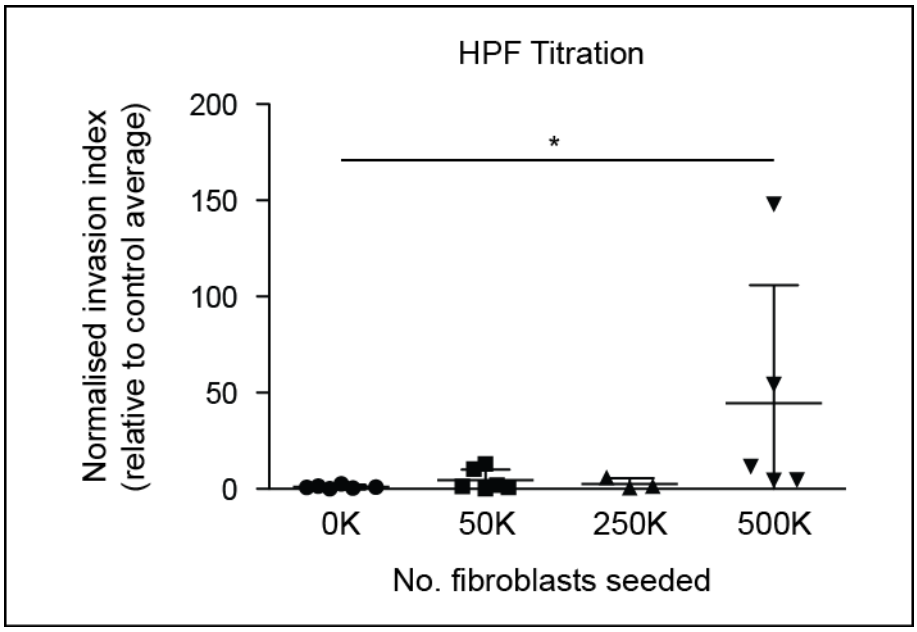

Figure 4-11 The effect of increasing numbers of fibroblasts on the invasion of the ovarian cancer cell line TOV21G in the 3D omental model.

Graph illustrating the invasion index of the ovarian cancer cell line TOV21G in the presence of increasing numbers of HPFs. Tumour cells were cultured on the 3D omental model containing zero to 500K HPFs for two weeks. Photographs of immunofluorescence stained sections were taken across the whole section of each model. Each treatment group was tested with triplicate models. The invasion index from each photograph was determined. The invasion index is a factor of the number of invading particles, tumour area (μm^2) and invasion distance (μm). Bars indicate the means and standard deviations across all measurements. Collective data from two experiments. $p = 0.035$*

Increasing the numbers of HPMCs co-cultured in the 3D omental model with the ovarian cancer cell line TOV21G also reproducibly caused an increase ($p = 0.0004$) in tumour cell invasion (Figure 4-12). The most significant promotion of invasion was observed when 80K HPMCs were co-cultured in the 3D omental model (Figure 4-12d & e). There were really no signs of invasion in the absence of these cells (Figure 4-12a & e).

The effect of ascitic fluid on TOV21G cell invasion was inconclusive (Table 4-2).

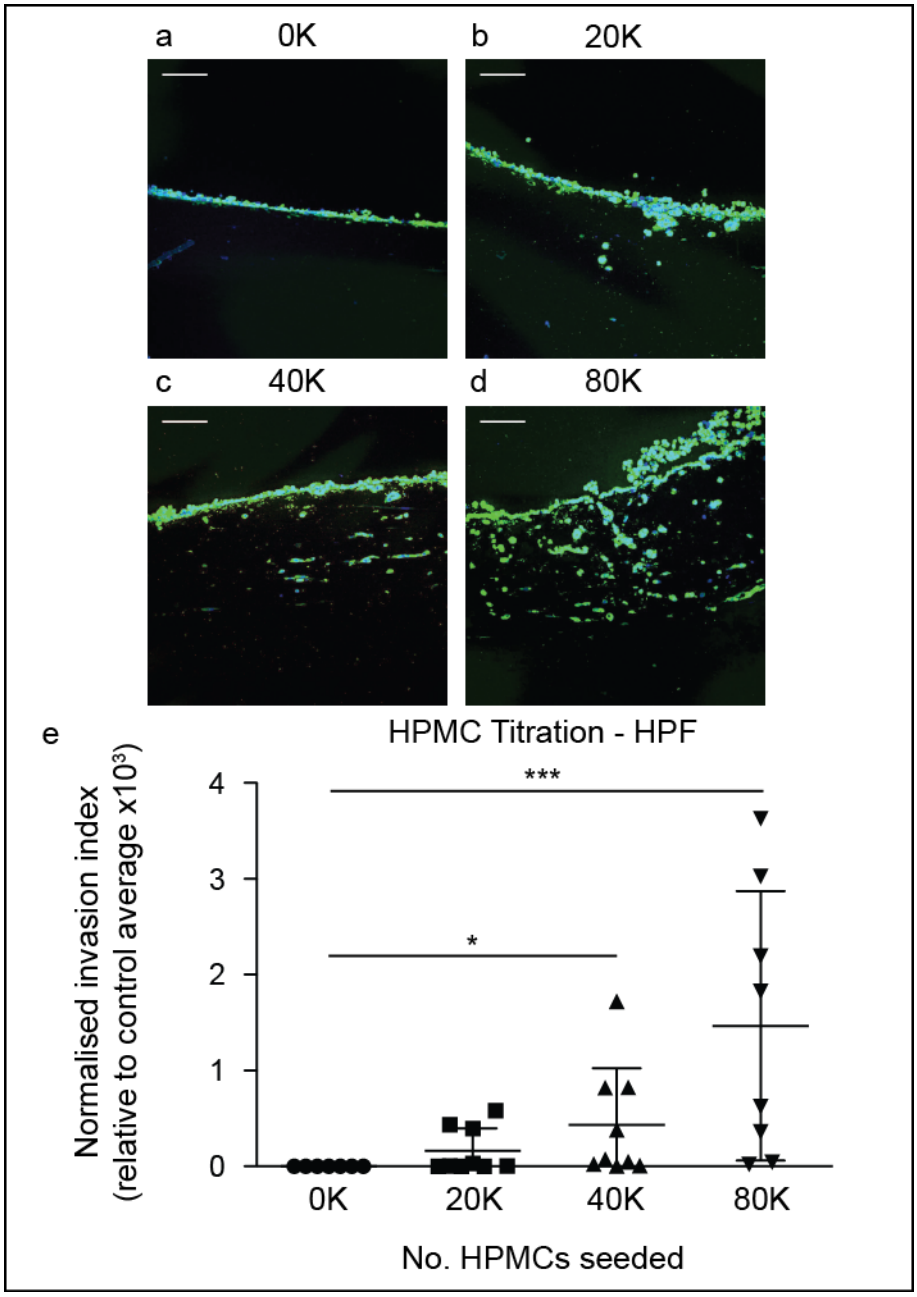

Figure 4-12 The effect of increasing numbers of HPMCs on the invasion of the ovarian cancer cell line TOV21G in the 3D omental model.

The GFP labelled human ovarian cancer cell line TOV21G cultured on the 3D omental model for two weeks. Representative immunofluorescence images of 5 μm thick cross sections of the 3D models when **a)** 0K, **b)** 20K, **c)** 40K and **d)** 80K HPMCs were grown on each model. Blue = Hoechst nuclei stain, Green = GFP. 20x magnification, bar = 200 μm. **e)** Graph illustrating the invasion index of the TOV21G cells in the presence of increasing numbers of HPMCs and co-cultured with HPFs. Photographs of immunofluorescence stained sections were taken across the whole section of each model. Each treatment group was tested with triplicate models. The invasion index is a factor of the number of invading particles, tumour area (μm^2) and invasion distance (μm). Bars indicate the means and standard deviations across all measurements. Collective data from three experiments. p = 0.0004***

4.6. Concluding remarks

4.6.1. Summary of the growth and invasion of ovarian cancer cell lines in the 3D omental model

4.6.1.1. Primary cell characterisation

Cultures of HPFs and HPMCs from several patients have been characterised by cytokeratin 8/18 and vimentin expression. The HPF populations contained a high percentage of cytokeratin 8/18 positive cells. The original publication for the establishment of the 3D omental model distinguished between the HPFs and HPMCs by the expression of the collagen synthesising enzyme prolyl-hydroxylase. They did not however show that their HPF populations were negative for cytokeratin 8/18 ((Kenny et al., 2007) and it can be argued that describing isolated fibroblasts only by their ability to produce collagen is insufficient. Due to the lack of specific cell surface markers to separate the two cell populations however, and due to the low cell yields, it was deduced that the most efficient means of identifying the cells would be by examining cell morphology at confluency. Arguably the potential for activated HPMCs to differentiate in to mesenchymal cells (Lansley et al., 2010) suggested that cell morphology was perhaps also not the best method for distinguishing the primary cell types. This in essence was the reason for predominantly performing experiments with the non tumour-associated HEFs.

4.6.1.2. Longevity of culture

3D omental cell culture models of a group of four ovarian cancer cell lines have been established. Previously no laboratories had cultured ovarian cancer cells on the model for longer periods than five days, but for this thesis the malignant cells were grown on the 3D model for at

least 14 days. Other publications describing work with this particular model (Cai et al., 2012; Kenny et al., 2008; Kenny et al., 2007; Zillhardt et al., 2011) only culture the models for 72 hours to study early tumour cell adhesion and invasion events. For the purpose of this thesis it was important to establish a long-term cell culture model that increases the interactions between the tumour cells and the cells of the tumour microenvironment. This was successfully done.

4.6.1.3. Tumour cell line variations

The optimal number of each of the ovarian cancer cell lines to be seeded on the 3D omental model for growth and invasion was established (Table 4-1). There was a significant level of variation in the pattern of growth and invasion in the 3D omental model between ovarian cancer cell lines. For example the TOV21G cell line demonstrated a single cell invasion pattern where as the SKOV3ip1 cells demonstrated collective cell invasion. The AOCS1 and RMG1 cell lines did not invade at all. The TOV21G cells were confirmed to be representative of the CCC subtype of ovarian cancer (Anglesio et al., 2013; Domcke et al., 2013). CCC is characterised by increased activation of cytokine, oxidative stress and hypoxia driven pathways, as well as the PI3K pathway (Jones et al., 2010), all of which may support the survival of single cells disseminated in a matrix. Comparably the SKOV3ip1 cells may not have an enrichment in these survival signalling pathways and therefore require more cell: cell contact for survival in a novel environment, encouraging them to invade collectively.

4.6.1.4. Fibroblasts

Fibroblasts had no effect on the growth of the tumour cells on the model as measured by tumour area, but the fibroblasts stimulated the invasion of the ovarian cancer cell line TOV21G. The release of chemokines, growth factors and MMPs from fibroblasts in the collagen matrix was

likely to be responsible for this stimulated invasion. 50,000 cells per model were optimal for cell growth, but 250,000 cells were optimal for invasion.

4.6.1.5. Mesothelial cells

Mesothelial cells were important for both the growth and invasion of ovarian cancer cell lines on the model. Induced HPMC contractility and clearance on the surface of the omentum by metastasising tumour cells has been reported to allow tumour cell access to the underlying matrix (Iwanicki et al., 2011). The HPMC titrations in the 3D omental model reinforced the importance of this cell: cell contact for tumour cell metastasis to the omentum, however excessive numbers of HPMCs in the co-culture also highlighted their capacity to form a physical defensive barrier to invading cells or pathogens from the peritoneal cavity. 40,000 cells per model were optimal for cell growth and invasion.

4.6.1.6. Ascitic fluid

Ascitic fluid from HGSC patients could stimulate the growth and invasion of the ovarian cancer cell lines in the model, but had minimal effect in the presence of more HPMCs. Ascitic fluid is rich in growth factors and inflammatory cytokines that potentially supported pro-survival signalling in the tumour cells, particularly in cells that displayed low autocrine inflammatory cytokine signalling. Cytokine signalling has been shown to stimulate cell contractility via the JAK (Janus kinase) pathway (Sanz-Moreno et al., 2011), which may have potentially attributed to the increase in tumour cell invasion in the 3D omental model in the presence of ascitic fluid. It was also possible that any detrimental effects of ascitic fluid on tumour cell growth and invasion observed was a consequence of an increased localised concentration of cellular waste products in the co-culture system.

4.6.2. Overall scope for 3D omental model development

One of the strengths of the 3D omental model was its ability to subject the tumour cells to a multicellular microenvironment, where the stromal cells were sourced from the actual human tissue that it set out to mimic. It was multi-dimensional and offered potential to assess several processes simultaneously, such as tumour cell adhesion, growth and invasion. There are multiple signaling pathways that regulate these processes (Hanahan and Weinberg, 2011). PI3 kinase and Akt signaling mediate tumour cell adhesion and survival. Growth factor signaling activates the MAP kinase pathway supporting cell proliferation. Tumour cell invasion is associated with EMT, which can also be stimulated by growth factor signaling. The reported interactions between CSF1 and EGF signaling promoting breast cancer invasion is an example of the role of growth factor signaling in tumour cell invasion (Boimel et al., 2012). Similarly the cytokine activated JAK-STAT3 signaling pathway promotes both proliferation and invasion (Coward et al., 2011; Sanz-Moreno et al., 2011). Therefore therapeutic agents that target these signaling pathways are desirable since they affect multiple processes involved in cancer progression. The 3D omental model would be an ideal model for testing these therapeutic agents since these processes can be measured concurrently.

Both RNA and protein could be extracted from the 3D omental models for qRT-PCR and western blot analysis respectively. Once cells had been cultured in the model they could also be re-extracted from the collagen matrix with collagenase treatment and separated by FACS for further analysis. Hence the model could be applied to studies into the effect of the tumour cells on the stroma and vice versa.

The normal omentum can be described as a fatty pad of tissue that lies from the stomach and over the bowels. Nieman el at (Nieman et al., 2011) recently described how the monopolisation of the adipocyte-rich tissue by the invading tumour cells is stimulated by adipokines such as

IL-8, and how the direct transfer of lipids from the adipocytes to the tumour cells provides the tumour cells with an energy source for proliferation. This suggests that the adipocytes in the omentum are a key cellular component in driving HGSC metastasis to this site. Communications with Prof Ernst Lengyel revealed that omentum sourced adipocytes have now been introduced to the established 3D omental cell culture model.

This highlights the most exciting challenge for the development of this 3D omental model. The tumour microenvironment contains many different cell types (Balkwill et al., 2012), including the malignant cells, the immune cells, fibroblasts, mesenchymal stem cells and endothelial cells. Incorporating additional cell types in the 3D omental model will bring the microenvironment even closer to the microenvironment found *in vivo*, which will not only reduce the need for animal experiments, but will generate results that will recapitulate the disease situation in patients with greater accuracy.

4.6.3. Conclusion

The major clinical problem with HGSC is late stage diagnosis and presentation with heavily spread tumour burden throughout the peritoneal cavity. Research into earlier diagnosis is critical, however difficult when patients are rarely seen at an early stage. There is therefore a demand for models to study the early events in HGSC metastasis. The 3D omental model has already proved its worth in studying these early events (Kenny et al., 2008) and may lead to improved therapies to reduce tumour cell attachment to areas of the peritoneal lining. Combinational therapies are though also critical when targeting HGSC. Cells that might become resistant to a single line of therapy may still colonise the peritoneal lining and develop to form significantly sized metastatic deposits. The fibroblasts and mesothelial cells are of course present at the early stages of HGSC metastasis, but

as the deposits develop there is an influx of infiltrating inflammatory cells (Leinster et al., 2012).

The aim of the next chapter was to use the 3D omental model to study the role of the chemokine CXCL12 in the development of metastatic deposits of ovarian cancer. Following this the accompanied influx of macrophages was further modelled and investigated within the *in vitro* system established in this chapter.

Chapter 5

5. Using the 3D omental model to test the efficacy of a neutralising antibody targeting CXCL12

Collaborative work with John McCafferty in Cambridge as a part of a Cancer Research UK Discovery committee grant provided our lab with an antibody, denoted 114_3H1 that targeted human CXCL12. The role of the CXCR4/CXCL12 signalling pathway in ovarian cancer is well established (Kulbe et al., 2012). CXCR4 signalling has been shown to promote tumour cell proliferation, survival and migration (Balkwill, 2004; Scotton et al., 2001; Scotton et al., 2002). These cellular responses can be measured in the established 3D omental model as described in chapter 4. Therefore I used this 3D omental model to test the efficacy of the antibody and the targeting of this pathway in ovarian cancer metastasis.

5.1. CXCL12 expression in the 3D omental model

The levels of secreted CXCL12 in the supernatant of the 3D omental models were measured by ELISA. The supernatants of the 3D omental models were collected and the models were fixed after two weeks in culture. The number of positive hematoxylin nuclear stained cells in each section was quantified using a computer-operated microscope and the Leica Ariol software, as previously described in chapter 3. These hematoxylin nuclear cell counts were then used as reference figures for normalisation of CXCL12 concentrations in the supernatant relative to one million cells (Figure 5-1).

These data collected showed that higher levels of CXCL12 were secreted from the SKOV3ip1 and TOV21G ovarian cancer cell lines on

the 3D omental model than the AOCS1 and RMG1 ovarian cancer cell lines (Figure 5-1). Interestingly these two cell lines were the most invasive of the four tested in the 3D omental model. When the ovarian cancer cells were cultured on plastic, negligible levels of CXCL12 can be detected from the supernatants (data not shown).

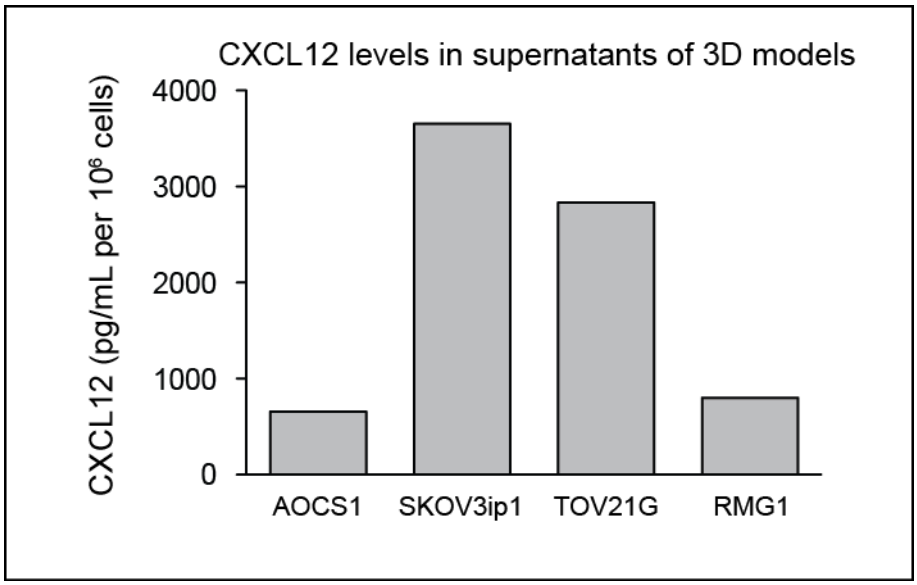

Figure 5-1 CXCL12 levels in the 3D omental model supernatants

Quantification of CXCL12 levels in cell culture supernatants measured by ELISA. CXCL12 concentrations (pg/mL) normalised per million cells as quantified from cross-sections of the 3D omental models with the Leica Ariol image analysis software. Data from a single experiment when a panel of ovarian cancer cell lines AOCS1, SKOV3ip1, TOV21G and RMG1 were co-cultured for two weeks with the 3D omental model.

5.2. Targeting CXCL12 in the 3D omental model

The expression of the CXCR4 receptor on the ovarian cancer cell lines was first confirmed by flow cytometry analysis after culture on plastic (Figure 5-2). All of the ovarian cancer cells were positive for the receptor relative to the isotype controls. The TOV21G and RMG1 cell lines (Figures 5-2 c & d) displayed a broader spectrum of high and low expressing cells within the population than the AOCS1 and SKOV3ip1 cell lines (Figures 5-2 a & b). It is possible that the spectrum of low and high CXCR4 expressing cells in Figures 5-2 c & d may be representative

of the higher levels of internalisation of the receptor in response to ligand binding.

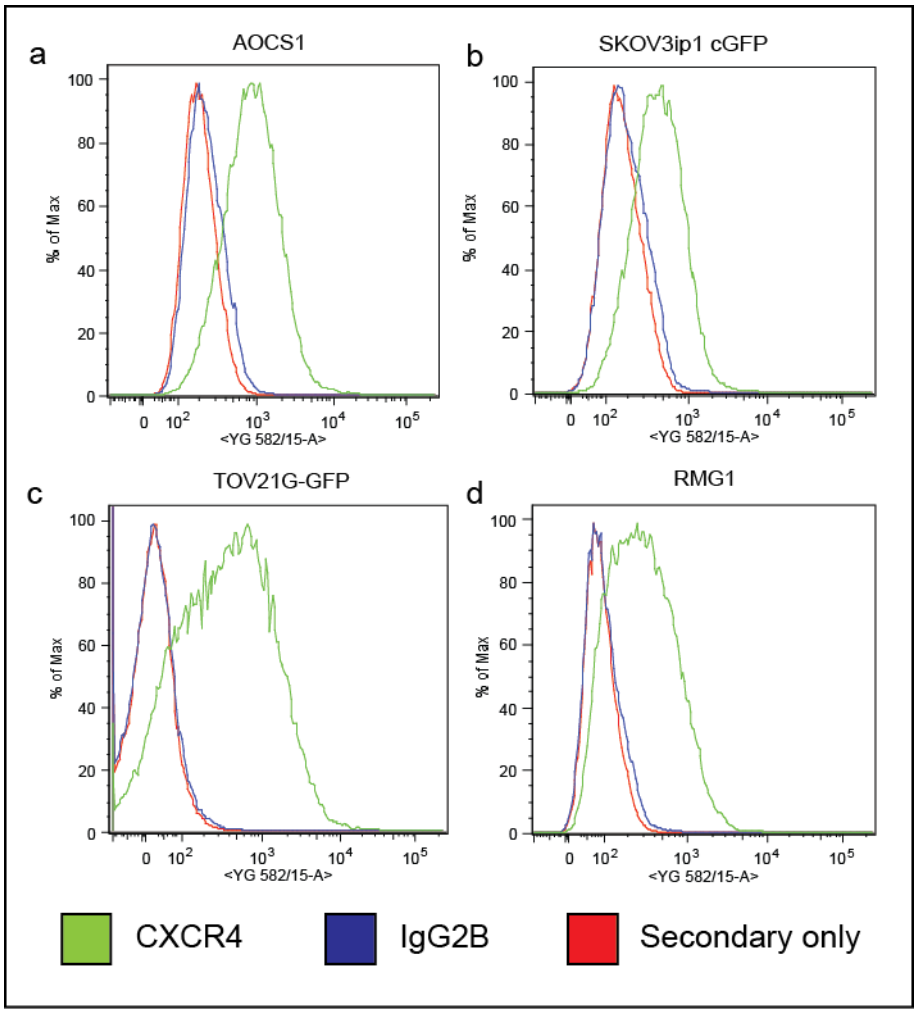

Figure 5-2 CXCR4 receptor expression on the surface of the ovarian cancer cell lines

Histograms of CXCR4 positive PE labelled cell populations as analysed by flow cytometry. CXCR4 expression profile of the cell lines **a)** AOCS1, **b)** SKOV3ip1, **c)** TOV21G and **d)** RMG1. All cells positive for the FVD450 viability stain were excluded from the analysis and due to the GFP positivity of the SKOV3ip1 and TOV21G cells, all analyses were compensated with FITC and PE labelled beads. Green = CXCR4 antibody, Blue = igG2B isotype control, Red = no primary antibody, secondary antibody only.

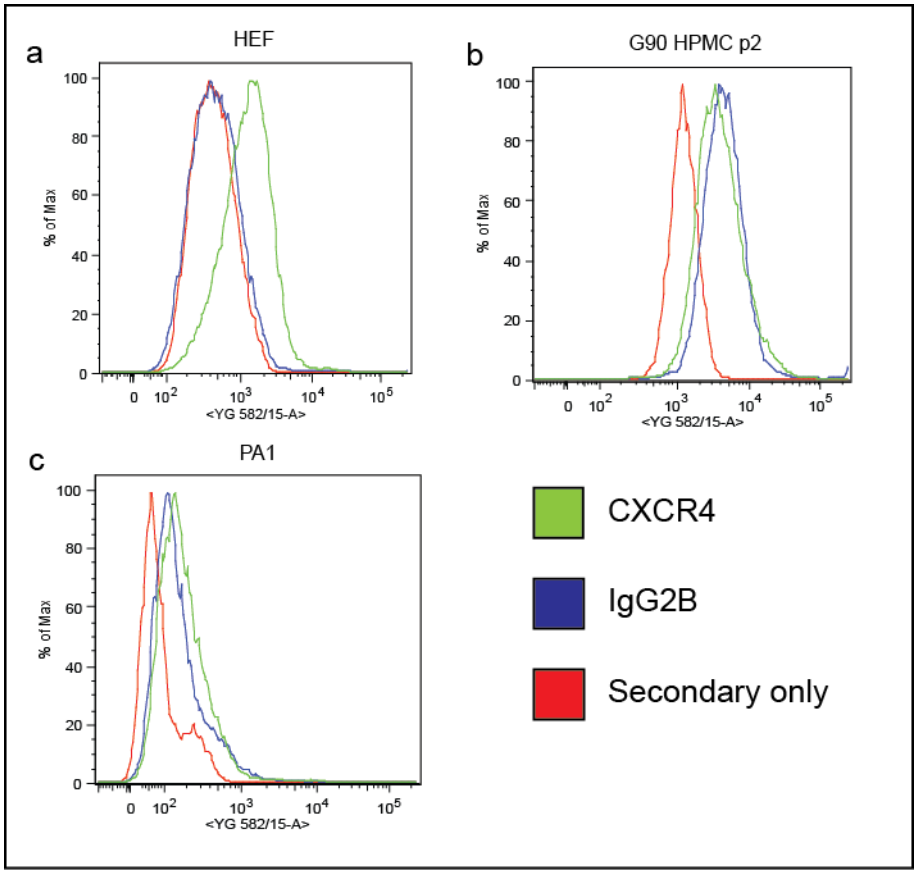

Figure 5-3 CXCR4 receptor expression on the surface of the fibroblasts and mesothelial cells

Histograms of CXCR4 positive PE labelled cell populations as analysed by flow cytometry. CXCR4 expression profile of the **a)** HEFs and **b)** HPMCs from patient G90. **c)** The ovarian teratocarcinoma cell line PA1 was used as a negative control cell line. All cells positive for the FVD450 viability stain were excluded from the analysis. All analyses were compensated with FITC and PE labelled beads. Green = CXCR4 antibody, Blue = igG2B isotype control, Red = no primary antibody, secondary antibody only.

The HEFs used in the 3D omental model were also positive for cell surface expression of CXCR4 subsequent to their culture on plastic (Figure 5-3a). During flow cytometry analysis the HPMCs displayed a high level of auto fluorescence and had a high affinity for the isotype control, therefore the expression status of the HPMCs for CXCR4 here was inconclusive (Figure 5-3b). General CXCR4 expression in HPMCs could be further studied by qRT-PCR and western blotting analysis. The localisation of the receptor could be identified by immunofluorescence and confocal microscopy. Immunofluorescence analysis could potentially

be affected by auto fluorescence, but could be informative of the intracellular trafficking of the cell surface receptor following ligand activation. However, it has previously been reported that omentum derived HPMCs express CXCR4 as analysed by western blot (Kajiyama et al., 2008a). Kajiyama and colleagues also showed that the HPMCs secreted higher levels of CXCL12 than their panel of epithelial ovarian cancer cell lines. In addition stimulation of the HPMCs with TGFβ1 increased the HPMC's migratory potential and also induced differentiation from that of cobblestone morphology to a mesenchymal morphology.

The ovarian teratocarcinoma cell line PA1 that was known to be negative for CXCR4 expression was used as an internal negative control (Figure 5-3c).

The expression of the chemokine CXCL12 in ovarian cancer was mimicked in the 3D omental cell culture model (Figure 5-1). Hugh Kikuchi, a research assistant in the laboratory previously utilised transwell migration assays to identify the concentration of the 114_3H1 antibody that optimally inhibited migration of the TOV21G ovarian cancer cell line. On the basis of Hugh Kikuchi's experiments, the 3D omental models were treated with 10μg/mL of 114_3H1. This was controlled with an equal concentration of an anti-lysozyme IgG2 isotype control antibody. The results of the 3D omental model experiments are summarised in the table below (Table 5-1).

Cell line	Decrease in growth	Ki67	Decrease in invasion	ELISA Control (pg/mL)	ELISA anti-CXCL12 (pg/mL)
AOCS1	0.7 p=0.012*	ns	No data	659.1	7356.7
SKOV3ip1	ns	ns	No data	3654.9	3749.8
TOV21G	No data	No data	0.6 p=0.029*	2834.9	8614.3
RMG1	ns	No data	No data	801.4	2435.0

Table 5-1 Results summary of 114_3H1 antibody treated 3D omental models

Table summarising the effects of 10μg/mL of the CXCL12 neutralising antibody 114_3H1 on ovarian cancer cell growth, proliferation (Ki67) and invasion in the 3D omental model. Four ovarian cancer cell lines were co-cultured on the model and treated with the antibody for two weeks. Experiments were controlled with equal concentrations of an IgG2 isotype control. No data were available for cell lines that did not grow collectively on the surface of the model or those that were non-invasive. Statistically significant fold changes in growth and invasion are denoted with the associated p-values. ns = not significant. ELISA measured CXCL12 concentrations (pg/mL) in the supernatants of the control and antibody treated 3D omental models are also summarised.

Figure 5-4 shows that the CXCL12 targeted antibody significantly reduced tumour growth of the AOCS1 ovarian cancer cells on the 3D omental model. The antibody had no significant effect on the tumour growth of the SKOV3ip1 and RMG1 (Table 5-1) ovarian cancer cell lines on the 3D omental model. The TOV21G ovarian cancer cell line does not display accumulative cell growth on the surface of the model, but is invasive. Therefore measuring tumour growth was not applied to this cell line (Table 5-1).

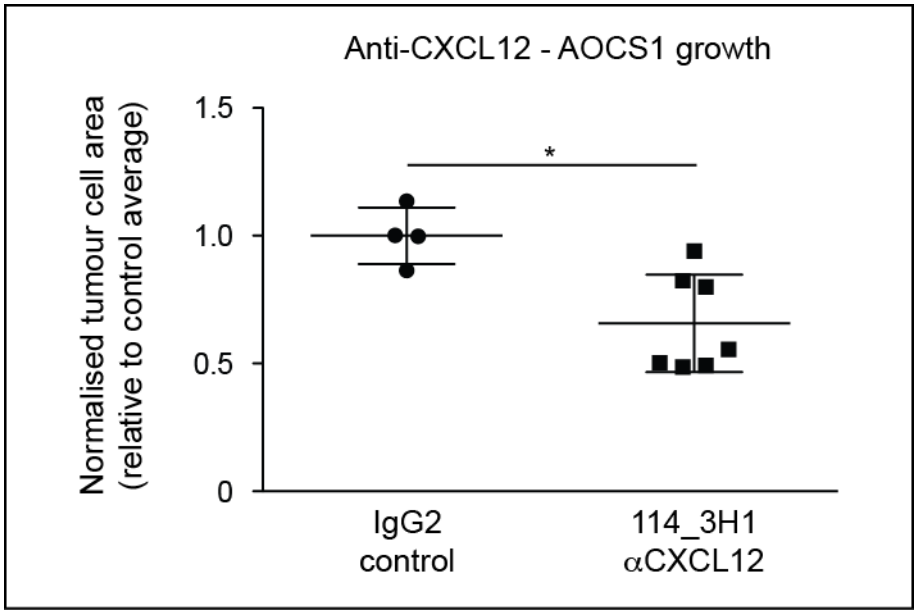

Figure 5-4 The effect of CXCL12 targeted antibody treatment on the growth of the AOCS1 ovarian cancer cell line on the 3D omental model

Graph illustrating the growth of the ovarian cancer cell line AOCS1 on the 3D omental model when treated with 10μg/mL of the CXCL12 targeted antibody 114_3H1. Control groups were treated with an equal concentration of an IgG2 isotype control. The 3D omental models were cultured for two weeks. Photographs of H & E stained sections were taken across the whole section of each model. Each treatment group was tested with triplicate models. The tumour area (μm^2) on each photograph was quantified as a measure of tumour growth. Bars indicate the means and standard deviations across all measurements. Collective data from three experiments. p = 0.012*

Ki67 positive epithelial cells in the 3D omental models were quantified with the aid of the computer-operated microscope and the Leica Ariol image analysis software. Where a significant reduction in AOCS1 tumour cell growth with CXCL12 targeted antibody treatment was observed (Figure 5-4), there was no associated reduction in tumour cell proliferation (Figure 5-5). This therefore suggests that CXCL12 is more implicated in the survival of the AOCS1 ovarian cancer cells in this 3D omental model than in the proliferation of the cells. In addition targeting CXCL12 had no significant effect on the proliferation of the SKOV3ip1 ovarian cancer cells in the 3D omental model (Table 5-1).

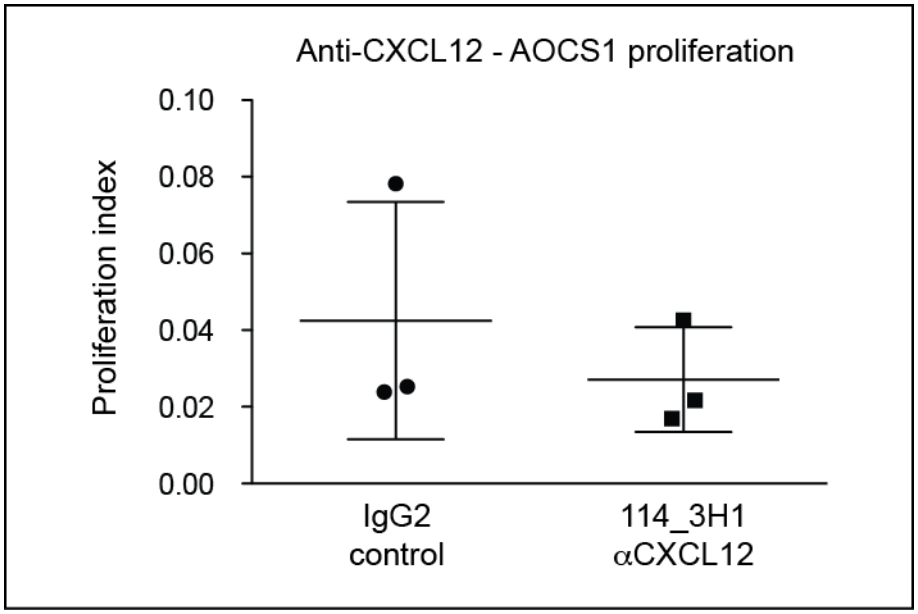

Figure 5-5 The effect of CXCL12 targeted antibody treatment on the proliferation of the AOCS1 ovarian cancer cell line in the 3D omental model

Quantification of the proliferation indices in the 3D omental models co-cultured with the ovarian cancer cell line AOCS1 in the presence of 10μg/mL of the CXCL12 targeted antibody-denoted 114_3H1 or equal concentrations of an IgG2 isotype control. Tumour cells were cultured on the 3D omental model for two weeks. Three 3D omental model cross-sections from each experiment were analysed by computer-aided microscopy and Leica Ariol software. Values are the number of Ki67 positively stained cells in relation to the haematoxylin nucleus counterstain. Bars indicate the means and standard deviations across all measurements. Collective data from three experiments. $p = 0.4$ Data not statistically significant.

Given the reported role of the chemokine CXCL12 as a chemoattractant for CXCR4 positive metastasising cells (Muller et al., 2001), the effect of the CXCL12 targeted antibody on invasion of CXCR4 receptor bearing ovarian cancer cells in the 3D omental model was then investigated.

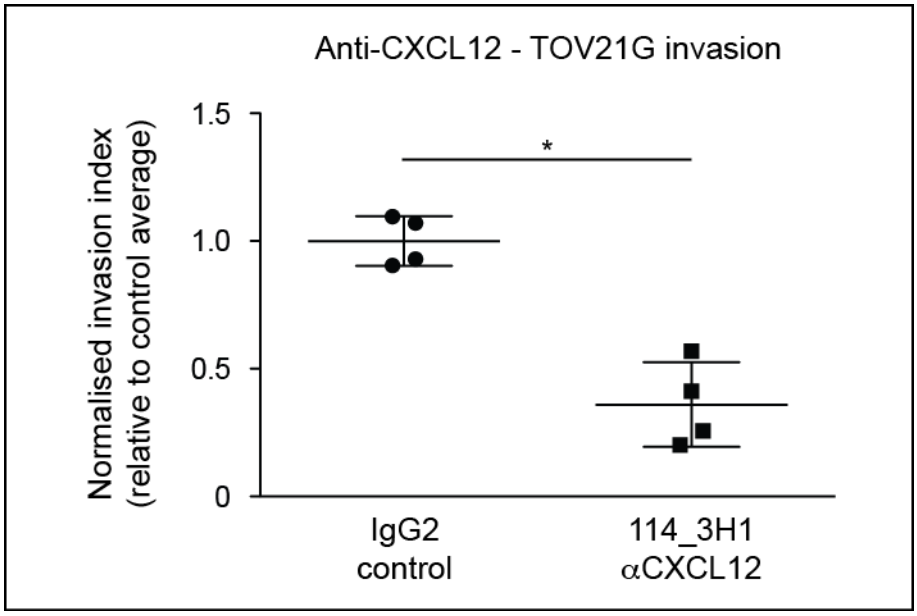

Figure 5-6 The effect of CXCL12 targeted antibody treatment on the invasion of the ovarian cancer cell line TOV21G in the 3D omental model

Graph illustrating the quantified invasion index of the ovarian cancer cell line TOV21G in the presence of 10μg/mL of the CXCL12 targeted antibody-denoted 114_3H1 or equal concentrations of an IgG2 isotype control. Tumour cells were cultured on the 3D omental model for two weeks. Photographs of H & E stained sections were taken across the whole section of each model. Each treatment group was tested with triplicate models. The invasion index from each photograph was determined. The invasion index is a factor of the number of invading particles, tumour area (μm^2) and invasion distance (μm). Bars indicate the means and standard deviations across all measurements. Collective data from two experiments. p = 0.029*.

The invasion of the ovarian cancer cell line TOV21G was tested in the presence of the CXCL12 targeted antibody relative to the isotype control (Figure 5-6). The treated 3D omental models demonstrated a significant decrease in invasion. The antibody had no significant effect on the invasion of the SKOV3ip1 ovarian cancer cells in the 3D omental model (Table 5-1).

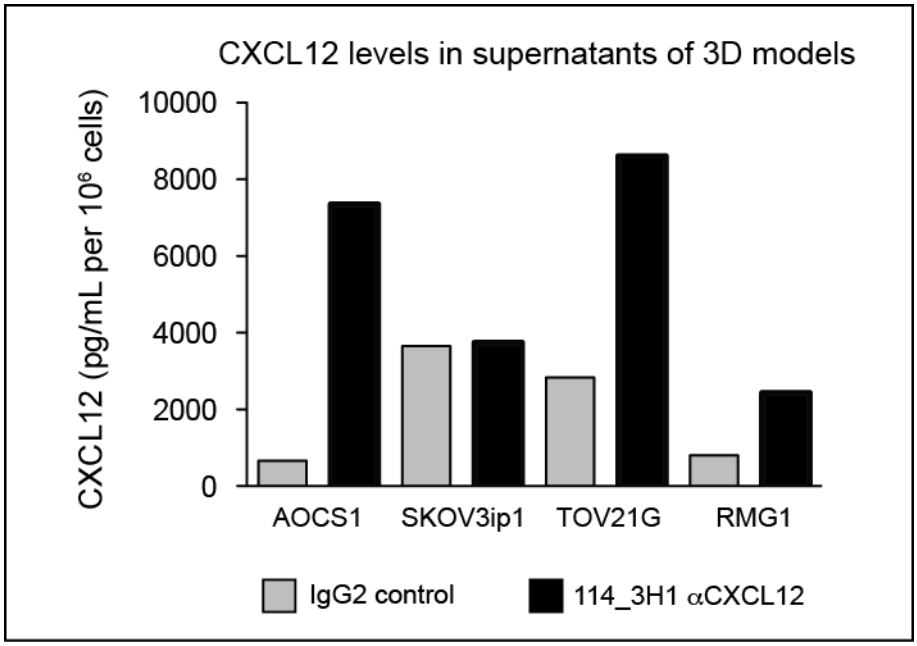

Figure 5-7 The effect of CXCL12 targeted antibody treatment on the CXCL12 levels in the 3D omental model supernatants

Quantification of CXCL12 levels in cell culture supernatants measured by ELISA. CXCL12 concentrations (pg/mL) normalised per million cells as quantified from cross-sections of the 3D omental models with the Leica Ariol image analysis software. Data from a single experiment when a panel of ovarian cancer cell lines AOCS1, SKOV3ip1, TOV21G and RMG1 were co-cultured for two weeks with the 3D omental model and treated with 10μg/mL of the CXCL12 targeted antibody-denoted 114_3H1 or equal concentrations of an IgG2 isotype control.

The supernatants from SKOV3ip1 3D omental cultures had relatively high levels of CXCL12 in comparison with the other cell lines of the panel tested (Figure 5-1). When treated with the CXCL12 targeted antibody there was no reduction in CXCL12 supernatant levels (Figure 5-7). Unexpectedly treatment of the remaining ovarian cancer cell lines in the panel on the 3D omental models appeared to increase the levels of CXCL12 in the cell culture supernatant (Figure 5-7). This could have been a result of the antibody sequestering the ligand in the culture and preventing its degradation. Alternatively it could have been a consequence of the cells secreting more CXCL12 as a compensatory mechanism for the lack of signalling.

5.3. Concluding comments

Overall the chemokine receptor CXCR4 and its ligand CXCL12 are expressed in both the malignant and stromal compartments of ovarian cancer omental metastases, therefore targeting the chemokine network would implicate both the tumour cells themselves and the supporting tumour microenvironment. The stroma is a more favourable target due to its greater genomic stability in relation to the highly adaptable malignant cells. Targeting the chemokine network may have a greater impact on the survival of tumour cells that do not so highly and inherently express a chemokine driven network (Jones et al., 2010; Wiegand et al., 2010), and that are more dependent on stromal cues. However tumour cells that do express high levels of the chemokine network facilitating single cell invasion through the ECM may also be impacted through inhibition of the pathway due to dependencies on chemokine gradients.

When the ovarian cancer cell lines were cultured on plastic very little CXCL12 could be detected in the supernatant in comparison to when they were cultured on the 3D omental model. It is impossible to know from the ELISA data collected in this chapter which cell types were the source of the CXCL12 in the 3D omental models. However the variable levels of CXCL12 secretion induced by different ovarian cancer cell lines in the model, emphasises the importance of the tumour-stroma interactions for chemokine production. This therefore highlights the significance of using this 3D model when studying inflammatory mediators in HGSC metastasis.

A broader titration of the antibody concentrations would need to be tested in the 3D omental model across a larger panel of ovarian cancer cell lines to consolidate this work. Chemokines are often sequestered on matrix proteins (Sorokin, 2010; Vaday and Lider, 2000), and therefore it would also be necessary to consider the penetrance of the therapeutic agent into the collagen matrix of the model.

In this chapter, the 3D omental model was used to test the efficacy of a therapeutic agent that generated statistically significant results. This therefore supports the potential for the use of this assay in future therapeutic studies. However the antibody tested here showed no efficacy in *in vivo* subcutaneous pancreatic cancer models or xenograft models of ovarian cancer (experiments performed by research assistant Lily Keane in the Cancer & Inflammation laboratory). Targeting an inflammatory mediator in models deficient or absent of immune cells such as xenograft *in vivo* models or the 3D omental model respectively, may render such models insufficient for the given experiment.

In parallel to the work of this chapter the potential association between CXCL12 and the up regulation of ECM genes was investigated in the HGSC omental metastases. The aim was to use the antibody targeting CXCL12 in the established 3D omental model as an *in vitro* system to further interrogate the CXCL12 and ECM gene expression link.

Chapter 6

6. Investigating the association between CXCL12 and extracellular matrix remodelling in HGSC omental metastases

6.1. Extracellular matrix remodelling in the tumour microenvironment

Stabilisation of the ECM provides an anchoring substrate for cellular adhesion to support cell survival, and for chemokines to generate suitable concentration gradients for chemotaxis. The ECM is also a physical scaffold for tissue regeneration and angiogenesis (Cox and Erler, 2011; Lopez-Novoa and Nieto, 2009).

Tissue desmoplasia and fibrosis describes an over-production, deposition and cross-linking of ECM proteins and is a key feature of inflammation and wound repair. Advanced solid tumours are characterised by a reactive stromal signature within a dense matrix (Erler and Weaver, 2009; Paszek et al., 2005). An increase in ECM density supports malignant and stromal cell survival and differentiation through an increase in focal adhesions and integrin signalling (Levental et al., 2009). MMPs cleave ECM proteins to aid malignant cell invasion (Kenny and Lengyel, 2009) and mediate growth factor and chemokine bioavailability (Kessenbrock et al., 2010).

Breast cancer development is associated with an increased ‘stiffness’ of the surrounding stroma (Butcher et al., 2009; Erler and Weaver, 2009; Paszek et al., 2005). 3D acini culture of the non-malignant MCF-10A mammary epithelial cells in increasing stiffened collagen gels disrupted the polarisation of the cells and their ability to form lumen. An increase in

the concentration of ECM proteins within the cellular microenvironment provides an abundance of substrate for cell adhesion. Within the acini culture, incremental tensional force on the cellular spheroid development drove the formation of focal adhesions, integrin signalling, and EGF-dependent ERK (extracellular signal related-kinase) activation (Levental et al., 2009).

The stability of the surrounding ECM can therefore positively regulate cell de-differentiation, growth and survival, supporting malignant transformation and chemoresistance. An Affymetrix Gene Expression Array of four drug resistant MCF-7 breast carcinoma cell lines identified 25 ECM genes with a two-fold or more up-regulation compared with the drug sensitive parental line (Iseri et al., 2010). Similarly a proteomic analysis of the cisplatin resistant COC1 ovarian cancer cell line compared with the parental control identified extracellular matrix proteins as one of the eight groups of differentially expressed proteins (Li et al., 2010).

6.2. ECM remodelling in ovarian cancer

Osteopontin is an ECM protein that is significantly over-expressed in ovarian clear cell carcinoma compared with the other histological subtypes (Matsuura et al., 2010). Osteopontin integrates with and up-regulates the expression of its receptors alpha V, alpha 5, beta 1, 3 and 5 integrins particularly in the ovarian carcinoma cell lines TOV21G and RMG-1. It has been found to promote matrix invasion of these cell lines.

In contrast to the increasingly developed argument that extracellular matrix proteins promote the acquisition of chemoresistance during malignant transformation, some ECM proteins are thought to elicit the opposite effect. The presence of the TGFβ-induced protein (TGFBI) in ovarian carcinomas was associated with paclitaxel cytotoxicity. The mechanism of this was established by the re-sensitisation of paclitaxel

resistant cells when they were treated with TGFBI. It is thought that TGFBI stabilises the microtubules of the resistant cells (Ahmed et al., 2007). However more recent work suggests that mesothelial cell interactions with ovarian cancer cell lines increases the expression of TGFBI, and promotes ovarian cancer cell motility, adhesion and invasion (Ween et al., 2011). Not only is tumour progression mapped by the balance of ECM degradation and stabilisation, but the ECM composition is also equally important, whereby proteins that may be crucial at earlier stages of cell attachment and invasion, may in fact be detrimental to tumour growth in a more established microenvironment.

In an analysis of gene expression in 285 ovarian cancer biopsies Tothill et al found that ECM remodelling processes correlate with poor overall patient survival (Tothill et al., 2008). The deposition of ECM proteins has also been identified as a possible mechanism for the development of chemoresistance in ovarian carcinomas (Etemadmoghadam et al., 2009). Serial analysis of gene expression in the A2780 ovarian cancer cell line compared with cisplatin resistant derived clones identified an up-regulation in both collagen 6 α3 and decorin (Sherman-Baust et al., 2003). Growth of the parental cell line on collagen 6 α3 increased their resistance to cisplatin in a colony-formation assay. Cytoplasmic and extracellular staining was observed in a TMA of ovarian cancer biopsies, and expression associated with tumour grade. Collagen 6 α3 expression was however more variable in HGSC compared with other subtypes, and further analysis was required to associate expression with chemotherapy response.

Overall there are very few reports describing the role of the extracellular matrix in HGSC metastasis. Very recently however a similar study to the work described in this chapter identified an ECM gene signature associated with poor survival in HGSC (Cheon et al., 2014). The ten genes were regulated by TGFβ1 and included periostin and versican.

The gene signature was also up regulated in the metastases in comparison with the primary tumours.

6.3. ECM remodelling and cell-matrix interaction processes are associated with high levels of CXCL12 expression in ovarian carcinoma.

Pathway and process enrichment analysis of an Affymetrix gene expression array of 245 ovarian cancer biopsies (GSE 6008 and 3149 sourced from the National Center for Biotechnology Information's (NCBI) Gene Expression Omnibus (GEO) (Barrett and Edgar, 2006)) suggested an association between CXCL12 mRNA expression and ECM remodelling and cell-matrix interactions (Kulbe H, unpublished data). The aim of this chapter was to confirm this link in a second data set, and validate correlations between CXCL12 and ECM remodelling gene expression in the human omental metastases by qRT-PCR.

Dr Probir Chakravarty at the London Research Institute conducted all of the bioinformatics analyses for this chapter. The gene selection and expression validation was completed in the Cancer and Inflammation laboratory. The cohort of 285 ovarian cancer biopsies from the Australian Ovarian Cancer Study (AOCS) was selected as a second data set to confirm the CXCL12 and extracellular matrix-remodelling link. The AOCS data set was interrogated by ranking the biopsies by their levels of CXCL12 expression. The 50 highest CXCL12-expressing biopsies were compared with the 50 lowest CXCL12-expressing biopsies with an eBayes t-test. Amongst these two groups of 50 biopsies, more than 95% of the biopsies were from HGSC, and the remaining biopsies were from endometrioid ovarian cancers. A total of 5167 probes for genes were differentially expressed between the two groups. Genes were identified with multiple probes. Only probe sets with p values equal to or less than 0.05 were considered differentially expressed.

The biological processes enriched in the 5167 differentially expressed probes were elucidated using the Metacore Analysis software (Figure 6-1). Processes expected to be associated with CXCL12 signalling such as inflammation, development and chemotaxis for example were enriched in high CXCL12 – expressing ovarian cancers. The processes of cell-matrix interactions and ECM remodelling were also enriched and associated with high levels of CXCL12. This confirmed the preliminary data that generated the hypothesis to be investigated in this chapter.

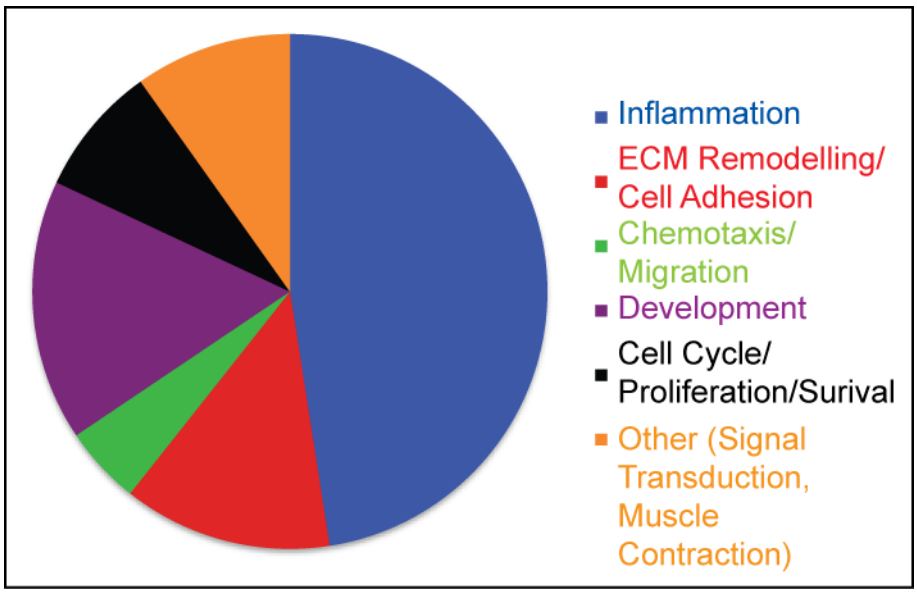

Figure 6-1 Gene set enrichment in high CXCL12 expressing ovarian cancer biopsies.

Pie chart generated by interrogation of the microarray gene expression data from the 285 ovarian cancer biopsies of the Australian Ovarian Cancer Study data set. The biopsies were ranked by their levels of CXCL12 mRNA expression and the top 50 CXCL12 - expressing biopsies were compared by an e-Bayes t-test with the 50 lowest CXCL12 - expressing biopsies. Metacore analysis of the differentially expressed genes elucidated the processes enriched in high CXCL12 expressing biopsies.

These two main category processes were sub-divided into seven more specific processes. Five sub-category processes were more definitively associated with cell adhesion (Cell-matrix interactions, Integrin-mediated cell-matrix adhesion, Glycoconjugates, Integrin priming, Attractive and repulsive receptors) and two sub-category processes were associated

with proteolysis (Connective tissue degradation, ECM remodelling). Most of the genes denoted by these seven processes were up regulated in the high CXCL12 - expressing biopsies (Figure 6-2).

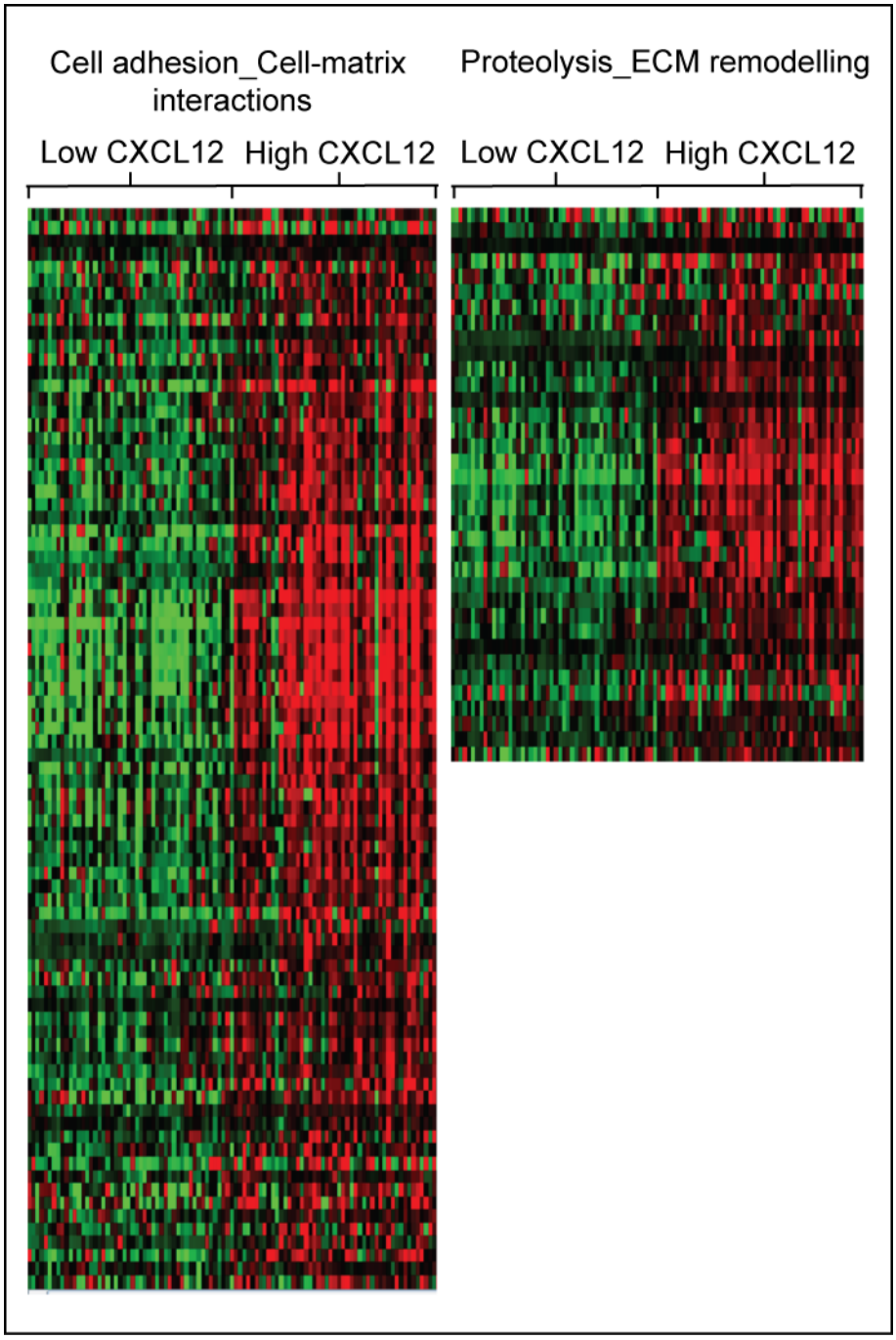

Figure 6-2 Extracellular matrix remodelling and cell-matrix interaction genes are up regulated in high CXCL12 – expressing biopsies.

Heat map generated by interrogation of the microarray gene expression data from the 285 ovarian cancer biopsies of the Australian Ovarian Cancer Study data set. Representation of the genes up regulated in ovarian cancers with associated high levels of CXCL12 expression in two of the seven enriched ECM remodelling and cell-matrix interaction processes; Cell adhesion_Cell-matrix interactions (80 genes), and Proteolysis_ECM remodelling (36 genes). p value ≤ 0.05. Green denotes low expression and red denotes high expression. Heat map kindly generated by Probir Chakravarty at the London Research Institute.

6.4. ECM remodelling and cell-matrix interaction gene selection for validation

The seven sub-category defined processes included a total of 201 genes out of the total 5167 (3.89%) differentially expressed probes for genes that were finally characterised as cell-matrix interactions and ECM remodelling genes associated with high levels of CXCL12. It was established that 89 of these 201 genes had a fold change in expression greater than two. The differential expression of genes was more likely to be detected by subsequent qRT-PCR analysis when there was a fold change in expression greater than two as determined by the bioinformatics analysis.

This work was repeated in the GSE 6008 and 3149 data set of the 245 ovarian cancer biopsies. The characterised cell-matrix interactions and ECM remodelling genes associated with high levels of CXCL12 from the AOCS and the GSE 6008 and 3149 data sets were then compared. 48 differentially expressed genes were found to be common to the two independent data sets (Tables 10-1 & 2 in Appendix I). The common genes within each data set were then ranked by their fold change values and the twenty common genes with the highest fold change values from each data set were subsequently compared. Table 6-1 details the top twenty common genes in each data set and highlights those that appear in the top twenty in both data sets.

The majority of genes listed in Table 6-1 encode for extracellular matrix proteins, suggesting that high levels of CXCL12 may associate with the deposition and establishment of the matrix. Five genes were selected for validation by qRT-PCR in the human omental metastases of HGSC. Decorin and collagen VI α3 were selected on the basis that they appeared in the top twenty common genes in both data sets. In addition these two genes were up regulated in a cisplatin resistant ovarian cancer cell line relative to the parental line (Sherman-Baust et al., 2003).

AOCS data set	Fold change	GSE 6008 & 3149 data set	Fold change
collagen X α 1	11.780	**lumican**	11.558
lumican	9.110	**collagen V α 2**	8.694
collagen III α 1	7.558	**fibronectin 1**	6.404
decorin	7.176	**SPARC (osteonectin)**	6.351
versican	6.290	**collagen III α 1**	6.240
TIMP metallopeptidase inhibitor 3	6.205	**collagen I α 1**	6.137
collagen V α 1	6.186	**TIMP metallopeptidase inhibitor 3**	6.060
collagen V α 2	6.032	**collagen V α 1**	5.635
collagen I α 1	5.942	**vascular cell adhesion molecule 1**	5.264
vascular cell adhesion molecule 1	5.742	**fibrillin 1**	5.057
cartilage oligomeric matrix protein	5.407	**thrombospondin 1**	5.045
fibrillin 1	4.912	**decorin**	4.923
actin, alpha 2, smooth muscle, aorta	4.825	**collagen VI α 3**	4.581
fibronectin 1	4.823	**actin, alpha 2, smooth muscle, aorta**	4.410
thrombospondin 1	4.775	matrix metallopeptidase 2 (type IV collagenase)	4.197
plasminogen activator, urokinase	4.769	**matrix metallopeptidase 11 (stromelysin 3)**	4.193
SPARC (osteonectin)	4.229	serpin peptidase inhibitor, clade E (nexin, plasminogen activator inhibitor type 1), member 1	3.556
collagen VI α 3	4.192	collagen XVI α 1	3.498
collagen I α 2	3.928	**cartilage oligomeric matrix protein**	3.280
matrix metallopeptidase 11 (stromelysin 3)	3.839	nidogen 2 (osteonidogen)	3.190

Table 6-1 The twenty genes up regulated in high CXCL12 expressing biopsies common to two independent data sets.

Table listing the twenty cell-matrix interactions and ECM remodelling genes with the greatest fold change values, when comparing their expression in the 50 highest versus the 50 lowest CXCL12 expressing ovarian cancer biopsies. The genes listed here are those common to the AOCS and the GSE 6008 and 3149 affymetrix gene expression array data sets. Those highlighted appear in the top twenty for both data sets. Fold change values are averaged from each gene probe set. p value ≤ 0.05.

Decorin is a member of the small leucine rich proteoglycan family and interestingly actually more renowned for its tumour growth inhibitory effects in many cancers through blockade interactions with EGFR (Sofeu Feugaing et al., 2013). Lumican was also one of the top twenty common genes in both data sets, and also falls within the same family of matrix proteins (Iozzo and Sanderson, 2011).

Versican is within the proteoglycan family and appeared in the top twenty common genes in the AOCS data set only. Versican secreted by myeloid progenitor cells in the lung were found to support the establishment of breast cancer metastases (Gao et al., 2012). To study the overall expression of the proteoglycan family matrix proteins in the omental metastases, both lumican and versican were selected for validation.

Absent from the genes listed in Table 6-1 is periostin. This gene had the greatest fold change in expression (fold change value = 24.051) when comparing high versus low CXCL12-expressing biopsies in the AOCS data set. Periostin is a cell adhesion protein originally identified in osteoblasts. It is involved in heart embryonic development, wound repair and tumour development and is up regulated in many cancers including ovarian cancer (Ismail et al., 2000; Matei et al., 2002). It has been suggested that periostin may play a role in metastasis and angiogenesis in an *in vivo* model of ovarian carcinoma (Zhu et al., 2010). Ovarian cancer cell derived lysophosphatidic acid may also stimulate periostin expression in adipose tissue derived stromal cells (Choi et al., 2011). Given the significance of this to the adipose tissue of the omentum and therefore the microenvironment HGSC metastases, periostin was also selected for validation.

6.5. Correlating the ECM genes selected for validation with CXCL12 in the biopsies of the AOCS and GSE 6008 & 3149 data sets

The genes selected for validation in the HGSC omental metastases, decorin, lumican, versican, collagen VI α3 and periostin were correlated with CXCL12 expression in the 285 and 245 ovarian cancer biopsies of the AOCS and GSE 6008 and 3149 data sets respectively (Table 6-2). A correlation coefficient was generated for each ECM gene with CXCL12 expression, where a value of 0.8 or more was considered a strong positive correlation. The strength of the correlations was moderate, but positive in each case. This confirmed the association of these genes with CXCL12 expression in the ovarian cancer biopsies of the AOCS and GSE 6008 and 3149 data sets.

Gene	AOCS data set correlation	GSE 6008 & 3149 data set correlation
Decorin	0.540	0.550
Lumican	0.704	0.668
Versican	0.580	0.535
Collagen VI α3	0.545	0.616
Periostin	0.579	0.425
CXCL12	0.970	0.908

Table 6-2 Correlation between CXCL12 and ECM gene expression in ovarian cancer biopsies.

The ECM genes listed were correlated with CXCL12 expression across all of the ovarian cancer biopsies of the AOCS (285 biopsies) and the GSE 6008 and 3149 (245 biopsies) data sets. The table indicates the correlation coefficients for each ECM gene. A correlation coefficient value of 0.8 or more was considered a strong positive correlation. p value ≤ 0.05.

6.6. Associating immune cell signatures with CXCL12 in the biopsies of the AOCS and GSE 6008 & 3149 data sets

Gene set signatures defining macrophage and other immune cell infiltrates (Abbas et al., 2005) were used to interrogate the differentially expressed genes associated with high levels of CXCL12. All immune cell signatures analysed were up regulated in high CXCL12 expressing biopsies (Table 6-3). This was with the exception of the neutrophils in the GSE 6008 and 3149 data set, where the gene set signature was not significantly up regulated ($p = 0.759$). Macrophage and monocyte gene signatures were amongst the most significantly up regulated of all the immune cell signatures analysed. Therefore the association between CXCL12 and increased macrophage infiltrates previously described in the laboratory (Kulbe et al., 2012) was further confirmed. Of the M1 and M2 macrophage phenotypes, the M1 gene signature was the most significantly up regulated in both data sets.

Immune cell type signatures	AOCS data set p-values		GSE 6008 & 3149 data set p-values	
	Up regulated	Down regulated	Up regulated	Down regulated
Monocytes	4.38E-25	1	8.04E-11	1
Macrophages	1.87E-17	1	1.95E-12	1
M1	1.65E-14	1	6.87E-08	0.999
M2	8.14E-08	0.999	7.29E-06	0.999
T cells	7.52E-24	1	3.89E-06	0.999
B cells	1.23E-15	1	5.86E-09	0.999
Neutrophils	7.19E-05	0.999	0.759	0.241

Table 6-3 Up regulation of immune cell signatures in high CXCL12 expressing ovarian cancer biopsies.

Publically available gene set signatures associated with immune cell subtypes were used to interrogate the gene expression microarray data of the AOCS and GSE 6008 and 3149 data sets. High CXCL12 expressing ovarian cancer biopsies showed enrichment in all immune cell signatures analysed. Table lists the associated p-values for up and down regulated immune cell signatures.

Genes within the macrophage gene set signature and differentially expressed in high CXCL12 expressing biopsies of the AOCS (Table 10-3 in Appendix I) and GSE 6008 and 3149 (Table 10-4 in Appendix I) were identified. These genes were analysed to question whether the selected ECM genes appeared in the list. None of the ECM genes selected were associated with both high levels of CXCL12 and macrophage infiltrates in the biopsies. However it was noted that CD36, which is the receptor for thrombospondin 1 (Lopez-Dee et al., 2011) was significantly associated with CXCL12 and macrophage infiltrates (AOCS; 2.709 fold change, GSE 6008 & 3149; 1.709 fold change, probe set p-values less than 0.05). Thrombospondin 1 appeared in the top twenty common genes in both data sets (Table 6-1).

In summary, decorin, lumican, versican, collagen VI α3, periostin and thrombospondin 1 were all selected to validate their association with CXCL12 by qRT-PCR in the human omental metastases of HGSC.

6.7. Optimisation and establishment of appropriate house-keeping genes for qRT-PCR gene expression validation in the human omental metastases of HGSC

The human omental metastases were very heterogeneous in their cellular composition and therefore it was likely that the expression of routinely used house keeping genes measured by qRT-PCR would vary significantly between samples. Vandesompele J and colleagues studied the expression of ten different house keeping genes in a cell line, primary cells and several different tissue samples (Vandesompele et al., 2002). These data were used to identify the error in gene expression data when single house keeping genes were used. A mathematical algorithm was generated to establish the combination and number of the most stably expressed house keeping genes that should be used in gene expression analyses within a given sample set. This algorithm is now publically available in the geNorm software (http://www.biogazelle.com/qbaseplus).

On the basis of this report and those routinely used in the laboratory ten house keeping genes were selected (GAPDH, 18s, β2M, RPL34, UBC, HMBS, HPRT1, TBP, ACTB, and YWHAZ) for optimisation in the human omental metastases. The measured expression data for these genes in the omental metastases was imported into the geNorm software that calculated an M value for each gene (Figure 6-3a). This was a measure of gene expression stability across all the samples. The lower the M value was the more stable the expression. The software also generated a V value, which was a measure of the systematic pairwise variation in expression between all the tested genes in each sample (Figure 6-3b). On the basis of the nature of the samples, the software generated a threshold for the most suitable V value for the sample set. In conclusion it was established that for the given set of omental metastases samples, the geometric mean of the expression values for HPRT1, TBP, ACTB

and YWHAZ in each sample should be used as a house keeping gene reference for further gene expression analyses.

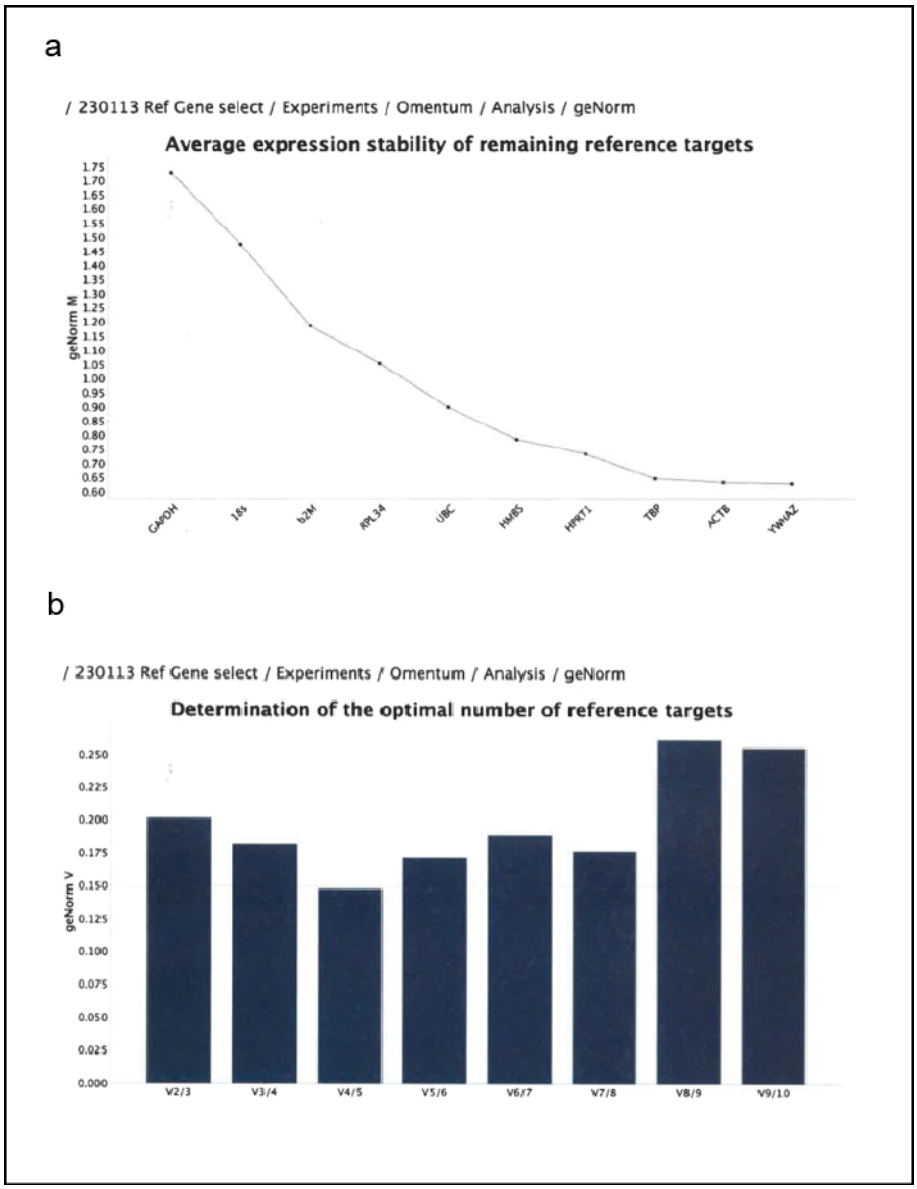

Figure 6-3 House keeping reference gene optimisation in the human omental metastases of HGSC.

Graphs generated by the geNorm software after input of the expression of ten house keeping reference genes in the omental metastases samples. **a)** The lowest geNorm calculated M value indicated the most stably expressed genes across all the samples. **b)** The geNorm V value was calculated by measuring the pairwise variation in expression of each gene in each sample. The V value below a given threshold suitable to the sample set identified the optimal number of house keeping genes to be used as a reference in subsequent experiments.

6.8. CXCL12 and ECM gene expression correlation validation in human omental metastases of HGSC

The mRNA expression of the selected ECM genes; decorin, lumican, versican, collagen 6 α 3, periostin, and thrombospondin 1 together with CXCL12 in whole HGSC omental metastasis samples were measured by qRT-PCR. The strength of the correlations between all the ECM genes and CXCL12 was tested. The only ECM gene to show a significant positive correlation with CXCL12 was decorin (Figure 6-4).

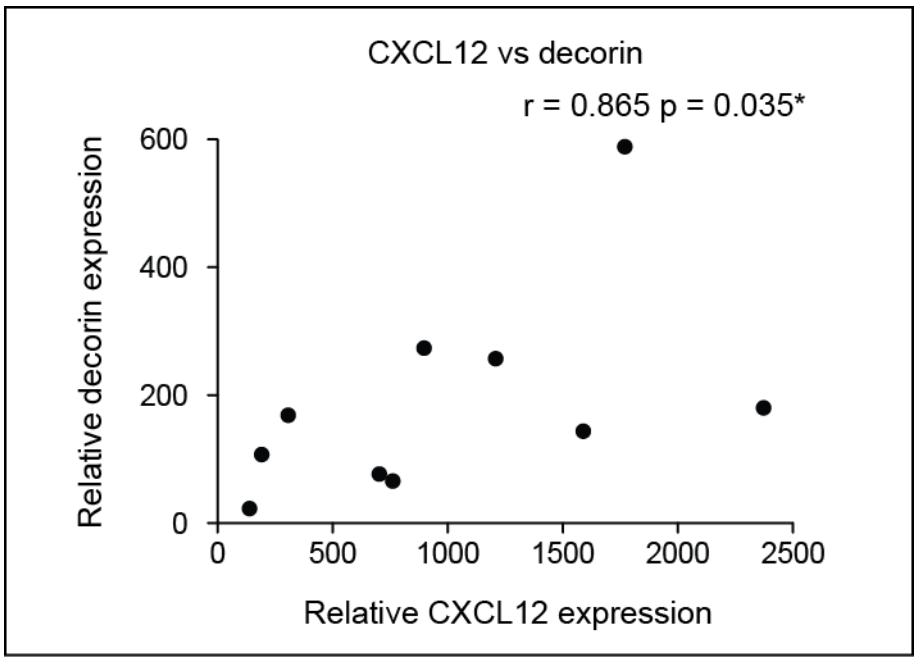

Figure 6-4 The correlation between CXCL12 and decorin mRNA expression in human omental metastases of HGSC.

The relative mRNA expression levels of CXCL12 and decorin were measured by quantitative real-time PCR in ten samples of HGSC omental metastasis. The fold change in gene expression was calculated relative to the geometric mean of the cycle threshold values for the reference genes ACTB, YWHAZ, TBP and HPRT1. r = Spearman rank correlation coefficient.

The expression of CXCR4, the receptor for CXCL12, was also measured in all the HGSC omental metastasis samples. CXCR4 showed a significant positive correlation with 50% of the ECM genes analysed (Figure 6-5).

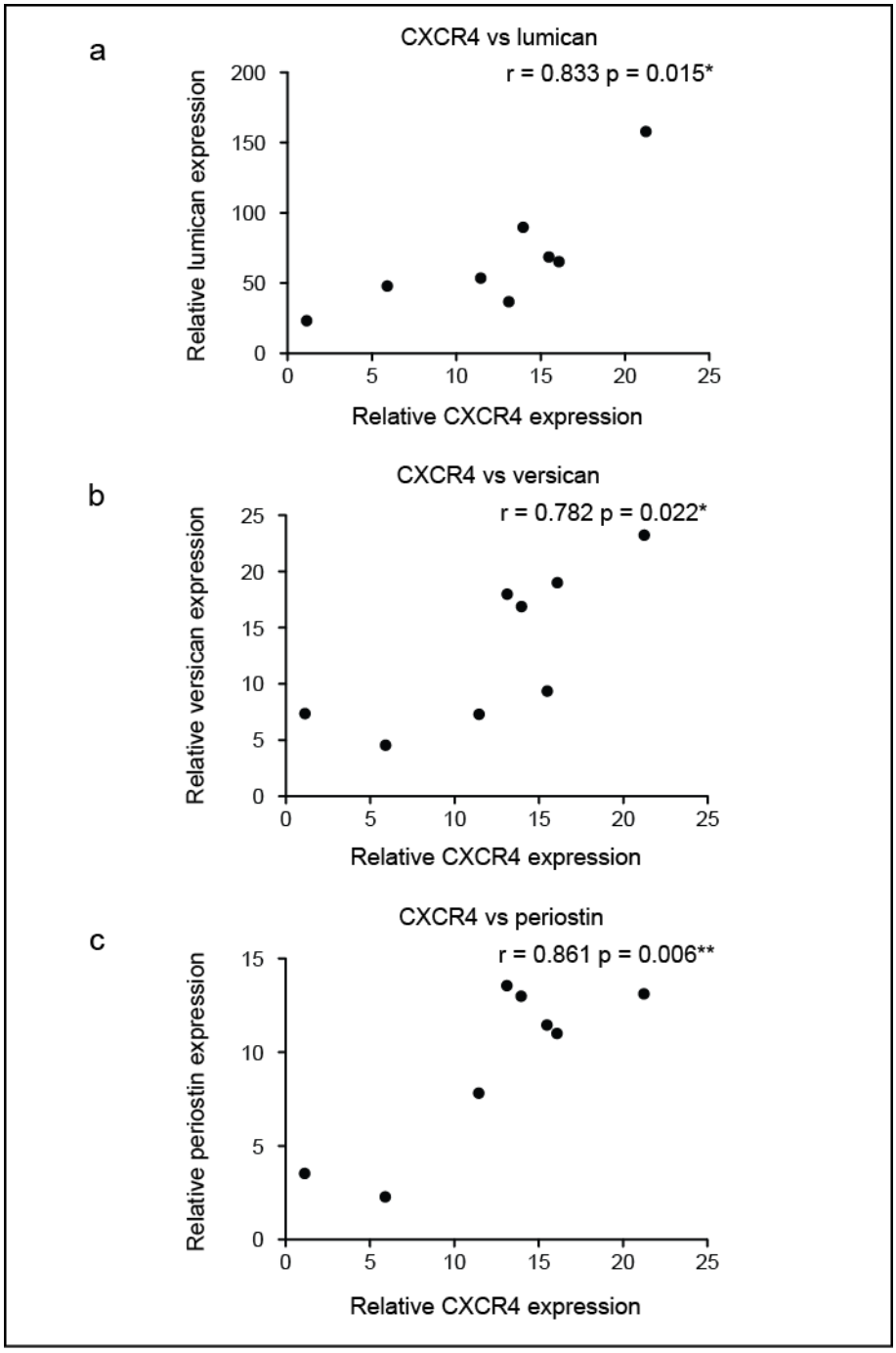

Figure 6-5 The correlation between CXCR4 and ECM gene mRNA expression in human omental metastases of HGSC.

The relative mRNA expression levels of CXCR4, **a)** lumican, **b)** versican and **c)** periostin were measured by quantitative real-time PCR in eight samples of HGSC omental metastasis. The fold change in gene expression was calculated relative to the geometric mean of the cycle threshold values for the reference genes ACTB, YWHAZ, TBP and HPRT1. r = **a)** Spearman or **b & c)** Pearson rank correlation coefficient.

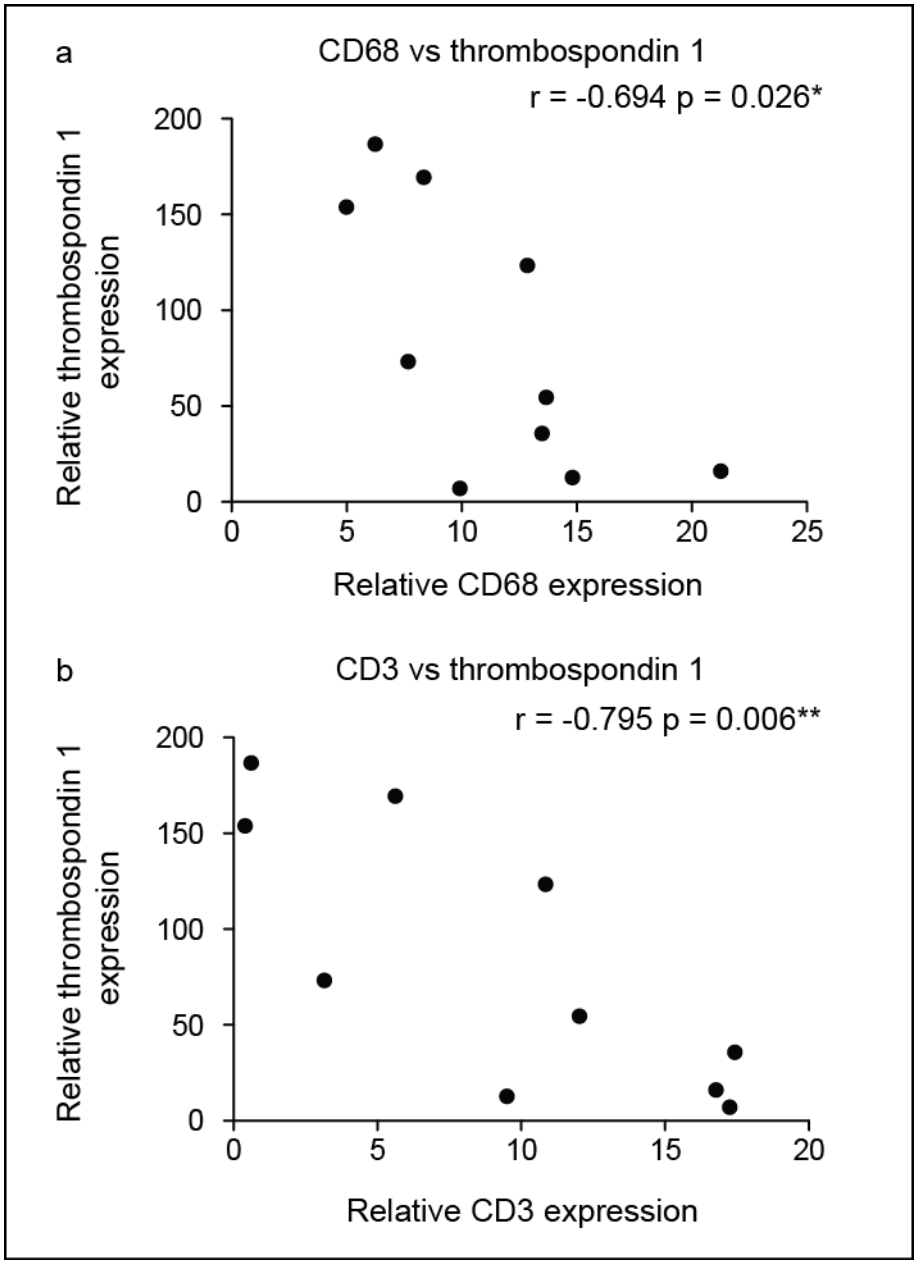

Figure 6-6 The correlation between immune cell infiltrates and thrombospondin 1 mRNA expression in human omental metastases of HGSC.

The relative mRNA expression levels of thrombospondin 1 were measured by quantitative real-time PCR in ten samples of HGSC omental metastasis. The fold change in gene expression was calculated relative to the geometric mean of the cycle threshold values for the reference genes ACTB, YWHAZ, TBP and HPRT1. The mRNA expression levels were correlated with the corresponding percentages of **a)** CD68 positive macrophages and **b)** CD3 positive T cells in relation to the hematoxylin nuclear counterstain (data collected in chapter 3). r = Pearson rank correlation coefficient.

The expression of CXCL12 associated with immune cell infiltrates in the ovarian cancer biopsies of the AOCS and the GSE 6008 and 3149 data sets (Table 6-3). Therefore the immune cell infiltrate and Ki67 data for each HGSC omental metastasis sample collected in chapter 3 was then also correlated with the CXCL12, CXCR4 and ECM gene expression data. Thrombospondin 1 showed a significant negative correlation with CD68 positive macrophages and CD3 positive T cells (Figure 6-6).

Periostin also showed a significant negative correlation with CD8 positive T cells (Figure 6-7). However CXCL12 and CXCR4 did not correlate with the immune cell infiltrates, and no other correlations with the ECM genes were identified.

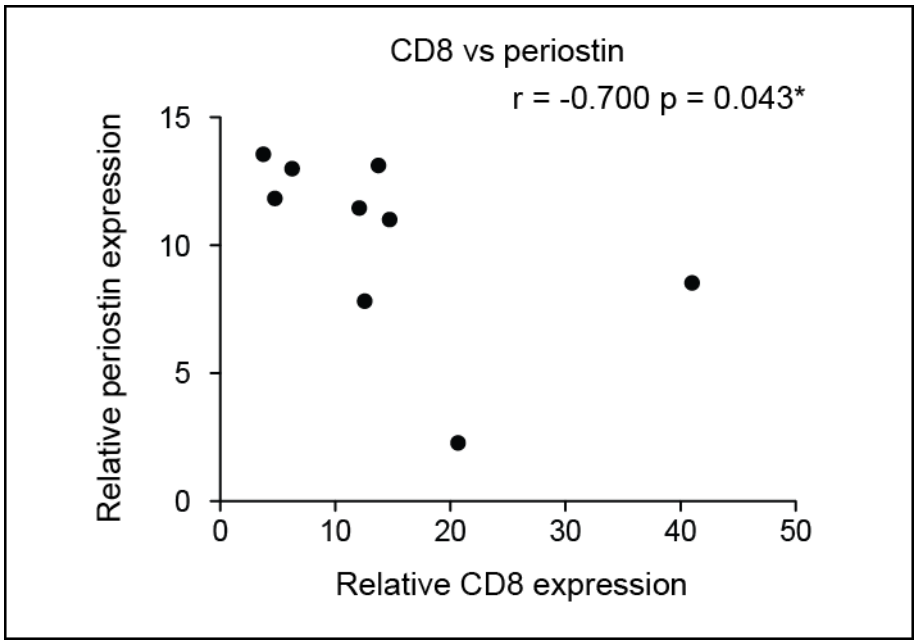

Figure 6-7 The correlation between CD8 positive T cells and periostin mRNA expression in human omental metastases of HGSC.

The relative mRNA expression levels of periostin were measured by quantitative real-time PCR in nine samples of HGSC omental metastasis. The fold change in gene expression was calculated relative to the geometric mean of the cycle threshold values for the reference genes ACTB, YWHAZ, TBP and HPRT1. The mRNA expression levels were correlated with the corresponding percentages of CD8 positive T cells in relation to the hematoxylin nuclear counterstain (data collected in chapter 3). r = Spearman rank correlation coefficient.

6.9. Concluding statements

Associations between CXCL12, ECM gene expression and immune cell infiltrates were identified in two independent gene expression microarray data sets. A small cohort of ECM genes was selected for validation by qRT-PCR in a sample set of human HGSC omental metastases. The GeNorm software established following a publication by Vandesompele and colleagues (Vandesompele et al., 2002) was used to test ten different house keeping genes across the sample set. The software generated an optimised house keeping reference for gene expression analysis.

Only decorin of the six ECM genes analysed correlated with CXCL12 when further analysed by qRT-PCR, and none of the immune cell infiltrates showed a significant correlation. This suggested that the associations observed in the primary ovarian cancer biopsies might not apply to the metastases. However CXCR4 did significantly correlate with lumican, versican and periostin, indicating that the expression of the receptor might be more relevant to these associations than the expression of the ligand. CXCR4 is a chemokine receptor within the described 'TNF Network' (Kulbe et al., 2005; Kulbe et al., 2007). The expression of inflammatory cytokines can activate the transcription factor NF-κB (Hagemann et al., 2005). Within a positive feedback loop, NF-κB itself can regulate the expression of inflammatory cytokines (Greten et al., 2004). Perhaps therefore, the associated expression of CXCR4 and the ECM genes lumican, versican and periostin are co-regulated by NF-κB.

Malek and colleagues recently reported that CXC chemokines inclusive of CXCL12 were amplified in the primary ovarian tumour but not in the metastases (Malek et al., 2011). CXCR4 is expressed on the malignant cells (Scotton et al., 2001) and the leukocytes (Tchernychev et al., 2010) within the ovarian cancer microenvironment. Perhaps at the site of

metastasis, the association between CXCR4 and ECM gene expression relates to enrichment in CXCR4 expressing cells and increased matrix deposition within the microenvironment that does not depend upon CXCR4 signalling *per se*.

CD36 was identified amongst the genes up regulated in high CXCL12 expressing biopsies and within the macrophage gene set signature. The ECM protein thrombospondin 1 is a ligand for the CD36 receptor, and inhibits angiogenesis through interaction with the receptor on endothelial cells (Hall et al., 2013; Lopez-Dee et al., 2011). Thrombospondin 1 negatively correlated with CD68 positive macrophages and CD3 positive T cells. This perhaps suggests that in a microenvironment rich in immune cells and actively angiogenic (Leinster et al., 2012; Yang et al., 2004), thrombospondin 1 may be down regulated.

An infiltrate of CD8 positive T cells is associated with a good survival rate in ovarian cancer patients (Fridman et al., 2012). Periostin showed a significant negative correlation with CD8 positive T cells in the HGSC omental metastases, which may indicate that periostin is also associated with a poor prognosis, however this requires further investigation.

6.10. Summary

• 48 ECM genes associated with high levels of CXCL12 expression in two independent gene expression microarray data sets of 285 (AOCS) and 245 (GSE 6008 & 3149) ovarian cancer biopsies.
• Six ECM genes were selected to validate the association with CXCL12 expression by qRT-PCR in human omental metastases of HGSC. These genes were lumican, versican, decorin, periostin, thrombospondin 1, and collagen VI α 3.
• CXCR4 positively correlated with lumican, versican and periostin.
• CXCL12 positively correlated with decorin.

• CD68 positive macrophages negatively correlated with thrombospondin 1.
• CD3 positive T cells negatively correlated with thrombospondin 1.
• CD8 positive T cells negatively correlated with periostin.

Overall there was no significant association between CXCL12 and ECM gene expression in the human omental metastases of HGSC identified in this chapter. Consequently there was no justification to study the effect of neutralising CXCL12 signalling on ECM gene expression in the 3D omental model. Therefore advancing the 3D omental model by introduction of an immune cell infiltrate became the focus of the next chapter.

Chapter 7

7. Introducing an immune cell infiltrate to the 3D omental model

The established 3D omental model described in chapter 4 lacks any immune cell component. Following a review of recent literature describing available 3D models of ovarian cancer (section 1.4), there was clearly room in the field for the development of 3D models incorporating immune cells. Therefore the effect of including an inflammatory cell type to the established 3D omental model was investigated. A recent report from the laboratory described an increase in CD68 positive macrophages in ovarian cancer biopsies expressing high levels of the cytokines and chemokines of the TNF network, which includes CXCL12 (Kulbe et al., 2012). In addition both CXCL12 signalling and macrophage infiltrates were both required for invasion and metastasis in a breast cancer *in vivo* model (Boimel et al., 2012). In chapter 3 an infiltrate of CD68 positive macrophages in human omental metastases of HGSC significantly correlated with increased Ki67 positive malignant epithelial cells (Figure 3-8). Therefore in this chapter macrophages were introduced into the 3D omental cell culture model and the influence of this on malignant cell proliferation was investigated.

7.1. Introducing THP1 monocytic cell line derived macrophages to the 3D omental model

The first experiments were carried out with the THP1 monocytic cell line that was established from a patient with acute monocytic leukaemia (Tsuchiya et al., 1980). These cells can be cultured in suspension in the presence of 0.05mM β-mercaptoethanol, and then differentiated into adherent macrophages through culture with 5ng/mL phorbol 12-

myristate 13-acetate (PMA) for a minimum of 48 hours (Park et al., 2007). The differentiated macrophages express the markers CD68, CD36, CD11b (Phillips et al., 2005) and CD14 (Daigneault et al., 2010).

Even without a differentiation step, the THP1 cells share similar characteristics to tumour-associated macrophages. For instance, co-culture of THP-1 cells with non-small cell lung cancer cell lines induced tumour cell expression of the angiogenic cytokine IL-8 (Chen et al., 2003). Additionally these cells have been used to demonstrate how macrophage-tumour cell interactions stimulate IL-1β in THP1 cells leading to the activation of Wnt signalling in colon cancer cells supporting tumour growth. (Kaler et al., 2009). A later study further suggested that the stimulation of IL-1β in the THP1 cells and paracrine signalling in the tumour cells, downstream stabilised Snail and blocked TRAIL-induced apoptosis (Kaler et al., 2010).

Initially THP1 derived macrophages were co-cultured in the 3D omental model with the ovarian cancer cell line AOCS1 (Figure 7-1). Analysis of immunohistochemistry stained omental metastases of HGSC demonstrated that CD68 positive macrophages were predominantly localised within the tumour deposits rather than in the surrounding stroma (Figure 3-5). Therefore to mimic these tumour-infiltrating macrophages in the 3D omental model, THP1 derived macrophages were detached and pooled together with the ovarian cancer cells to seed on the surface of the model. The numbers of macrophages to test in the model were deduced on the basis that CD68 positive macrophages constituted for 11.3% of the total tumour microenvironment in human omental metastases of HGSC as determined in chapter 3 (Figure 3-6). When co-culturing the AOCS1 ovarian cancer cells on the 3D omental model, 11.3% of the total number of cells in the model equated to approximately 37,000 macrophages. A titration of macrophage numbers ranging below and above this value was also tested in the 3D omental model.

Cross-sections of the 3D omental model were stained by immunofluorescence with a pan-cytokeratin antibody to identify the tumour cells and for CD68 to distinguish the macrophages (Figure 7-1a). The THP1 derived macrophages were also cultured on the 3D omental model without the tumour cells (Figure 7-1b). The immunofluorescence staining was controlled with tonsil sections illustrating the presence of pan-cytokeratin positive epithelial cells (Figure 7-1c) and CD68 positive macrophages (Figure 7-1d). This staining revealed that the THP1-derived macrophages incorporated themselves into the collagen matrix, whilst the AOCS1 ovarian cancer cells remained viable on the surface of the model.

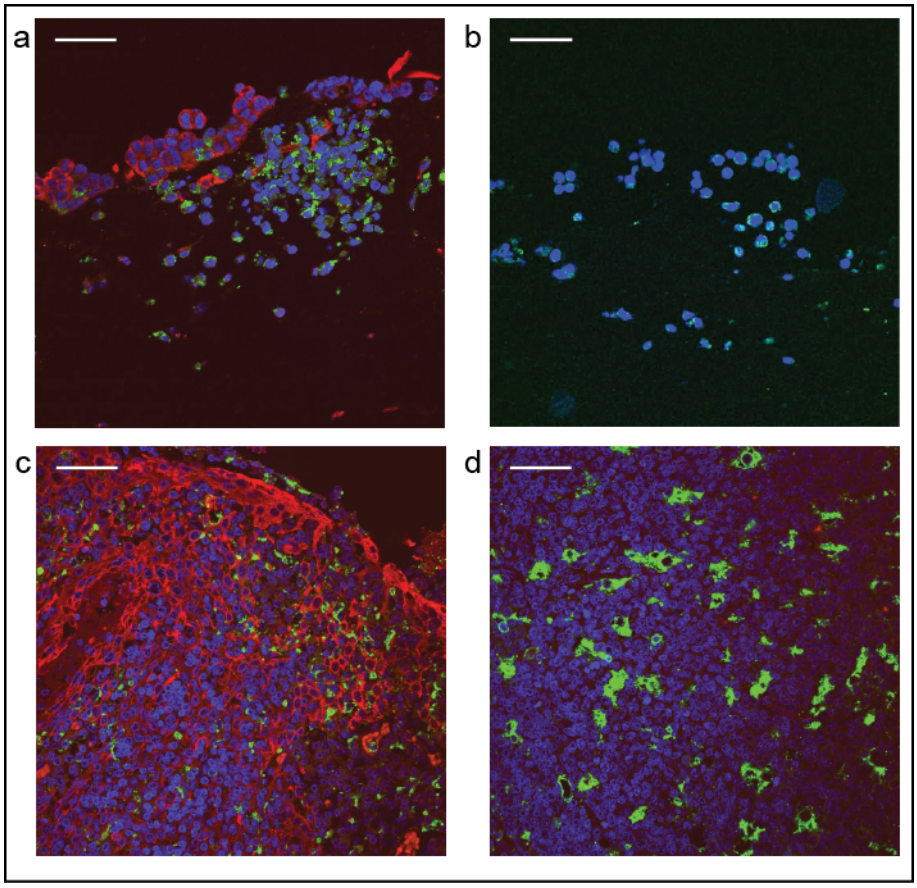

Figure 7-1 Co-culture of AOCS1 ovarian cancer cells and THP1 derived macrophages in the 3D omental model.

Representative immunofluorescence images of 5 μm thick cross sections of the 3D omental models when 25K tumour-infiltrating mimicking THP1 derived macrophages (mϕ) were co-cultured **a)** with and **b)** without the ovarian cancer cell line AOCS1 for two weeks. Sections of human tonsil were used as a positive control for **c)** pan-cytokeratin positive epithelial cells and **d)** CD68 positive macrophages. Blue = Hoechst nuclei stain, Green = CD68, Red = pan-cytokeratin. 40x magnification, bar = 50 μm.

To assess whether the ovarian cancer cells were proliferating in the culture, immunohistochemistry stained sections of the 3D omental models were analysed using the Leica Ariol software to quantify the Ki67 positive epithelial cells relative to the total cell counts (Figure 7-2). The AOCS1 ovarian cancer cells were proliferating in the model. However increasing the number of co-cultured THP1 derived macrophages had no significant effect on the proliferation of the ovarian cancer cell line AOCS1 in the 3D omental model.

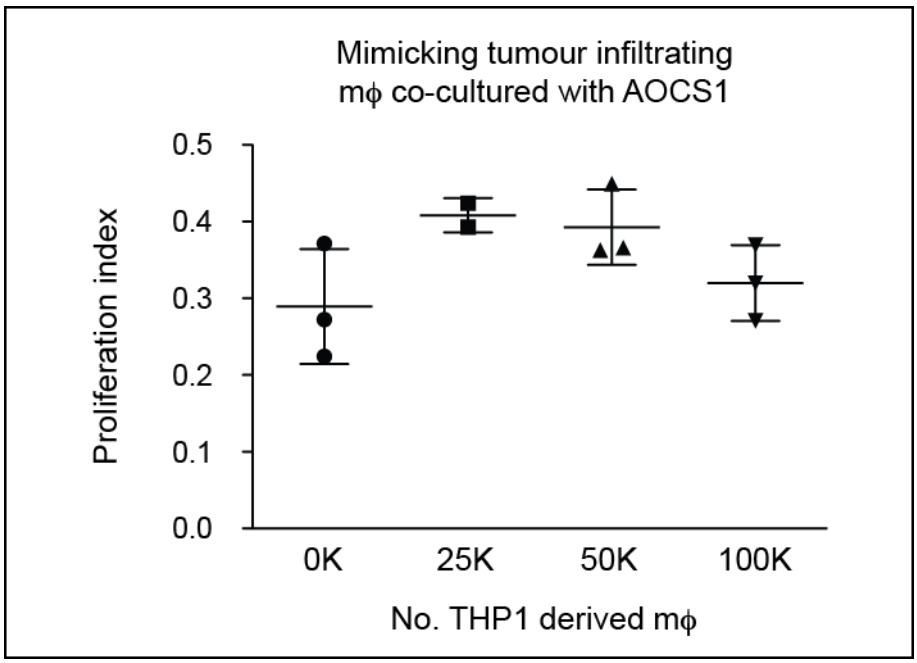

Figure 7-2 The effect of increasing numbers of THP1 derived macrophages on the proliferation of the ovarian cancer cell line AOCS1 in the 3D omental model

Quantification of the proliferation indices of the ovarian cancer cell line AOCS1 on the 3D omental models co-cultured with 0 – 100K of tumour-infiltrating mimicking THP1 derived macrophages (mϕ). Tumour cells were cultured on the 3D omental model for two weeks. 3D omental model cross-sections were analysed by computer-aided microscopy and Leica Ariol software. Values are the number of Ki67 positively stained cells in relation to the hematoxylin nuclear counterstain. Bars indicate the means and standard deviations across all measurements. Collective data from three experiments. Data not statistically significant.

Following the successful co-culture of the THP1 derived macrophages in the 3D omental model, collaboration with MedImmune, Cambridge offered the opportunity to pursue introducing macrophages to the model further. A recent publication comparing the PMA differentiated THP1 monocytic cell line with PBMCs suggested that PBMCs show significant increased LPS induced release of cytokines such as IL1-β, TNF-α, IL-6 and IL-8 compared with the THP1 cells (Daigneault et al., 2010). In addition the phagocytosis function of the PMA differentiated THP1 cells was less efficient than that of PBMCs. However the differentiation of PBMCs to monocyte-derived macrophages reduced their capacity to phagocytose opsonised latex beads to a level that was comparable to the differentiated THP1 cells. Ultimately THP1 monocytic cells were originally established from a patient with acute monocytic leukaemia (Tsuchiya et al., 1980). Therefore the THP1 cells are likely to carry oncogenic mutations that could interfere with the growth of other cells within the 3D omental model and distort studies on the mutation status of co-cultured ovarian cancer cells. It was advised to discontinue work with this cell line and start to evaluate introducing PBMC derived macrophages to the 3D omental model. It was also advised to co-culture GFP labelled ovarian cancer cells in the model since this would aid differentiation between the macrophages and tumour cells within the matrix.

7.2. Introducing peripheral blood monocytic cell (PBMC) derived macrophages to the 3D omental model

PBMCs were extracted from the blood of a healthy human donor by density gradient centrifugation. The monocytes were isolated from this preparation by adherence and cultured in the presence of macrophage colony-stimulating factor (M-CSF) for one week to allow differentiation into macrophages.

PBMC-derived macrophages were co-cultured with the GFP positive SKOV3ip1 ovarian cancer cell line (Figure 7-3). The aim of the experiments was to investigate the effect of introducing the macrophages on ovarian cancer cell growth, proliferation, invasion and cytokine expression. The SKOV3ip1 cells were selected for co-culture since they were thought to be HGSC cells (section 4.1) and were invasive in the 3D omental model as described in chapter 4 (Figure 4-10), whereas the AOCS1 cells were not invasive (Table 4-2). The SKOV3ip1 cells were co-cultured in the 3D model with (Figure 7-3c & d) and without (Figure 7-3a & b) the PBMC derived macrophages to determine what effect the macrophages may have on ovarian cancer cell invasion. Malignant cells may lose cytokeratin expression during the process of invasion (Huang et al., 2012). Hence, GFP-labelled ovarian cancer cells can be distinguished from other cell types in the model with greater accuracy than using pan-cytokeratin as a marker (Figure 7-1).

11.3% of the total cell population in the microenvironment of the 3D omental model culturing the SKOV3ip1 ovarian cancer cells equated to approximately 17,800 macrophages. 20,000 PBMC derived macrophages were therefore introduced to the models (Figure 7-3). The CD68 positive macrophages can be clearly identified in immunofluorescence labelled cross-sections of the model (Figure 7-3c). The macrophages not only survived in the model, but they also incorporated themselves into the matrix (Figure 7-3c & d). Figure 7-3d demonstrates co-localised staining of GFP and CD68, suggesting that the CD68 positive macrophages may have a tendency to phagocytose the tumour cells cultured in the model. Alternatively, the co-localised staining may be a result of direct interactions between the tumour cells and macrophages. Such interactions mediated by integrins have been reported to promote tumour cell viability during metastasis (Chen and Massague, 2012). In addition, macrophage differentiation increases auto fluorescence (Daigneault et al., 2010), which may have also contributed to the fluorescence of the macrophages in the 488nm green channel as observed in Figure 7-3d.

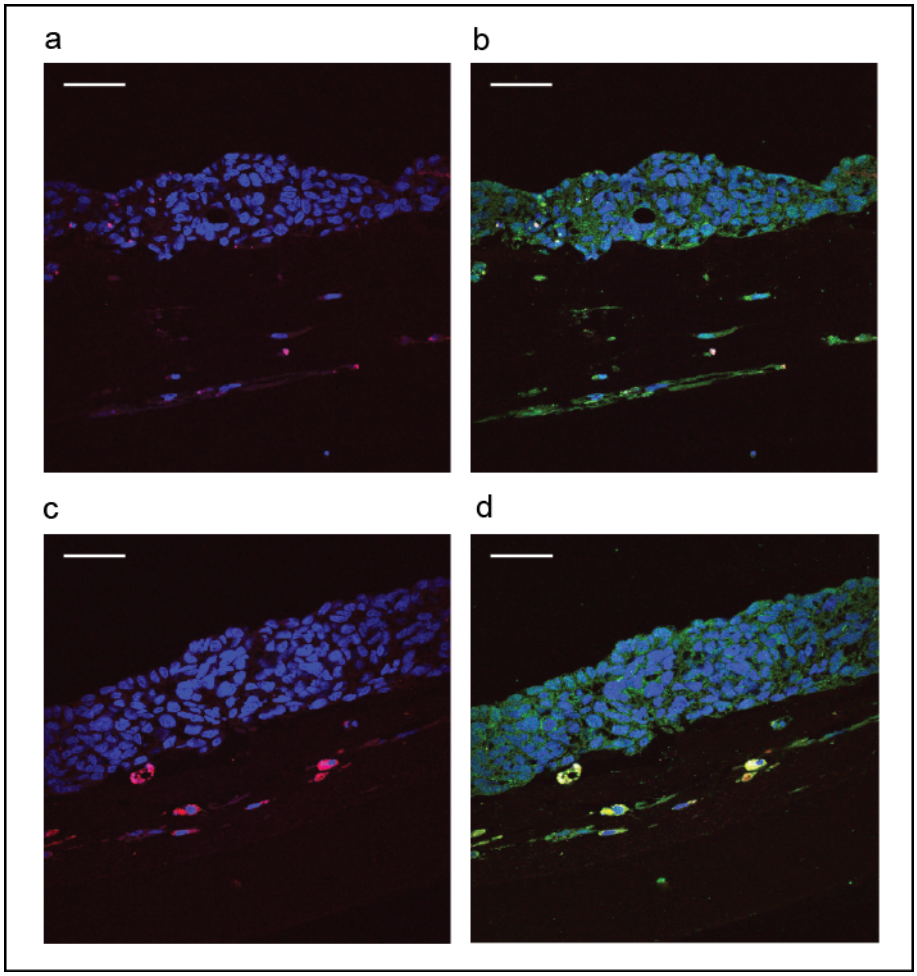

Figure 7-3 Co-culture of SKOV3ip1 ovarian cancer cells and PBMC derived macrophages in the 3D omental model.

Representative immunofluorescence images of 5 μm thick cross sections of the 3D omental models when ovarian cancer cell line SKOV3ip1 was co-cultured for two weeks **a & b)** without and **c & d)** with 20K tumour-infiltrating mimicking PBMC derived macrophages (mϕ). PBMCs were isolated from the blood of a healthy donor. **a & c)** Images showing CD68 immunostaining. **b & d)** Images showing merged CD68 and GFP immunostaining. Blue = Hoechst nuclei stain, Green = GFP, Red = CD68. 40x magnification, bar = 50 μm.

Expression of CD68 observed in the 543nm red channel was specific to macrophages in the immunofluorescence labelled cross-sections of the model (Figure 7-3c). Therefore images of the CD68 staining alone were used to eliminate the macrophages from the images using the image analysis software ImageJ. Subsequently these images were used to quantify the tumour cell area and invasion as previously described in chapter 4.

There was time for only one experiment to be carried out in collaboration with MedImmune. However the observable trend of the data illustrated a decline in SKOV3ip1 ovarian cancer cell growth (Figure 7-4a), proliferation (Figure 7-4b) and invasion (Figure 7-5) in the presence of PBMC derived macrophages. This may support the concept that macrophages introduced into the 3D omental model undergo phagocytosis of the co-cultured tumour cells. Additionally the macrophages may be producing cytotoxic reactive nitrogen and oxygen intermediates and TNF-α that can induce apoptosis in the ovarian cancer cells (Sica and Mantovani, 2012). These tumoricidal activities of macrophages may be collectively contributing to the potential decline in tumour growth and invasion observed in the 3D omental model (Figure 7-4 & 5).

However, in ovarian cancer an infiltrate of macrophages is associated with a poor patient prognosis (Kryczek et al., 2007; Vaughan et al., 2011). The 3D omental co-culture system may not have sufficient time for the microenvironment to polarise the macrophages into a tumour-promoting phenotype. Therefore the macrophages may need to be polarised before incorporated into the model. Alternatively it would be interesting to maintain the cultures for an even longer time period than two weeks to determine whether the macrophages eventually become polarised and promote tumour cell growth.

In more recent years the polarisation status of macrophages has been better appreciated as a continuum of phenotypes (Wynn et al., 2013), but for simplicity macrophages have been sub-categorised by their classical (M1) and tumour-associated (M2) phenotypes (Section 1.2.3). M2 macrophages have previously been further sub-divided to M2a, b and c macrophages in accordance with the activating stimuli (Mantovani et al., 2004). Broadly speaking, the M2a macrophages activated by IL-4 and IL-13 are involved in phagocytosis, and would therefore have tumoricidal capabilities. Whereas at the opposite end of the spectrum,

the M2c macrophages activated by IL-10, are more driven towards regulation of the immune system. These macrophages would be more representative of those that promote tumour progression. Interestingly, the M2c macrophages also have greater involvement in ECM deposition. It would be important to consider polarising the macrophages more specifically towards an M2c phenotype to better support the malignant microenvironment of the developing 3D omental model, and to establish a system where ECM remodelling could be measured.

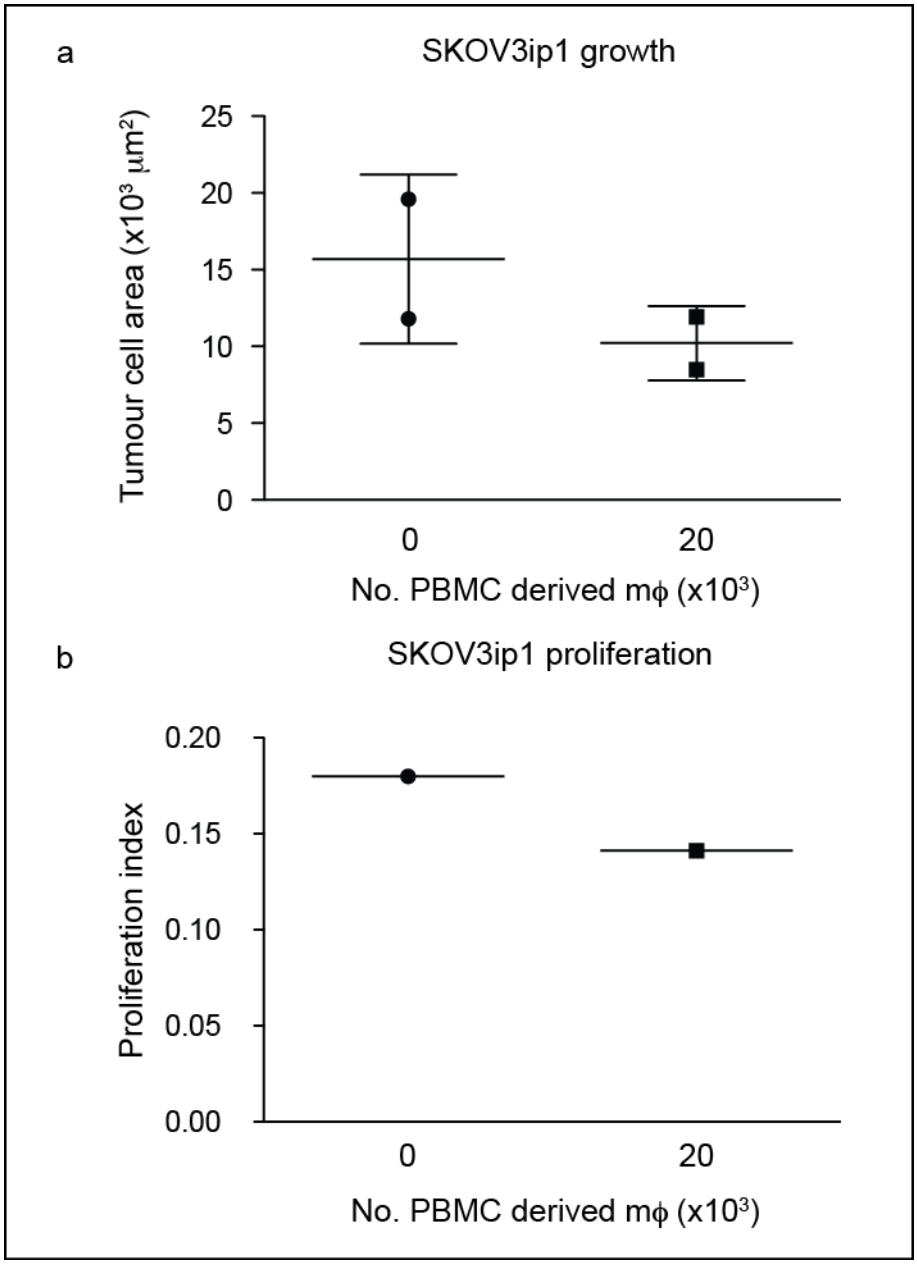

Figure 7-4 The effect of PBMC derived macrophages on the growth and proliferation of the SKOV3ip1 ovarian cancer cell line on the 3D omental model

Graphs illustrating the quantified **a)** growth and **b)** proliferation indices of the ovarian cancer cell line SKOV3ip1 on the 3D omental models co-cultured with and without 20K tumour-infiltrating mimicking PBMC derived macrophages (mϕ). PBMCs were isolated from the blood of a healthy donor. Tumour cells were cultured on the 3D omental model for two weeks. Photographs of immunofluorescence stained sections were taken across the whole section of each model. Each treatment group was tested with duplicate models. The tumour area (μm^2) on each photograph was quantified as a measure of tumour growth. To quantify proliferation indices, 3D omental model cross-sections were analysed by computer-aided microscopy and Leica Ariol software. Values are the number of Ki67 positively stained cells in relation to the hematoxylin nuclear counterstain. Bars indicate the means and standard deviations across all measurements. Data from a single experiment. Data not statistically significant.

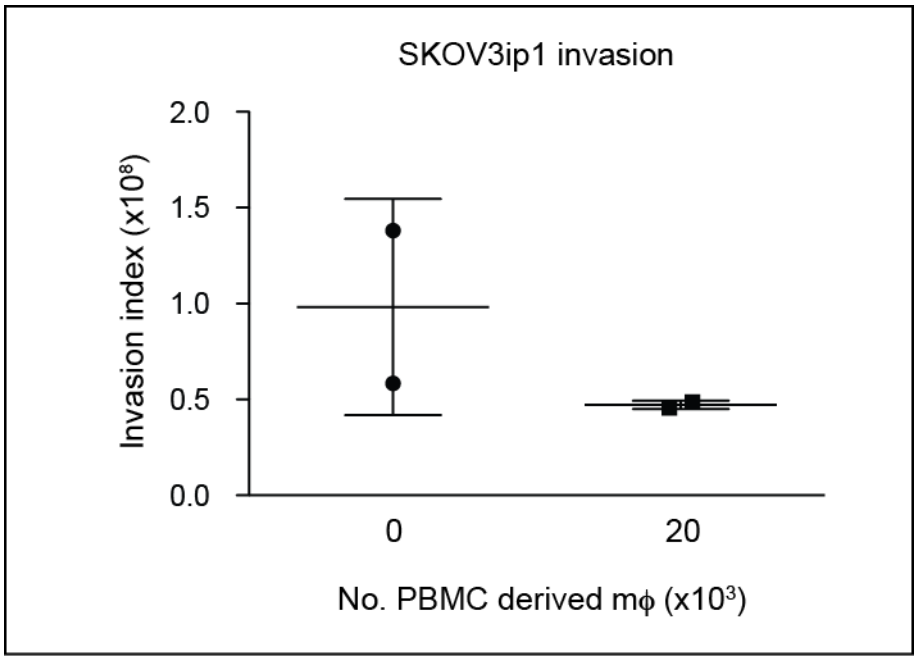

Figure 7-5 The effect of PBMC derived macrophages on the invasion of the SKOV3ip1 ovarian cancer cell line in the 3D omental model

Graph illustrating the quantified invasion index of the ovarian cancer cell line SKOV3ip1 in the 3D omental models co-cultured with and without 20K tumour-infiltrating mimicking PBMC derived macrophages (mϕ). PBMCs were isolated from the blood of a healthy donor. Tumour cells were cultured on the 3D omental model for two weeks. Photographs of immunofluorescence stained sections were taken across the whole section of each model. Each treatment group was tested with duplicate models. The invasion index from each photograph was determined. The invasion index is a factor of the number of invading particles, tumour area (μm^2) and invasion distance (μm). Bars indicate the means and standard deviations across all measurements. Data from a single experiment. Data not statistically significant.

Cytokine production can be used as a measure of macrophage polarisation. The inflammatory cytokines TNF-α and IL1-β are known to promote malignant transformation and metastasis (Balkwill and Mantovani, 2012). In addition, many oncogenic mutations are drivers of inflammatory signalling pathways. For example RET activation in thyroid carcinomas induces the expression of the pro-inflammatory cytokine IL1-β, the angiogenesis inducing cytokine IL-8, and also CXCR4 in the malignant cells. (Grivennikov et al., 2010; Mantovani et al., 2008). Therefore in this 3D omental model where there are direct cell interactions between immune, malignant and stromal cell types, the

levels of cytokines and chemokines were investigated compared to control models which were absent for the PBMC derived macrophages (Figure 7-6). RNA was extracted from the 3D omental models and qRT-PCR was performed on the reverse transcribed cDNA to analyse the relative expression of a panel of cytokines and chemokines. There were detectable increases in cytokine and chemokine levels in the presence of PBMC derived macrophages (Figure 7-6). There was an increase in the relative expression levels of the pro-inflammatory and classical macrophage associated cytokines IFN-γ (Figure 7-6a), IL-12 (Figure 7-6c), IL1-β (Figure 7-6e) and IL-6 (Figure 7-6f), however there was no detectable increase in TNF-α (Figure 7-6b). Given the high levels of TNF-α already expressed by ovarian cancer cells as previously described by the TNF network (Kulbe et al., 2012), any increase in the levels of TNF-α within the metastatic microenvironment mimicked by the 3D omental model, may not be easily measured by qRT-PCR.

Interestingly there was an increase in the anti-inflammatory, tumour-associated macrophage related cytokine IL-10 (Figure 7-6d). Tumour-associated macrophages promote angiogenesis (Wynn et al., 2013) and there was also an increase in the angiogenic cytokine IL-8 (Figure 7-6g) in the 3D omental model in the presence of PBMC derived macrophages. There was however no detectable increase in VEGF (Figure 7-6h). This may be consequential to the absence of vascular endothelial cells in the model system, or due to the normoxic growth conditions that the 3D omental models were cultured in, as angiogenic macrophages are driven by hypoxia (Wynn et al., 2013).

In addition, following the significant but minimal effect of an antibody targeting CXCL12 in the 3D omental model as described in chapter 5, introducing PBMC derived macrophages to the model increased the relative expression levels of CXCL12 (Figure 7-6i). Therefore the CXCL12 targeted antibody may have a greater impact on the growth,

survival and invasion of ovarian cancer cells co-cultured in a 3D omental model that includes a macrophage infiltrate.

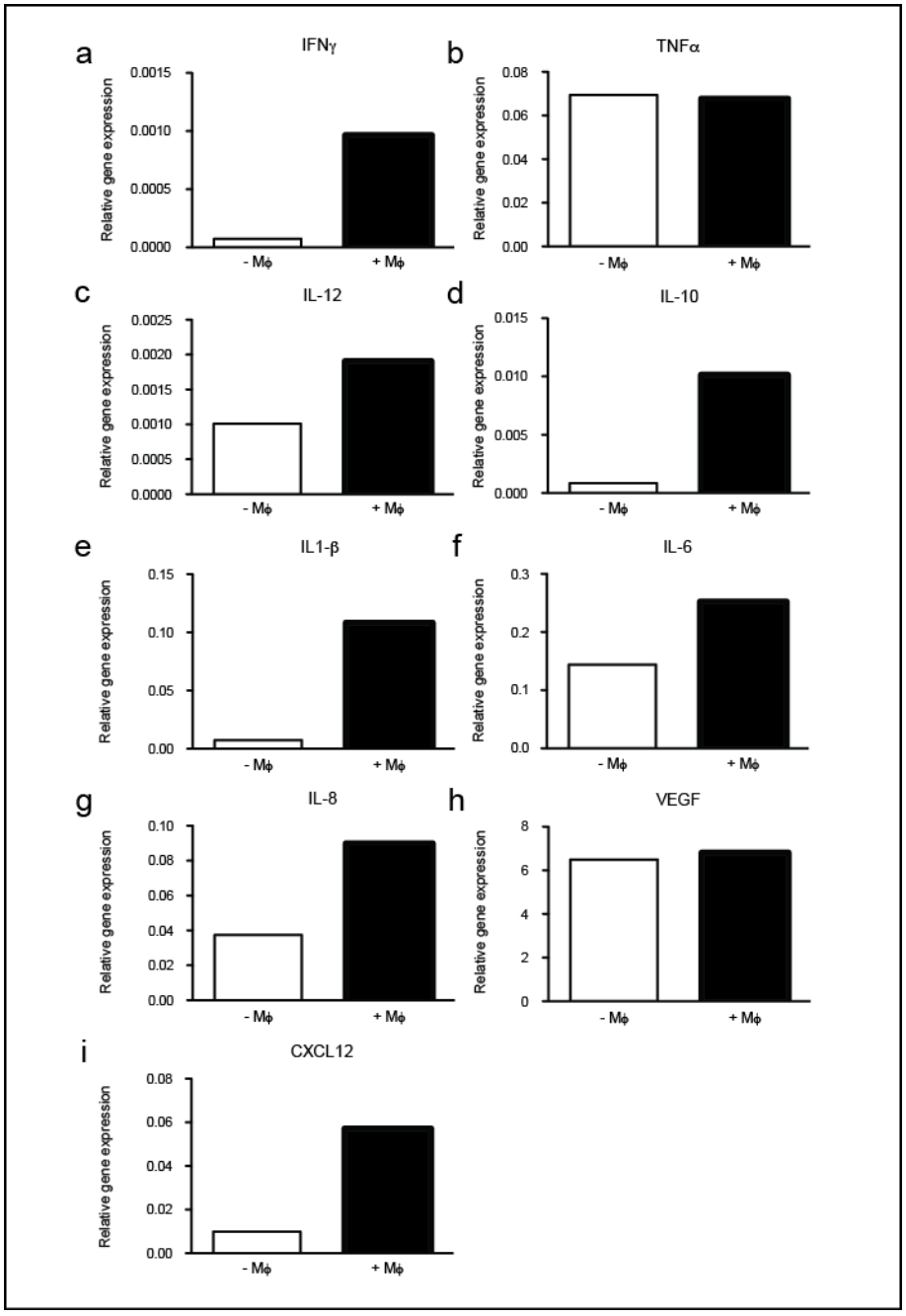

Figure 7-6 The effect of PBMC derived macrophages on the relative gene expression of cytokines and chemokines in the 3D omental model

The relative mRNA expression levels measured by quantitative real-time PCR of **a)** IFNγ, **b)** TNFα, **c)** IL-12, **d)** IL-10, **e)** IL1-β, **f)** IL-6, **g)** IL-8, **h)** VEGF and **i)** CXCL12 in the 3D omental model when the ovarian cancer cell line SKOV3ip1 were co-cultured with and without 20K tumour-infiltrating mimicking PBMC derived macrophages (mϕ). PBMCs were isolated from the blood of a healthy donor. Tumour cells were cultured on the 3D omental model for two weeks. Bars represent the fold change in gene expression calculated relative to the geometric mean of the cycle threshold values for the reference genes ACTB, YWHAZ, TBP and HPRT1. n = 1.

7.3. Conclusions and future work

These data shown here in this chapter is preliminary work that sets scope for much further optimisation and development. From this chapter the following points can be considered for future work:

- Complete titrations and ratio controls between the numbers of macrophages versus the other cells in the 3D omental model needs to be established and optimised.
- Are the macrophages phagocytosing the co-cultured tumour cells? Are the macrophages active in other tumoricidal mechanisms within the model?
- PBMC derived macrophages are a better cell type to use in the co-culture system than THP1 derived macrophages.
- The expression of any genes of interest in the 3D omental model can be analysed by qRT-PCR.
- Gene expression and cellular interactions in the 3D omental model with an introduced macrophage infiltrate may be more accurate to the clinical situation if the models were cultured in hypoxic conditions.
- Ovarian cancer cell lines that are grown on the 3D omental model must now be chosen with greater caution.

Once established, a 3D cell culture model mimicking an inflammatory infiltrate of macrophages in omental metastases of HGSC, could be used to study the impact of macrophage polarisation on the tumour microenvironment. Similarly the influence of the stromal and malignant components of the microenvironment on the macrophages themselves could also be investigated. With an inflammatory cell component the model would be more appropriate for ovarian cancer and inflammation studies, and would be a phenomenal tool for testing potential therapeutic targets. Data from this thesis provided preliminary data for the CANBUILD project grant proposal, for which the European Research

Council awarded €2.43 million to the laboratory earlier this year. The CANBUILD project will continue and advance the work of the 3D omental model development including incorporation of immune cell subtypes.

Chapter 8

8. Discussion

8.1. Implications to the field of ovarian cancer research

The work of this thesis approaches two important areas of current research into HGSC. The first is the study of the metastases. In the clinic HGSC patients present with widespread peritoneal metastases and it is this aggressive dissemination of the disease that is reflected in the poor overall survival rates. Yet there still seems to be a strong focus in the field of research around the development of the primary tumours. Without disputing the importance of this work, survival rates have not changed in the last 30 years. This somewhat suggests that a shift in paradigm towards what distinguishes the metastases from the primary mass is required when it is the metastases that pose the real clinical problem.

The metastasis of HGSC is different from many other cancers. HGSC cells disseminate freely in the peritoneal fluids and do not necessarily require access to the blood or lymphatic vessels to colonise other organs. Women predominantly present at such a late stage in disease progression, that the opportunity to monitor metastasis development has long passed. There is therefore a demand for appropriate models of HGSC to study this stage of the disease hence the other topic investigated in this thesis.

8.2. Future work on inflammatory infiltrates in the tumour microenvironment of HGSC

Inflammation in the tumour microenvironment was recently recognised as one of the hallmarks of tumour development (Hanahan and Weinberg, 2011). The work of chapter 3 aimed to characterise the inflammatory cell infiltrates of HGSC omental metastases, and identified a positive correlation between CD68 positive macrophages and Ki67 positive epithelial cells (Figure 8-1). The next question would be to delineate the polarisation of those macrophages in the selected patient samples.

Since the completion of this work, Dr Steffen Boehm in the laboratory established a TMA of all the omental metastases with additional samples collected. However TMA cores cover an even smaller localised area of the metastases than the whole tissue sections. If malignant cells from the centre of an omental deposit dominate a TMA core, immune infiltrates surrounding that deposit (as observed in chapter 3), may fail to be included in the analysis.

By immunohistochemistry, classically polarised macrophages expressing the cell surface receptors CD40, CD80 and MHC class II could be quantified with the Leica Ariol imaging software. TAMs expressing CD163 in the ascites of HGSC patients were recently associated with reduced relapse free survival (Reinartz et al., 2013). This could also be used as a marker of TAMs by immunohistochemistry in the omental metastases. It may also be possible to digest the omental specimens and measure inflammatory cell infiltrates by flow cytometry, however it is important here to be wary of the disruption of cell surface proteins by the digestion method. In addition the observation of inflammatory cell localisation within the metastases is lost using FACS analysis.

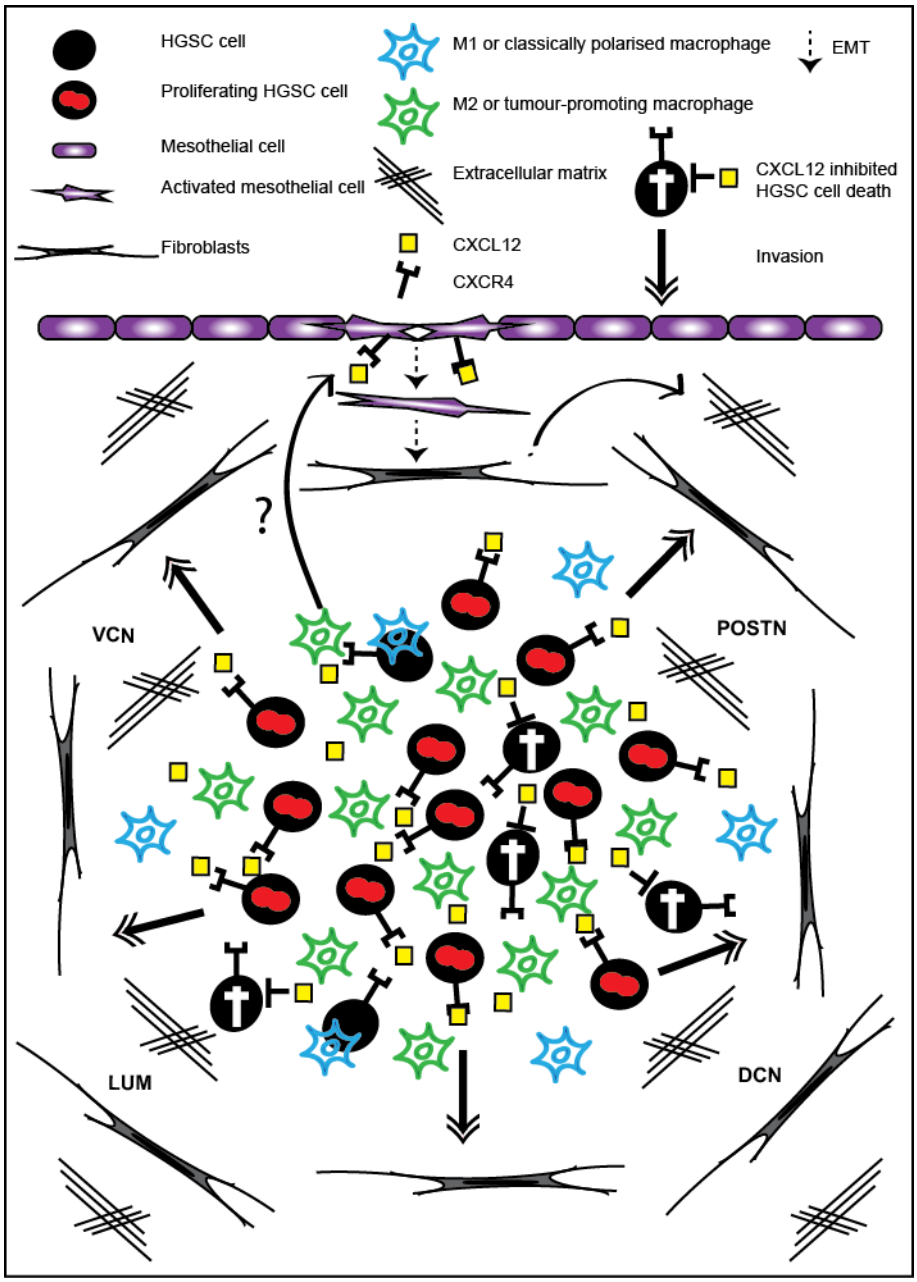

Figure 8-1 Summary of cellular interactions in HGSC metastasis.

An increase in tumour-promoting macrophages within the microenvironment of HGSC correlated with an increase in proliferative Ki67 positive tumour cells. The mesothelial cells promoted tumour growth and invasion. The expression of CXCL12 may increase tumour cell survival. The expression of CXCR4 and its ligand associated with the expression of the extracellular matrix genes decorin (DCN), lumican (LUM), versican (VCN) and periostin (POSTN). M1 classically polarised macrophages may engulf tumour cells within the metastatic microenvironment. M2 tumour-promoting macrophages could potentially interplay with the mesothelial cells, stimulating their contractility, activation and EMT, leading to increased matrix deposition.

Dr Steffen Boehm was able to further define the T cell populations in the established TMA, and identified a significant reduction in Ki67 positive epithelial cells with increased CD8 positive T cells (manuscript in preparation). This agrees with previous studies associating a CD8 positive T cell infiltrate with improved patient prognosis (Fridman et al., 2012).

In the human omental metastases TMA, no significant correlations were identified with CD4 positive T cells and Ki67 positive epithelial cells. Perhaps further discrimination of memory, FOXP3 positive regulatory and helper T cells would prove otherwise.

Descriptive analyses of inflammatory infiltrates in the metastases really carry little meaning unless the numbers are correlated with a cellular function, such as malignant epithelial cell proliferation for example (as described in chapter 3). By immunohistochemistry it would also be possible to quantify the number of apoptotic cells using the TUNEL (Terminal Transferase dUTP Nick End Labelling) assay. TUNEL is a marker of DNA degradation. This would give a better indication of how well tumour cells are surviving in the metastases especially after chemotherapy.

The TMA cores would be beneficial here also to correlate the inflammatory cell infiltrates with the scored expression of inflammatory cytokines and chemokines such as CXCL12 (Figure 8-1). An understanding of this may give an indication of the cytokines and chemokines predisposing the omental metastasis microenvironment to support the infiltrate of particular inflammatory cells. These cytokines and chemokines may then be targeted to diminish the tumour supporting inflammatory cell population, and recruit the tumour-targeting inflammatory cells.

Cytokeratin 7 (Lengyel, 2010) and CA-125 expression (Bast, 2003; Perets et al., 2013) are markers often used as a measure of ovarian

cancer epithelial cell content in immunohistochemistry sections. However cytokeratin 7 expression can be very heterogeneous (data not shown). In chapter 3 the malignant epithelial cell areas of whole tissue sections were defined to quantify the number of Ki67 positive cells. These areas could therefore be better defined with CA-125 immunostaining. These areas could then be used to calculate an index for the tumour versus stroma content of each of the samples. This may be useful to correlate with the expression of certain cytokines and chemokines to define where in the metastases they are predominantly expressed.

The intensity of immunohistochemical stains can be quantified on the Ariol. Therefore the intensity of Herovici staining and expression of αSMA for example, could be quantified to give an indication of collagen deposition and stromal activation respectively in the omental metastases.

In time it would be particularly interesting to relate all the collated data on these omental metastases to clinical data, such as patient survival and response to chemotherapy. However the collection of samples for this particular tissue bank started with the beginning of the work for this thesis four years ago, therefore at the time of writing this thesis it was too early to establish five-year survival rates. In addition, when collecting the samples, if there was a more severe case, the surgeons ethically chose not to operate, and we did not receive a sample. Consequently the patients from whom we received samples are likely to survive longer, which will further increase the time before survival data can be recorded. This also meant that a high percentage of the samples collected were not colonized with disease, rendering them unsuitable for the immunohistochemistry studies.

The ascites are also rich in inflammatory cells. It would perhaps be useful diagnostically to examine and compare the inflammatory infiltrates

of the ascites with those of the metastases. It could then be questioned whether the immune cell composition of the ascites is predictive of that in the metastases. An established data set such as this could then later be compared with potential blood biomarkers. The difficulty with such a study is the logistics of acquiring all the necessary samples from each patient. For this thesis ascites could not be collected from the same patients that omental specimens were received from. The procedure of draining the ascites was carried out some time before surgery and in a completely different hospital that was not easily accessible to Barts Cancer Institute.

8.3. Future work on the 3D omental model of HGSC metastasis

One focus of this thesis was to establish, optimise and develop a 3D omental cell culture model that mimics HGSC colonisation in the omentum. The model was originally established in Ernst Lengyel's laboratory at the University of Chicago (Kenny et al., 2007). Lengyel and colleagues isolated their primary fibroblasts and mesothelial cells from benign omental specimens. The patients they collected samples from did not have cancer, endometriosis or any inflammation. All of the omental samples collected for this thesis were from ovarian cancer patients, and this was one difference between the model established here and the original Lengyel model. Normal omentum was not accessible for the work in this thesis. The potential to obtain small samples of omentum when surgeons routinely remove scarred tissue from previous abdominal surgeries was investigated, however this has been awaiting ethical approval.

The original model was designed to study early adhesion events in ovarian cancer metastasis, whereas the model established in this thesis was intended for studying more developed omental deposits. Hence the models for this thesis were composed with cancer-associated primary

cells and successfully kept in culture for two weeks as opposed to five days. The Lengyel laboratory has now scaled their 3D omental model to be suitable for 384 well high throughput adhesion assays (communication from Prof Ernst Lengyel). Generating high throughput assays with this model will be of significant interest to pharmaceutical companies for testing therapeutic targets.

Patient sourced samples with varying levels of disease are likely to yield primary cells with different levels of activation. This often implicated the reproducibility of results experimenting with the 3D omental model in this thesis. Ideally several experimental replicates are required to produce results with statistical significance, which was limited by the availability of samples and the number of primary cells isolated.

Lengyel and colleagues characterised their HPMCs by the positive expression of cytokeratin 8/18 and vimentin, and the negative expression of the collagen synthesising enzyme prolyl-hydroxylase. The HPFs were proved to be positive for vimentin, prolyl-hydroxylase and trichrome staining which indicated the presence of collagen fibrils. However it was not clearly illustrated that the HPFs were negative for cytokeratin 8/18. A large proportion of the HPFs collected for this thesis were positive for cytokeratin 8/18 suggesting that these cells were activated HPMCs (Figure 8-1). With the controversy in the field about the legitimate markers that define a fibroblast, it seems insufficient to characterise the HPFs purely by their ability to synthesise collagen. At the beginning of the work for this thesis, the primary cells cultured on coverslips were studied for E-Cadherin and α-SMA positivity by immunofluorescence (data not shown). The E-Cadherin expression was not significantly different in the HPMCs compared with the HPFs however α-SMA expression was higher in the HPFs, further supporting the concept that these cells were activated. The primary cells were also stained as cytospins for FAPα and $\alpha V\beta 1$ integrin, to try and differentiate the HPMCs from the HPFs, but this also came with little success.

HPMCs are also negative for the epithelial marker EpCam (Ranieri et al., 2013). Despite the absence of distinguishing cell surface markers, the primary cells were autofluorescent and particularly sensitive to the processing required for FACS (Figure 5-3). The auto fluorescence would have interfered with the cell sorting process even if cell surface markers were available. Without definitive markers for distinguishing the primary cells, it was concluded that the HPMCs would be identified by their morphology, and that the 3D omental models would be predominantly cultured with cytokeratin negative human embryonic fibroblasts instead of the HPFs. HPFs were used when they were available.

The key finding from the establishment of the 3D omental model in this thesis was the importance of the HPMCs in promoting tumour cell growth and invasion (Figure 8-1). As previously mentioned the availability of human omentum samples and primary cell yields limited the rate at which experiments could be carried out. To investigate the role of the HPMCs further, it would be hugely beneficial to immortalise the HPMCs from at least three patients, and use these cells in subsequent experiments. A method for the immortalisation of primary cells often involves the exogenous expression of Telomerase Reverse Transcriptase (hTERT) (Fridman and Tainsky, 2008). This method alone is not usually successful for the immortalisation of epithelial cells, however it was used in combination with small interfering RNA silencing of p53 (Yang et al., 2007b) and retinoblastoma (Yang et al., 2007a) to immortalise human primary ovarian surface epithelial cells. An alternative method of immortalising primary cells involves transfecting the cells with Simian Virus 40 T antigen (Lundberg et al., 2000). This inactivates tumour suppressor proteins. Such interference with the expression and activation of tumour suppressor genes and proteins respectively may however generate undesirable oncogenic attributes in the immortalised cells.

At the beginning of this thesis, the LP-9 mesothelial cell line was used to establish the 3D omental model (data not shown). Unfortunately these

cells have a mesenchymal morphology and do not resemble the cobblestone appearance of the primary mesothelial cells described in the Lengyel 3D model (Kenny et al., 2007). Therefore the use of these cells in the 3D omental model established for this thesis was discontinued. The mesenchymal morphology of these cells may be an indication that these cells were activated in the immortalisation process.

Several measurable read outs could be used to study the activation of HPMCs, for example α-SMA expression, migration and the secretion of growth factors and cytokines. Iwanicki and colleagues demonstrated the interactions between the myosin network, talin I and $\alpha V\beta 1$ integrin in ovarian cancer cells that drive the contractility and displacement of mesothelial cells in the presence of invading spheroids (Iwanicki et al., 2011). Time-lapse video microscopy and the displacement of fluorescent beads in matrices were assays used in this study that could be used to investigate the effect of therapeutic targets on the role of HPMCs in HGSC metastasis.

It is possible that the cytokine and chemokine signalling network that is up-regulated in HGSC (Kulbe et al., 2012) is contributing to the contractile nature of the HPMCs in response to invading tumour cells. Sanz-Moreno and colleagues describe how cytokine signalling via JAK1 and the phosphorylation of myosin light chain (MLC) 2 in myosin II leads to increased contractility in stromal fibroblasts and melanoma cells (Sanz-Moreno et al., 2011). As the siRNA silencing of myosin II in invading ovarian cancer cells leads to the reduced contractility and clearance of interacting mesothelial cells (Iwanicki et al., 2011), perhaps similar cytokine signalling mechanisms are involved more directly in mesothelial cell contractility. Matrix contraction assays and the 3D omental model itself could be used to evaluate this.

Matrix deposition is also indicative of stromal activation (Erler and Weaver, 2009) . Communications with Ernst Lengyel reveal that ovarian

cancer cells do in fact activate the HPMCs through TGFβ signalling, which leads to an increase in fibronectin production (manuscript in preparation). TGFβ is a driver of EMT. Therefore it would be interesting to investigate the implication of potential therapeutic targets on the expression of mesenchymal markers such as the loss of E-Cadherin and cytokeratins and the increase in N-Cadherin and vimentin (Wan et al., 2013) in the activation of HPMCs. Proving that HGSC drives activation and EMT in HPMCs would have clinical relevance given that the CLOVAR model described by Veerhaak RG and colleagues associates a mesenchymal signature with the worst prognosis in HGSC patients (Verhaak et al., 2013).

The 3D omental model as a whole will offer its greatest value to pharmaceutical companies where there is a necessity to bridge the void between cells grown on plastic that provide quick results, to *in vivo* experiments which take a long time and are expensive to run. The void is of course made greater by the fact that the results from the *in vitro* experiments often do not reproduce *in vivo*. Supernatants from the 3D omental models can be collected and could be analysed on a multiplex cytokine secretion platform such as the Luminex. Equally both RNA and protein can be extracted from the 3D models for the performance of gene expression and protein arrays. The recently described CLOVAR (Verhaak et al., 2013) and PROVAR (Yang et al., 2013b) models could be applied to the 3D omental model after treatment with a potential therapeutic agent, to predict whether the therapy could improve patient survival. In addition the 3D omental model could be used to test therapies in combination with Paclitaxal and Carboplatin. Potentially treatment of the model with less than optimal concentrations of current chemotherapy drugs over a period of one week or more could recapitulate molecular changes in the model associated with the development of chemoresistance.

What is critical to the translation of results from the 3D omental model to the clinical situation is that the model truly resembles the subtype of

ovarian cancer under question. This involves insuring that the correct cell line subtype is co-cultured with the model. In light of the recent reports from Domcke et al (Domcke et al., 2013) and Anglesio et al (Anglesio et al., 2013), it has become clear that many of the ovarian cancer cell lines that we were using were not representative of the subtype that it was classified to be. The significance of these reports to this thesis was that the SKOV3ip1 cells were not representative of HGSC (Domcke et al., 2013) and the RMG1 cells were unclassified (Anglesio et al., 2013). The AOCS1 cells were confirmed to have TP53 mutations characteristic of HGSC (communication from Dr Carla Milagre) and the TOV21G cells were classified as CCC (Anglesio et al., 2013). The TOV21G cells were also found to be hypermutated (Domcke et al., 2013), which perhaps suggests that they have the capacity to evolve quickly and readily adapt to novel environments, owing to their level of chemoresistance.

Despite recent revelations regarding the identity of cell lines (Anglesio et al., 2013; Domcke et al., 2013), the original aim in chapter 4 was to optimise the growth of HGSC and CCC cell lines on the 3D omental model. Although HGSC is the focus of this thesis, the work of this chapter illustrates that the 3D omental model could be used for research into more than one subtype of the disease.

During the course of this thesis, over one hundred human omental specimens were digested to isolate HPMCs. One particular specimen from patient G33 was especially diseased. The digestion process yielded no HPMCs or HPFs, however after a period of time in culture colonies of HGSC cells were growing. Over the course of a year these cells were expanded and used as model cell line in the laboratory. The cells were wild type for the R175H mutation in exon 5 and the R273H mutation in exon 8 of the TP53 gene which are two of the most frequently occurring TP53 mutations in HGSC (Ahmed et al., 2010; Cancer Genome Atlas Research, 2011; Lee et al., 2007b). However, the cells carried a W146* substitution mutation in exon 5 (data not shown).

This mutation introduces a premature stop codon, and translates a truncated protein (IARC TP53 database). It is yet to be confirmed whether the truncated protein in this new cell line is stable enough to be detected by western blot.

The new HGSC G33 cell line was successfully grown on the 3D omental model. In other projects in the laboratory it was shown to be relatively inert in terms of cytokine production (communication from Dr Hagen Kulbe) and it formed spheroids in hanging drop cell culture plates (communication from Dr Oliver Pearce).

The low levels of cytokines produced by this cell line may indicate that the cells have a greater dependency on the tumour microenvironment for survival. Since the recent publications by Domcke et al (Domcke et al., 2013) and Anglesio et al (Anglesio et al., 2013), the value of the new HGSC G33 cell line to the laboratory has increased, and could be a great resource in future studies, particularly those involving the 3D omental model.

It was clear from the work optimising the growth of four cell lines on the 3D omental model, that individual cell lines will react quite differently to the omental microenvironment that cannot always be predicted by their growth in animal models. For instance, IGROV1 cells that grow very well in animal models did not grow at all on the 3D omental model. The translation of *in vitro* data to animal model data will always present limitations, however a human 3D model mimicking metastasis such as this will produce more reliable and accurate results than any other *in vitro* system currently available.

8.4. Chemokine signalling in a the 3D omental model

The efficacy of an antibody targeting the chemokine ligand CXCL12 was tested in the 3D omental model. The purpose of this was to develop an *in vitro* model for further studies into the association between CXCL12 and ECM remodelling in HGSC metastasis. These data generated by the model showed a statistically significant reduction in tumour cell growth with antibody treatment (Figure 8-1). The concentration of the antibody tested in the 3D model was determined from previous work in the laboratory. This previous work demonstrated an optimal inhibition of the migration of the CCC cell line TOV21G in the transwell migration assay at 10µg/mL of antibody. Ideally, given accessibility to larger volumes of the 114_3H1 antibody, a greater range of concentrations would have been tested in the 3D omental model to further confirm that the observed effect of the antibody was truly dependent upon the activity of the compound tested. In addition, the dosing experiment would have been particularly relevant since the effects therapeutic agents would have on cells grown in the 2D transwell migration assay, would differ quite significantly to their effects when cells are cultured in the 3D omental model.

A commercially available antibody targeting CXCL12 also showed a trend towards a decrease in tumour growth with increasing antibody concentrations (data not shown). Although these data were not statistically significant, the observed trends were reproducible of those seen with the antibody 114_3H1. This therefore supported the conclusion that the 114_3H1 antibody was active and effective at neutralising CXCL12 in the 3D omental model.

The 114_3H1 antibody elicited no significant effect on tumour cell proliferation in the 3D omental model as measured by Ki67 positivity. However using tumour cell area as a measure of growth, the CXCL12 targeted antibody significantly reduced tumour growth. Together this

suggested that CXCL12 was more important in the survival of the tumour cells in the 3D omental model rather than their proliferation (Figure 8-1). This conclusion could be consolidated further using alternative cell viability assays in the model such as the CellTiter blue assay.

In chapter 6 more ECM genes correlated with CXCR4 than CXCL12 expression. In future studies it could be important to consider targeting the receptor CXCR4 with the molecular inhibitor AMD3100. The 3D omental models were treated with AMD3100 in a single experiment during the work for this thesis. Conversely to targeting the ligand CXCL12, targeting the receptor had no inhibitory effect on the growth of the HGSC cell line AOCS1 or the invasion of the CCC cell line TOV21G in the 3D omental model (data not shown). Further experiments with AMD3100 were required, however greater confidence was gained in the efficacy of the ligand targeted antibody 114_3H1.

Success with the efficacy of this therapeutic agent and others in the 3D omental model further supported its potential role in the drug discovery process. Furthermore the 3D omental model could now be used to develop current concepts and investigate hypotheses surrounding the TNF network in HGSC metastasis. For instance, in this thesis the importance of the HPMCs in tumour growth in the model was identified (Figure 8-1). The role of the CXCR4 pathway in cell adhesion and integrin signalling is also well known (Hartmann et al., 2005). Therefore perhaps chemokine signalling plays an important role in HPMC activation and in αVβ1-fibronectin interaction mediated HPMC clearance (Iwanicki et al., 2011). Chemokine gradients could be incorporated into the 3D collagen matrix of the model, to determine whether they play a role in driving the clearance of the HPMCs.

Collaborative studies with the postdoctoral scientists in the laboratory using the 3D omental model proved that the model could be used to validate the expression of any genes of interest associated with the TNF

network, and its cross-talk with other networks, such as EGFR signalling. CXCL12 has been described to be amplified in primary ovarian tumours, but not in the matched peritoneal metastases (Malek et al., 2011). This signalling pathway may therefore carry greater significance in the growth of the primary tumour, which might explain the conclusive but not so greatly potent inhibitory effect of the CXCL12 targeted antibody 114_3H1 on tumour growth when mimicking metastasis in the 3D omental model. Overall however the important role of CXCL12 in ovarian cancer progression is reflected in the correlation of its expression in patient biopsies with poor survival (Popple et al., 2012). Hence targeting CXCL12 in the 3D omental model and measuring its impact on tumour growth will be an important model system for studying HGSC progression.

8.5. Association between CXCL12 and ECM remodelling

The association between CXCL12, ECM remodelling and cell-matrix interactions was identified in two independent gene expression microarray data sets. Efforts were employed to validate this by qRT-PCR in human omental metastases of HGSC.

Bioinformatics and interrogation of these data sets can generate a wealth of information about the sample set. It would perhaps be useful to generate similar microarray data from the HGSC omental metastasis samples. Despite the quantity of data generated from these high-throughput gene expression platforms, it can often be difficult to find the most appropriate and accurate method to analyse such large volumes of data. Over 5,000 genes were differentially expressed in high CXCL12 expressing ovarian cancer biopsies, which was filtered to 48 genes of interest. Six of these 48 genes were finally validated in the omental metastases therefore there are many genes that could still be validated. Consequently, due to the very small number of genes measured by

qRT-PCR, strong conclusions cannot be drawn from the results, but the results to this chapter can be considered as an indication of what may be occurring in the HGSC metastatic microenvironment. Likewise, comparatively to the 285 and 245 ovarian cancer biopsies of the AOCS and GSE 6008 and 3149 data sets, only ten samples of HGSC omental metastases were analysed in this chapter.

However, of the genes and samples analysed in this chapter, only an increase in decorin expression significantly correlated with an increase in CXCL12 expression (Figure 8-1). The geNorm software used to validate the house keeping reference for the sample set was considered a reliable tool for data analysis. The software developers claim the method (Vandesompele et al., 2002) has been cited more than 3,000 times, and that more than 16,000 scientists across more than 126 countries use the software (http://www.biogazelle.com/qbaseplus).

The lack of consistency of the qRT-PCR results with the analyses of the gene expression microarray data may have been consequential to the differences between the microenvironment of primary tumours and metastases (Malek et al., 2011). More ECM genes did however positively correlate with CXCR4 (Figure 8-1), providing some confirmation of the link between CXCR4 and CXCL12 signalling and ECM remodelling in HGSC metastasis.

CD36, the receptor for thrombospondin 1 associated with a macrophage infiltrate in high CXCL12 ovarian cancer biopsies. The expression of the ECM gene thrombospondin 1 was evaluated in the HGSC omental metastases, but correlated negatively with CD68 positive macrophages. In future studies it would be important to also analyse the expression of CD36 itself in the metastases to better validate the bioinformatics data. However given ECM genes were the interest of this chapter, priority was given to studying thrombospondin 1 expression.

Periostin displayed a negative correlation with CD8 positive T cells. It would be interesting to link the CD8 positive T cell infiltrate associated good prognosis in ovarian cancer with a reduction in periostin expression. However as previously mentioned, at the time of writing this thesis the established bank of omental metastases was not mature enough to acquire patient survival data to test this. Correlating the ECM gene expression with patient survival and response to chemotherapy when the clinical data becomes available would be an important future study to consider. In addition work analysing further immune cell infiltrates could also be later correlated with the ECM gene expression data. For instance it would be of particular interest to investigate the association between M1 and M2 macrophage subtypes and ECM gene expression in the HGSC metastatic microenvironment.

In future work it may also be of interest to investigate and differentiate the expression of ECM genes by the tumour cells and the surrounding stroma. Digestion of the omental metastases and subsequent FACS analysis could be used to isolate individual cell types for RNA extraction and gene expression analysis. Alternatively laser-capture microdissection could also be used to separate tumour and stromal areas from tissue sections.

It is also very important to consider here that gene expression analysed at the mRNA level may not necessarily translate to expression at the protein level. Expression of the ECM proteins could now be analysed by immunohistochemistry and correlated with CXCL12 and CXCR4 in the omental metastases TMA established by Dr Steffen Boehm in the laboratory. This TMA includes more than ten samples, which would also increase the statistical significance of the results.

The work of the new CANBUILD project team in the Balkwill laboratory of Barts Cancer Institute, London will involve building a matrix that is representative of that in HGSC omental metastases. Therefore the work of this chapter initiates an indication of the ECM composition of the

metastatic microenvironment. The ambition is to be able to modulate and control the properties of the matrix, to study the impact on tumour progression. Preliminary to this, the CANBUILD team are studying the matrix density of the omental metastases, which could later be associated with the immune cell infiltrate and clinical data connected to the samples.

8.6. Introducing a macrophage infiltrate to the 3D omental model

The network of inflammatory cytokines and chemokines in the tumour microenvironment regulates an influx of immune cells (Balkwill et al., 2012). The established multicellular 3D omental model lacked an inflammatory infiltrate, and the culture of immune cells in 3D models of ovarian cancer was absent in the field (Lengyel et al., 2013). Previous work in the laboratory described an association with CXCL12 expression and CD68 positive macrophage infiltrates in ovarian cancer biopsies (Kulbe et al., 2012)(Figure 8-1). In addition work for this thesis correlated CD68 positive macrophages with Ki67 positive epithelial cells in omental metastases of HGSC. Given this collectively, for the final chapter of this thesis macrophages were introduced to the 3D omental model in collaboration with MedImmune, Cambridge. This work demonstrated that PBMC derived macrophages incorporated and survived within the matrix of the 3D omental model, and induced measurable changes in cytokine and chemokine expression.

GFP and CD68 expression levels could be measured in parallel by qRT-PCR to normalise the cytokine and chemokine expression levels to the number of tumour cells and macrophages in the models respectively. Of course it would also be important to confirm the changes detected at the mRNA level with secreted cytokine and chemokine levels in the 3D omental model supernatants measured by ELISA or Luminex. For normalisation in this instance, the number of GFP positive tumour cells

and CD68 positive macrophages in the 3D models could be quantified from immunohistochemistry staining with the Leica Ariol software as described in chapters 3 and 5. Alternatively, it would be useful to develop a method to separate the cells post culture in the 3D omental model. Enzymatic degradation of the matrix, and subsequent FACS of the cells could further aid the delineation of which cells in the model are interacting with each other.

When the 3D omental model inclusive of macrophages was co-cultured with the SKOV3ip1 cells, there was a reduction in tumour cell growth, proliferation and invasion, which was potentially due to the phagocytic and tumoricidal activities of the macrophages (Figure 8-1). Whether phagocytosis of tumour cells is taking place in the 3D omental model is a question that needs to be answered. To further study whether phagocytosis is occurring in the 3D omental model, the macrophages could be treated with an inhibitor that perturbs their phagocytic function. The impact of this on tumour growth in the model could then be investigated.

GFP positive tumour cells and CD68 positive macrophages co-stained by immunofluorescence could also be studied in detail at high magnifications to endeavour to identify double nuclei as an indicator of phagocytosis. However given the macrophages in the 3D omental model sections were fluorescing in the red and green channels of the confocal microscope (Figure 7-3) after immunofluorescence staining, perhaps the use of fluorescent-labelled cell tracker dyes would be a more accurate method of detecting the cell subtypes. This way a relatively strong detected fluorescence in the 405nm wavelength could be used to distinguish the macrophages, whilst fluorescence in the 568nm wavelength that can often omit greater background levels could be used for the nuclei. Even when the THP1 and PBMC derived macrophages were cultured alone in the model, the macrophages were fluorescing in the 488nm and 568nm channels of the confocal microscope. This suggests that there was some auto fluorescence generated from these

cells, which can occur through their interactions with the ECM (communication from MedImmune).

As previously mentioned alternative cell viability assays could be used to consolidate the observed reduction in tumour cell proliferation in this final chapter. In light of the recent studies on the legitimacy of characterised ovarian cancer cell lines (Anglesio et al., 2013; Domcke et al., 2013) the SKOV3 cell line was not confirmed as HGSC. On the basis that the positive correlation between CD68 positive macrophages and Ki67 positive epithelial cells described in chapter 1 was observed in omental metastases of HGSC, work with the SKOV3ip1 cells in the 3D omental model was stopped. Since the completion of this thesis and the establishment of the novel G33 HGSC ovarian cancer cell line, further work to study the interactions between macrophages and G33 spheroids in the 3D omental model is being addressed in the laboratory.

It was concluded from this final chapter that PBMC derived macrophages were a better model cell type to use in the 3D omental model than the THP1 derived macrophages. The THP1 cells were reported to secrete lower levels of pro-inflammatory cytokines when stimulated and were less efficient at phagocytosis than PBMCs (Daigneault et al., 2010). In addition the THP1 cells were likely to bear an oncogenic phenotype since they originated from an acute monocytic leukaemia patient (Tsuchiya et al., 1980). However the former report also suggested that differentiated THP1 cells better resemble PBMC derived macrophages when they are treated with PMA for 48 hours and then subsequently allowed to rest in culture before used in an assay (Daigneault et al., 2010). At times when primary cells are unavailable, supporting experimentation with THP1 cells using this method may be an option. This may have even greater value particularly when primary cells can elicit significant degrees of variation between donors, which could affect the accuracy of data collected from 3D omental models co-cultured with these cells.

For the collaborative work with MedImmune in this final chapter, PBMCs were differentiated in M-CSF. Human serum can also be used to differentiate PBMCs (Daigneault et al., 2010)(communication from Dr Cristina Ghirelli), which may be more physiologically relevant and may drive the cells into a less polarised phenotype. For the purpose of this thesis, the aim was to mimic the microenvironment of a developing omental metastasis; a phase where the tumour deposits are within their growth phase and the proliferation of cells could be measured and experimentally influenced. Therefore non-polarised macrophages were introduced to the model in an effort to represent infiltrating leukocytes from the vasculature. Arguably the original observation correlating CD68 positive macrophages with Ki67 positive epithelial cells was determined from more established omental metastases, but many of those analysed were of a microscopic scale, and would therefore be within their growth phase. For future work the differentiation and polarisation status of the macrophages introduced to the 3D omental model would have to be evaluated on the basis of the experimental question being tested. To study the influence of the tumour microenvironment on the macrophages, less polarised macrophages may have to be introduced to the model, and vice versa the macrophages may need to be driven to a particular polarisation status prior to their co-culture in the 3D omental model. In addition to better replicate the clinical situation, tumour cells may need to be cultured on or in the model for a greater length of time before the macrophages are introduced, to mimic macrophages infiltrating a developing tumour deposit. The work of this final chapter clearly demonstrated that the macrophages invade and incorporate within the matrix of the model; therefore introducing the macrophages at a later stage in the co-culture system should be feasible. Again, arguably it is important to consider the localisation of the macrophages under question. In chapter 1 macrophages were found localised within and surrounding the tumour deposits of omental metastases (Figures 3-5 & 8-1). As well as supporting the growth and proliferation of tumour deposits, at the periphery of a tumour macrophages can facilitate the remodelling of the ECM to allow tumour cell invasion (Wynn et al.,

2013). Therefore to study these cellular mechanisms it may be more relevant to culture the macrophages in the 3D omental model for a period of time to encourage their incorporation into the matrix, prior to introducing the tumour cells. By this method the macrophages would be in a suitable position to localise at the invasive margin of the developing tumour growth on the surface of the model. Pre-established spheroids within the matrix could on the other hand be introduced to the macrophages in the model secondly, to mimic their localisation surrounding the developing deposit.

Discussion thus far has emphasised the preliminary nature of the work in this final chapter, but has highlighted the wealth of options for future model development. Recent work has endeavoured to better define intermediate macrophage phenotypes, where a binary classification is no longer sufficient. Differences between the origins of tissue resident and peripheral blood macrophages were reported for instance (Gomez Perdiguero and Geissmann, 2013). The effect of each of these subtypes on the growth of HGSC deposits in the omentum could be evaluated in the 3D model.

Previous publications have described differences in the transcriptional profiles of PBMCs from patients of pancreatic, lung and renal cancers for example compared with control patients (Baine et al., 2011; Burczynski et al., 2005; Chang et al., 2013; Showe et al., 2009). PBMC-derived macrophages co-cultured in the 3D omental model could be used to study the molecular switches that drive this change in transcriptional signatures in HGSC.

Furthermore introducing to the 3D omental model macrophages derived from the ascites of HGSC patients would even better resemble the real clinical situation. Recently Ko SY and colleagues described how expression of the homeobox gene HOXA9 that is associated with a poor prognosis in ovarian cancer, increases chemotaxis in peritoneal macrophages and increases their expression of M2 tumour associated

markers including CD163 (Ko et al., 2014). In human tumour samples with increased expression of the HOXA9 gene, there was a decrease in CD8 positive T cell infiltrates and an increase in T regulatory cells and tumour-associated macrophages. Therefore a 3D omental model co-culturing peritoneal or ascites derived macrophages could be used to further study tumour-macrophage interactions such as those described in this report.

Once such a 3D omental model with a mimicking macrophage infiltrate has been appropriately established, many of the questions raised in other chapters of this thesis could be further addressed. For instance the role of the CXCR4-CXCL12 chemokine pathway that drives inflammatory cell recruitment in tumours (Balkwill, 2004; Leinster et al., 2012; Schioppa et al., 2003) could be studied in the development of omental metastases of HGSC. In addition models with and without exposure to chemotherapy agents such as Paclitaxal and Carboplatin could be used to determine whether such therapies beneficially or detrimentally polarise the macrophages in the tumour microenvironment for metastatic colonisation of the omentum. The potential benefits of non-steroidal anti-inflammatory drugs (NSAIDs) to cancer patients are currently topical in the field (Balkwill and Mantovani, 2012; Rothwell, 2013). A human inflammatory 3D model could equally be used to underpin the molecular mechanisms involved in disease stabilisation or regression following treatment.

The work of chapter 4 identified the importance of the HPMCs in the development of omental tumour deposits in the 3D model, and proposed the potential for cytokine driven HPMC contractility and activation (Sanz-Moreno et al., 2011)(Figure 8-1). The influx of immune cells into the omental microenvironment following disease colonisation may play a significant role in this. An established inflammatory 3D model could be used to mimic and study these potential mesothelial cells: macrophage interactions.

An increasingly complex 3D omental model opens options for investigating many cell type interactions in the development of HGSC omental deposits. Ernst Lengyel's laboratory recently described the how the lipids and adipokines in adipose tissue promote tumour cell proliferation and invasion respectively (Nieman et al., 2011). Communications with Ernst Lengyel also indicated that their laboratory was endeavouring to incorporate adipocytes into their previously established 3D omental model. Previous reports described how macrophages were recruited to adipose tissue (Sun et al., 2011; Weisberg et al., 2003), and that these adipose associated macrophages secreted increased levels of pro-inflammatory cytokines such as TNF-α and IL-6. Combining Ernst Lengyel's adipocyte 3D omental model with one containing macrophages, could aid the investigation into the possible relationship between macrophages and adipocytes in driving HGSC metastasis in a microenvironment that is already naturally rich with adipocytes.

The opportunity to incorporate an immune cell infiltrate to the 3D omental model goes beyond only macrophages. Other immune cell subtypes such as CD4 positive and regulatory T cells could be introduced to the model either singly or together with the macrophages. αFAP positive fibroblasts in the tumour microenvironment have been suggested to play a very significant role in suppressing a tumour-targeted immune response (Kraman et al., 2010). Matthew Kraman and colleagues used a transgenic mouse model to delete the αFAP positive cell population that perturbed the development of Lewis lung and pancreatic carcinomas. This effect was only observed in the cancers where an immune response had already been initiated. Treatment with TNF-α and IFN-γ neutralising antibodies reversed the induced hypoxic necrosis of the tumour and stromal cells caused by the depletion of αFAP positive cells. More recently a report from the same laboratory described how CXCL12 sourced from this small population of αFAP positive fibroblasts coated the tumour cells in a mouse model of

pancreatic cancer and inhibited the cytotoxicity of CD8 positive T cells (Feig et al., 2013). Treatment with the CXCR4 inhibitor AMD3100 allowed the recruitment of T cells and promoted tumour regression. Given the 3D omental model already includes fibroblasts, potentially the significance of the small subset of αFAP positive stromal cells in the progression of HGSC within an inflammatory microenvironment could be tested if the model also incorporated T cells.

8.7. Concluding statements

Undeniably, there are several further cell types that play pivotal roles in the tumour microenvironment that have not been mentioned here (Balkwill et al., 2012). In *ex vivo* cultures ovarian cancer spheroids interacted extensively with mesenchymal stem cells (Touboul et al., 2013). The omentum is also very well vascularised, giving rise to further signalling pathways communicating with endothelial cells and pericytes of both pre-established vessels and those involved in the process of angiogenesis. Chemokine signalling and tumour progression are furthermore driven by a hypoxic microenvironment (Anglesio et al., 2011b; Schioppa et al., 2003) that conventional cell culture techniques do not convey. Ideally the perfect 3D cell culture model would include all the cell types and conditions of the tumour microenvironment. Often this cannot even be achieved in animal models where mice with impaired adaptive immune systems are utilised to avoid human xenograft rejection. The establishment of such a complex cell culture model is the ambition of the recently founded CANBUILD project team in the Balkwill laboratory of Barts Cancer Institute, London. The European Research Council funds the team and the work of this thesis provided the preliminary data for the project's proposal.

In the realms of the drug discovery process, there is forever a disconnection between the *in vitro* and animal experiments, which creates difficulties to justify pushing targets through to clinical trials. A

3D multicellular *in vitro* model could bridge this gap and become an essential tool for testing combination, and even personalised therapies. In addition, the use of this complex model mimicking the omentum will also carry value in testing therapies for other cancers that metastasise to the peritoneum, including colorectal cancers.

It is without dispute that this 3D omental model will not make *in vivo* models completely redundant in research and drug development, however experiments using the 3D model will be far less expensive in terms of financial and time costs, which are favourable attributes for both academic and industrial institutions. It has already been proved by the work of Prof Ernst Lengyel and colleagues, that the 3D omental model can be reproduced in a 384 well format, rendering it a suitable assay for small scale or high throughput screens. In addition each cellular and extracellular component of the 3D model can be more easily manipulated and regulated in than in an *in vivo* model. Ultimately the 3D model is a human model, which will always recapitulate the human disease setting better than a murine counterpart. The assay is neither restricted by ethics and fully supports the focus of the three R's (reduction, replacement and refinement) when conducting animal experiments. The 3D omental model can be generated to represent ovarian cancer metastases of a particular subtype or mutation status, and it can be hoped that with further development, autologous models could be created for testing patient specific therapies.

The poor prognosis associated with HGSC stems from the late stage disease presentation and the widespread metastasis throughout the peritoneum. It is becoming increasingly evident that the metastatic microenvironment is quite different from the primary tumours in ovarian cancer (Malek et al., 2011). Following recent developments in our understanding of the origins of ovarian cancer (Kurman, 2013), we are now more astute to treating ovarian cancer subtypes as individual diseases, which must translate in our experimental design and choice of cell lines. However given the real clinical problem associated with this

disease is the peritoneal spread it is critical that we seek therapeutic targets associated with the metastases. The 3D omental model established in this thesis and further developed by the CANBUILD team will aid the identification of these targets, and the development of therapeutic interventions. With this it can be hoped that following thirty years of little improvement in the survival rates of ovarian cancer patients, a shift in paradigm and progression in treatment regimes may reduce the severity of diagnosis and offer patients confidence that they can live with a better quality of life for longer.

9. References

9.1. Web and text book references

Cancer Research UK

http://www.cancerresearchuk.org/cancer-info/cancerstats/types/ovary/

CANBUILD project YouTube video

(http://www.youtube.com/watch?v=V61eD9oJD48)

IARC TP53 database

http://p53.iarc.fr/

Gene Expression Omnibus

http://www.ncbi.nlm.nih.gov/geo/

Metacore analysis

http://thomsonreuters.com/metacore/

Statistical computing

R Development Core Team (2008). R: A language and environment for statistical computing. R Foundation for Statistical Computing, Vienna, Austria.

Limma package

Smyth, GK (2005). Limma: linear models for microarray data. In: 'Bioinformatics and Computational Biology Solutions using R and Bioconductor'. R. Gentleman, V. Carey, S.Dudoit, R. Irizarry, W. Huber (eds), Springer, New York, pages 397-420.

Multiple testing

Benjamini, Y., and Hochberg, Y. Controlling the False Discovery Rate:A Practical and Powerful Approach to Multiple Testing. J.Roy Stat. Soc,Ser B. 57:289-300.

9.2. Journal references

Abbas, A. R., Baldwin, D., Ma, Y., Ouyang, W., Gurney, A., Martin, F., Fong, S., van Lookeren Campagne, M., Godowski, P., Williams, P. M.*, et al.* (2005). Immune response in silico (IRIS): immune-specific genes identified from a compendium of microarray expression data. Genes Immun *6*, 319-331.

Ahmed, A. A., Etemadmoghadam, D., Temple, J., Lynch, A. G., Riad, M., Sharma, R., Stewart, C., Fereday, S., Caldas, C., Defazio, A.*, et al.* (2010). Driver mutations in TP53 are ubiquitous in high grade serous carcinoma of the ovary. J Pathol *221*, 49-56.

Ahmed, A. A., Mills, A. D., Ibrahim, A. E., Temple, J., Blenkiron, C., Vias, M., Massie, C. E., Iyer, N. G., McGeoch, A., Crawford, R.*, et al.* (2007). The extracellular matrix protein TGFBI induces microtubule stabilization and sensitizes ovarian cancers to paclitaxel. Cancer Cell *12*, 514-527.

Aiuti, A., Webb, I. J., Bleul, C., Springer, T., and Gutierrez-Ramos, J. C. (1997). The chemokine SDF-1 is a chemoattractant for human CD34+ hematopoietic progenitor cells and provides a new mechanism to explain the mobilization of CD34+ progenitors to peripheral blood. J Exp Med *185*, 111-120.

Andreu, P., Johansson, M., Affara, N. I., Pucci, F., Tan, T., Junankar, S., Korets, L., Lam, J., Tawfik, D., DeNardo, D. G.*, et al.* (2010). FcRgamma activation regulates inflammation-associated squamous carcinogenesis. Cancer Cell *17*, 121-134.

Ang, J. E., Gourley, C., Powell, C. B., High, H., Shapira-Frommer, R., Castonguay, V., De Greve, J., Atkinson, T., Yap, T. A., Sandhu, S.*, et al.* (2013). Efficacy of chemotherapy in BRCA1/2 mutation carrier ovarian

cancer in the setting of PARP inhibitor resistance: a multi-institutional study. Clin Cancer Res *19*, 5485-5493.

Anglesio, M. S., Carey, M. S., Kobel, M., Mackay, H., and Huntsman, D. G. (2011a). Clear cell carcinoma of the ovary: A report from the first Ovarian Clear Cell Symposium, June 24th, 2010. Gynecol Oncol.

Anglesio, M. S., George, J., Kulbe, H., Friedlander, M. L., Rischin, D., Lemech, C., Power, J., Coward, J., Cowin, P. A., House, C. M.*, et al.* (2011b). Il6-Stat3-Hif Signalling and Therapeutic Response to the Angiogenesis Inhibitor, Sunitinib, in Ovarian Clear Cell Cancer. Clin Cancer Res.

Anglesio, M. S., Wiegand, K. C., Melnyk, N., Chow, C., Salamanca, C., Prentice, L. M., Senz, J., Yang, W., Spillman, M. A., Cochrane, D. R.*, et al.* (2013). Correction: Type-Specific Cell Line Models for Type-Specific Ovarian Cancer Research. PLoS One *8(10).*

Archibald, K. M., Kulbe, H., Kwong, J., Chakravarty, P., Temple, J., Chaplin, T., Flak, M. B., McNeish, I. A., Deen, S., Brenton, J. D.*, et al.* (2012). Sequential genetic change at the TP53 and chemokine receptor CXCR4 locus during transformation of human ovarian surface epithelium. Oncogene *31*, 4987-4995.

Baine, M. J., Chakraborty, S., Smith, L. M., Mallya, K., Sasson, A. R., Brand, R. E., and Batra, S. K. (2011). Transcriptional profiling of peripheral blood mononuclear cells in pancreatic cancer patients identifies novel genes with potential diagnostic utility. PLoS One *6.*

Balkwill, F. (2002). Tumor necrosis factor or tumor promoting factor? Cytokine Growth Factor Rev *13*, 135-141.

Balkwill, F. (2004). The significance of cancer cell expression of the chemokine receptor CXCR4. Semin Cancer Biol *14*, 171-179.

Balkwill, F. (2009). Tumour necrosis factor and cancer. Nat Rev Cancer *9*, 361-371.

Balkwill, F., and Mantovani, A. (2001). Inflammation and cancer: back to Virchow? Lancet *357*, 539-545.

Balkwill, F., Montfort, A., and Capasso, M. (2013). B regulatory cells in cancer. Trends Immunol *34*, 169-173.

Balkwill, F. R., Capasso, M., and Hagemann, T. (2012). The tumor microenvironment at a glance. J Cell Sci *125*, 5591-5596.

Balkwill, F. R., and Mantovani, A. (2012). Cancer-related inflammation: common themes and therapeutic opportunities. Semin Cancer Biol *22*, 33-40.

Banerjee, S., Kaye, S. B., and Ashworth, A. (2010). Making the best of PARP inhibitors in ovarian cancer. Nat Rev Clin Oncol *7*, 508-519.

Banerjee, S., Rustin, G., Paul, J., Williams, C., Pledge, S., Gabra, H., Skailes, G., Lamont, A., Hindley, A., Goss, G.*, et al.* (2013). A multicenter, randomized trial of flat dosing versus intrapatient dose escalation of single-agent carboplatin as first-line chemotherapy for advanced ovarian cancer: an SGCTG (SCOTROC 4) and ANZGOG study on behalf of GCIG. Ann Oncol *24*, 679-687.

Bankert, R. B., Balu-Iyer, S. V., Odunsi, K., Shultz, L. D., Kelleher, R. J., Jr., Barnas, J. L., Simpson-Abelson, M., Parsons, R., and Yokota, S. J. (2011). Humanized mouse model of ovarian cancer recapitulates patient solid tumor progression, ascites formation, and metastasis. PLoS One *6*.

Barrett, T., and Edgar, R. (2006). Mining microarray data at NCBI's Gene Expression Omnibus (GEO). Methods Mol Biol *338*, 175-190.

Bast, R. C., Jr. (2003). Status of tumor markers in ovarian cancer screening. J Clin Oncol *21*, 200s-205s.

Bates, G. J., Fox, S. B., Han, C., Leek, R. D., Garcia, J. F., Harris, A. L., and Banham, A. H. (2006). Quantification of regulatory T cells enables the identification of high-risk breast cancer patients and those at risk of late relapse. J Clin Oncol *24*, 5373-5380.

Beyer, M., Mallmann, M. R., Xue, J., Staratschek-Jox, A., Vorholt, D., Krebs, W., Sommer, D., Sander, J., Mertens, C., Nino-Castro, A.*, et al.* (2012). High-resolution transcriptome of human macrophages. PLoS One *7*.

Bhowmick, N. A., Neilson, E. G., and Moses, H. L. (2004). Stromal fibroblasts in cancer initiation and progression. Nature *432*, 332-337.

Boimel, P. J., Smirnova, T., Zhou, Z. N., Wyckoff, J., Park, H., Coniglio, S. J., Qian, B. Z., Stanley, E. R., Cox, D., Pollard, J. W.*, et al.* (2012).

Contribution of CXCL12 secretion to invasion of breast cancer cells. Breast Cancer Res *14*, R23.

Bonecchi, R., Locati, M., and Mantovani, A. (2011). Chemokines and cancer: a fatal attraction. Cancer Cell *19*, 434-435.

Bowen, N. J., Logani, S., Dickerson, E. B., Kapa, L. B., Akhtar, M., Benigno, B. B., and McDonald, J. F. (2007). Emerging roles for PAX8 in ovarian cancer and endosalpingeal development. Gynecol Oncol *104*, 331-337.

Bowtell, D. D. (2010). The genesis and evolution of high-grade serous ovarian cancer. Nat Rev Cancer *10*, 803-808.

Buhtoiarov, I. N., Sondel, P. M., Wigginton, J. M., Buhtoiarova, T. N., Yanke, E. M., Mahvi, D. A., and Rakhmilevich, A. L. (2011). Anti-tumour synergy of cytotoxic chemotherapy and anti-CD40 plus CpG-ODN immunotherapy through repolarization of tumour-associated macrophages. Immunology *132*, 226-239.

Burczynski, M. E., Twine, N. C., Dukart, G., Marshall, B., Hidalgo, M., Stadler, W. M., Logan, T., Dutcher, J., Hudes, G., Trepicchio, W. L.*, et al.* (2005). Transcriptional profiles in peripheral blood mononuclear cells prognostic of clinical outcomes in patients with advanced renal cell carcinoma. Clin Cancer Res *11*, 1181-1189.

Burger, J. A., and Kipps, T. J. (2006). CXCR4: a key receptor in the crosstalk between tumor cells and their microenvironment. Blood *107*, 1761-1767.

Butcher, D. T., Alliston, T., and Weaver, V. M. (2009). A tense situation: forcing tumour progression. Nat Rev Cancer *9*, 108-122.

Cai, J., Tang, H., Xu, L., Wang, X., Yang, C., Ruan, S., Guo, J., Hu, S., and Wang, Z. (2012). Fibroblasts in omentum activated by tumor cells promote ovarian cancer growth, adhesion and invasiveness. Carcinogenesis *33*, 20-29.

Campbell, I. G., Russell, S. E., Choong, D. Y., Montgomery, K. G., Ciavarella, M. L., Hooi, C. S., Cristiano, B. E., Pearson, R. B., and Phillips, W. A. (2004). Mutation of the PIK3CA gene in ovarian and breast cancer. Cancer Res *64*, 7678-7681.

Cancer Genome Atlas Research, N. (2011). Integrated genomic analyses of ovarian carcinoma. Nature *474*, 609-615.

Carus, A., Gurney, H., Gebski, V., Harnett, P., Hui, R., Kefford, R., Wilcken, N., Ladekarl, M., von der Maase, H., and Donskov, F. (2013). Impact of baseline and nadir neutrophil index in non-small cell lung cancer and ovarian cancer patients: Assessment of chemotherapy for resolution of unfavourable neutrophilia. J Transl Med *11*, 189.

Casey, R. C., Burleson, K. M., Skubitz, K. M., Pambuccian, S. E., Oegema, T. R., Jr., Ruff, L. E., and Skubitz, A. P. (2001). Beta 1-integrins regulate the formation and adhesion of ovarian carcinoma multicellular spheroids. Am J Pathol *159*, 2071-2080.

Cavallo, F., De Giovanni, C., Nanni, P., Forni, G., and Lollini, P. L. (2011). 2011: the immune hallmarks of cancer. Cancer Immunol Immunother *60*, 319-326.

Chang, D. H., Rutledge, J. R., Patel, A. A., Heerdt, B. G., Augenlicht, L. H., and Korst, R. J. (2013). The effect of lung cancer on cytokine expression in peripheral blood mononuclear cells. PLoS One *8.*

Chen, J. J., Yao, P. L., Yuan, A., Hong, T. M., Shun, C. T., Kuo, M. L., Lee, Y. C., and Yang, P. C. (2003). Up-regulation of tumor interleukin-8 expression by infiltrating macrophages: its correlation with tumor angiogenesis and patient survival in non-small cell lung cancer. Clin Cancer Res *9*, 729-737.

Chen, Q., and Massague, J. (2012). Molecular pathways: VCAM-1 as a potential therapeutic target in metastasis. Clin Cancer Res *18*, 5520-5525.

Cheon, D. J., Tong, Y., Sim, M. S., Dering, J., Berel, D., Cui, X., Lester, J., Beach, J. A., Tighiouart, M., Walts, A. E.*, et al.* (2014). A Collagen-Remodeling Gene Signature Regulated by TGF-beta Signaling Is Associated with Metastasis and Poor Survival in Serous Ovarian Cancer. Clin Cancer Res, 16.

Cheung, H. W., Cowley, G. S., Weir, B. A., Boehm, J. S., Rusin, S., Scott, J. A., East, A., Ali, L. D., Lizotte, P. H., Wong, T. C.*, et al.* (2011). Systematic investigation of genetic vulnerabilities across cancer cell

lines reveals lineage-specific dependencies in ovarian cancer. Proc Natl Acad Sci U S A *108*, 12372-12377.

Choi, K. U., Yun, J. S., Lee, I. H., Heo, S. C., Shin, S. H., Jeon, E. S., Choi, Y. J., Suh, D. S., Yoon, M. S., and Kim, J. H. (2011). Lysophosphatidic acid-induced expression of periostin in stromal cells: Prognoistic relevance of periostin expression in epithelial ovarian cancer. Int J Cancer *128*, 332-342.

Connolly, D. C., Bao, R., Nikitin, A. Y., Stephens, K. C., Poole, T. W., Hua, X., Harris, S. S., Vanderhyden, B. C., and Hamilton, T. C. (2003). Female mice chimeric for expression of the simian virus 40 TAg under control of the MISIIR promoter develop epithelial ovarian cancer. Cancer Res *63*, 1389-1397.

Cooke, S. L., Ng, C. K., Melnyk, N., Garcia, M. J., Hardcastle, T., Temple, J., Langdon, S., Huntsman, D., and Brenton, J. D. (2010). Genomic analysis of genetic heterogeneity and evolution in high-grade serous ovarian carcinoma. Oncogene *29*, 4905-4913.

Coussens, L. M., and Werb, Z. (2002). Inflammation and cancer. Nature *420*, 860-867.

Coward, J., Kulbe, H., Chakravarty, P., Leader, D., Vassileva, V., Leinster, D. A., Thompson, R., Schioppa, T., Nemeth, J., Vermeulen, J., *et al.* (2011). Interleukin-6 as a therapeutic target in human ovarian cancer. Clin Cancer Res *17*, 6083-6096.

Cox, T. R., and Erler, J. T. (2011). Remodeling and homeostasis of the extracellular matrix: implications for fibrotic diseases and cancer. Dis Model Mech *4*, 165-178.

Cramer, D. W., Hutchison, G. B., Welch, W. R., Scully, R. E., and Knapp, R. C. (1982). Factors affecting the association of oral contraceptives and ovarian cancer. N Engl J Med *307*, 1047-1051.

Cramer, D. W., and Welch, W. R. (1983). Determinants of ovarian cancer risk. II. Inferences regarding pathogenesis. J Natl Cancer Inst *71*, 717-721.

Crum, C. P., Drapkin, R., Miron, A., Ince, T. A., Muto, M., Kindelberger, D. W., and Lee, Y. (2007). The distal fallopian tube: a new model for pelvic serous carcinogenesis. Curr Opin Obstet Gynecol *19*, 3-9.

Crum, C. P., McKeon, F. D., and Xian, W. (2012). The oviduct and ovarian cancer: causality, clinical implications, and "targeted prevention". Clin Obstet Gynecol *55*, 24-35.

Curiel, T. J., Coukos, G., Zou, L., Alvarez, X., Cheng, P., Mottram, P., Evdemon-Hogan, M., Conejo-Garcia, J. R., Zhang, L., Burow, M.*, et al.* (2004). Specific recruitment of regulatory T cells in ovarian carcinoma fosters immune privilege and predicts reduced survival. Nat Med *10*, 942-949.

Daigneault, M., Preston, J. A., Marriott, H. M., Whyte, M. K., and Dockrell, D. H. (2010). The identification of markers of macrophage differentiation in PMA-stimulated THP-1 cells and monocyte-derived macrophages. PLoS One *5*.

DeCaprio, J. A., Ludlow, J. W., Figge, J., Shew, J. Y., Huang, C. M., Lee, W. H., Marsilio, E., Paucha, E., and Livingston, D. M. (1988). SV40 large tumor antigen forms a specific complex with the product of the retinoblastoma susceptibility gene. Cell *54*, 275-283.

Delort, L., Lequeux, C., Dubois, V., Dubouloz, A., Billard, H., Mojallal, A., Damour, O., Vasson, M. P., and Caldefie-Chezet, F. (2013). Reciprocal interactions between breast tumor and its adipose microenvironment based on a 3D adipose equivalent model. PLoS One *8*.

Dijkgraaf, E. M., Heusinkveld, M., Tummers, B., Vogelpoel, L. T., Goedemans, R., Jha, V., Nortier, J. W., Welters, M. J., Kroep, J. R., and van der Burg, S. H. (2013). Chemotherapy alters monocyte differentiation to favor generation of cancer-supporting m2 macrophages in the tumor microenvironment. Cancer Res *73*, 2480-2492.

Doitsidou, M., Reichman-Fried, M., Stebler, J., Koprunner, M., Dorries, J., Meyer, D., Esguerra, C. V., Leung, T., and Raz, E. (2002). Guidance of primordial germ cell migration by the chemokine SDF-1. Cell *111*, 647-659.

Domanska, U. M., Kruizinga, R. C., Nagengast, W. B., Timmer-Bosscha, H., Huls, G., de Vries, E. G., and Walenkamp, A. M. (2013). A review on CXCR4/CXCL12 axis in oncology: no place to hide. Eur J Cancer *49*, 219-230.

Domcke, S., Sinha, R., Levine, D. A., Sander, C., and Schultz, N. (2013). Evaluating cell lines as tumour models by comparison of genomic profiles. Nat Commun *4:2126.*

Donskov, F. (2013). Immunomonitoring and prognostic relevance of neutrophils in clinical trials. Semin Cancer Biol *23*, 200-207.

Donzella, G. A., Schols, D., Lin, S. W., Este, J. A., Nagashima, K. A., Maddon, P. J., Allaway, G. P., Sakmar, T. P., Henson, G., De Clercq, E., and Moore, J. P. (1998). AMD3100, a small molecule inhibitor of HIV-1 entry via the CXCR4 co-receptor. Nat Med *4*, 72-77.

Dowsett, M., Nielsen, T. O., A'Hern, R., Bartlett, J., Coombes, R. C., Cuzick, J., Ellis, M., Henry, N. L., Hugh, J. C., Lively, T.*, et al.* (2011). Assessment of Ki67 in breast cancer: recommendations from the International Ki67 in Breast Cancer working group. J Natl Cancer Inst *103*, 1656-1664.

Dranoff, G. (2004). Cytokines in cancer pathogenesis and cancer therapy. Nat Rev Cancer *4*, 11-22.

Duraiswamy, J., Freeman, G. J., and Coukos, G. (2013). Therapeutic PD-1 pathway blockade augments with other modalities of immunotherapy T-cell function to prevent immune decline in ovarian cancer. Cancer Res *73*, 6900-6912.

Dvorak, H. F. (1986). Tumors: wounds that do not heal. Similarities between tumor stroma generation and wound healing. N Engl J Med *315*, 1650-1659.

Erez, N., and Coussens, L. M. (2011). Leukocytes as paracrine regulators of metastasis and determinants of organ-specific colonization. Int J Cancer *128*, 2536-2544.

Erickson, B. K., Conner, M. G., and Landen, C. N., Jr. (2013). The role of the fallopian tube in the origin of ovarian cancer. Am J Obstet Gynecol *209*, 409-414.

Erler, J. T., and Weaver, V. M. (2009). Three-dimensional context regulation of metastasis. Clin Exp Metastasis *26*, 35-49.

Etemadmoghadam, D., deFazio, A., Beroukhim, R., Mermel, C., George, J., Getz, G., Tothill, R., Okamoto, A., Raeder, M. B., Harnett, P.*, et al.* (2009). Integrated genome-wide DNA copy number and expression

analysis identifies distinct mechanisms of primary chemoresistance in ovarian carcinomas. Clin Cancer Res *15*, 1417-1427.

Fathalla, M. F. (1971). Incessant ovulation--a factor in ovarian neoplasia? Lancet *2*, 163.

Feig, C., Jones, J. O., Kraman, M., Wells, R. J., Deonarine, A., Chan, D. S., Connell, C. M., Roberts, E. W., Zhao, Q., Caballero, O. L.*, et al.* (2013). Targeting CXCL12 from FAP-expressing carcinoma-associated fibroblasts synergizes with anti-PD-L1 immunotherapy in pancreatic cancer. Proc Natl Acad Sci U S A *110*, 20212-20217.

Feng, Y., Broder, C. C., Kennedy, P. E., and Berger, E. A. (1996). HIV-1 entry cofactor: functional cDNA cloning of a seven-transmembrane, G protein-coupled receptor. Science *272*, 872-877.

Frankenberger, M., Hofer, T. P., Marei, A., Dayyani, F., Schewe, S., Strasser, C., Aldraihim, A., Stanzel, F., Lang, R., Hoffmann, R.*, et al.* (2012). Transcript profiling of CD16-positive monocytes reveals a unique molecular fingerprint. Eur J Immunol *42*, 957-974.

Fridlender, Z. G., Sun, J., Kim, S., Kapoor, V., Cheng, G., Ling, L., Worthen, G. S., and Albelda, S. M. (2009). Polarization of tumor-associated neutrophil phenotype by TGF-beta: "N1" versus "N2" TAN. Cancer Cell *16*, 183-194.

Fridman, A. L., and Tainsky, M. A. (2008). Critical pathways in cellular senescence and immortalization revealed by gene expression profiling. Oncogene *27*, 5975-5987.

Fridman, W. H., Pages, F., Sautes-Fridman, C., and Galon, J. (2012). The immune contexture in human tumours: impact on clinical outcome. Nat Rev Cancer *12*, 298-306.

Friedl, P., and Alexander, S. (2011). Cancer invasion and the microenvironment: plasticity and reciprocity. Cell *147*, 992-1009.

Friedl, P., and Gilmour, D. (2009). Collective cell migration in morphogenesis, regeneration and cancer. Nat Rev Mol Cell Biol *10*, 445-457.

Friedl, P., and Wolf, K. (2010). Plasticity of cell migration: a multiscale tuning model. J Cell Biol *188*, 11-19.

Gao, D., Vahdat, L. T., Wong, S., Chang, J. C., and Mittal, V. (2012). Microenvironmental regulation of epithelial-mesenchymal transitions in cancer. Cancer Res *72*, 4883-4889.

Garson, K., Gamwell, L. F., Pitre, E. M., and Vanderhyden, B. C. (2012). Technical challenges and limitations of current mouse models of ovarian cancer. J Ovarian Res *5*, 39.

Gautier, E. L., Shay, T., Miller, J., Greter, M., Jakubzick, C., Ivanov, S., Helft, J., Chow, A., Elpek, K. G., Gordonov, S.*, et al.* (2012). Gene-expression profiles and transcriptional regulatory pathways that underlie the identity and diversity of mouse tissue macrophages. Nat Immunol *13*, 1118-1128.

Gautier, L., Cope, L., Bolstad, B. M., and Irizarry, R. A. (2004). affy--analysis of Affymetrix GeneChip data at the probe level. Bioinformatics *20*, 307-315.

Gentleman, R. C., Carey, V. J., Bates, D. M., Bolstad, B., Dettling, M., Dudoit, S., Ellis, B., Gautier, L., Ge, Y., Gentry, J.*, et al.* (2004). Bioconductor: open software development for computational biology and bioinformatics. Genome Biol *5*, R80.

George, J., Alsop, K., Etemadmoghadam, D., Hondow, H., Mikeska, T., Dobrovic, A., deFazio, A., Smyth, G. K., Levine, D. A., Mitchell, G., and Bowtell, D. D. (2013). Nonequivalent gene expression and copy number alterations in high-grade serous ovarian cancers with BRCA1 and BRCA2 mutations. Clin Cancer Res *19*, 3474-3484.

Gierach, G. L., Lacey, J. V., Jr., Schatzkin, A., Leitzmann, M. F., Richesson, D., Hollenbeck, A. R., and Brinton, L. A. (2008). Nonsteroidal anti-inflammatory drugs and breast cancer risk in the National Institutes of Health-AARP Diet and Health Study. Breast Cancer Res *10*, R38.

Goff, B. A., Sainz de la Cuesta, R., Muntz, H. G., Fleischhacker, D., Ek, M., Rice, L. W., Nikrui, N., Tamimi, H. K., Cain, J. M., Greer, B. E., and Fuller, A. F., Jr. (1996). Clear cell carcinoma of the ovary: a distinct histologic type with poor prognosis and resistance to platinum-based chemotherapy in stage III disease. Gynecol Oncol *60*, 412-417.

Gomez Perdiguero, E., and Geissmann, F. (2013). Myb-Independent Macrophages: A Family of Cells That Develops with Their Tissue of

Residence and Is Involved in Its Homeostasis. Cold Spring Harb Symp Quant Biol, 11.

Granot, Z., Henke, E., Comen, E. A., King, T. A., Norton, L., and Benezra, R. (2011). Tumor entrained neutrophils inhibit seeding in the premetastatic lung. Cancer Cell *20*, 300-314.

Green, S. K., Francia, G., Isidoro, C., and Kerbel, R. S. (2004). Antiadhesive antibodies targeting E-cadherin sensitize multicellular tumor spheroids to chemotherapy in vitro. Mol Cancer Ther *3*, 149-159.

Gregoire, L., Munkarah, A., Rabah, R., Morris, R. T., and Lancaster, W. D. (1998). Organotypic culture of human ovarian surface epithelial cells: a potential model for ovarian carcinogenesis. In Vitro Cell Dev Biol Anim *34*, 636-639.

Greten, F. R., Eckmann, L., Greten, T. F., Park, J. M., Li, Z. W., Egan, L. J., Kagnoff, M. F., and Karin, M. (2004). IKKbeta links inflammation and tumorigenesis in a mouse model of colitis-associated cancer. Cell *118*, 285-296.

Grivennikov, S. I., Greten, F. R., and Karin, M. (2010). Immunity, inflammation, and cancer. Cell *140*, 883-899.

Grugan, K. D., McCabe, F. L., Kinder, M., Greenplate, A. R., Harman, B. C., Ekert, J. E., van Rooijen, N., Anderson, G. M., Nemeth, J. A., Strohl, W. R.*, et al.* (2012). Tumor-associated macrophages promote invasion while retaining Fc-dependent anti-tumor function. J Immunol *189*, 5457-5466.

Guruswamy, S., Lightfoot, S., Gold, M. A., Hassan, R., Berlin, K. D., Ivey, R. T., and Benbrook, D. M. (2001). Effects of retinoids on cancerous phenotype and apoptosis in organotypic cultures of ovarian carcinoma. J Natl Cancer Inst *93*, 516-525.

Hagemann, T., Lawrence, T., McNeish, I., Charles, K. A., Kulbe, H., Thompson, R. G., Robinson, S. C., and Balkwill, F. R. (2008). "Re-educating" tumor-associated macrophages by targeting NF-kappaB. J Exp Med *205*, 1261-1268.

Hagemann, T., Wilson, J., Burke, F., Kulbe, H., Li, N. F., Pluddemann, A., Charles, K., Gordon, S., and Balkwill, F. R. (2006). Ovarian cancer

cells polarize macrophages toward a tumor-associated phenotype. J Immunol *176*, 5023-5032.

Hagemann, T., Wilson, J., Kulbe, H., Li, N. F., Leinster, D. A., Charles, K., Klemm, F., Pukrop, T., Binder, C., and Balkwill, F. R. (2005). Macrophages induce invasiveness of epithelial cancer cells via NF-kappa B and JNK. J Immunol *175*, 1197-1205.

Hahn, W. C., Counter, C. M., Lundberg, A. S., Beijersbergen, R. L., Brooks, M. W., and Weinberg, R. A. (1999). Creation of human tumour cells with defined genetic elements. Nature *400*, 464-468.

Halama, N., Michel, S., Kloor, M., Zoernig, I., Benner, A., Spille, A., Pommerencke, T., von Knebel, D. M., Folprecht, G., Luber, B.*, et al.* (2011). Localization and density of immune cells in the invasive margin of human colorectal cancer liver metastases are prognostic for response to chemotherapy. Cancer Res *71*, 5670-5677.

Hall, M., Gourley, C., McNeish, I., Ledermann, J., Gore, M., Jayson, G., Perren, T., Rustin, G., and Kaye, S. (2013). Targeted anti-vascular therapies for ovarian cancer: current evidence. Br J Cancer *108*, 250-258.

Hamanishi, J., Mandai, M., Iwasaki, M., Okazaki, T., Tanaka, Y., Yamaguchi, K., Higuchi, T., Yagi, H., Takakura, K., Minato, N.*, et al.* (2007). Programmed cell death 1 ligand 1 and tumor-infiltrating CD8+ T lymphocytes are prognostic factors of human ovarian cancer. Proc Natl Acad Sci U S A *104*, 3360-3365.

Hamilton, J. A., and Achuthan, A. (2013). Colony stimulating factors and myeloid cell biology in health and disease. Trends Immunol *34*, 81-89.

Hamilton, T. C., Young, R. C., Louie, K. G., Behrens, B. C., McKoy, W. M., Grotzinger, K. R., and Ozols, R. F. (1984). Characterization of a xenograft model of human ovarian carcinoma which produces ascites and intraabdominal carcinomatosis in mice. Cancer Res *44*, 5286-5290.

Hanahan, D., and Weinberg, R. A. (2011). Hallmarks of cancer: the next generation. Cell *144*, 646-674.

Hartmann, T. N., Burger, J. A., Glodek, A., Fujii, N., and Burger, M. (2005). CXCR4 chemokine receptor and integrin signaling co-operate in

mediating adhesion and chemoresistance in small cell lung cancer (SCLC) cells. Oncogene *24*, 4462-4471.

Hiraoka, N., Onozato, K., Kosuge, T., and Hirohashi, S. (2006). Prevalence of FOXP3+ regulatory T cells increases during the progression of pancreatic ductal adenocarcinoma and its premalignant lesions. Clin Cancer Res *12*, 5423-5434.

Huang, R. Y., Guilford, P., and Thiery, J. P. (2012). Early events in cell adhesion and polarity during epithelial-mesenchymal transition. J Cell Sci *125*, 4417-4422.

Iozzo, R. V., and Sanderson, R. D. (2011). Proteoglycans in cancer biology, tumour microenvironment and angiogenesis. J Cell Mol Med *15*, 1013-1031.

Iseri, O. D., Kars, M. D., Arpaci, F., and Gunduz, U. (2010). Gene expression analysis of drug-resistant MCF-7 cells: implications for relation to extracellular matrix proteins. Cancer Chemother Pharmacol *65*, 447-455.

Ismail, R. S., Baldwin, R. L., Fang, J., Browning, D., Karlan, B. Y., Gasson, J. C., and Chang, D. D. (2000). Differential gene expression between normal and tumor-derived ovarian epithelial cells. Cancer Res *60*, 6744-6749.

Iwanicki, M. P., Davidowitz, R. A., Ng, M. R., Besser, A., Muranen, T., Merritt, M., Danuser, G., Ince, T. A., and Brugge, J. S. (2011). Ovarian cancer spheroids use myosin-generated force to clear the mesothelium. Cancer Discov *1*, 144-157.

Jaafar, F., Righi, E., Lindstrom, V., Linton, C., Nohadani, M., Van Noorden, S., Lloyd, T., Poznansky, J., Stamp, G., Dina, R.*, et al.* (2009). Correlation of CXCL12 expression and FoxP3+ cell infiltration with human papillomavirus infection and clinicopathological progression of cervical cancer. Am J Pathol *175*, 1525-1535.

Jacobson, O., Weiss, I. D., Szajek, L., Farber, J. M., and Kiesewetter, D. O. (2009). 64Cu-AMD3100--a novel imaging agent for targeting chemokine receptor CXCR4. Bioorg Med Chem *17*, 1486-1493.

Jones, S., Wang, T. L., Shih Ie, M., Mao, T. L., Nakayama, K., Roden, R., Glas, R., Slamon, D., Diaz, L. A., Jr., Vogelstein, B.*, et al.* (2010).

Frequent mutations of chromatin remodeling gene ARID1A in ovarian clear cell carcinoma. Science *330*, 228-231.

Kajiyama, H., Shibata, K., Terauchi, M., Ino, K., Nawa, A., and Kikkawa, F. (2008a). Involvement of SDF-1alpha/CXCR4 axis in the enhanced peritoneal metastasis of epithelial ovarian carcinoma. Int J Cancer *122*, 91-99.

Kajiyama, H., Shibata, K., Terauchi, M., Ino, K., Nawa, A., and Kikkawa, F. (2008b). Involvement of SDF-1alpha/CXCR4 axis in the enhanced peritoneal metastasis of epithelial ovarian carcinoma. Int J Cancer *122*, 91-99.

Kaler, P., Augenlicht, L., and Klampfer, L. (2009). Macrophage-derived IL-1beta stimulates Wnt signaling and growth of colon cancer cells: a crosstalk interrupted by vitamin D3. Oncogene *28*, 3892-3902.

Kaler, P., Galea, V., Augenlicht, L., and Klampfer, L. (2010). Tumor associated macrophages protect colon cancer cells from TRAIL-induced apoptosis through IL-1beta-dependent stabilization of Snail in tumor cells. PLoS One *5*.

Kalloger, S. E., Kobel, M., Leung, S., Mehl, E., Gao, D., Marcon, K. M., Chow, C., Clarke, B. A., Huntsman, D. G., and Gilks, C. B. (2011). Calculator for ovarian carcinoma subtype prediction. Mod Pathol *24*, 512-521.

Kelm, J. M., Timmins, N. E., Brown, C. J., Fussenegger, M., and Nielsen, L. K. (2003). Method for generation of homogeneous multicellular tumor spheroids applicable to a wide variety of cell types. Biotechnol Bioeng *83*, 173-180.

Kennedy, A. W., Biscotti, C. V., Hart, W. R., and Webster, K. D. (1989). Ovarian clear cell adenocarcinoma. Gynecol Oncol *32*, 342-349.

Kenny, H. A., Kaur, S., Coussens, L. M., and Lengyel, E. (2008). The initial steps of ovarian cancer cell metastasis are mediated by MMP-2 cleavage of vitronectin and fibronectin. J Clin Invest *118*, 1367-1379.

Kenny, H. A., Krausz, T., Yamada, S. D., and Lengyel, E. (2007). Use of a novel 3D culture model to elucidate the role of mesothelial cells, fibroblasts and extra-cellular matrices on adhesion and invasion of ovarian cancer cells to the omentum. Int J Cancer *121*, 1463-1472.

Kenny, H. A., and Lengyel, E. (2009). MMP-2 functions as an early response protein in ovarian cancer metastasis. Cell Cycle *8*, 683-688.

Kessenbrock, K., Plaks, V., and Werb, Z. (2010). Matrix metalloproteinases: regulators of the tumor microenvironment. Cell *141*, 52-67.

Khan, S. M., Funk, H. M., Thiolloy, S., Lotan, T. L., Hickson, J., Prins, G. S., Drew, A. F., and Rinker-Schaeffer, C. W. (2010a). In vitro metastatic colonization of human ovarian cancer cells to the omentum. Clin Exp Metastasis *27*, 185-196.

Khan, S. M., Funk, H. M., Thiolloy, S., Lotan, T. L., Hickson, J., Prins, G. S., Drew, A. F., and Rinker-Schaeffer, C. W. (2010b). In vitro metastatic colonization of human ovarian cancer cells to the omentum. Clin Exp Metastasis *27*, 185-196.

Kierstead, T. D., and Tevethia, M. J. (1993). Association of p53 binding and immortalization of primary C57BL/6 mouse embryo fibroblasts by using simian virus 40 T-antigen mutants bearing internal overlapping deletion mutations. J Virol *67*, 1817-1829.

Kim, J., Coffey, D. M., Creighton, C. J., Yu, Z., Hawkins, S. M., and Matzuk, M. M. (2012). High-grade serous ovarian cancer arises from fallopian tube in a mouse model. Proc Natl Acad Sci U S A *109*, 3921-3926.

Kindelberger, D. W., Lee, Y., Miron, A., Hirsch, M. S., Feltmate, C., Medeiros, F., Callahan, M. J., Garner, E. O., Gordon, R. W., Birch, C.*, et al.* (2007). Intraepithelial carcinoma of the fimbria and pelvic serous carcinoma: Evidence for a causal relationship. Am J Surg Pathol *31*, 161-169.

Ko, S. Y., Ladanyi, A., Lengyel, E., and Naora, H. (2014). Expression of the homeobox gene HOXA9 in ovarian cancer induces peritoneal macrophages to acquire an M2 tumor-promoting phenotype. Am J Pathol *184*, 271-281.

Kraman, M., Bambrough, P. J., Arnold, J. N., Roberts, E. W., Magiera, L., Jones, J. O., Gopinathan, A., Tuveson, D. A., and Fearon, D. T. (2010). Suppression of antitumor immunity by stromal cells expressing fibroblast activation protein-alpha. Science *330*, 827-830.

Kryczek, I., Lange, A., Mottram, P., Alvarez, X., Cheng, P., Hogan, M., Moons, L., Wei, S., Zou, L., Machelon, V.*, et al.* (2005). CXCL12 and vascular endothelial growth factor synergistically induce neoangiogenesis in human ovarian cancers. Cancer Res *65*, 465-472.

Kryczek, I., Wei, S., Zhu, G., Myers, L., Mottram, P., Cheng, P., Chen, L., Coukos, G., and Zou, W. (2007). Relationship between B7-H4, regulatory T cells, and patient outcome in human ovarian carcinoma. Cancer Res *67*, 8900-8905.

Kucia, M., Jankowski, K., Reca, R., Wysoczynski, M., Bandura, L., Allendorf, D. J., Zhang, J., Ratajczak, J., and Ratajczak, M. Z. (2004). CXCR4-SDF-1 signalling, locomotion, chemotaxis and adhesion. J Mol Histol *35*, 233-245.

Kulbe, H., Chakravarty, P., Leinster, D. A., Charles, K. A., Kwong, J., Thompson, R. G., Coward, J. I., Schioppa, T., Robinson, S. C., Gallagher, W. M.*, et al.* (2012). A dynamic inflammatory cytokine network in the human ovarian cancer microenvironment. Cancer Res *72*, 66-75.

Kulbe, H., Hagemann, T., Szlosarek, P. W., Balkwill, F. R., and Wilson, J. L. (2005). The inflammatory cytokine tumor necrosis factor-alpha regulates chemokine receptor expression on ovarian cancer cells. Cancer Res *65*, 10355-10362.

Kulbe, H., Levinson, N. R., Balkwill, F., and Wilson, J. L. (2004). The chemokine network in cancer--much more than directing cell movement. Int J Dev Biol *48*, 489-496.

Kulbe, H., Thompson, R., Wilson, J. L., Robinson, S., Hagemann, T., Fatah, R., Gould, D., Ayhan, A., and Balkwill, F. (2007). The inflammatory cytokine tumor necrosis factor-alpha generates an autocrine tumor-promoting network in epithelial ovarian cancer cells. Cancer Res *67*, 585-592.

Kumar, R., Crouthamel, M. C., Rominger, D. H., Gontarek, R. R., Tummino, P. J., Levin, R. A., and King, A. G. (2009). Myelosuppression and kinase selectivity of multikinase angiogenesis inhibitors. Br J Cancer *101*, 1717-1723.

Kurman, R. J. (2013). Origin and molecular pathogenesis of ovarian high-grade serous carcinoma. Ann Oncol *24*, x16-21.

Kurman, R. J., and Shih Ie, M. (2010). The origin and pathogenesis of epithelial ovarian cancer: a proposed unifying theory. Am J Surg Pathol *34*, 433-443.

Kurman, R. J., and Shih Ie, M. (2011). Molecular pathogenesis and extraovarian origin of epithelial ovarian cancer--shifting the paradigm. Hum Pathol *42*, 918-931.

Lansley, S. M., Searles, R. G., Hoi, A., Thomas, C., Moneta, H., Herrick, S. E., Thompson, P. J., Newman, M., Sterrett, G. F., Prele, C. M., and Mutsaers, S. E. (2010). Mesothelial Cell Differention into Osteoblast- and Adipocyte-Like Cells. J Cell Mol Med.

Lee, S., Garner, E. I., Welch, W. R., Berkowitz, R. S., and Mok, S. C. (2007a). Over-expression of hypoxia-inducible factor 1 alpha in ovarian clear cell carcinoma. Gynecol Oncol *106*, 311-317.

Lee, Y., Miron, A., Drapkin, R., Nucci, M. R., Medeiros, F., Saleemuddin, A., Garber, J., Birch, C., Mou, H., Gordon, R. W.*, et al.* (2007b). A candidate precursor to serous carcinoma that originates in the distal fallopian tube. J Pathol *211*, 26-35.

Leinster, D. A., Kulbe, H., Everitt, G., Thompson, R., Perretti, M., Gavins, F. N., Cooper, D., Gould, D., Ennis, D. P., Lockley, M.*, et al.* (2012). The peritoneal tumour microenvironment of high-grade serous ovarian cancer. J Pathol *227*, 136-145.

Lengyel, E. (2010). Ovarian cancer development and metastasis. Am J Pathol *177*, 1053-1064.

Lengyel, E., Burdette, J. E., Kenny, H. A., Matei, D., Pilrose, J., Haluska, P., Nephew, K. P., Hales, D. B., and Stack, M. S. (2013). Epithelial ovarian cancer experimental models. Oncogene *12*, 321.

Levanon, K., Ng, V., Piao, H. Y., Zhang, Y., Chang, M. C., Roh, M. H., Kindelberger, D. W., Hirsch, M. S., Crum, C. P., Marto, J. A., and Drapkin, R. (2010). Primary ex vivo cultures of human fallopian tube epithelium as a model for serous ovarian carcinogenesis. Oncogene *29*, 1103-1113.

Levental, K. R., Yu, H., Kass, L., Lakins, J. N., Egeblad, M., Erler, J. T., Fong, S. F., Csiszar, K., Giaccia, A., Weninger, W.*, et al.* (2009). Matrix crosslinking forces tumor progression by enhancing integrin signaling. Cell *139*, 891-906.

Li, J., Abushahin, N., Pang, S., Xiang, L., Chambers, S. K., Fadare, O., Kong, B., and Zheng, W. (2011). Tubal origin of 'ovarian' low-grade serous carcinoma. Mod Pathol *24*, 1488-1499.

Li, S. L., Ye, F., Cai, W. J., Hu, H. D., Hu, P., Ren, H., Zhu, F. F., and Zhang, D. Z. (2010). Quantitative proteome analysis of multidrug resistance in human ovarian cancer cell line. J Cell Biochem *109*, 625-633.

Liles, W. C., Broxmeyer, H. E., Rodger, E., Wood, B., Hubel, K., Cooper, S., Hangoc, G., Bridger, G. J., Henson, G. W., Calandra, G., and Dale, D. C. (2003). Mobilization of hematopoietic progenitor cells in healthy volunteers by AMD3100, a CXCR4 antagonist. Blood *102*, 2728-2730.

Lin, E. Y., Nguyen, A. V., Russell, R. G., and Pollard, J. W. (2001). Colony-stimulating factor 1 promotes progression of mammary tumors to malignancy. J Exp Med *193*, 727-740.

Liu, J., Yang, G., Thompson-Lanza, J. A., Glassman, A., Hayes, K., Patterson, A., Marquez, R. T., Auersperg, N., Yu, Y., Hahn, W. C.*, et al.* (2004). A genetically defined model for human ovarian cancer. Cancer Res *64*, 1655-1663.

Lopez-Dee, Z., Pidcock, K., and Gutierrez, L. S. (2011). Thrombospondin-1: multiple paths to inflammation. Mediators Inflamm *2011:296069.*

Lopez-Novoa, J. M., and Nieto, M. A. (2009). Inflammation and EMT: an alliance towards organ fibrosis and cancer progression. EMBO Mol Med *1*, 303-314.

Lumeng, C. N., Bodzin, J. L., and Saltiel, A. R. (2007). Obesity induces a phenotypic switch in adipose tissue macrophage polarization. J Clin Invest *117*, 175-184.

Lundberg, A. S., Hahn, W. C., Gupta, P., and Weinberg, R. A. (2000). Genes involved in senescence and immortalization. Curr Opin Cell Biol *12*, 705-709.

Malek, J. A., Mery, E., Mahmoud, Y. A., Al-Azwani, E. K., Roger, L., Huang, R., Jouve, E., Lis, R., Thiery, J. P., Querleu, D., and Rafii, A. (2011). Copy number variation analysis of matched ovarian primary tumors and peritoneal metastasis. PLoS One *6*.

Mantovani, A., Allavena, P., Sica, A., and Balkwill, F. (2008). Cancer-related inflammation. Nature *454*, 436-444.

Mantovani, A., Sica, A., Sozzani, S., Allavena, P., Vecchi, A., and Locati, M. (2004). The chemokine system in diverse forms of macrophage activation and polarization. Trends Immunol *25*, 677-686.

Masiakos, P. T., MacLaughlin, D. T., Maheswaran, S., Teixeira, J., Fuller, A. F., Jr., Shah, P. C., Kehas, D. J., Kenneally, M. K., Dombkowski, D. M., Ha, T. U.*, et al.* (1999). Human ovarian cancer, cell lines, and primary ascites cells express the human Mullerian inhibiting substance (MIS) type II receptor, bind, and are responsive to MIS. Clin Cancer Res *5*, 3488-3499.

Matei, D., Graeber, T. G., Baldwin, R. L., Karlan, B. Y., Rao, J., and Chang, D. D. (2002). Gene expression in epithelial ovarian carcinoma. Oncogene *21*, 6289-6298.

Matsuura, M., Suzuki, T., and Saito, T. (2010). Osteopontin is a new target molecule for ovarian clear cell carcinoma therapy. Cancer Sci *101*, 1828-1833.

Mesher, D., Soldan, K., Howell-Jones, R., Panwar, K., Manyenga, P., Jit, M., Beddows, S., and Gill, O. N. (2013). Reduction in HPV 16/18 prevalence in sexually active young women following the introduction of HPV immunisation in England. Vaccine *5*, 01492-01498.

Mhawech-Fauceglia, P., Wang, D., Ali, L., Lele, S., Huba, M. A., Liu, S., and Odunsi, K. (2013). Intraepithelial T cells and tumor-associated macrophages in ovarian cancer patients. Cancer Immun *13*, 1.

Mills, G. B., May, C., Hill, M., Campbell, S., Shaw, P., and Marks, A. (1990). Ascitic fluid from human ovarian cancer patients contains growth factors necessary for intraperitoneal growth of human ovarian adenocarcinoma cells. J Clin Invest *86*, 851-855.

Moore, R. J., Owens, D. M., Stamp, G., Arnott, C., Burke, F., East, N., Holdsworth, H., Turner, L., Rollins, B., Pasparakis, M.*, et al.* (1999).

Mice deficient in tumor necrosis factor-alpha are resistant to skin carcinogenesis. Nat Med *5*, 828-831.

Moradi, M. M., Carson, L. F., Weinberg, B., Haney, A. F., Twiggs, L. B., and Ramakrishnan, S. (1993). Serum and ascitic fluid levels of interleukin-1, interleukin-6, and tumor necrosis factor-alpha in patients with ovarian epithelial cancer. Cancer *72*, 2433-2440.

Moser, B., and Loetscher, P. (2001). Lymphocyte traffic control by chemokines. Nat Immunol *2*, 123-128.

Motohara, T., Tashiro, H., Miyahara, Y., Sakaguchi, I., Ohtake, H., and Katabuchi, H. (2010). Long-term oncological outcomes of ovarian serous carcinomas with psammoma bodies: a novel insight into the molecular pathogenesis of ovarian epithelial carcinoma. Cancer Sci *101*, 1550-1556.

Mukhopadhyay, A., Plummer, E. R., Elattar, A., Soohoo, S., Uzir, B., Quinn, J. E., McCluggage, W. G., Maxwell, P., Aneke, H., Curtin, N. J., and Edmondson, R. J. (2012). Clinicopathological features of homologous recombination-deficient epithelial ovarian cancers: sensitivity to PARP inhibitors, platinum, and survival. Cancer Res *72*, 5675-5682.

Muller, A., Homey, B., Soto, H., Ge, N., Catron, D., Buchanan, M. E., McClanahan, T., Murphy, E., Yuan, W., Wagner, S. N.*, et al.* (2001). Involvement of chemokine receptors in breast cancer metastasis. Nature *410*, 50-56.

Mural, R. J., Adams, M. D., Myers, E. W., Smith, H. O., Miklos, G. L., Wides, R., Halpern, A., Li, P. W., Sutton, G. G., Nadeau, J.*, et al.* (2002). A comparison of whole-genome shotgun-derived mouse chromosome 16 and the human genome. Science *296*, 1661-1671.

Murdoch, C. (2000). CXCR4: chemokine receptor extraordinaire. Immunol Rev *177*, 175-184.

Nervi, B., Ramirez, P., Rettig, M. P., Uy, G. L., Holt, M. S., Ritchey, J. K., Prior, J. L., Piwnica-Worms, D., Bridger, G., Ley, T. J., and DiPersio, J. F. (2009). Chemosensitization of acute myeloid leukemia (AML) following mobilization by the CXCR4 antagonist AMD3100. Blood *113*, 6206-6214.

Nieman, K. M., Kenny, H. A., Penicka, C. V., Ladanyi, A., Buell-Gutbrod, R., Zillhardt, M. R., Romero, I. L., Carey, M. S., Mills, G. B., Hotamisligil, G. S.*, et al.* (2011). Adipocytes promote ovarian cancer metastasis and provide energy for rapid tumor growth. Nat Med *17*, 1498-1503.

Nik, N. N., Vang, R., Shih Ie, M., and Kurman, R. J. (2014). Origin and pathogenesis of pelvic (ovarian, tubal, and primary peritoneal) serous carcinoma. Annu Rev Pathol *9:27-45.*

Nystrom, M. L., Thomas, G. J., Stone, M., Mackenzie, I. C., Hart, I. R., and Marshall, J. F. (2005). Development of a quantitative method to analyse tumour cell invasion in organotypic culture. J Pathol *205*, 468-475.

O Donnell, R. L., McCormick, A., Mukhopadhyay, A., Woodhouse, L. C., Moat, M., Grundy, A., Dixon, M., Kaufman, A., Soohoo, S., Elattar, A.*, et al.* (2014). The use of ovarian cancer cells from patients undergoing surgery to generate primary cultures capable of undergoing functional analysis. PLoS One *9*.

Park, E. K., Jung, H. S., Yang, H. I., Yoo, M. C., Kim, C., and Kim, K. S. (2007). Optimized THP-1 differentiation is required for the detection of responses to weak stimuli. Inflamm Res *56*, 45-50.

Paszek, M. J., Zahir, N., Johnson, K. R., Lakins, J. N., Rozenberg, G. I., Gefen, A., Reinhart-King, C. A., Margulies, S. S., Dembo, M., Boettiger, D.*, et al.* (2005). Tensional homeostasis and the malignant phenotype. Cancer Cell *8*, 241-254.

Pease, J. C., Brewer, M., and Tirnauer, J. S. (2012). Spontaneous spheroid budding from monolayers: a potential contribution to ovarian cancer dissemination. Biol Open *1*, 622-628.

Perets, R., Wyant, G. A., Muto, K. W., Bijron, J. G., Poole, B. B., Chin, K. T., Chen, J. Y., Ohman, A. W., Stepule, C. D., Kwak, S.*, et al.* (2013). Transformation of the fallopian tube secretory epithelium leads to high-grade serous ovarian cancer in Brca;Tp53;Pten models. Cancer Cell *24*, 751-765.

Phillips, R. J., Lutz, M., and Premack, B. (2005). Differential signaling mechanisms regulate expression of CC chemokine receptor-2 during monocyte maturation. J Inflamm (Lond) *2*, 14.

Pollard, J. W. (2008). Macrophages define the invasive microenvironment in breast cancer. J Leukoc Biol *84*, 623-630.

Polyak, K., Haviv, I., and Campbell, I. G. (2009). Co-evolution of tumor cells and their microenvironment. Trends Genet *25*, 30-38.

Popple, A., Durrant, L. G., Spendlove, I., Rolland, P., Scott, I. V., Deen, S., and Ramage, J. M. (2012). The chemokine, CXCL12, is an independent predictor of poor survival in ovarian cancer. Br J Cancer *106*, 1306-1313.

Pusic, I., and DiPersio, J. F. (2010). Update on clinical experience with AMD3100, an SDF-1/CXCL12-CXCR4 inhibitor, in mobilization of hematopoietic stem and progenitor cells. Curr Opin Hematol *17*, 319-326.

Qian, B. Z., Li, J., Zhang, H., Kitamura, T., Zhang, J., Campion, L. R., Kaiser, E. A., Snyder, L. A., and Pollard, J. W. (2011). CCL2 recruits inflammatory monocytes to facilitate breast-tumour metastasis. Nature *475*, 222-225.

Qin, Z., Richter, G., Schuler, T., Ibe, S., Cao, X., and Blankenstein, T. (1998). B cells inhibit induction of T cell-dependent tumor immunity. Nat Med *4*, 627-630.

Radisavljevic, S. V. (1977). The pathogenesis of ovarian inclusion cysts and cystomas. Obstet Gynecol *49*, 424-429.

Ranieri, D., Raffa, S., Parente, A., Rossi Del Monte, S., Ziparo, V., and Torrisi, M. R. (2013). High adhesion of tumor cells to mesothelial monolayers derived from peritoneal wash of disseminated gastrointestinal cancers. PLoS One *8*.

Raz, E., and Mahabaleshwar, H. (2009). Chemokine signaling in embryonic cell migration: a fisheye view. Development *136*, 1223-1229.

Reinartz, S., Schumann, T., Finkernagel, F., Wortmann, A., Jansen, J. M., Meissner, W., Krause, M., Schworer, A. M., Wagner, U., Muller-Brusselbach, S., and Muller, R. (2013). Mixed-polarization phenotype of ascites-associated macrophages in human ovarian carcinoma: Correlation of CD163 expression, cytokine levels and early relapse. Int J Cancer *20*, 28335.

Rhim, A. D., Mirek, E. T., Aiello, N. M., Maitra, A., Bailey, J. M., McAllister, F., Reichert, M., Beatty, G. L., Rustgi, A. K., Vonderheide, R. H.*, et al.* (2012). EMT and dissemination precede pancreatic tumor formation. Cell *148*, 349-361.

Rizvi, I., Gurkan, U. A., Tasoglu, S., Alagic, N., Celli, J. P., Mensah, L. B., Mai, Z., Demirci, U., and Hasan, T. (2013). Flow induces epithelial-mesenchymal transition, cellular heterogeneity and biomarker modulation in 3D ovarian cancer nodules. Proc Natl Acad Sci U S A *110*, E1974-1983.

Robinson-Smith, T. M., Isaacsohn, I., Mercer, C. A., Zhou, M., Van Rooijen, N., Husseinzadeh, N., McFarland-Mancini, M. M., and Drew, A. F. (2007). Macrophages mediate inflammation-enhanced metastasis of ovarian tumors in mice. Cancer Res *67*, 5708-5716.

Roby, K. F., Taylor, C. C., Sweetwood, J. P., Cheng, Y., Pace, J. L., Tawfik, O., Persons, D. L., Smith, P. G., and Terranova, P. F. (2000). Development of a syngeneic mouse model for events related to ovarian cancer. Carcinogenesis *21*, 585-591.

Rothwell, P. M. (2013). Aspirin in prevention of sporadic colorectal cancer: current clinical evidence and overall balance of risks and benefits. Recent Results Cancer Res *191:121-42.*

Rothwell, P. M., Fowkes, F. G., Belch, J. F., Ogawa, H., Warlow, C. P., and Meade, T. W. (2011). Effect of daily aspirin on long-term risk of death due to cancer: analysis of individual patient data from randomised trials. Lancet *377*, 31-41.

Rothwell, P. M., Wilson, M., Price, J. F., Belch, J. F., Meade, T. W., and Mehta, Z. (2012). Effect of daily aspirin on risk of cancer metastasis: a study of incident cancers during randomised controlled trials. Lancet *379*, 1591-1601.

Salomonnson, E., Stacer, A. C., Ehrlich, A., Luker, K. E., and Luker, G. D. (2013). Imaging CXCL12-CXCR4 signaling in ovarian cancer therapy. PLoS One *8*, e51500.

Sanz-Moreno, V., Gaggioli, C., Yeo, M., Albrengues, J., Wallberg, F., Viros, A., Hooper, S., Mitter, R., Feral, C. C., Cook, M.*, et al.* (2011).

ROCK and JAK1 signaling cooperate to control actomyosin contractility in tumor cells and stroma. Cancer Cell *20*, 229-245.

Sanz-Moreno, V., and Marshall, C. J. (2010). The plasticity of cytoskeletal dynamics underlying neoplastic cell migration. Curr Opin Cell Biol *22*, 690-696.

Sato, E., Olson, S. H., Ahn, J., Bundy, B., Nishikawa, H., Qian, F., Jungbluth, A. A., Frosina, D., Gnjatic, S., Ambrosone, C.*, et al.* (2005). Intraepithelial CD8+ tumor-infiltrating lymphocytes and a high CD8+/regulatory T cell ratio are associated with favorable prognosis in ovarian cancer. Proc Natl Acad Sci U S A *102*, 18538-18543.

Sawada, K., Mitra, A. K., Radjabi, A. R., Bhaskar, V., Kistner, E. O., Tretiakova, M., Jagadeeswaran, S., Montag, A., Becker, A., Kenny, H. A.*, et al.* (2008). Loss of E-cadherin promotes ovarian cancer metastasis via alpha 5-integrin, which is a therapeutic target. Cancer Res *68*, 2329-2339.

Schafer, M., and Werner, S. (2008). Cancer as an overhealing wound: an old hypothesis revisited. Nat Rev Mol Cell Biol *9*, 628-638.

Schioppa, T., Uranchimeg, B., Saccani, A., Biswas, S. K., Doni, A., Rapisarda, A., Bernasconi, S., Saccani, S., Nebuloni, M., Vago, L.*, et al.* (2003). Regulation of the chemokine receptor CXCR4 by hypoxia. J Exp Med *198*, 1391-1402.

Schulz, C., Gomez Perdiguero, E., Chorro, L., Szabo-Rogers, H., Cagnard, N., Kierdorf, K., Prinz, M., Wu, B., Jacobsen, S. E., Pollard, J. W.*, et al.* (2012). A lineage of myeloid cells independent of Myb and hematopoietic stem cells. Science *336*, 86-90.

Scotton, C. J., Wilson, J. L., Milliken, D., Stamp, G., and Balkwill, F. R. (2001). Epithelial cancer cell migration: a role for chemokine receptors? Cancer Res *61*, 4961-4965.

Scotton, C. J., Wilson, J. L., Scott, K., Stamp, G., Wilbanks, G. D., Fricker, S., Bridger, G., and Balkwill, F. R. (2002). Multiple actions of the chemokine CXCL12 on epithelial tumor cells in human ovarian cancer. Cancer Res *62*, 5930-5938.

Sehouli, J., Senyuva, F., Fotopoulou, C., Neumann, U., Denkert, C., Werner, L., and Gulten, O. O. (2009). Intra-abdominal tumor

dissemination pattern and surgical outcome in 214 patients with primary ovarian cancer. J Surg Oncol *99*, 424-427.

Shah, S., Divekar, A. A., Hilchey, S. P., Cho, H. M., Newman, C. L., Shin, S. U., Nechustan, H., Challita-Eid, P. M., Segal, B. M., Yi, K. H., and Rosenblatt, J. D. (2005). Increased rejection of primary tumors in mice lacking B cells: inhibition of anti-tumor CTL and TH1 cytokine responses by B cells. Int J Cancer *117*, 574-586.

Shchors, K., Shchors, E., Rostker, F., Lawlor, E. R., Brown-Swigart, L., and Evan, G. I. (2006). The Myc-dependent angiogenic switch in tumors is mediated by interleukin 1beta. Genes Dev *20*, 2527-2538.

Sherman-Baust, C. A., Weeraratna, A. T., Rangel, L. B., Pizer, E. S., Cho, K. R., Schwartz, D. R., Shock, T., and Morin, P. J. (2003). Remodeling of the extracellular matrix through overexpression of collagen VI contributes to cisplatin resistance in ovarian cancer cells. Cancer Cell *3*, 377-386.

Shield, K., Ackland, M. L., Ahmed, N., and Rice, G. E. (2009). Multicellular spheroids in ovarian cancer metastases: Biology and pathology. Gynecol Oncol *113*, 143-148.

Showe, M. K., Vachani, A., Kossenkov, A. V., Yousef, M., Nichols, C., Nikonova, E. V., Chang, C., Kucharczuk, J., Tran, B., Wakeam, E.*, et al.* (2009). Gene expression profiles in peripheral blood mononuclear cells can distinguish patients with non-small cell lung cancer from patients with nonmalignant lung disease. Cancer Res *69*, 9202-9210.

Sica, A., and Bronte, V. (2007). Altered macrophage differentiation and immune dysfunction in tumor development. J Clin Invest *117*, 1155-1166.

Sica, A., and Mantovani, A. (2012). Macrophage plasticity and polarization: in vivo veritas. J Clin Invest *122*, 787-795.

Sodek, K. L., Ringuette, M. J., and Brown, T. J. (2009). Compact spheroid formation by ovarian cancer cells is associated with contractile behavior and an invasive phenotype. Int J Cancer *124*, 2060-2070.

Sofeu Feugaing, D. D., Gotte, M., and Viola, M. (2013). More than matrix: the multifaceted role of decorin in cancer. Eur J Cell Biol *92*, 1-11.

Son, D. S., Kabir, S. M., Dong, Y. L., Lee, E., and Adunyah, S. E. (2012). Inhibitory effect of tumor suppressor p53 on proinflammatory chemokine expression in ovarian cancer cells by reducing proteasomal degradation of IkappaB. PLoS One *7*.

Sorokin, L. (2010). The impact of the extracellular matrix on inflammation. Nat Rev Immunol *10*, 712-723.

Sparmann, A., and Bar-Sagi, D. (2004). Ras-induced interleukin-8 expression plays a critical role in tumor growth and angiogenesis. Cancer Cell *6*, 447-458.

Stumpf, M., Hasenburg, A., Riener, M. O., Jutting, U., Wang, C., Shen, Y., Orlowska-Volk, M., Fisch, P., Wang, Z., Gitsch, G.*, et al.* (2009). Intraepithelial CD8-positive T lymphocytes predict survival for patients with serous stage III ovarian carcinomas: relevance of clonal selection of T lymphocytes. Br J Cancer *101*, 1513-1521.

Sun, K., Kusminski, C. M., and Scherer, P. E. (2011). Adipose tissue remodeling and obesity. J Clin Invest *121*, 2094-2101.

Tchernychev, B., Ren, Y., Sachdev, P., Janz, J. M., Haggis, L., O'Shea, A., McBride, E., Looby, R., Deng, Q., McMurry, T.*, et al.* (2010). Discovery of a CXCR4 agonist pepducin that mobilizes bone marrow hematopoietic cells. Proc Natl Acad Sci U S A *107*, 22255-22259.

Tothill, R. W., Tinker, A. V., George, J., Brown, R., Fox, S. B., Lade, S., Johnson, D. S., Trivett, M. K., Etemadmoghadam, D., Locandro, B.*, et al.* (2008). Novel molecular subtypes of serous and endometrioid ovarian cancer linked to clinical outcome. Clin Cancer Res *14*, 5198-5208.

Touboul, C., Lis, R., Al Farsi, H., Raynaud, C. M., Warfa, M., Althawadi, H., Mery, E., Mirshahi, M., and Rafii, A. (2013). Mesenchymal stem cells enhance ovarian cancer cell infiltration through IL6 secretion in an amniochorionic membrane based 3D model. J Transl Med *11:28.*

Tsuchiya, A., Sakamoto, M., Yasuda, J., Chuma, M., Ohta, T., Ohki, M., Yasugi, T., Taketani, Y., and Hirohashi, S. (2003). Expression profiling in ovarian clear cell carcinoma: identification of hepatocyte nuclear factor-1 beta as a molecular marker and a possible molecular target for therapy of ovarian clear cell carcinoma. Am J Pathol *163*, 2503-2512.

Tsuchiya, S., Yamabe, M., Yamaguchi, Y., Kobayashi, Y., Konno, T., and Tada, K. (1980). Establishment and characterization of a human acute monocytic leukemia cell line (THP-1). Int J Cancer *26*, 171-176.

Vaday, G. G., and Lider, O. (2000). Extracellular matrix moieties, cytokines, and enzymes: dynamic effects on immune cell behavior and inflammation. J Leukoc Biol *67*, 149-159.

Vandesompele, J., De Preter, K., Pattyn, F., Poppe, B., Van Roy, N., De Paepe, A., and Speleman, F. (2002). Accurate normalization of real-time quantitative RT-PCR data by geometric averaging of multiple internal control genes. Genome Biol *3*.

Vaughan, S., Coward, J. I., Bast, R. C., Jr., Berchuck, A., Berek, J. S., Brenton, J. D., Coukos, G., Crum, C. C., Drapkin, R., Etemadmoghadam, D.*, et al.* (2011). Rethinking ovarian cancer: recommendations for improving outcomes. Nat Rev Cancer *11*, 719-725.

Verhaak, R. G., Tamayo, P., Yang, J. Y., Hubbard, D., Zhang, H., Creighton, C. J., Fereday, S., Lawrence, M., Carter, S. L., Mermel, C. H.*, et al.* (2013). Prognostically relevant gene signatures of high-grade serous ovarian carcinoma. J Clin Invest *123*, 517-525.

Wan, L., Pantel, K., and Kang, Y. (2013). Tumor metastasis: moving new biological insights into the clinic. Nat Med *19*, 1450-1464.

Wang, Y., Krushel, L. A., and Edelman, G. M. (1996). Targeted DNA recombination in vivo using an adenovirus carrying the cre recombinase gene. Proc Natl Acad Sci U S A *93*, 3932-3936.

Webb, J. R., Milne, K., Watson, P., Deleeuw, R. J., and Nelson, B. H. (2014). Tumor-Infiltrating Lymphocytes Expressing the Tissue Resident Memory Marker CD103 Are Associated with Increased Survival in High-Grade Serous Ovarian Cancer. Clin Cancer Res *20*, 434-444.

Ween, M. P., Lokman, N. A., Hoffmann, P., Rodgers, R. J., Ricciardelli, C., and Oehler, M. K. (2011). Transforming growth factor-beta-induced protein secreted by peritoneal cells increases the metastatic potential of ovarian cancer cells. Int J Cancer *128*, 1570-1584.

Weisberg, S. P., McCann, D., Desai, M., Rosenbaum, M., Leibel, R. L., and Ferrante, A. W., Jr. (2003). Obesity is associated with macrophage accumulation in adipose tissue. J Clin Invest *112*, 1796-1808.

Wiegand, K. C., Shah, S. P., Al-Agha, O. M., Zhao, Y., Tse, K., Zeng, T., Senz, J., McConechy, M. K., Anglesio, M. S., Kalloger, S. E.*, et al.* (2010). ARID1A mutations in endometriosis-associated ovarian carcinomas. N Engl J Med *363*, 1532-1543.

Witz, C. A., Montoya-Rodriguez, I. A., Cho, S., Centonze, V. E., Bonewald, L. F., and Schenken, R. S. (2001). Composition of the extracellular matrix of the peritoneum. J Soc Gynecol Investig *8*, 299-304.

Wynn, T. A., Chawla, A., and Pollard, J. W. (2013). Macrophage biology in development, homeostasis and disease. Nature *496*, 445-455.

Yang, C., Lee, H., Jove, V., Deng, J., Zhang, W., Liu, X., Forman, S., Dellinger, T. H., Wakabayashi, M., Yu, H., and Pal, S. (2013a). Prognostic significance of B-cells and pSTAT3 in patients with ovarian cancer. PLoS One *8*.

Yang, G., Rosen, D. G., Colacino, J. A., Mercado-Uribe, I., and Liu, J. (2007a). Disruption of the retinoblastoma pathway by small interfering RNA and ectopic expression of the catalytic subunit of telomerase lead to immortalization of human ovarian surface epithelial cells. Oncogene *26*, 1492-1498.

Yang, G., Rosen, D. G., Mercado-Uribe, I., Colacino, J. A., Mills, G. B., Bast, R. C., Jr., Zhou, C., and Liu, J. (2007b). Knockdown of p53 combined with expression of the catalytic subunit of telomerase is sufficient to immortalize primary human ovarian surface epithelial cells. Carcinogenesis *28*, 174-182.

Yang, J. Y., Yoshihara, K., Tanaka, K., Hatae, M., Masuzaki, H., Itamochi, H., Takano, M., Ushijima, K., Tanyi, J. L., Coukos, G.*, et al.* (2013b). Predicting time to ovarian carcinoma recurrence using protein markers. J Clin Invest *123*, 3740-3750.

Yang, L., DeBusk, L. M., Fukuda, K., Fingleton, B., Green-Jarvis, B., Shyr, Y., Matrisian, L. M., Carbone, D. P., and Lin, P. C. (2004). Expansion of myeloid immune suppressor Gr+CD11b+ cells in tumor-bearing host directly promotes tumor angiogenesis. Cancer Cell *6*, 409-421.

Zhang, L., Conejo-Garcia, J. R., Katsaros, D., Gimotty, P. A., Massobrio, M., Regnani, G., Makrigiannakis, A., Gray, H., Schlienger, K., Liebman, M. N.*, et al.* (2003). Intratumoral T cells, recurrence, and survival in epithelial ovarian cancer. N Engl J Med *348*, 203-213.

Zhu, M., Fejzo, M. S., Anderson, L., Dering, J., Ginther, C., Ramos, L., Gasson, J. C., Karlan, B. Y., and Slamon, D. J. (2010). Periostin promotes ovarian cancer angiogenesis and metastasis. Gynecol Oncol *119*, 337-344.

Zillhardt, M., Park, S. M., Romero, I. L., Sawada, K., Montag, A., Krausz, T., Yamada, S. D., Peter, M. E., and Lengyel, E. (2011). Foretinib (GSK1363089), an orally available multikinase inhibitor of c-Met and VEGFR-2, blocks proliferation, induces anoikis, and impairs ovarian cancer metastasis. Clin Cancer Res *17*, 4042-4051.

10. Appendices

10.1. Appendix I: Supplementary data

Gene	Fold change
chemokine (C-X-C motif) ligand 12	14.33127613
collagen, type X, alpha 1	11.77985505
lumican	9.109582398
collagen, type III, alpha 1	7.558319183
decorin	7.175963403
versican	6.289583754
TIMP metallopeptidase inhibitor 3	6.205274356
collagen, type V, alpha 1	6.185612833
collagen, type V, alpha 2	6.03244568
collagen, type I, alpha 1	5.942290308
vascular cell adhesion molecule 1	5.74151157
cartilage oligomeric matrix protein	5.407498397
fibrillin 1	4.912413639
actin, alpha 2, smooth muscle, aorta	4.824726047
fibronectin 1	4.822990822
thrombospondin 1	4.775156404
plasminogen activator, urokinase	4.768927985
SPARC (osteonectin)	4.22897384
collagen, type VI, alpha 3	4.192198622
collagen, type I, alpha 2	3.928224315
matrix metallopeptidase 11 (stromelysin 3)	3.83949525
protein tyrosine phosphatase receptor type C	3.834024497
plasminogen activator inhibitor type 1	3.725180397
actin, gamma 2, smooth muscle, enteric	3.642892403
ADAM metallopeptidase domain 12	3.607230262
transforming growth factor beta 1 induced transcript 1	3.373300685
nidogen 2 (osteonidogen)	3.283834603
laminin, alpha 4	3.06510418
matrix metallopeptidase 2 (type IV collagenase)	2.904500569

nidogen 1	2.886898881
gap junction protein, alpha 1, 43kDa	2.883873436
plexin C1	2.756617893
collagen, type XVI, alpha 1	2.655875711
cysteine-rich, angiogenic inducer, 61	2.638213266
lectin, galactoside-binding, soluble, 1	2.550982506
biglycan	2.540618456
collagen, type IV, alpha 1	2.47126342
integrin, beta 2	2.446855377
elastin microfibril interfacer 1	2.438230988
myosin, light chain 9, regulatory	2.397138418
myosin light chain kinase	2.297410958
spondin 2, extracellular matrix protein	2.232495807
neuropilin 1	2.205313558
transforming growth factor, beta-induced	2.204489896
microfibrillar-associated protein 2	2.196129265
collagen, type IV, alpha 2	2.135848543
plasminogen activator, tissue	2.090273259
laminin, beta 1	2.028368486

Table 10-1 The fold change values of 48 genes up regulated in the high CXCL12 expressing biopsies of the AOCS data set also common to the GSE 6008 and 3149 data set.

Table listing the 48 differentially expressed cell-matrix interactions and ECM remodelling genes when comparing their expression in the 50 highest versus the 50 lowest CXCL12 expressing ovarian cancer biopsies. The genes listed here are those in the AOCS data set and common to the GSE 6008 and 3149 affymetrix gene expression array data set. Fold change values are averaged from each gene probe set. p value ≤ 0.05.

Gene	Fold change
lumican	11.558
collagen, type V, alpha 2	8.694
fibronectin 1	6.404
SPARC (osteonectin)	6.351
collagen, type III, alpha 1	6.240
collagen, type I, alpha 1	6.137
TIMP metallopeptidase inhibitor 3	6.060
collagen, type V, alpha 1	5.635
vascular cell adhesion molecule 1	5.264
fibrillin 1	5.057
thrombospondin 1	5.045
decorin	4.923
collagen, type VI, alpha 3	4.581
actin, alpha 2, smooth muscle, aorta	4.410
matrix metallopeptidase 2 (type IV collagenase)	4.197
matrix metallopeptidase 11 (stromelysin 3)	4.193
plasminogen activator inhibitor type 1	3.556
collagen, type XVI, alpha 1	3.498
cartilage oligomeric matrix protein	3.280
nidogen 2 (osteonidogen)	3.190
cysteine-rich, angiogenic inducer, 61	3.167
versican	3.164
transforming growth factor beta 1 induced transcript 1	3.162
collagen, type I, alpha 2	3.144
transforming growth factor, beta-induced	3.029
collagen, type X, alpha 1	3.019
ADAM metallopeptidase domain 12	2.973
biglycan	2.892
myosin, light chain 9, regulatory	2.856
chemokine (C-X-C motif) ligand 12	2.764
nidogen 1	2.749
plasminogen activator, urokinase	2.717
microfibrillar-associated protein 2	2.679
myosin light chain kinase	2.678
elastin microfibril interfacer 1	2.655

laminin, beta 1	2.603
laminin, alpha 4	2.559
collagen, type IV, alpha 1	2.504
gap junction protein, alpha 1, 43kDa	2.481
plasminogen activator, tissue	2.436
lectin, galactoside-binding, soluble, 1	2.379
plexin C1	2.328
integrin, beta 2	2.191
collagen, type IV, alpha 2	2.184
protein tyrosine phosphatase receptor type C	2.140
actin, gamma 2, smooth muscle, enteric	2.124
spondin 2, extracellular matrix protein	2.083
neuropilin 1	2.058

Table 10-2 The fold change values of 48 genes up regulated in the high CXCL12 expressing biopsies of the GSE 6008 and 3149 data set also common to the AOCS data set.

Table listing the 48 differentially expressed cell-matrix interactions and ECM remodelling genes when comparing their expression in the 50 highest versus the 50 lowest CXCL12 expressing ovarian cancer biopsies. The genes listed here are those in the GSE 6008 and 3149 affymetrix gene expression array data set and common to the AOCS data set. Fold change values are averaged from each gene probe set. p value $\leq$ 0.05.

Gene	Fold change
lymphotoxin beta receptor (TNFR superfamily, member 3)	-1.131616039
protein tyrosine phosphatase, receptor type, C	1.13505687
CD300c molecule	1.15173752
CD84 molecule	1.19923003
colony stimulating factor 2 receptor, alpha, low-affinity (granulocyte-macrophage)	1.210582268
colony stimulating factor 2 receptor, alpha, low-affinity (granulocyte-macrophage)	1.210903576
leukocyte immunoglobulin-like receptor, subfamily B (with TM and ITIM domains), member 3	1.214603058
colony stimulating factor 2 receptor, alpha, low-affinity (granulocyte-macrophage)	1.218547541
CD33 molecule	1.269361861
signaling lymphocytic activation molecule family member 1	1.269852752
SLAM family member 7	1.269981022
interleukin 10	1.280623156
CD209 molecule	1.310874507
low density lipoprotein-related protein 1 (alpha-2-macroglobulin receptor)	1.321366842
toll-like receptor 4	1.324133329
interferon gamma receptor 1	1.33809499
CD80 molecule	1.35002511
integrin, alpha X (complement component 3 receptor 4 subunit)	1.351124152
tumor necrosis factor (ligand) superfamily, member 14	1.364360028
macrophage receptor with collagenous structure	1.364737939
colony stimulating factor 2 receptor, alpha, low-affinity (granulocyte-macrophage)	1.39067681
egf-like module containing, mucin-like, hormone receptor-like 2	1.391370913
interferon gamma receptor 1	1.393709641

C-type lectin domain family 4, member A	1.412309433
CD40 molecule, TNF receptor superfamily member 5	1.463765592
CD163 molecule	1.470314972
leukocyte immunoglobulin-like receptor, subfamily B (with TM and ITIM domains), member 1	1.472273846
leukocyte immunoglobulin-like receptor, subfamily B (with TM and ITIM domains), member 2	1.491065131
integrin, alpha 4 (antigen CD49D, alpha 4 subunit of VLA-4 receptor)	1.49365124
endoglin	1.509373226
CD300a molecule	1.517304571
leukocyte immunoglobulin-like receptor, subfamily B (with TM and ITIM domains), member 1	1.51897657
leukocyte immunoglobulin-like receptor, subfamily B (with TM and ITIM domains), member 2	1.534522657
integrin, alpha 4 (antigen CD49D, alpha 4 subunit of VLA-4 receptor)	1.540794702
sialic acid binding Ig-like lectin 1, sialoadhesin	1.593832955
toll-like receptor 4	1.597868185
toll-like receptor 4	1.614484659
CD300 molecule-like family member f	1.648166427
secreted phosphoprotein 1	1.67216327
chemokine (C-C motif) ligand 18 (pulmonary and activation-regulated)	1.712673294
chemokine (C-C motif) ligand 18 (pulmonary and activation-regulated)	1.733217618
CD74 molecule, major histocompatibility complex, class II invariant chain	1.736459907
low density lipoprotein-related protein 1 (alpha-2-macroglobulin receptor)	1.764913502
triggering receptor expressed on myeloid cells 2	1.765413442
toll-like receptor 4	1.804733734

C-type lectin domain family 4, member A	1.831602731
stabilin 1	1.840315916
leukocyte immunoglobulin-like receptor, subfamily B (with TM and ITIM domains), member 4	1.852621159
CD300a molecule	1.870152775
stabilin 1	1.9033815
Fc fragment of IgG, low affinity IIIb, receptor (CD16b)	1.908836469
SLAM family member 8	1.911165522
lymphocyte antigen 86	1.934924438
CD84 molecule	2.01648301
platelet/endothelial cell adhesion molecule	2.033580494
CD74 molecule, major histocompatibility complex, class II invariant chain	2.058409447
Fc fragment of IgG, low affinity IIc, receptor for (CD32)	2.118460086
leukocyte immunoglobulin-like receptor, subfamily B (with TM and ITIM domains), member 1	2.139579706
latexin	2.163830519
glycoprotein (transmembrane) nmb	2.218326743
sialic acid binding Ig-like lectin 1, sialoadhesin	2.26871802
Fc fragment of IgG, low affinity IIc, receptor for (CD32)	2.296616299
integrin, alpha 4 (antigen CD49D, alpha 4 subunit of VLA-4 receptor)	2.318384464
platelet/endothelial cell adhesion molecule	2.326640299
integrin, beta 2 (complement component 3 receptor 3 and 4 subunit)	2.425879093
platelet/endothelial cell adhesion molecule	2.428000064
integrin, beta 2 (complement component 3 receptor 3 and 4 subunit)	2.446855377
insulin-like growth factor 1 (somatomedin C)	2.467476991
insulin-like growth factor 1 (somatomedin C)	2.551831551
chemokine (C-X-C motif) ligand 11	2.556396115
CD36 molecule (thrombospondin receptor)	2.686326408

protein tyrosine phosphatase, receptor type, C	2.692544941
CD36 molecule (thrombospondin receptor)	2.703676107
CD36 molecule (thrombospondin receptor)	2.738252745
CD14 molecule	2.760683304
SLAM family member 7	2.838395853
Fc fragment of IgG, low affinity IIb, receptor (CD32)	2.903086451
SLAM family member 8	3.062866033
protein tyrosine phosphatase, receptor type, C	3.114887339
chemokine (C-X-C motif) ligand 11	3.170899496
glycoprotein (transmembrane) nmb	3.211112872
Fc fragment of IgG, high affinity Ib, receptor (CD64)	3.355217161
CD163 molecule	3.379356064
CD163 molecule	3.558453751
protein tyrosine phosphatase, receptor type, C	3.834024497
lymphocyte antigen 96	4.018962142
insulin-like growth factor 1 (somatomedin C)	4.304344053
chemokine (C-X-C motif) ligand 10	4.484603172
insulin-like growth factor 1 (somatomedin C)	4.684374381
chemokine (C-X-C motif) ligand 9	5.770426244

Table 10-3 Macrophage signature genes in high CXCL12 expressing ovarian cancer biopsies of the AOCS data set.

A publically available gene set signature associated with macrophages was used to interrogate the gene expression microarray data of the AOCS data set. High CXCL12 expressing ovarian cancer biopsies showed enrichment in macrophage gene signatures. Table lists all the genes associated with macrophages and high expression of CXCL12 in the biopsies with the corresponding fold change values for each gene probe set. p value ≤ 0.05.

Gene	Fold change
poliovirus receptor	-1.094811277
integrin, beta 3 (platelet glycoprotein IIIa, antigen CD61)	-1.088293523
chemokine (C-C motif) ligand 17	-1.055380932
integrin, beta 3 (platelet glycoprotein IIIa, antigen CD61)	-1.048696369
CD300c molecule	1.068651148
C-type lectin domain family 4, member A	1.085003434
CD163 molecule	1.098397774
poliovirus receptor	1.100142278
signaling lymphocytic activation molecule family member 1	1.110156307
chemokine (C-C motif) ligand 18 (pulmonary and activation-regulated)	1.120202175
leukocyte immunoglobulin-like receptor, subfamily B (with TM and ITIM domains), member 2	1.122434874
SLAM family member 8	1.142414091
toll-like receptor 4	1.150457705
C-type lectin domain family 4, member A	1.154750033
leukocyte immunoglobulin-like receptor, subfamily B (with TM and ITIM domains), member 2	1.155149407
CD40 molecule, TNF receptor superfamily member 5	1.1611291
integrin, alpha 4 (antigen CD49D, alpha 4 subunit of VLA-4 receptor)	1.169747631
endoglin	1.179377571
sialic acid binding Ig-like lectin 1, sialoadhesin	1.186170149
leukocyte immunoglobulin-like receptor, subfamily B (with TM and ITIM domains), member 4	1.190080308
triggering receptor expressed on myeloid cells 2	1.195460247
CD300a molecule	1.195911812

integrin, alpha 4 (antigen CD49D, alpha 4 subunit of VLA-4 receptor)	1.196499459
chemokine (C-C motif) ligand 18 (pulmonary and activation-regulated)	1.199596037
CD84 molecule	1.208472952
CD40 molecule, TNF receptor superfamily member 5	1.22393359
Fc fragment of IgG, low affinity IIc, receptor for (CD32)	1.25512673
Fc fragment of IgG, low affinity IIIb, receptor (CD16b)	1.267594021
interferon gamma receptor 1	1.290301376
sialic acid binding Ig-like lectin 1, sialoadhesin	1.304110673
scavenger receptor class B, member 2	1.314859149
lymphocyte antigen 86	1.326899064
scavenger receptor class B, member 2	1.338297334
integrin, alpha 4 (antigen CD49D, alpha 4 subunit of VLA-4 receptor)	1.35163333
Fc fragment of IgG, low affinity IIc, receptor for (CD32)	1.361960092
low density lipoprotein-related protein 1 (alpha-2-macroglobulin receptor)	1.493771381
protein tyrosine phosphatase, receptor type, C	1.502458085
endoglin	1.504804445
stabilin 1	1.509919671
Fc fragment of IgG, low affinity IIb, receptor (CD32)	1.522381822
Fc fragment of IgG, high affinity Ib, receptor (CD64)	1.532299878
latexin	1.550880539
stabilin 1	1.605912238
platelet/endothelial cell adhesion molecule	1.616925083
platelet/endothelial cell adhesion molecule	1.622624317
chemokine (C-X-C motif) ligand 11	1.630053469
chemokine (C-X-C motif) ligand 11	1.641899621
SLAM family member 8	1.647210931

CD36 molecule (thrombospondin receptor)	1.703728151
chemokine (C-X-C motif) ligand 10	1.711583601
CD36 molecule (thrombospondin receptor)	1.712641394
platelet/endothelial cell adhesion molecule	1.712653905
insulin-like growth factor 1 (somatomedin C)	1.872892105
low density lipoprotein-related protein 1 (alpha-2-macroglobulin receptor)	2.050509235
protein tyrosine phosphatase, receptor type, C	2.092077389
protein tyrosine phosphatase, receptor type, C	2.14001381
insulin-like growth factor 1 (somatomedin C)	2.165799688
integrin, beta 2 (complement component 3 receptor 3 and 4 subunit)	2.191357554
CD14 molecule	2.195483266
chemokine (C-X-C motif) ligand 9	2.249026866
CD163 molecule	2.303025895
lymphocyte antigen 96	2.381283658
CD163 molecule	2.562992321
glycoprotein (transmembrane) nmb	2.814810658
insulin-like growth factor 1 (somatomedin C)	2.942212048
insulin-like growth factor 1 (somatomedin C)	4.259370331

Table 10-4 Macrophage signature genes in high CXCL12 expressing ovarian cancer biopsies of the GSE 6008 and 3149 data set.

A publically available gene set signature associated with macrophages was used to interrogate the gene expression microarray data of the GSE 6008 and 3149 data set. High CXCL12 expressing ovarian cancer biopsies showed enrichment in macrophage gene signatures. Table lists all the genes associated with macrophages and high expression of CXCL12 in the biopsies with the corresponding fold change values for each gene probe set. p value ≤ 0.05.

10.2. Appendix II: Publication

Journal of Pathology
J Pathol 2012; **227:** 136–145
Published online in Wiley Online Library
(wileyonlinelibrary.com) DOI: 10.1002/path.4002

ORIGINAL PAPER

The peritoneal tumour microenvironment of high-grade serous ovarian cancer

D Andrew Leinster,[1,2] Hagen Kulbe,[1] Gemma Everitt,[1] Richard Thompson,[1] Mauro Perretti,[2] Felicity N. E Gavins,[2] Dianne Cooper,[2] David Gould,[2] Darren P Ennis,[1] Michelle Lockley,[1] Iain A McNeish,[1] Sussan Nourshargh[2] and Frances R Balkwill[1]*

[1] *Barts Cancer Institute, Barts and The London School of Medicine and Dentistry, Queen Mary University of London, Charterhouse Square, London EC1M6BQ, UK*
[2] *William Harvey Research Institute, Barts and The London School of Medicine and Dentistry, Queen Mary University of London, Charterhouse Square, London EC1M6BQ, UK*

**Correspondence to: Frances R Balkwill, Barts Cancer Institute, Barts and The London School of Medicine and Dentistry, Queen Mary University of London, Charterhouse Square, London EC1M6BQ, UK. e-mail: f.balkwill@qmul.ac.uk*

Abstract

High-grade serous ovarian cancer (HGSC) disseminates early and extensively throughout the peritoneal space, causing multiple lesions that are a major clinical problem. The aim of this study was to investigate the cellular composition of peritoneal tumour deposits in patient biopsies and their evolution in mouse models using immunohistochemistry, intravital microscopy, confocal microscopy, and 3D modelling. Tumour deposits from the omentum of HGSC patients contained a prominent leukocyte infiltrate of $CD3^+$ T cells and $CD68^+$ macrophages, with occasional neutrophils. Alpha-smooth muscle $actin^+$ (α-SMA^+) pericytes and/or fibroblasts surrounded these well-vascularized tumour deposits. Using the murine bowel mesentery as an accessible mouse peritoneal tissue that could be easily imaged, and two different transplantable models, we found multiple microscopic tumour deposits after i.p. injection of malignant cells. Attachment to the peritoneal surface was rapid (6–48 h) with an extensive $CD45^+$ leukocyte infiltrate visible by 48 h. This infiltrate persisted until end point and in the syngeneic murine ID8 model, it primarily consisted of $CD3^+$ T lymphocytes and $CD68^+$ macrophages with α-SMA^+ cells also involved from the earliest stages. A majority of tumour deposits developed above existing mesenteric blood vessels, but in avascular spaces new blood vessels tracked towards the tumour deposits by 2–3 weeks in the IGROV-1 xenografts and 6 weeks in the ID8 syngeneic model; a vigorous convoluted blood supply was established by end point. Inhibition of tumour cell cytokine production by stable expression of shRNA to CXCR4 in IGROV-1 cells did not influence the attachment of cells to the mesentery but delayed neovascularization and reduced tumour deposit size. We conclude that the multiple peritoneal tumour deposits found in HGSC patients can be modelled in the mouse. The techniques described here may be useful for assessing treatments that target the disseminated stage of this disease.

Keywords: ovarian cancer; peritoneum; metastases; inflammation; chemokines; CXCR4; intravital microscopy

Received 15 November 2011; Revised 12 January 2012; Accepted 27 January 2012

No conflicts of interest were declared.

Introduction

There may be controversy about the cell and tissue origin of high-grade serous ovarian cancer (HGSC) [1,2], but there is no doubt that by the time of diagnosis, this most common and lethal of the 'ovarian' malignancies has spread extensively throughout the peritoneal space [3,4], presenting a fundamental clinical problem. After optimal cytoreduction by surgery and chemotherapy, many microscopic nodules remain, and in these areas chemoresistant cells may develop. The reason why high-grade serous cancers are only detected once they have spread throughout the peritoneum is that small asymptomatic primary lesions, whether they develop on the surface of the ovary or the distal fimbria of the Fallopian tube, are able to generate multiple micro-metastases by the dissemination of malignant cells into the peritoneum [2,5].

There is as yet no appropriate genetic model of HGSC that accurately recapitulates the p53 mutation and general genomic instability characteristic of this malignancy [6], but intraperitoneal injection of malignant cells in xenogeneic or syngeneic models generates large intraperitoneal tumours and ascites fluid with tumour growth usually measured by bioluminescent imaging of luciferase-transfected cells or weight of macroscopic resected tumours [7–10]. The development of microscopic peritoneal metastases has not been studied in detail and it is not known if this is a valid model for the human situation. Our aim was to study the natural history and cellular composition of peritoneal metastases in mouse models and relate

our findings to the human disease. We conclude that this clinical problem can be reproduced in mouse models; describe techniques that could enhance our understanding of peritoneal tumour spread and be useful in the development of novel treatments; and show how shRNA to the chemokine receptor CXCR4 had a significant effect on the development of intraperitoneal tumour deposits.

Materials and methods

Cell lines

IGROV-1 (NCI) and the ID8 (MOSEC) malignant cells (provided by K Roby, University of Kansas, Kansas City, KS, USA) were used for this study. IGROV-1 cells were cultured in RPMI with 10% FCS and ID8 cells were cultured in DMEM with 4% FCS and insulin transferrin sodium selenite supplement (Sigma Aldrich, Dorset, U.K.). The human cell line most recently underwent 16 loci STR authentication (LGC Standards, London, UK) in September 2011. Both cell lines were infected with a lentiviral eGFP construct (pHRSIN-CSGW-dNotI) to express an eGFP construct (kindly provided by Dr Y Ikeda, Mayo Clinic, Rochester, MN, USA), as described previously by Kulbe *et al* [8]. IGROV-1 cells were also transfected with SUPER RNAi™ plasmids containing two different shRNA sequences targeting CXCR4, or a control plasmid containing scrambled RNA (IGROV-Scrambled). Cells were transfected using Lipofectamine 2000 (Invitrogen, Paisley, UK) following the manufacturer's instructions.

Animal models

ICRF nude mice (Cancer Research UK) were used for the IGROV-1 experiments. C57 Black6 mice (Charles River, Margate, UK) were used for all ID8 experiments. Briefly, IGROV-1 (5×10^6 cells) and ID8 (1×10^7 cells) were injected in 0.3 ml of sterile, endotoxin-free PBS. The animals would reach UKCCCR guidelines for end-point tumour burden [11] in approximately 5 and 12 weeks, respectively.

Intravital microscopy (IVM)

The protocol for mesenteric IVM has been described previously [12]. Body temperature was maintained at 37 °C and mice were anaesthetized with i.p. ketamine (150 mg/kg) and xylazine (7.5 mg/kg). A midline incision (1.5 cm) was made through the skin and the peritoneal wall. The mesentery was positioned over a Perspex viewing stage and observed using a water immersion objective on a Zeiss Axioskop FS microscope (Carl Zeiss, Welwyn Garden City, UK). The number and size of the tumour deposits were recorded in a 0.4 mm^2 area.

Fluorescent labelling of the mesentery

Functional blood vessel labelling was achieved by injecting (i.v.) 100 µl of 2 mg/ml lectin solution (TRITC-conjugated *Bandeiraea simplicifolia* lectin; Sigma Aldrich, Dorset, UK) or streptavidin Alexa 633 conjugated to biotin-tagged *Lycopersicon esculentum* lectin (Invitrogen and Vector Labs, Peterborough, UK, respectively) under terminal anaesthesia. The animals were then killed via cardiac perfusion of a 4% paraformaldehyde (PFA) solution. The mesenteric tissue was removed, washed, and fixed in 4% PFA for 1 hour. The tissue was then blocked and permeabilized in a blocking solution of 3% goat serum, 1% BSA, and 1% Triton-X100. Staining for a variety of cell markers was achieved using both fluorophore-conjugated primary antibodies (eg SMA-Cy3 from Sigma; MRP14 conjugated to Alexafluor 555, a kind gift from Professor N Hogg, CRUK; and CD3-Alexa 647 from eBioscience, Hatfield, UK) and primary antibodies with fluorescently labelled secondary antibodies [eg F4/80 (a mouse macrophage-specific marker) with anti-rat DyLight™ 405 from ABD Serotec, Kidlington, UK and CD45 (a common marker for all nucleated haemopoietic cells) from BD, Oxford, UK with anti-rat Alexa 633]. MRP14 was used as a tissue neutrophil marker as it labels calcium-binding proteins highly expressed on neutrophils and monocytes. Tissues were washed in PBS and arranged on a slide. The intestine was then removed before embedding the tissue onto the slide in Prolong Gold (Invitrogen). The mesenteric tissue was imaged on both an Ariol computer-controlled microscope (Leica Microsystems, Gateshead, UK) and image analysis system and a Zeiss LSM 510 confocal microscope.

Human tumour samples

Human omentum samples were collected from surgery on ovarian cancer patients at St Bartholomew's Hospital. Samples were taken from patients who had given prior consent under the Research Ethical Committee Project number 10/H0304/14 and stored within the Barts Gynae Tissue Bank. Sections of human omental tissue were stained for the immunohistochemical markers CD68 (a marker for all human cells of the macrophage lineage) (Dako, Ely, UK) and CD3 (found on all mature human T cells) (Labvision, Cuncorn, UK) using a Dako Autostainer Plus with a Super Sensitive Polymer—HRP DAB (Launch Diagnistics Ltd, Longfield, U.K.). Neutrophil elastase (a marker for human neutrophils) (Dako) and α-SMA (a marker for fibroblasts and pericytes) (Sigma) staining was visualized with a biotinylated HRP secondary antibody and DAB staining (Vector Labs). Quantification of the tumour-infiltrating inflammatory cells was determined using the Ariol computer-controlled microscope (Leica Microsystems) and image analysis system. Six of the samples were obtained from patients who had interval debulking surgery after three cycles of carboplatin

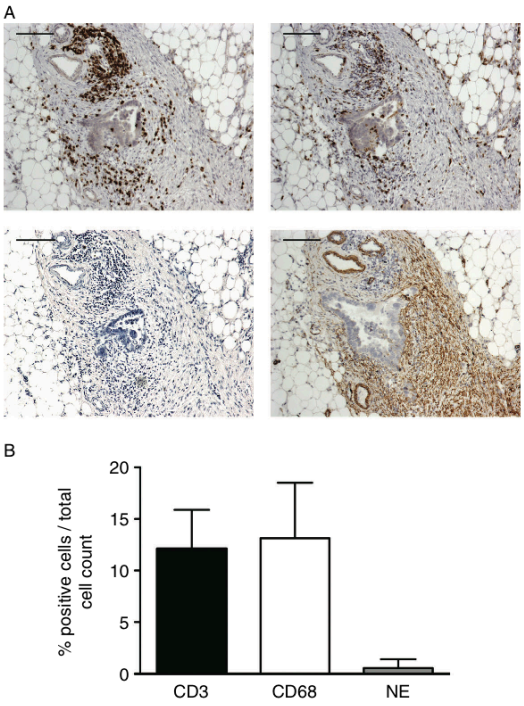

Figure 1. Leukocytes and α-smooth muscle actin (α-SMA)-positive cells in omental tumour deposits of high-grade serous ovarian cancer. Immunohistochemistry was carried out on omental tumour deposits removed at surgery. (A) Representative images of a section from patient G11. Clockwise from top left: $CD3^+$, $CD68^+$, α-SMA^+, and neutrophil $elastase^+$ (NE^+) cells. Scale bar = 400 μm. (B) The tumour-infiltrating leukocytes were measured in each entire tissue section using the Ariol computer-controlled microscope and are expressed as a percentage of positively stained cells relative to a haematoxylin nucleus counterstain. All values represent mean and standard deviations. $n = 8$ patients.

and paclitaxel chemotherapy; two were obtained from patients undergoing primary debulking surgery.

Results

Peritoneal metastases of human high-grade serous ovarian cancer

We first examined the cellular composition of microscopic peritoneal tumour deposits from eight patients with HGSC, using omentum removed during cytoreductive surgery. All deposits had prominent infiltrates of $CD3^+$ lymphocytes and $CD68^+$ macrophages, but there were few neutrophil elastase-positive cells. The deposits were well-vascularized and had many α-SMA-positive pericytes and fibroblasts (Figure 1A). Using Ariol computer-controlled microscopy, we calculated the percentage of each leukocyte population per total number of cells in the peritoneal tumour islands, assessing an entire tissue section for each of the deposits. Figure 1B shows that 12% of the cells were $CD3^+$ T cells and 14% of the cells were $CD68^+$ macrophages. Less than 1% of the cells in the tumour deposits were neutrophils.

Peritoneal metastases of ovarian cancer cells in mice

We used the bowel mesentery as a readily accessible murine peritoneal location for temporal analysis of cellular and molecular changes using both confocal and intravital microscopy. In all experiments, we used two well-characterized transplantable models of ovarian cancer that grow intraperitoneally: IGROV-1 human HGSC xenografts [8,10] and the ID8 syngeneic mouse ovarian cancer model [7,9]. Both cell lines expressed eGFP. An Ariol computer-controlled microscope imaged the entire bowel mesentery for deposits of eGFP-expressing tumour cells. Vasculature was labelled with red TRITC-labelled *Bandeiraea*

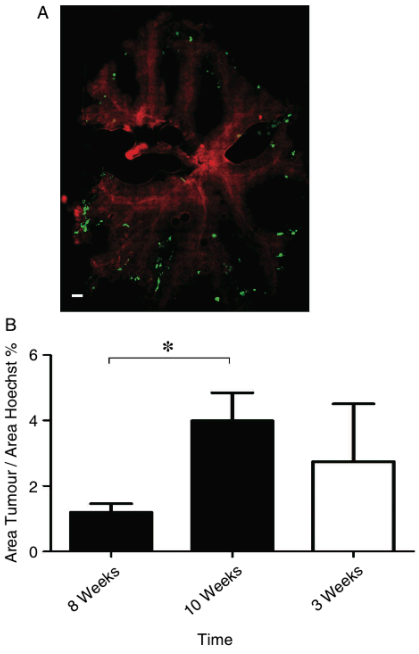

Figure 2. The development of ovarian cancer deposits on the bowel mesentery. Ariol computer-controlled microscopy provided a global view of the colonization of malignant cells on the surface of the mesothelium. (A) A representative image of the colonization of the bowel mesentery with ID8 tumour deposits (green) and the functional vasculature (BS-1 lectin–red). Scale bar = 1 mm. (B) The colonization of the bowel mesentery by tumour cell deposits was measured by the Ariol microscope software by comparing the area of Hoechst staining with the area of the eGFP tumour staining. (Solid bars are the ID8 tumour deposits and the open bars are the IGROV-1 tumour deposits.) The results for the ID8 cells showed a significant increase in the tumour cell area over a 2-week period ($p = 0.01$, Student's t-test). $n = 6$ animals per time point for ID8 and $n = 3$ animals for IGROV-1.

simplicifolia lectin. Figure 2A shows a representative image of the bowel mesentery 10 weeks after injection of eGFP-expressing ID8 cells. Similar patterns of spread were observed in a xenograft setting with IGROV-1 cells. A majority of the deposits were located close to existing peritoneal vessels, although some developed in avascular areas. The area of the mesentery that was occupied by eGFP-labelled cells also increased with time, as shown in a typical experiment with ID8 cells (Figure 2B). At 3 weeks, comparable values for IGROV-1 cells were approximately 3% of the mesenteric area (Figure 2B). This reflected the natural history of these two models in our laboratory; the end point of the ID8 model was approximately 12 weeks [9], whereas the IGROV-1 end point was 4–6 weeks [8].

Intravital microscopy of the tumour-bearing bowel mesentery

To enable us to study the development of tumour deposits in live animals, an intravital microscopy technique established for studying peritoneal inflammation [12] was used to study peritoneal tumour growth and attachment in more detail. For this purpose, mice were injected with eGFP-labelled malignant cells and at time points between 48 h and 10 weeks, the bowel mesentery was exteriorized under terminal anaesthesia (Figure 3A). Malignant cells were clearly visible in the avascular areas of the mesentery, as observed by both phase contrast and fluorescence microscopy (Figures 3B and 3C). As deposits above and around the existing blood vessels were difficult to image because of surrounding adipose tissue, we focused on areas between the vessels (see Figure 3A).

All such IGROV-1 deposits were avascular for the first 2 weeks. However, by 3 weeks, blood vessels began to spread across the avascular mesenteric spaces towards the malignant cells. At 3 weeks, these vessels had poor flow and were mostly incomplete. After this time, tumour blood vessels developed rapidly and within 6 weeks, most tumours larger than 100 μm in diameter were vascularized with apparently viable structures that could support a fast-moving and convoluted blood flow. (Figure 3C shows this sequence for IGROV-1.) The peritoneal deposits formed by ID8 murine ovarian cancer cells took longer to develop, as expected from our knowledge of the natural history, with new blood vessels developing at 4–6 weeks.

Supplementary Movie 1 (Supporting information) shows the development of IGROV-1 tumours on the bowel mesentery. The normal mesothelium is shown at the beginning, followed by an early time point (6 h post-i.p. injection of cells) where single malignant cells are visible on the mesothelium. After 1 week, the malignant cells showed signs of aggregation. Two weeks after injection, IGROV-1 cells had formed large deposits without a vasculature. The development of a vasculature to the tumour was visible at 3 weeks post-i.p. injection of IGROV-1 cells. The initial vessels appeared as fine structures, and as can be seen in the film, the single red blood cells within them were moving slowly and were sometimes static. By 4 and 6 weeks, the vessels had developed into large structures with an increased flow rate. These images are typical of those obtained from at least three mice at each time point. The images shown at different time points of peritoneal development are from individual mice.

Colony number and size were recorded throughout the experiments. For both the xenogeneic and the syngeneic model, single cells and smaller deposits of less than 100 μm in diameter were visible by 48 h (Figures 3D and 3E). In the IGROV-1 model, the number of small deposits decreased by 1 week and remained constant thereafter. Deposits larger than 100 μm increased in number steadily over the 6-week time course of the experiment. The deposits also grew

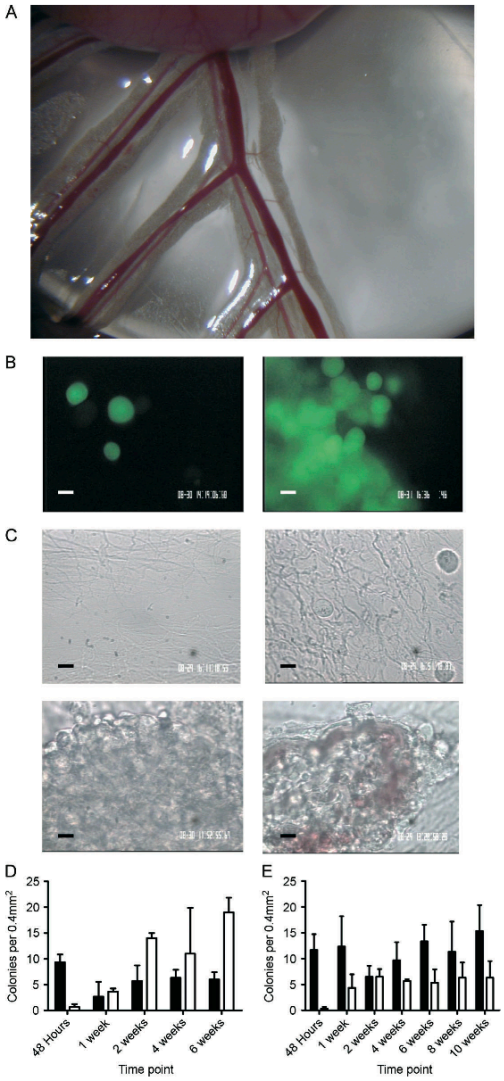

Figure 3. Imaging of tumour deposits on the bowel mesentery by intravital microscopy (IVM). (A) Image of a bowel mesentery preparation as used for the IVM protocols from a dissecting microscope (original magnification ×10). (B) eGFP-transfected malignant cells clearly show the colonization of the bowel mesothelium. Both single cells and larger tumour colonies could be seen. Scale bar = 10 μm. (C) Composite panel showing the development of the IGROV-1 malignant cells on the bowel mesothelium. As mice were sacrificed after imaging, each picture is taken from a different animal. Scale bar = 10 μm. Clockwise from top left: the pre-tumour bowel mesothelium with no malignant cells; the initial colonization process of the malignant cells 48 h post-injection of malignant cells with single cells attached to the mesothelium; the tumour 2 weeks post-i.p. injection with an avascular tumour formed on the surface of the tissue; a vascularized tumour 4 weeks after injection of the cells. (D) Tumour deposits were counted by assessing 40 regions of the bowel mesentery (0.4 mm^2). The growth of the IGROV-1 malignant cells is shown over a 6-week time course ($n = 3$ animals per time point). (E) ID8 tumour deposits were counted as in D but over a 10-week time course ($n = 3$ per time point). (D, E) Solid bars are colonies smaller than 100 μm in diameter. Open bars are colonies larger than 100 μm.

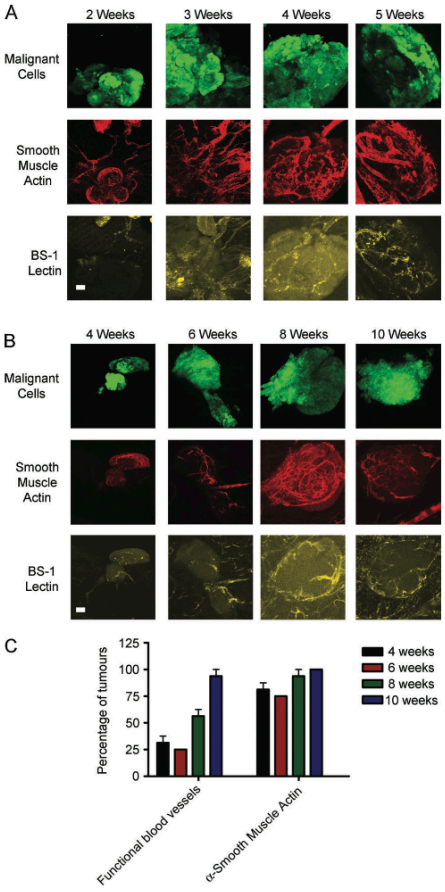

Figure 4. Mesenteric tumour angiogenesis visualized using the whole mount method. (A) The development of IGROV-1 tumours on the bowel mesentery showing the recruitment of functional blood vessels (LE lectin—yellow) and pericytes (anti-SMA—red). Scale bar = 50 μm. (B) ID8 tumours develop over a longer time course compared with the IGROV-1 tumours. However, the similar recruitment of pericytes and functional vessels is visible. Scale bar = 50 μm. (C) Comparison of the pericyte labelling and functional blood vessels in the ID8 tumour model. The percentage of tumours with either BS-1 lectin or anti-SMA labelling is displayed (six tumours analysed per time point).

out from the surface of the bowel mesentery, reaching estimated heights of between 2 and 3 mm at end point. With ID8, the smaller deposits persisted throughout the experiment and larger deposits were observed by 2 weeks. With both models, clusters of cells from the larger deposits could be dislodged, suggesting that they too may be able to disseminate elsewhere through the peritoneal cavity.

The 'angiogenic switch' in the peritoneal tumour islands

We next used confocal microscopy to further study the development of blood vessels in the peritoneal deposits, staining the mesothelium for functional blood vessels (*Lycopersicon esculentum* lectin — yellow), fibroblasts, and pericytes (α-SMA — red) with eGFP-positive malignant cells. Figure 4A shows a typical image of IGROV-1 tumour colony development, with vasculature first evident between 3 and 4 weeks. Of note is that α-SMA-positive 'vascular shapes' resembling blood vessels were seen before functional blood vessels were observed. In the ID8 model, the vasculature first developed between 4 and 8 weeks post-tumour cell injection (Figure 4B); 25% of tumour deposits were vascularized at 4 weeks but 100% at 10 weeks (Figure 4C). In contrast, the percentage of tumour deposits containing α-SMA-positive cells remained constant over the 4- to 10-week observation period (Figure 4C), suggesting that the pericyte 'sheaths' preceded functional blood flow.

The leukocyte infiltrate in the peritoneal tumour deposits

We next examined the leukocyte component of the peritoneal tumour deposits by confocal microscopy using CD45 as a pan-leukocyte marker and red TRITC-labelled lectin as a marker of functional blood vessels. $CD45^+$ cells were rarely detected on the bowel mesentery from control mice or in areas of mesentery from tumour-bearing mice that were tumour-free. Within 48 hours of IGROV-1 cell injection, we found leukocytes accumulating around the tumour cell deposits. This leukocyte infiltrate persisted and preceded the development of blood vessels at 3–4 weeks (Figure 5A). As the ID8 model had a slower natural history, we studied this from 2 to 10 weeks after tumour cell injection. Once again, a prominent $CD45^+$ leukocyte infiltrate preceded the development of a vasculature to the deposits (Figure 5B). As we had observed with the omental tumour deposits from the HGSC patients, the leukocytes were predominantly $CD3^+$ T cells and $F4/80^+$ macrophages in the ID8 model (Figures 5C and 5D). There were few $MRP14^+$ cells after 2 weeks.

Manipulation of CXCR4 expression

The results described above show that we can model the development of peritoneal deposits of ovarian cancer in mice and that the leukocyte populations resemble those seen in human HGSC. We therefore asked if we could use our methods to measure changes in tumour development. We chose to assess the effects of manipulating expression of the chemokine receptor CXCR4 on peritoneal tumour deposits, as we, and others, have found this receptor to be important in ovarian cancer growth and spread [8,13–15]. Moreover, we recently reported that stable knockdown of CXCR4

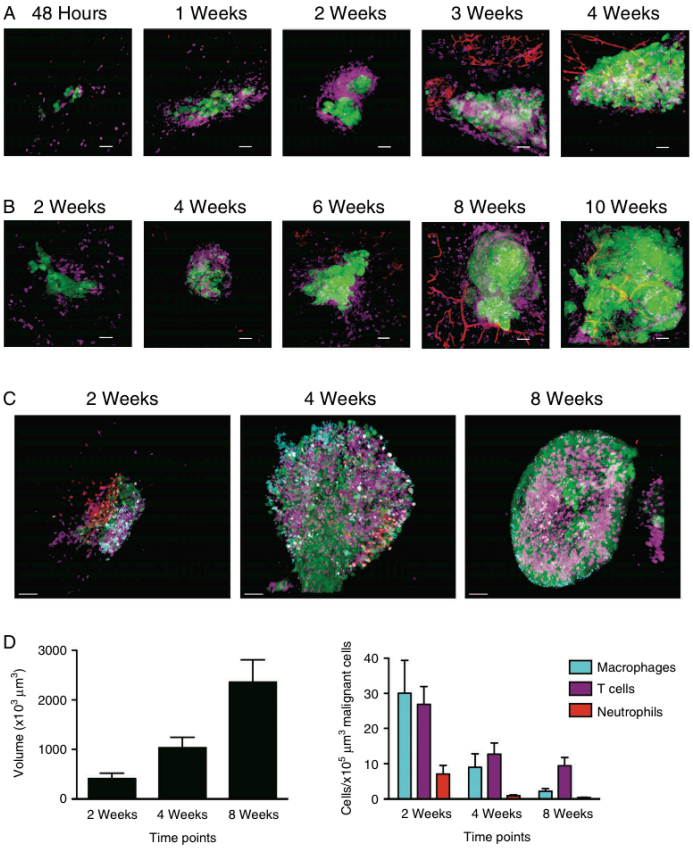

Figure 5. Imaging and quantifying the leukocyte recruitment to mesenteric ovarian tumour deposits. (A) Using immunofluorescence, the IGROV-1 tumours (green) on the bowel mesentery were labelled for immune infiltrate (anti-CD45—purple) and functional blood flow (red). Representative images over a 4-week time course are shown. (B) Using the same labelling as in A, the immune infiltrate and functional blood flow are shown in the ID8 tumour model over a 10-week time period. (C) The different immune cell infiltrate within the ID8 tumour (green) was further characterized by staining for $CD3^+$ (purple), $F4/80^+$ (turquoise), and $MRP14^+$ cells (red) (representative images shown). (D) The tumour volume and immune infiltrate (expressed as number of each cell type per 100000 μm^3 tumour volume) from the ID8 tumour were quantified using IMARIS analysis software of the CLSM images (18 tumours from six mice). All scale bars = 50 µm. The increase in tumour volume with time was statistically significant ($p < 0.01$, Student's *t*-test). All differences in composition of the leukocyte infiltrate between 2 and 4 or 8 weeks were also significant ($p < 0.05$, Student's *t*-test).

reduced tumour growth *in vivo*, as measured by imaging of luciferase-transfected cells [10]. The efficacy of the CXCR4 knockdown and the lack of effect on *in vitro* growth and viability of these cells have already been published by us [10]. IGROV-1 cells mock-transfected or transfected with shRNA to CXCR4 were injected i.p. and peritoneal tumour colony formation was assessed over a 6-week time period using intravital and confocal microscopy. Intravital microscopy showed that more mock-transfected than shCXCR4 tumour cells had adhered to the mesentery in the time period 48 h–2 weeks. Control deposits developed and grew in size as expected. Viable single cells and small deposits remained on the mesentery in the shCXCR4 group but the number of deposits 100 µm in diameter or more was greatly reduced ($p < 0.001$) (Figures 6A and 6B). Confocal microscopy revealed a diminished vasculature in the shCXCR4 deposits (Figure 6C). We also used IMARIS analysis to measure tumour volume and $CD45^+$ leukocyte density. At 4 weeks, there was a significant decrease in tumour volume and at 1 week a significant decrease in leukocyte count standardized to tumour volume (Figures 6D and 6E) (both $p < 0.001$).

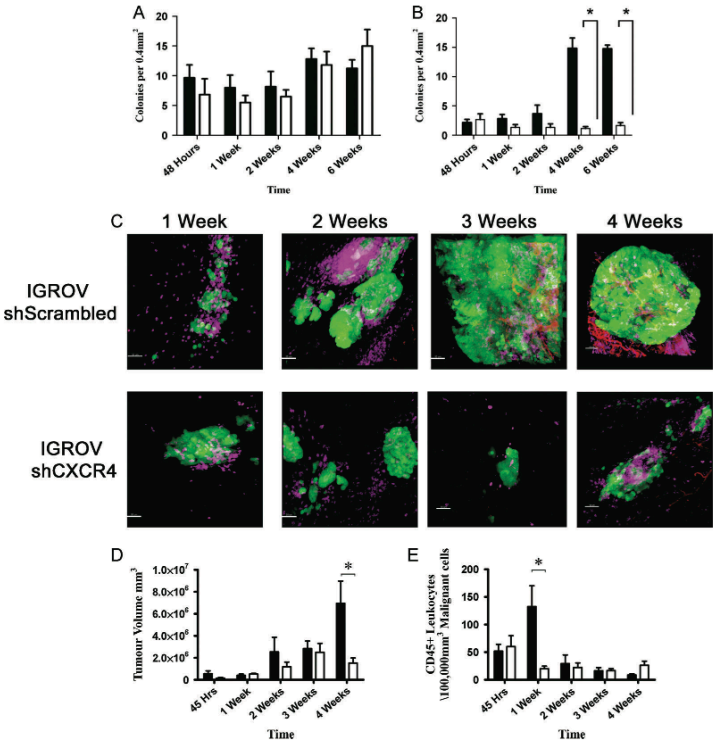

Figure 6. Measuring the effect of CXCR4 shRNAi on the mesenteric development of IGROV-1 ovarian tumours. IVM analysis of the growth of the CXCR4 shRNA IGROV-1 tumours is displayed on the two graphs (black bars—shScrambled IGROV-1 cells; open bars—shCXCR4 IGROV-1).(A) Effect of shCXCR4 on the growth of IGROV-1 cell colonies smaller than 100 μm. (B) Effect of shCXCR4 on the growth of IGROV-1 cell colonies larger than 100 μm. Inhibition of tumour growth was recorded in the larger IGROV-1 deposits, $p < 0.001$ (six mice per time point). (C) Representative images of the leukocyte recruitment ($CD45^+$ cells—purple) and functional blood (BS-1 lectin—red) in both mock and shCXCR4 IGROV-1 tumours over a 4-week time period. (D) Measurement of the tumour volume using IMARIS analysis software. $^*p < 0.001$, Bonferroni post-test. (E) The density of $CD45^+$ leukocytes. $^*p < 0.001$, Bonferroni post-test). All scale bars = 50 μm.

Discussion

Traditional concepts of metastasis may not apply to some types of ovarian cancer. In HGSC, there is no anatomical barrier to seeding throughout the peritoneal cavity. At the earliest detectable stage, the disease may have already formed multiple small peritoneal deposits and these can probably be generated from a primary cancer no larger than a few centimetres [2,5]. Any therapeutic approach to this disease therefore needs to take into account an understanding of the development of peritoneal deposits and their response to treatment. Here we have shown that in experimental mouse models, ovarian cancer cells injected intraperitoneally attach rapidly to avascular areas of the peritoneal surface, forming vascularized deposits. These tumour deposits contain substantial infiltrates of lymphocytes, macrophages, and fibroblasts/pericytes that mimic the composition of those found in patients with advanced HGSC. After i.p. injection, the malignant cells also formed deposits over the vascular areas of the bowel mesentery and some of these may have been associated with milky spots as described by Gerber *et al* [16]. However, we conclude that, at least on the bowel mesentery, malignant cells can attach to mesothelial cell monolayers and then recruit their own microenvironment of leukocytes and new blood vessels.

The infiltrating leukocytes found in primary human HGSC tumours are related to both good and bad prognosis, depending on subtype. Increased infiltration of $CD8^+$ lymphocytes in solid tumour islets predicts longer survival [17] and correlates significantly with BRCA loss [18]. On the other hand, high numbers of $CD4^+$ T-regulatory cells, which can mediate immune suppression, predict poor patient survival

[19,20]. Additional immunosuppressive leukocyte subtypes, such as B7-H4-expressing tumour macrophages [21], have also been correlated with poor outcome in ovarian cancer.

Six of the eight patients studied had already received three cycles of chemotherapy. As a majority of HGSC patients in the UK are now pretreated before surgery, we could only obtain two chemo-naïve samples. We could see no difference between untreated and treated in terms of deposit size, location or the $CD3^+$ and NE^+ infiltrate but there did seem to be fewer $CD68^+$ cells in the treated patients.

We believe that any pre-clinical studies of HGSC in mouse models should study peritoneal spread, as this is the major clinical challenge. There is evidence for a cancer stem cell (CSC) population in HGSC with the capacity for both self-renewal and generating heterogeneous lineages [22–25], and we expect that this stem cell component will be a major determinant of cell behaviour *in vivo* [23]. It is likely that the tumour deposits that have colonized the peritoneum in the mouse models are derived from these CSCs. We have shown that in HGSC there is an autocrine cytokine network in the malignant cells, with the major players being CXCR4, CXCL12, TNF-α, and IL-6. We have named this the TNF network. This network has paracrine tumour-promoting actions on the leukocyte infiltrate and angiogenesis [10]. The results presented here show that inhibiting the TNF network via stable CXCR4 knockdown can have profound effects on the development of peritoneal deposits. Viable malignant cells survived attached to the peritoneal surface but few developed any vasculature. Treatment of HGSC with cytokine or chemokine antagonists, eg anti-IL-6 antibodies [26], may be one way to delay or inhibit further development of peritoneal disease after diagnosis and initial chemotherapy and surgery.

Acknowledgment

This study was supported by the Wellcome Trust (081172/Z/06/Z and 088407/Z/09/Z), BBSRC, Barts and the London Charity, and Cancer Research UK.

Abbreviations

BS-1	*Bandeiraea simplicifolia*
HGSC	high-grade serous ovarian cancer
i.p.	intraperitoneal
i.v.	intravenous
IVM	intravital microscopy
LE	*Lycopersicon esculentum*
NE	neutrophil elastase

Author contribution statement

DAL conducted most of the mouse model experiments. HK constructed the shRNA CXCR4 cells and assisted in the mouse experiments. RT provided expert technical assistance with the mouse experiments. GE conducted the experiments with the human biopsies. MP, FG, and DC provided expertise with the intravital microscopy. DG made the eGFP-expressing cells. ML, DE, and IAM obtained the clinical samples and provided the clinical information. SN provided the expertise on confocal microscopy. FB devised and supervised the study and wrote the manuscript.

References

1. Bowtell DD. The genesis and evolution of high-grade serous ovarian cancer. *Nature Rev Cancer* 2010; **10**: 803–808.
2. Vaughan S, Coward J, Bast RC Jr, *et al*. Rethinking ovarian cancer: recommendations for improving outcomes. *Nature Rev Cancer* 2011; **11**: 719–725.
3. Tan DS, Agarwal R, Kaye SB. Mechanisms of transcoelomic metastasis in ovarian cancer. *Lancet Oncol* 2006; **7**: 925–934.
4. Kyriazi S, Kaye SB, deSouza NM. Imaging ovarian cancer and peritoneal metastases — current and emerging techniques. *Nature Rev Clin Oncol* 2010; **7**: 381–393.
5. Brown PO, Palmer C. The preclinical natural history of serous ovarian cancer: defining the target for early detection. *PLoS Med* 2009; **6**: e1000114.
6. Consortium TCGA. Integrated analysis of ovarian carcinoma. *Nature* 2011; **474**: 609–615.
7. Roby KF, Taylor CC, Sweetwood JP, *et al*. Development of a syngeneic mouse model for events related to ovarian cancer. *Carcinogenesis* 2000; **21**: 585–591.
8. Kulbe H, Thompson RT, Wilson J, *et al*. The inflammatory cytokine TNF-α generates an autocrine tumour-promoting network in epithelial ovarian cancer cells. *Cancer Res* 2007; **67**: 585–592.
9. Charles KA, Kulbe H, Soper R, *et al*. The tumour-promoting actions of TNF-alpha involve TNFR1 and IL-17 in ovarian cancer in mice and humans. *J Clin Invest* 2009; **119**: 3011–3023.
10. Kulbe H, Chakravarty P, Leinster DA, *et al*. A dynamic inflammatory cytokine network in the human ovarian cancer microenvironment. *Cancer Res* 2012; **72**: 66–75.
11. Workman P, Aboagye EO, Balkwill F, *et al*. Guidelines for the welfare and use of animals in cancer research. *Br J Cancer* 2010; **102**: 1555–1577.
12. Gavins FN, Chatterjee BE. Intravital microscopy for the study of mouse microcirculation in anti-inflammatory drug research: focus on the mesentery and cremaster preparations. *J Pharmacol Toxicol Methods* 2004; **49**: 1–14.
13. Kulbe H, Hagermann T, Szlosarek PW, *et al*. The inflammatory cytokine TNF-α upregulates chemokine receptor expression on ovarian cancer cells. *Cancer Res* 2005; **65**: 10355–10362.
14. Scotton CJ, Wilson JL, Scott K, *et al*. Multiple actions of the chemokine CXCL12 on epithelial tumour cells in human ovarian cancer. *Cancer Res* 2002; **62**: 5930–5938.
15. Scotton CJ, Wilson JL, Milliken D, *et al*. Epithelial cancer cell migration: a role for chemokine receptors? *Cancer Res* 2001; **61**: 4961–4965.
16. Gerber SA, Rybalko VY, Bigelow CE, *et al*. Preferential attachment of peritoneal tumour metastases to omental immune aggregates and possible role of a unique vascular microenvironment in metastatic survival and growth. *Am J Pathol* 2006; **169**: 1739–1752.
17. Zhang L, Conejo-Garcia JR, Katsaros D, *et al*. Intratumoural T cells, recurrence, and survival in epithelial ovarian cancer. *N Engl J Med* 2003; **348**: 203–213.

18. Clarke B, Tinker AV, Lee CH, *et al*. Intraepithelial T cells and prognosis in ovarian carcinoma: novel associations with stage, tumour type, and BRCA1 loss. *Mod Pathol* 2009; **22**: 393–402.
19. Curiel TJ, Coukos G, Zou L, *et al*. Specific recruitment of regulatory T cells in ovarian carcinoma fosters immune privilege and predicts reduced survival. *Nature Med* 2004; **10**: 942–949.
20. Sato E, Olson SH, Ahn J, *et al*. Intraepithelial $CD8^+$ tumour-infiltrating lymphocytes and a high $CD8^+$/regulatory T cell ratio are associated with favorable prognosis in ovarian cancer. *PNAS* 2005; **102**: 18538–18543.
21. Kryczek I, Wei S, Zhu G, *et al*. Relationship between B7-H4, regulatory T cells, and patient outcome in human ovarian carcinoma. *Cancer Res* 2007; **67**: 8900–8905.
22. Chien JR, Aletti G, Bell DA, *et al*. Molecular pathogenesis and therapeutic targets in epithelial ovarian cancer. *J Cell Biochem* 2007; **102**: 1117–1129.
23. Curley MD, Garrett LA, Schorge JO, *et al*. Evidence for cancer stem cells contributing to the pathogenesis of ovarian cancer. *Front Biosci* 2011; **16**: 368–392.
24. Rizzo S, Hersey JM, Mellor P, *et al*. Ovarian cancer stem cell like side populations are enriched following chemotherapy and overexpress EZH2. *Mol Cancer Ther* 2011; **10**: 325–335.
25. Strauss R, Li ZY, Liu Y, *et al*. Analysis of epithelial and mesenchymal markers in ovarian cancer reveals phenotypic heterogeneity and plasticity. *PLoS One* 2011; **6**: e16186.
26. Coward J, Kulbe H, Chakravarty P, *et al*. Interleukin-6 as a therapeutic target in human ovarian cancer. *Clin Cancer Res* 2011; **17**: 6083–6096.

SUPPORTING INFORMATION ON THE INTERNET

The following supporting information may be found in the online version of this article.

Supplementary Movie 1. Intravital microscopy of the bowel mesentery showing the development of peritoneal tumour deposits.